Probabilistic Modeling of Wind Turbine Drivetrain Components

Rafsanjani, Hesam Mirzaei

DOI (link to publication from Publisher):
10.5278/vbn.phd.engsci.00170

Publication date:
2016

Document Version
Publisher's PDF, also known as Version of record

PROBABILISTIC MODELING OF WIND TURBINE DRIVETRAIN COMPONENTS

BY
HESAM MIRZAEI RAFSANJANI

DISSERTATION SUBMITTED 2016

AALBORG UNIVERSITY
DENMARK

PROBABILISTIC MODELING OF WIND TURBINE DRIVETRAIN COMPONENTS

BY

HESAM MIRZAEI RAFSANJANI

AALBORG UNIVERSITY
DENMARK

Dissertation submitted 2016

.

Dissertation submitted: December 23, 2016

PhD supervisor: Prof. John Dalsgaard Sørensen
Aalborg University

PhD committee: Associate Professor Thomas Lykke Andersen (chair.)
Aalborg University

Professor Carlos Guedes Soares
Universidade de Lisboa

Associate Professor Sebastian Thöns
Technical University of Denmark

PhD Series: Faculty of Engineering and Science, Aalborg University

ISSN (online): 2246-1248
ISBN (online): 978-87-7112-859-8

Published by:
Aalborg University Press
Skjernvej 4A, 2nd floor
DK – 9220 Aalborg Ø
Phone: +45 99407140
aauf@forlag.aau.dk
forlag.aau.dk

Printed in Denmark by Rosendahls, 2017

THESIS DETAILS

Thesis title:

Probabilistic Modeling of Wind Turbine Drivetrain Components

PhD student:

Hesam Mirzaei Rafsanjani

Supervisor:

John Dalsgaard Sørensen

List of published paper:

Papers included in the appendix of the thesis:

1. Mirzaei Rafsanjani, H., & Sørensen, J.D. (2015). Reliability of analysis of fatigue failure of cast components for wind turbines. *Energies*, 8(4), 2908-2923.
2. Mirzaei Rafsanjani, H., & Sørensen, J. D. (2014). Stochastic models of defects in wind turbine drivetrain components, In *Multiscale Modeling and Uncertainty Quantification of Materials and Structures* (pp. 287-298). Springer International Publishing.
3. Mirzaei Rafsanjani, H., Sørensen, J. D., Mukherjee, K., Fæster, S., & Sturlason, A. (2014). Statistical analysis of manufacturing defects on fatigue life of a wind turbine casted component, International Conference on Safety & Reliability of Ship, Offshore & Subsea Structures, Glasgow, UK, 18th – 20th August.
4. Mirzaei Rafsanjani, H., Sørensen, J.D., Fæster, S., & Sturlason, A. (2016). Fatigue reliability analysis of wind turbine cast components. Submitted to Energies.
5. Mirzaei Rafsanjani, H., & Sørensen, J. D. (2015). Fatigue reliability of casted wind turbine components due to defects, 12th International Conference on Applications of Statistics and Probability in Civil Engineering, ICASP12, Vancouver, Canada, 12th – 15th July.
6. Mirzaei Rafsanjani, H., & Sørensen, J. D. (2015) Effect of defects distribution on fatigue life of wind turbine components. *Procedia IUTAM*, 13, 144-150.

Other papers:

7. Mirzaei Rafsanjani, H. & Sørensen, J. D. (2013). Stochastic modeling of wind turbine drivetrain components, Safety, Reliability and Risk Anaysis:

Beyond the Horizon: Proccedings of the European safety and reliability conference, Esrel 2013, Amsterdam, The Netherlands, 29 september - 2 October 2013. ed. / R.D.J.M. Steenbergen; P.H.A.J.M. van Gelder; S. Miraglia; A.C.W.M. Vrouwenvelder. London : C R C Press LLC, 2014. p. 1221-1228.

CURRICULUM VITAE

Hesam Mirzaei Rafsanjani

Email: hesam.mirzaei@gmail.com
hmr@civil.aau.dk
Date of Birth: September 19th, 1984
Place of Birth: Tehran, Iran
Degree: Master of Science in Mechanical Engineering
Alumni: Aalborg University, Denmark

Education

PhD Fellow (November 2012 – October 2015)
Aalborg University, Aalborg, Denmark
Civil Engineering Department
Thesis: Probabilistic modeling of wind turbine drivetrain components
Supervisor: John Dalsgaard Sørensen

Master of Science (September 2006 – January 2009)
Sharif University of Technology, Tehran, Iran
Mechanical Engineering Department
Thesis: Rolling bearing lifetime prognosis with damage mechanics method
Supervisor: Mehdi Behzad

Bachelor of Science (September 2002 – September 2006)
Amirkabir University of Technology, Tehran, Iran
Marine Engineering Department
Thesis: Analysis of torsional vibration of ship transmission shaft
Supervisor: Firooz Bakhtiari Nezhad

Work Experience

Project Engineer (November 2015 – Present)
Dansk Ingeniør Service, Aarhus, Denmark

Mechanical Engineer (November 2010 – November 2012)
MAPNA Turbine Company, Karaj, Iran

Field Engineer (November 2009 – November 2010)
Petropart, South Pars Gas Field Development, Iran

Mechanical Engineer (February 2009 – November 2009)
Marine Propulsion Institute, Tehran, Iran

Research Experience

Sharif University of Technology, Tehran, Iran
Research Assistant in Condition Monitoring Center
Supervisor: Mehdi Behzad

Teaching Experience

Sharif University of Technology, Tehran, Iran
Department of Mechanical Engineering
Strength of Material Laboratory, Teaching Assistant
May 2007 – September 2007

Amir Kabir University of Technology, Tehran, Iran
Department of Marine Engineering
Hydrostatic Laboratory, Teaching Assistant
October 2005 – June 2006

Amir Kabir University of Technology, Tehran, Iran
Department of Marine Engineering
Fluid Mechanics Course, Teaching Assistant
January 2005 – June 2006

Publications

Mirzaei Rafsanjani, H., & Sørensen, J. D. (2015). Reliability analysis of fatigue failure of cast components for wind turbines. *Energies*, 8(4), 2908- 2923.

Mirzaei Rafsanjani, H., & Sørensen, J. D. (2015) Effect of defects distribution on fatigue life of wind turbine components. *Procedia IUTAM*, 13, 144-150.

Mirzaei Rafsanjani, H., & Sørensen, J. D. (2014). Stochastic models of defects in wind turbine drivetrain components, In *Multiscale Modeling and Uncertainty Quantification of Materials and Structures* (pp. 287-298). Springer International Publishing.

Mirzaei Rafsanjani, H., & Rezaei nasab, A. (2012). Risk Assessment of failure modes of gas diffuser liner of V94.2 siemens gas turbine by FMEA method, *Journal of Physics: Conference Series*, 364, 012137

Mehdigholi, H., Mirzaei Rafsanjani, H., & Behzad, M. (2011). Estimation of rolling bearing life with damage curve approach, *Polish Maritime Research*, 3 (70), pp. 66-70.

Presentation

Mirzaei Rafsanjani, H., & Sørensen, J. D. (2015). Fatigue reliability of casted wind turbine components due to defects, 12th International Conference on Applications of Statistics and Probability in Civil Engineering, ICASP12, Vancouver, Canada,

12th – 15th July.

Mirzaei Rafsanjani, H., Sørensen, J. D., Mukherjee, K., Fæster, S., & Sturlason, A. (2014). Statistical analysis of manufacturing defects on fatigue life of a wind turbine casted component, International Conference on Safety & Reliability of Ship, Offshore & Subsea Structures, Glasgow, UK, 18th – 20th August.

Mirzaei Rafsanjani, H. & Sørensen, J. D. (2013). Stochastic modeling of wind turbine drivetrain components, Safety, Reliability and Risk Anaysis: Beyond the Horizon: Proccedings of the European safety and reliability conference, Esrel 2013, Amsterdam, The Netherlands, 29 september - 2 October 2013. ed. / R.D.J.M. Steenbergen; P.H.A.J.M. van Gelder; S. Miraglia; A.C.W.M. Vrouwenvelder. London : C R C Press LLC, 2014. p. 1221-1228.

Behzad, M., Golestani, M., Rohani Bastami, A., & Mirzaei Rafsanjani, H. (2009). Vibration Analysis of Main Mill Electromotor in Momtazan Cement Plant, 3rd National Condition Monitoring and Failure Diagnosis Conference, March, Tehran, Iran.

Behzad, M., Alandi Hallaj, A., Mirzaei Rafsanjani, H., & Rohani Bastami, A. (2009). Common Failure Modes of Electro-pumps in Industries, 3rd National Condition Monitoring and Failure Diagnosis Conference, March, Tehran, Iran.

ENGLISH SUMMARY

Wind energy is one of several energy sources in the world and a rapidly growing industry in the energy sector. Like other industries, the wind turbine manufactures try to increase reliability and decrease the costs. Hence, we must develop wind turbines that are cheaper and more efficient than other energy sources.

When placed in offshore or onshore locations, wind turbines are exposed to wave excitations, highly dynamic wind loads and/or the wakes from other wind turbines. Therefore, most components in a wind turbine experience highly dynamic and time-varying loads. These components may fail due to wear or fatigue, and this can lead to unplanned shutdown repairs that are very costly. The design of mechanical components in the wind turbine drivetrain by deterministic methods using safety factors is generally unable to account for the many uncertainties. Thus, a reliability assessment should be based on probabilistic methods where stochastic modeling of failures is performed.

The probabilistic models include uncertainties such as statistical uncertainty and model uncertainty. The statistical uncertainties are related to the limited number of samples for evaluation of the strength of a material and model uncertainties are related to imperfections of theoretical models compared to reality. This thesis focuses on probabilistic models and the stochastic modeling of the fatigue life of the wind turbine drivetrain using structural reliability methods allowing a rational modeling of all uncertainties.

Hence, two approaches are considered for stochastic modeling of the fatigue life. One method is based on the classical Weibull approach and the other on application of a log-normal distribution as done, e.g., for the fatigue life of welded steel details. The statistical parameters in both models are estimated and applied in reliability assessments.

Furthermore, the thesis includes a study of the effect of defects/nodules on fatigue life of cast iron samples (for two different casting methods). The cast iron samples scanned by 3D tomography equipment at the DTU Wind Energy (Risø campus), and the distribution of nodules are used to estimate the fatigue life and the most critical section of specimens. The GEV distribution is used to statistical analysis of nodules configurations. Moreover, the samples are divided in different volumes, and for each volume the distribution of nodules is evaluated in order to study the homogeneous scattering of nodules in component volume for each casting method.

DANSK RESUME

Vindenergi er en af adskillige energikilder i verdenen og er en kraftigt voksende industri i energisektoren. Som i andre industrier forsøger vindmølleproducenterne at øge pålideligheden og mindske omkostningerne. Derfor må vi udvikle vindmøller der er billigere og mere effektive end andre energikilder.

Om de er placeret offshore eller onshore udsættes vindmøller for energitilførsel fra bølger, yderst dynamiske vindbelastninger og/eller slipstrøm fra andre vindmøller. Derfor oplever de fleste komponenter i en vindmølle højt dynamiske og tidsvarierende belastninger. Disse komponenter kan fejle på grund af slid eller træthed, og dette kan føre til spontane lukningsreparationer der er meget bekostelige. Designet af mekaniske komponenter i vindmølletransmissionen med deterministiske metoder med brug af sikkerhedsfaktorer er generelt ikke i stand til at medregne de mange usikkerheder. Således skal en pålidelighedsvurdering baseres på probalistiske metoder hvor stokastisk modellering af svigt foretages.

De probalistiske modeller inkluderer usikkerheder så som statistiske usikkerheder og model usikkerhed. De statistiske usikkerheder er relaterede til det begrænsede antal af prøver til evaluering af materialets styrke, og model usikkerhederne er relaterede til mangelfuldheder i teoretiske modeller sammenlignet med virkeligheden. Denne afhandling fokuserer på probalistiske modeller og den stokastiske modellering af træthedslevetiden for vindmølletransmissionen ved brug af strukturelle pålidelighedsmetoder der tillader en rationel modellering af alle usikkerheder.

Herved betragtes to tilgange til stokastisk modellering af træthedslevetiden. En metode er baseret på den klassiske Weibull-tilgang og den anden på anvendelsen af en log-normal distribution som der f.eks. bruges for træthedslevetiden for svejsestålsdetaljer. Den statistiske parametre i begge modeller estimeres og anvendes i pålidelighedsvurderinger.

Ydermere inkluderer denne afhandling undersøgelse af effekten af mangler/noduler på træthedslevetiden af støbejernsprøver (for to forskellige støbemetoder). Støbejernsprøver scannes med 3D tomografiudstyr fra DTU Vindenergi (Risø), og distributionen af noduler bruges til at estimere træthedslevetiden og de mest kritiske sektioner af prøverne. GEV-distributionen bruges til statistisk analyse af nodulkonfigurationer. Ydermere deles prøverne i forskellige mængder og for hver mængde evalueres distributionen af noduler for at undersøge den homogene spredning af noduler i komponentmængden for hver støbemetode.

ACKNOWLEDGEMENTS

Firstly, I would like to express my sincere gratitude to my supervisor Prof. John Dalsgaard Sørenesen for his great support of my Ph.D study, for his motivation, for his supports and for all efforts on every aspects during of my 3 years of study. His guidance helped tremendously during all the time of research, presentations, writing the articles and writing of this thesis. I would also like to thanks all my helpful colleagues in our department who provide a fruitful collaborations.

My sincere thanks also goes to Søren Fæster, who provided me an opportunity to join DTU Wind Energy (Risø campus) as visiting researcher, and who gave access to the laboratory and research facilities. I really appreciate all that and my experiences during two-month stay in Risø campus were tremendously valuable for me and it was a productive collaboration. I would like to thank Asger Sturlason who provided valuable test samples and materials for the experiment and for all his supports. Without they precious support it would not be possible to conduct this research.

Last but not the least, my greatest and deep from my heart thanks goes to my strong, supportive and lovely wife Mahdieh for supporting me spiritually, and for all her patience during all these years and she have been so amazing and I definitely believe without her supports and encouragements, I would never ever finish this long and difficult journey. She left her country and family and all the beloved persons in Iran and during all this days stand side by side of me and I am really indebted to her for my success and achievement.

December 2016

Hesam Mirzaei Rafsanjani

TABLE OF CONTENTS

TABLE OF FIGURES

CHAPTER 1. INTRODUCTION

Wind energy is a rapidly growing industry in the renewable energy sector with large potential for contributing significantly to future renewable energy production (Mirzaei Rafsanjani & Sørensen, 2015a). Denmark was a pioneer in developing commercial wind power, and today Danish manufacturers produce a substantial share of the wind turbines around the world. Wind power produced the equivalent of 33% of Denmark's total electricity in 2013 and 39% in 2014 (Vittrup, 2014; Nørskov, 2015). In 2012 the Danish government adopted a plan to increase the share of electricity production from wind to 50% by 2020 and 84% in 2035 (The Guardian, 2012).

A main focus for wind turbine manufacturers and operators is how to increase the reliability of wind turbines and how to decrease their cost (Shirani & Härkegård, 2014). Hence, cheaper and more efficient wind turbine components have to be developed in order to have an optimal balance between initial costs related to the required reliability level on the one hand and the cost of operation and maintenance on the other hand (Mirzaei Rafsanjani & Sørensen, 2015a). In addition, the energy production should be high in order to minimize the Levelized Cost of Energy (LcoE). In order to perform this optimization, it is important to be able to estimate the reliability of the components (Marquez-Dominguez & Sørensen, 2012).

Depending on whether they are placed in offshore or onshore locations, wind turbines are exposed to wave excitations, highly dynamic wind loads, and the wakes from other wind turbines (Mirzaei Rafsanjani & Sørensen, 2015a); also, they are highly influenced by the control system. Therefore, drivetrain components in a wind turbine experience highly dynamic and time-varying loads (Mirzaei Rafsanjani & Sørensen, 2015a). The drivetrain is the component of the wind turbine that transforms the mechanical energy generated by the rotor into electrical energy (Oyague, 2009). There are many possible configurations for the power train depending upon the designer criteria. Four common configurations include the modular drive, the integrated drivetrain, the partially integrated drivetrain, and the direct drivetrain. There is currently no common consensus with respect to which configuration is most advantageous (Oyague, 2009).

The most common drivetrain configuration consists of the main shaft, the main bearings, the gearbox, and the generator (Hau, 2006). Modeling of the reliability of the drivetrain components is important for predicting the expected time-to-failure which is an important indicator to be used in planning of operation and maintenance (Mirzaei Rafsanjani & Sørensen, 2015a). In order to estimate the probability of failure of the drivetrain components, there should be a careful modeling of the aleatory (physical) and epistemic (model, statistical and measurement) uncertainties (Sheng & Veers, 2011; Mirzaei Rafsanjani & Sørensen, 2015a).

The drivetrain components may fail due to wear or fatigue and this can lead to unplanned shutdown repairs that are very costly (Mirzaei Rafsanjani & Sørensen, 2015b). The design of mechanical components in the wind turbine drivetrain by deterministic methods using safety factors is generally unable to account, in a rational way, for the many uncertainties (Mirzaei Rafsanjani & Sørensen, 2015a). Thus, a reliability-based assessment should be performed using probabilistic methods where stochastic modeling of failures is performed (Mirzaei Rafsanjani & Sørensen, 2015b).

The reliability of wind turbine gearboxes has been studied in a number of research projects, e.g., the Gearbox Reliability Collaboration (GRC) project at the U.S. National Renewable Energy Laboratory (NREL) (Link, et al., 2011). This includes important research areas on fault diagnosis and condition monitoring (Mirzaei Rafsanjani & Sørensen, 2015a). Studies have investigated several methods for obtaining information about the reliability, such as vibration and acoustic emissions (Soua, Lieshout, Perera, Gan, & Bridge, 2013) and local mean decomposition (Liu, Zhang, Han, & Wang, 2012).

Moreover, some studies consider the financial aspects of condition monitoring of gearboxes (Horenbeek, Ostaeyen, Duflou, & Pintelon, 2013). Further, some studies on probabilistic modeling of failures in wind turbine drivetrain components have been carried out, (Dong W. , Xing, Moan, & Gao, 2013; Shirani & Härkegård, 2011) but without a detailed stochastic modeling of the uncertainties related to the parameters in the limit state equations modeling each failure mode (Mirzaei Rafsanjani & Sørensen, 2015a).

This thesis focuses on probabilistic models and the stochastic modeling of fatigue lives in the wind turbine drivetrain using structural reliability methods (Madsen, Krenk, & Lind, 1986), allowing for a rational modeling of all uncertainties. An important aspect in modeling fatigue failure of large cast steel components is to take into account initial, random defects and scale effects (Mirzaei Rafsanjani & Sørensen, 2014). Two approaches are considered in this thesis for stochastic modeling of the fatigue life. One method is based on the classical Weibull approach and the other on the application of a log-normal distribution. The statistical parameters in both models are estimated and applied in reliability assessments.

The following section will give a short introduction into wind turbine drivetrain components.

1.1. Wind turbine drivetrain

As mentioned in the previous section, there are four common configurations of drivetrains. Currently, most operating turbines follow the modular configuration. All individual components of the drivetrain are mounted onto the bedplate, and the bedplate is designed to be torsionally stiff (Oyague, 2009). Nevertheless, there is a debate about the actual behavior of the bedplate that suggests that it is not as stiff as it should be and that its flexibilities influence not only the interaction between the

different components of the drivetrain but also its vibrational behavior (Oyague, 2009). The main components of the drivetrain are the rotor shaft or low-speed shaft, the gearbox, the brakes, and the generator.

The modular configuration allows for a non-vertical design process, which means that different suppliers can contribute to the development of the different components of the drivetrain. This inherently reduces the overall cost by creating a competitive environment among suppliers and reduces the in-house requirements of the turbine manufacturer. Figure 1-1 shows the typical configuration for a modular drivetrain (Gasch & Twele, 2011).

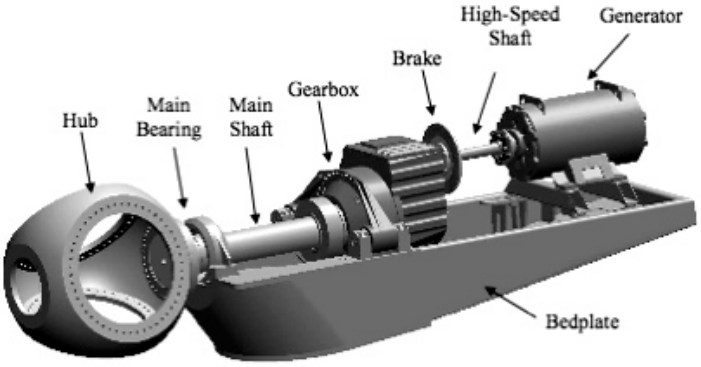

Figure 1-1 Modular drivetrain configuration (Oyague, 2009)

The low-speed shaft transmits loads from the rotor to the gearbox. Its configuration is also intended to minimize the transferred non-torsional load to the gearbox. The low-speed shaft supports the weight of the rotor and transmits all the reaction forces to the main frame through the main bearing. These reaction forces are composed of all non-torsional loads such as axial thrust from the wind as well as disturbances from turbulence caused by uneven wind distribution or wind shear.

While operating, dynamical effects such as vibration imbalances from the blades and gyroscopic loads from yaw movement also contribute to non-torsional loading. Although the low-speed shaft is a simple mechanical device it is very important, because the unintended transmission of reaction forces to the other components of the drivetrain could reduce its operating life (Manwell, McGowan, & Rogers, 2009).

The gearbox is a mechanical device capable of transferring torque loads from a primary mover to a rotary output, typically with a different relation of angular velocity and torque. In the case of wind turbines the gearbox connects the low-speed shaft and the generator; therefore, its gear ratio is generally dictated by the requirement of the generator and the angular velocity of the rotor.

In the case of electrical power production with an asynchronous generator, the output of the gearbox (which is connected to the generator) usually operates in the

ranges from 50Hz to 60 Hz or 1,500 rpm to 1,800 rpm. This depends on the frequency of the grid to which the generator is connected and on the number of poles of the generator (Manwell, McGowan, & Rogers, 2009).

Brakes are mechanical devices designed to slow or stop a machine (Saleh, El-Betar, & El-Assal, 2014). Brakes are also intended to prevent a device from moving after it has been stopped. In wind turbines there are typically two distinctive brake classifications: aerodynamic brakes and mechanical brakes (Saleh, El-Betar, & El-Assal, 2014).

Generators are devices that transform mechanical energy into electrical energy. The electrical power is produced by passing a conductor through a uniform magnetic field at a right angle to the lines of electric flux. The voltage generated is a function of the velocity, the conductor length, and the magnetic flux density. The magnetic field used by the generators is obtained by the use of electromagnets or permanent magnets (Gasch & Twele, 2011).

The induction generator is the most common generator used in the wind industry. This is largely because it has a simple configuration and a low price. Its main disadvantage is that it does not use permanent magnets, thus it has to be connected to the grid to be capable of producing power (Ackermann, 2012).

1.2. Defects in cast iron components

Cast iron is an iron-carbon cast alloy with other elements that is made by remelting iron and other additions (Radzikowska, 2004). For differentiation of steel and cast steel, cast iron is defined as a cast alloy with a minimum 2.03% carbon content (Radzikowska, 2004). In general the types of cast iron are as follows:

- Gray cast iron: it is characterized by its graphitic microstructure, which causes fractures of the material to have a grey appearance. Gray cast iron has less tensile strength and shock resistance than steel, but its compressive strength is comparable to low- and medium-carbon steel (Singh & Agarwal, 2011).
- White cast iron: In these cast irons, carbon is present in the form of iron carbide (Fe_3C) that is hard and brittle. The presence of iron carbide increases hardness and makes it difficult to machine. Consequently these cast irons are abrasion resistant (Berns & Thesen, 2008).
- Malleable iron: It starts as a white iron casting that is then heat-treated at about 900 ºC. It is tougher than gray cast iron and can be twisted or bent without fracture (Singh & Agarwal, 2011).
- Spheroidal or nodular graphite cast iron: In these cast irons, graphite is present in the form of spheres or nodules. They have high tensile strength and good elongation properties. In this thesis, the material that is used for fatigue tests is EN-GJS-400-18 which is nodular cast iron.

Further, Table 1-1 lists the range of compositions for the cast irons listed above (Radzikowska, 2004).

Ductile cast iron that is considered in this thesis has much more impact and fatigue resistance due to its nodular graphite (Shirani & Härkegård, 2014). The common specification of this group of materials is the shape (morphology) of the graphite that has the form of nodules rather than flakes (as in gray iron) (Shirani & Härkegård, 2014).

Table 1-1 Range of chemical compositions for typical nonalloyed and low-alloyed cast irons (Radzikowska, 2004)

Type of iron	Composition, %				
	C	Si	Mn	P	S
Gray	2.5 – 4.0	1.0 – 3.0	0.2 – 1.0	0.002 – 1.0	0.02 – 0.025
White	1.8 – 3.6	0.5 – 1.9	0.25 – 0.8	0.06 – 0.2	0.06 – 0.2
Malleable	2.2 – 2.9	0.9 – 1.9	0.15 – 1.2	0.02 – 0.2	0.02 – 0.2
Ductile (Nodular)	3.0 – 4.0	1.8 – 2.8	0.1 – 1.0	0.01 – 0.1	0.01 – 0.03

In cast iron components of wind turbine, metallurgical defects such as vermicular, spiky, coral, exploded, and chunky graphite (Shirani & Härkegård, 2014) are not acceptable on the component surface, and major defects should be removed from the surface and, if not possible, the component is mostly rejected. Common defects may be divided into two basic categories (Ecob, 2005):

- Those related to nodule shape and size, such as compacted graphite structures, exploded and chunky graphite, graphite floatation, spiky graphite and nodules alignment (Shirani & Härkegård, 2014).
- Those related to inclusions/abnormalities, such as flake graphite, slag inclusions, carbides, gas pores and shrinkage cavities (Shirani & Härkegård, 2014).

The following will briefly explain these defects.

1.2.1. Compacted graphite

Figure 1-2 shows a good example of compacted graphite in the structure (Ecob, 2005). There are several causes of this; the most common being that the nodularisation process has partly failed (Shirani & Härkegård, 2014).

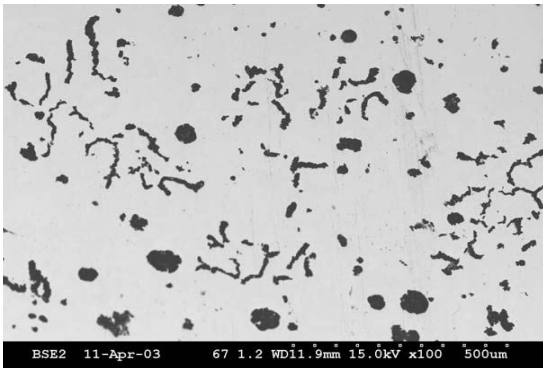

Figure 1-2 Compacted graphite (Shirani & Härkegård, 2014)

1.2.2. Exploded graphite

Figure 1-3 shows exploded graphite within the structure (Ecob, 2005). Exploded graphite looks exactly as the name might suggest that the graphite has been blown apart. Exploded graphite is normally found in thicker section castings with slow cooling rates or at very high carbon equivalent levels (Shirani & Härkegård, 2014).

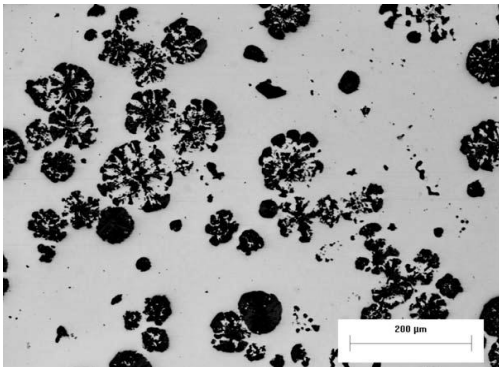

Figure 1-3 Exploded graphite (Shirani & Härkegård, 2014)

1.2.3. Chunky graphite

Figure 1-4 shows an example of chunky graphite (shown with arrows). This defect occurs in the thermal centers of heavy section castings – those with sections greater than 50 mm (Shirani & Härkegård, 2014). The location of chunky graphite normally, but not exclusively, indicates the location of the thermal center of a casting (Källboma, Hambergb, Wessénc, & Björkegrena, 2005). Low-carbon equivalent and the use of chills prevent chunky graphite formation. The result of this graphite shape is that the mechanical properties, such as ultimate tensile strength, in these defective areas are dramatically reduced (Shirani & Härkegård, 2014). The presence of chunky graphite decreases the mechanical strength, that is, the ultimate

tensile strength and especially the elongation to fracture are severely lowered (Källboma, Hambergb, Wessénc, & Björkegrena, 2005).

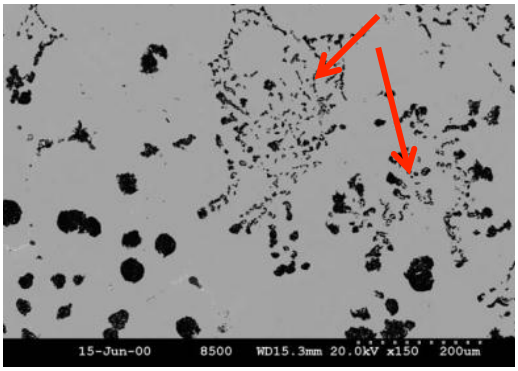

Figure 1-4 Chunky graphite (Shirani & Härkegård, 2014)

1.2.4. Graphite nodule floatation

Flotation is normally revealed by the presence of dark patches on the top surface (Shirani & Härkegård, 2014). When large, low density graphite nodules are formed during the solidification of thick sections or otherwise slow cooling castings, graphite nodule flotation is formed (Shirani & Härkegård, 2014). Slower solidification rate in heavy section castings is typically responsible for this defect. The nodules, being of a lower density than the matrix, tend to float towards the surface of the casting and thus can have a negative effect on the mechanical properties (and surface finish) in that region (Ecob, 2005). Figure 1-5 shows an example of graphite floatation (Ecob, 2005). In critical areas, it can have a devastation effect on fatigue properties, which are extremely important for wind turbine castings (Shirani & Härkegård, 2014).

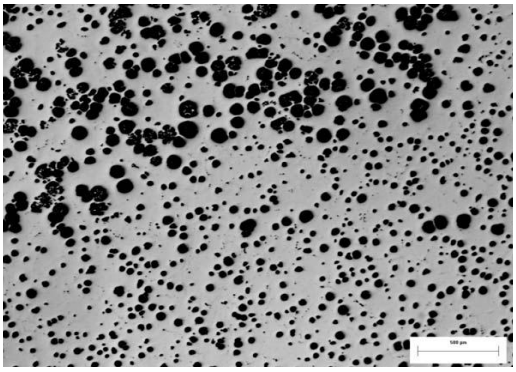

Figure 1-5 Graphite floatation (Shirani & Härkegård, 2014)

1.2.5. Spiky graphite

The effect of spiky graphite is a dramatic reduction in the mechanical properties of the iron; the spikes provide points of weakness in the structure (Shirani & Härkegård, 2014). Figure 1-6 shows a typical example of spiky graphite (Ecob, 2005).

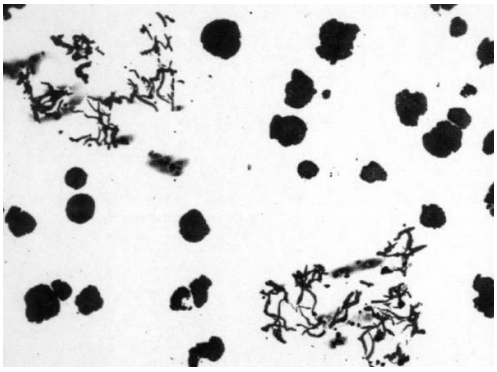

Figure 1-6 Spiky graphite (Ecob, 2005)

1.2.6. Nodule alignment

Figure 1-7 shows a classic case of nodule alignment. Whilst not normally a serious problem, this can have detrimental effects on such properties as tensile strength or impact resistance (Ecob, 2005). The normal causes are low carbon equivalent where not enough graphite is precipitated during the cooling, under inoculation or too high a pouring temperature (Ecob, 2005).

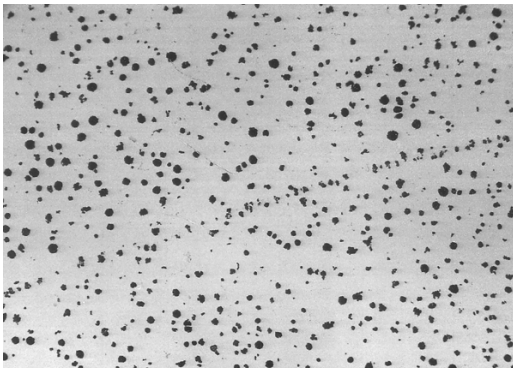

Figure 1-7 Nodule alignment (Ecob, 2005)

1.2.7. Flake graphite

Flake graphite is normally seen on the component surface (Shirani & Härkegård, 2014). However, it usually forms part of the machining allowance and can be

ignored (Shirani & Härkegård, 2014). This is mainly caused by a buildup of sulphur in the sand, which reacts with the magnesium in the iron to form magnesium sulphide and effectively denodularises the iron (Ecob, 2005). Figure 1-8 shows flake graphite on the surface of the casting due to high sulphur content in the moulding sand (Ecob, 2005).

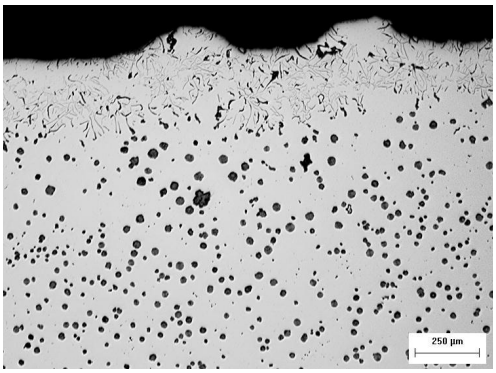

Figure 1-8 Flake alignment (Shirani & Härkegård, 2014)

1.2.8. Carbides

Ductile cast iron is particularly prone to the formation of primary carbides during solidification (Ecob, 2005). In the production of ductile iron, it must be remembered that magnesium is one of the most powerful carbide promoters (Shirani & Härkegård, 2014). Coupled with this, the violence of the magnesium reaction during the nodularisation process tends to destroy nuclei (Ecob, 2005). Another factor is that the S content in ductile iron is purposely lowered to less than 0.02%, to facilitate the formation of spherical graphite nodules (Shirani & Härkegård, 2014). Figure 1-9 shows the existence of carbides.

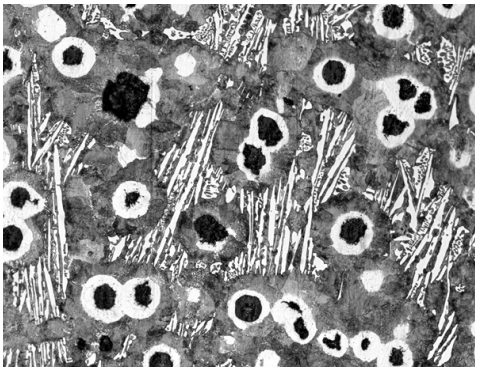

Figure 1-9 Sample with carbide present (Ecob, 2005)

1.2.9. Shrinkage cavities

Many different causes can lead to shrinkage formation in ductile iron (Shirani & Härkegård, 2014). Global experience shows that about 50% of shrinkage defects are related to sand systems, feeding, and gating (Ecob, 2005). The other 50% may be attributed to metallurgical factors such as carbon equivalent, temperature, inoculation or high magnesium residuals (Ecob, 2005). Casting section size can influence both the volume fraction and size of graphite nodules (Shirani & Härkegård, 2014). Increased section size reduces the cooling rate of the casting. The lower cooling rates of the larger diameter bars also affect graphite nucleating conditions, resulting in reduced nodule count but increased nodule size (Shirani & Härkegård, 2014).

1.2.10. The considered defects in thesis

In summary of section 1.2, the nodules of cast iron component are considered for study. On the other hand, the defects related to nodule shape and size such as “nodule alignment”, “chunky”, “spiky” and “graphite nodule floatation” have been considered. In Chapter 4, the test specimens for two different casting methods (Sand casting and chill casting) had been scanned to visualize the 3D distribution of defects. By visual inspection of scans, it was concluded that the defects such as “chunky graphite” and “ spiky graphite” do not exist in chill casting samples and the nodule count in chill casting samples is higher than in sand casting samples. On the other hand, the nodule size of sand casting samples is bigger than chill casting samples and the defects such as “chunky graphite” and “ spiky graphite” exist in sand casting samples. Chapter 4 and Chapter 5 studied the configuration of nodules in each casting process.

1.3. Reliability and probabilistic modeling

Reliability of wind turbine drivetrain components is very important for wind turbine manufacturers and owners (Mirzaei Rafsanjani & Sørensen, 2015a). These components may fail due to overload or extreme loads (e.g. Design load cases 1.1 , 1.3 or 6.1 based on IEC 61400), wear or fatigue loads (i.g. Design load case 1.2 based on IEC 61400) and this can lead to unplanned shut down repairs (IEC 61400, 2015). The failure of each component of the drivetrain will lead to economic losses such as the cost of lost energy, the cost of repair, the cost of crew, and the cost of transportation (Mirzaei Rafsanjani & Sørensen, 2015a). The environmental exposure affects the repair & maintenance of offshore wind turbine. Sometimes for offshore wind turbines, because of the harsh environment, the maintenance team cannot operate properly and, therefore, the wind turbine cannot be accessed for several days. Consequently, the cost of lost energy increases drastically.

Hence, modeling the reliability of drivetrain component failures will help in predicting the expected time-to-failure and in planning operation and maintenance in order to avoid unexpected failures (Mirzaei Rafsanjani & Sørensen, 2015a). Stochastic modeling of uncertain parameters related to failure of components will be

important in order to estimate the reliability of the drivetrain (Mirzaei Rafsanjani & Sørensen, 2015a).

This thesis focuses on fatigue failure initiated by defects related to nodules in the cast components. In order to estimate the probability of failure of the drivetrain components, it is important to carefully model physical and epistemic uncertainties (model, statistical, and measurement uncertainties). These uncertainties are to be used in the limit state equations for each of the considered failure modes. Finally, the limit state equations are used for estimating the probability of failure.

1.4. Objective of thesis

The primary objective of this work has been to develop, implement, and verify probabilistic models for fatigue failure of wind turbine drivetrain cast components and study to effects of defects by casting process. This is achieved by:

- Development of a probabilistic damage accumulation model for possible defects in wind turbine drivetrain, especially in cast metallic components.
- Development of probabilistic models for associated loads and load effects.
- Stochastic modeling for initial damage/defect sizes and distribution in time and space for selected, critical components in the nacelle.
- Modeling the effects of defects, estimating the resulting probability of failure and discussing the reliability requirements (related to consequence of failure).

Due to available test samples from industrial partners, the thesis focuses on the main shaft component. Therefore, the transfer of the results to other working components could be considered with some changes and the presented methodologies are considered relevant also for other wind turbine drivetrain components.

1.5. Thesis outline

The thesis is organized as a collection of papers, which are presented in the appendices. Chapter 1 gives the introduction of the thesis. Chpater 2 describes the main aspects needed for reliability assessment and probabilistic modeling. This includes discussion of the target reliability level to be used for fatigue damage assessment of wind turbine components where different failure modes are considered taking into account various uncertainties. Reliability methods for estimation of the probability of failure are also described including the FORM method.

The first step of thesis is stochastic modeling of initial damage/defects sizes and distribution in time and space for selected cast iron components. The main subject is modeling the defects/nodules. Further, the defects affect the fatigue life of component, and the relationship between existance of defect and fatigue life is considered in the thesis. The fatigue life is considered by safe life design method, and the *SN* curve is extracted from test samples and also the uncertainties considered

for modeling the strength distribution of components. In addition, based on *SN* curve and stochastic models of defects, the probabilistic damage accumulation models have been formulated. Finally, the reliability assessment and sensitivity analysis based on the stochastic models and probabilistic models are carried out. Chapter 1 explains the various types of defects in cast iron components. Moreover, stochastic models for initial damage/defect sizes and distribution are explained Chapter 4.

Furthermore, Chapter 3 considers fatigue modeling by *SN* curve. The basic fatigue failure model is developed based on the *SN* curve and the Miner's rule. This chapter explains the *SN* curve, Miner's rule, and the related uncertainties for strength distribution. Moreover, the chapter explains the probabilistic damage accumulation model for fatigue failure and presents reliability assessment based on strength distributions, load distributions, and related uncertainties. Furthermore, the chapter describes the statistical technique "Analysis of Covariance" and its application to establish *SN* curves. By using "Analysis of Covariance", it is possible to study the effect of different manufacturing factors such as suppliers' production process.

In addition, the effect of defects and probabilistic model of fatigue failure (based on existence of defects) are also considered in Chapter 5. This chapter presents a study of the effect of nodules in cast iron on the fatigue life of the components. Chapter 6 presents reliability assessments of cast component. Finally, Chapter 7 establish conclusions and future work.

CHAPTER 2. RELIABILITY ASSESSMENT

A wind turbine should be designed, dimensioned, and manufactured in such a way that, if correctly used and maintained over its anticipated service life, it can withstand the assumed loads within the prescribed level of safety and possess a sufficient degree of durability and robustness. Calculation, or a combination of calculation and testing, can be used to demonstrate that the structural elements of a wind turbine meet the prescribed level of safety.

A number of definitions of the term "reliability" are used in the literature and in national and international documents. (ISO 2394, 2015) provides a definition of reliability as "the ability of a structure or structural member to fulfil the requirement, during the working life, for which it was designed" (ISO 2394, 2015). In a quantitative sense, reliability may be defined as the complement of the probability of failure. Whether or not a certain probability of failure resulting from a probabilistic reliability assessment of a structural detail or system can be accepted may be based on a risk-based design approach. The risk-based design considers the consequences in case of failure and is used to define target reliability levels.

The probabilistic reliability assessment can be done by the following steps (Madsen, Krenk, & Lind, 1986):

1. Identification of failure modes and modeling of corresponding limit state equation $g(\boldsymbol{X})$.
2. Quantification of uncertainties and modeling by stochastic variables $\boldsymbol{X}$.
3. Applying reliability methods to estimate the probability of failure.

2.1. Failure modes

Structural reliability from an engineering point of view can be understood as the ability of a structure to fulfill the structural design request for a defined period (ISO 2394, 2015). Design requests can be fixed to specific design limits that are often denoted limit state conditions or failure modes. The failure modes (limit states) are generally divided in (Sørensen J. D., 2011; ISO 2394, 2015):

- **Ultimate limit states (ULS):** Ultimate limit states which can be defined by limit state connected to the maximum load carrying capacity or maximum material strength capacity (Sørensen J. D., 2011). ULS conditions are related to the structural collapse of one structural component or the whole structure caused by rupture due to extreme loads, fatigue of the material, corrosion, fracture, buckling, and large deformations.

- **Conditional limit states (CLS):** Conditional limit states correspond to the load-carrying capacity if a local part of the structure has failed (Sørensen J. D., 2011). A local failure can be caused by e.g. an accidental action. The conditional loads are generally caused by instantaneous actions that can exceed the material strength or can even cause the instability of the structure.
- **Serviceability limit states (SLS):** Serviceability limit states are related to normal use of the structure, e.g. excessive deflections, local damage, and excessive vibrations (Sørensen J. D., 2011).

In a deterministic structural design, the design limits are formulated in design equations. A deterministic design can be improved by a probabilistic design which takes into account the uncertainties related to environmental loads and material strength. The probabilistic design can be performed by limit state equations.

Reliability of wind turbine drivetrain components is very important for wind turbine manufacturers and owners (Mirzaei Rafsanjani & Sørensen, 2014). Offshore wind turbines are large structures exposed to wave excitations, highly dynamic wind loads influenced by the wind turbine control system and wakes from other wind turbines (Mirzaei Rafsanjani & Sørensen, 2014). Therefore, most components in a wind turbine experience highly dynamic and time-varying loads. These components may fail due to extreme loads, wear or fatigue, and this can lead to unplanned shutdown and repairs (Mirzaei Rafsanjani & Sørensen, 2014). Due to fluctuating loads, fatigue is one of the main failure modes in wind turbine components (Mirzaei Rafsanjani & Sørensen, 2015a). The current design of large wind turbines against fatigue is usually based on the life design approach (Campbell, 2008). In the safe life design, fatigue testing is carried out on baseline materials to produce S-N curves (Shirani & Härkegård, 2012). For many years it has been assumed in designs that all loads and strengths are deterministic (Mirzaei Rafsanjani & Sørensen, 2014). The strength of an element was determined in such a way that it exceeded the load with a certain margin and is accounted for by a (partial) safety factor defined as the ratio between the strength and the load (Dong W. , Xing, Moan, & Gao, 2013). Characteristic values of the uncertain loads and resistances are specified and partial safety factors are applied to the loads and strengths in order to ensure that the structure is safe enough (Sørensen J. D., 2011). Hence, the uncertainties in the loads, strengths and the modeling can be accounted partially for in such a semi-probabilistic safety format (Mirzaei Rafsanjani & Sørensen, 2014). The following subsection presents a brief review of uncertainties and the reliability assessment used in this thesis.

2.2. Uncertainties

The considered uncertainties can be classified as epistemic or aleatory uncertainties (Sørensen J. D., 2011). Epistemic uncertainties should be accounted for in a

probabilistic design. The epistemic uncertainties can be divided in the following groups (Sørensen J. D., 2011):

- **Measurement Uncertainty:** caused by imperfect measurements of, for example, a geometrical quantity (Sørensen J. D., 2011).
- **Statistical Uncertainty:** caused by limited sample sizes of observed quantities (Sørensen J. D., 2011).
- **Model Uncertainty:** related to imperfect knowledge or idealization of the mathematical models used or uncertainty related to the choice of probability distribution types for the stochastic variables (Sørensen J. D., 2011).

The aleatory uncertainty is represented by the physical uncertainty related to the natural randomness of a quantity (Sørensen J. D., 2011). Other references, e.g. (Melchers, 1999) and (Moan, 2008), mention a detailed classification about uncertainties in reliability assessment. The above types of uncertainty are usually treated by the reliability methods (Sørensen J. D., 2011) which will be described in the following subsections.

2.3. Probability of failure

In order to estimate the probability of failure P_f, it is assumed that the uncertain parameters related to the structural behavior may be described by a set of basic stochastic variables $\boldsymbol{X} = [X_1, X_2, \ldots, X_n]$ characterizing actions, mechanical properties, geometrical data, and model uncertainties. Furthermore, it is assumed that the limit state (ultimate, serviceability, conditional or fatigue) of a structure can be modelled by a limit state equation defined by equation (2-1) (Sørensen J. D., 2011):

$$g(\boldsymbol{X}) = R(\boldsymbol{X}) - S(\boldsymbol{X}) \tag{2-1}$$

where $R(\boldsymbol{X})$ indicates the resistance and $S(\boldsymbol{X})$ the load effects. Failure occurs if the limit state equation is smaller than or equal to zero (Ambühl, Kramer, & Sørensen, 2016). Further, the probability of failure is defined as

$$P_f = \mathrm{P}\left\{g\left(\boldsymbol{X}\right) < 0\right\} \tag{2-2}$$

The failure probability P_f can be assessed if basic variables $\boldsymbol{X} = [X_1, X_2, \ldots, X_n]$ are described by appropriate probabilistic models (EN 1990, 2002). In equation (2-2), the failure state of the structure is defined by $g(\boldsymbol{X}) < 0$, and $g(\boldsymbol{X}) = 0$, $g(\boldsymbol{X}) > 0$ define the failure surface and the safe states, respectively.

In structural reliability, the safety margin typically results from a mechanical analysis of the structure. This safety margin can be established by linear or non-linear functions with correlated or independent stochastic variables which can be Normal or Non-normal distributed. In order to estimate the reliability of the

structures, FORM[1]/SORM[2] and simulations techniques can be applied (Sørensen J. D., 2011).

2.4. Reliability index

An equivalent term to the failure probability is the reliability index β, formally defined as a negative value of a standardized normal variable corresponding to the probability of failure P_f (EN 1990, 2002). Thus, the following relationship may be considered as a definition (Sørensen J. D., 2011)

$$\beta = -\Phi^{-1}\left(P_f\right) \tag{2-3}$$

where $\Phi()$ is the standardized normal distribution function (EN 1990, 2002). The reliability index is commonly used as a measure of the structural reliability (Sørensen J. D., 2011). It should be emphasized that the failure probability P_f and the reliability index β represent fully equivalent reliability measures with one to one mutual correspondence given by equation (2-3) and numerically illustrated in Table 2-1 (EN 1990, 2002).

Table 2-1 Relationship between the failure probability P_f and the reliability index β (EN 1990, 2002)

P_f	10^{-1}	10^{-2}	10^{-3}	10^{-4}	10^{-5}	10^{-6}	10^{-7}
β	1.3	2.3	3.1	3.7	4.2	4.7	5.2

In (EN 1990, 2002) and (ISO 2394, 2015), the basic recommendation concerning a required reliability level is often formulated in terms of the reliability index β related to a certain reference time.

In First Order Reliability Methods (FORM) as well as in Second Order Reliability Methods (SORM), the stochastic variables, '$\boldsymbol{X}$', are transformed into a standardized, independent normal distributed space called 'u-space' (Figure 2-1). The failure surface (limit state equation) is approximated by a tangent plane in the design point (u^*) which is the point with the largest likelihood of failure. The reliability index β is equal to the distance between the origin and the most probable failure point u^* in the standardized normal space. The direction unit vector α at u^* indicates the importance of the different stochastic variables (Sørensen J. D., 2011).

[1] First Order Reliability Method
[2] Second Order Reliability Method

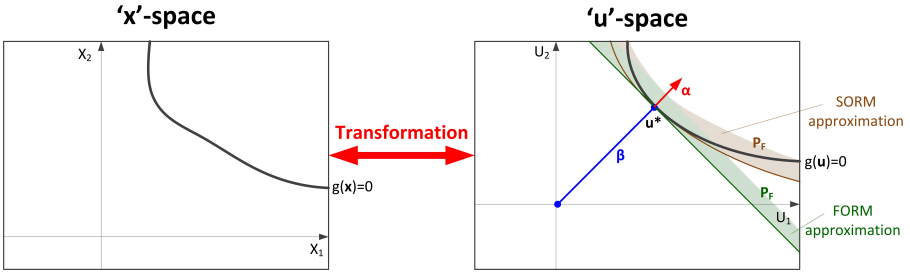

Figure 2-1 FORM/SORM techniques, graphic representation (Ambuhl, 2015)

2.5. Target reliability level

In terms of application of a reliability-based approach it is important to define a structural risk acceptance criterion related to a required minimum reliability index herein defined as *target reliability*. The requirements to the safety of the structure are consequently expressed in terms of *the accepted minimum reliability index* or *the accepted maximum failure probability* (Ambuhl, 2015).

Before performing probabilistic designs, a certain target reliability level should be defined in order to verify whether the chosen design is optimal for a certain application. Target reliability levels are often defined based on socio-economic considerations where the financial and social consequences are judged (Ambuhl, 2015). Table 2-2 shows the resulting target reliability level indices for ultimate limit state dependent on the consequences and the costs of safety measures.

Table 2-2 Target annual reliability index, Δβ, and the corresponding annual probability of failure ΔP_f (JCSS, 2001; Ambuhl, 2015)

Relative cost of safety measure	Consequences of failure		
	Minor	Moderate	Large
Large	$\Delta\beta$=3.1 ($P_f \approx 10^{-3}$)	$\Delta\beta$=3.3 ($P_f \approx 5*10^{-3}$)	$\Delta\beta$=3.7 ($P_f \approx 10^{-4}$)
Normal	$\Delta\beta$=3.7 ($P_f \approx 10^{-4}$)	$\Delta\beta$=4.2 ($P_f \approx 10^{-5}$)	$\Delta\beta$=4.4 ($P_f \approx 5*10^{-5}$)
Small	$\Delta\beta$=4.2 ($P_f \approx 10^{-5}$)	$\Delta\beta$=4.4 ($P_f \approx 5*10^{-5}$)	$\Delta\beta$=4.7 ($P_f \approx 10^{-6}$)

For wind turbines the risk of loss of human lives in case of failure of a structural element is generally very small. Further, it can be assumed that wind turbines are systematically reconstructed in case of collapse or end of lifetime (Sørensen J. , 2015). The optimal reliability level can be found by considering representative cost-benefit based optimization problems where the life-cycle expected cost of energy is minimized (Sørensen & Toft, 2014).

It is assumed that for wind turbines:

- A systematic reconstruction policy is used (a new wind turbine is erected in case of failure or expiry of lifetime) (Sørensen J. , 2015).
- Consequences of a failure are only economic (no fatalities and no pollution) (Sørensen J. , 2015).
- Cost of energy is important which implies that the relative cost of safety measures can be considered large (material cost savings are important) (Sørensen J. , 2015).
- Wind turbines are designed to a certain wind turbine class, i.e. not all wind turbines are 'designed to the limit' (Sørensen J. , 2015).

Based on (IEC 61400, 2015; ISO 19902, 2007), a target value for the nominal failure probability for structural design for extreme and fatigue failure modes for a reference period of 1 year is

$$P_f^t = 5 \cdot 10^{-4} \tag{2-4}$$

The corresponding target value for the reliability index is β^t = 3,3. Application of this target value assumes that the risk of human lives is negligible in case of failure of a structural element (Sørensen & Toft, 2014). Further it is noted that this reliability level corresponds to the reliability level for offshore structures that are unmanned or evacuated in severe storms and where other consequences of failure are not very significant.

CHAPTER 3. FATIGUE MODELING BY THE *SN* APPROACH

This section describes theoretical background on modeling fatigue of cast components by the *SN* approach. The drivetrain components of wind turbines are exposed to highly dynamic and time-varying loads. Hence, these components may fail due to fatigue. Fatigue failures occur due to the application of fluctuating stresses that are lower than the extreme stress required to cause failure during a single application of stress (Campbell, 2008). This thesis uses the *SN* curve model and the Palmgren-Miner rule to model the fatigue failure. The fatigue life of a component is assumed to be modelled as the sum of the crack initiation time and crack propagation time. In the *SN* curve model, no distinction is made between initiation and propagation (Nielsen, 2013).

3.1. *SN* curves

Fatigue failures typically occur due to the application of fluctuating stresses much lower than the stress required for causing failure during a single application of an extreme load (Mirzaei Rafsanjani & Sørensen, 2014). The fatigue life is the number of cycles to failure at a specified stress level, while the fatigue strength is the stress level below which failure does not occur for the given number of cycles with constant amplitude (Sørensen J. , 2015). When the applied stress level decreases, the number of cycles to failure increases.

SN curve baseline data is generated by imposing fully reversed fluctuating stresses in a standard specimen (Rothbart & Brown, 2006). Fully reversed loading refers to the fact that $\sigma_{max} = -\sigma_{min}$ (or, the alternating stress amplitude, $\sigma_a = \sigma_{max}$). *SN* curves are usually presented as a plot of stress range, *S*, versus the number of cycles to failure, *N*. Based on the *SN* curve, the fatigue strength of metals is often assumed to follow the Basquin equation (Campbell, 2008) and (Mirzaei Rafsanjani & Sørensen, 2015a):

$$\sigma_a = \sigma_f \left(2N\right)^{-\frac{1}{m}} \tag{3-1}$$

where σ_a is the alternating stress amplitude, σ_f is the fatigue strength, *N* is the number of load cycles to failure, and *m* is the fatigue strength exponent. σ_f and *m* can be determined empirically using tests (Mirzaei Rafsanjani & Sørensen, 2014). Hence, these values are associated with statistical uncertainties and by increasing the number of tests, the effect of the statistical uncertainties can be reduced.

Furthermore, when a component is considerably larger than the specimen used for generating the baseline fatigue data, a greater volume of material is subjected to the particular stress amplitude. This increases the statistical probability that a

microscopic flaw, defect, or slip system will exist that is susceptible to fatigue-crack development (Rothbart & Brown, 2006) and thereby reduce the fatigue life – due to this so-called size effect. Thus, the geometrical size effect affects the resistance of materials against fatigue failure (Shirani & Härkegård, 2011). Hence, σ_a is affected by geometrical size effects (Mirzaei Rafsanjani & Sørensen, 2015a). According to this, equation (3-1) can be written as (Mirzaei Rafsanjani & Sørensen, 2014):

$$N = \frac{1}{2}\left(\frac{\sigma_{a0}}{\sigma_f}\right)^{-m}\left(\frac{V}{V_0}\right)^{1/b_n} = \frac{1}{2}\left(\frac{\sigma_{a0}}{\sigma_f}\right)^{-m}\left(s_V\right)^{1/b_n} \tag{3-2}$$

where V_0 is the reference volume and σ_{a0} is the reference fatigue strength amplitude corresponding to reference volume of V_0. The exponent b_n determines the effect of the specimen size on the fatigue life and V is the volume of the component (Mirzaei Rafsanjani & Sørensen, 2014).

3.2. Palmgren-Miner rule

Engineering components are seldom subjected to constant-amplitude loading for their entire life. More often, load fluctuations occur with means and amplitudes that vary. Besides, *SN* curves specify the number of cycles to failure at different constant stress ranges (Sørensen & Toft, 2010). Thus, it is important to be able to predict the life of a component subjected to variable amplitude loading by using data generated in constant amplitude laboratory tests (Mirzaei Rafsanjani & Sørensen, 2015a).

According to this, cumulative damage theories consider the fatigue process to be one of damage accumulation until the life of the component is exhausted (Mirzaei Rafsanjani & Sørensen, 2015a). The most widely utilized damage concept is that of linear damage (also called Miner's rule or the Palmgren-Miner rule) (Rothbart & Brown, 2006). With the Palmgren-Miner rule, it is assumed that the total life can be estimated by adding up the percentage of life consumed at each stress level (Marquez-Dominguez & Sørensen, 2012):

$$D = \frac{n_1}{N_1} + \frac{n_2}{N_2} + ... + \frac{n_k}{N_k} = \sum_{j=1}^{k}\frac{n_j}{N_j} = 1 \tag{3-3}$$

where n_1, n_2, ..., n_k represent the number of cycles at a specific stress level (Mirzaei Rafsanjani & Sørensen, 2014), and N_1, N_2, ..., N_k represent the fatigue life in cycles at the same stress level and they are determined by the *SN* curve. A limit state equation for fatigue failure can thus be specified as:

$$g = \Delta - D \tag{3-4}$$

where Δ models model the uncertainty related to Miner's rule for linear damage accumulation (Marquez-Dominguez & Sørensen, 2012).

3.3. Fatigue strength modeled by a Log-Normal distribution

Fatigue strength can be modeled using the Basquin equation. This model is subject to uncertainties which must be considered in a reliability assessment. For instance, a log-normal distribution could be used for modeling the uncertainty related to the fatigue strength (Mirzaei Rafsanjani & Sørensen, 2015a). In a log-log format, equation (3-2) is linear and can be rewritten introducing an uncertainty term ε, see (Mirzaei Rafsanjani & Sørensen, 2015a):

$$\log N = m\log\sigma_f - m\log\sigma_{a0} + \frac{1}{b_n}\log s_V - \log\left(2\right) + \varepsilon \tag{3-5}$$

where ε is assumed to be normal distributed with mean value = 0 and standard deviation = σ_ε (Sørensen & Toft, 2010). ε models the scatter in fatigue life and can be considered here to cover both physical and model uncertainties related to imperfect knowledge or idealizations of the mathematical models used or uncertainty related to the choice of probability distribution types for the stochastic variables (Mirzaei Rafsanjani & Sørensen, 2015a; Sørensen & Toft, 2010). It is noted that the test data applied in this thesis does not allow a bilinear *SN* curve to be fitted. However, the above model can easily be extended to model a bi-linear *SN* curve and also a lower threshold (Mirzaei Rafsanjani H. , et al., 2014).

The parameters in (3-5) can be estimated using available test data (Mirzaei Rafsanjani & Sørensen, 2015a). In this thesis, test data extracted from industrial partners of project is used to exemplify the procedure for the stochastic modeling (Mirzaei Rafsanjani H. , et al., 2014). The Maximum Likelihood Method is used for the statistical analysis. The log-likelihood function as a function of the statistical parameters σ_f, m and σ_ε to be estimated is written as follows accounting both for test results where failure occurs and test results where failure does not occur (run-outs) (note, the uncertainty related to σ_f and m model statistical uncertainties and ε models model uncertainty) (Mirzaei Rafsanjani & Sørensen, 2015a):

$$\begin{aligned} L\left(\sigma_f, m, \sigma_\varepsilon\right) = &\prod_{i=1}^{n_F} P\left[\log n_i = m\log\sigma_f - m\log\sigma_{a0,i} + \frac{1}{b_n}\log s_V - \log\left(2\right) + \varepsilon\right] \\ \times &\prod_{i=1}^{n_R} P\left[\log n_i > m\log\sigma_f - m\log\sigma_{a0,i} + \frac{1}{b_n}\log s_V - \log\left(2\right) + \varepsilon\right] \end{aligned} \tag{3-6}$$

where n_i is the number of stress cycles to failure or run-out (no failure) with stress range equal to test number i. n_F is the number of tests where failure occurs, and n_R is the number of tests where failure does not occur after n_i stress cycles (run-outs) (Mirzaei Rafsanjani H. , et al., 2014).

$n = n_F + n_R$ is the total number of tests. σ_f, m and σ_ε are estimated solving the optimization problem: max $L(\sigma_f, m, \sigma_\varepsilon)$ (Mirzaei Rafsanjani H. , et al., 2014). This can be done using a standard nonlinear optimizer, e.g., the NLPQL algorithm (Schittkowski, 1986). Since the parameters σ_f, m and σ_ε are estimated by the

Maximum-Likelihood technique, they become asymptotically (number of data should be larger than 25-30) normally distributed stochastic variables with expected values equal to Maximum-Likelihood estimate and covariance matrix equal to (Lindley, 1976; Mirzaei Rafsanjani & Sørensen, 2015a):

$$C_{\sigma_f,m,\sigma_\varepsilon} = \left[-H_{\sigma_f,m,\sigma_\varepsilon}\right]^{-1} = \begin{bmatrix} \sigma_{\sigma_f}^2 & \rho_{\sigma_f,m}\sigma_{\sigma_f}\sigma_m & \rho_{\sigma_f,\sigma_\varepsilon}\sigma_{\sigma_f}\sigma_{\sigma_\varepsilon} \\ \rho_{\sigma_f,m}\sigma_{\sigma_f}\sigma_m & \sigma_m^2 & \rho_{m,\sigma_\varepsilon}\sigma_m\sigma_{\sigma_\varepsilon} \\ \rho_{\sigma_f,\sigma_\varepsilon}\sigma_{\sigma_f}\sigma_{\sigma_\varepsilon} & \rho_{m,\sigma_\varepsilon}\sigma_m\sigma_{\sigma_\varepsilon} & \sigma_{\sigma_\varepsilon}^2 \end{bmatrix} \tag{3-7}$$

where $H_{\sigma_f,m,\sigma_\varepsilon}$ is the Hessian matrix with second-order derivatives of the log-likelihood function. σ denotes the standard deviation, and ρ indicates correlation coefficients (Sørensen & Toft, 2010; Marquez-Dominguez & Sørensen, 2012).

Moreover, in deterministic approaches, code-based design safety is introduced though application of deterministic values in terms of characteristic values and safety factors to obtain design values of both loads and strengths (Mirzaei Rafsanjani & Sørensen, 2015a). If uncertainty is not taken into account then corresponding to a stress range, $\sigma_{a0,c}$ a characteristic value of the fatigue life, n_c defined as the 5% quantile can be estimated directly from the distribution function of the fatigue life (Mirzaei Rafsanjani & Sørensen, 2014).

If statistical uncertainty is to be taken into account and the physical/model uncertainties for the fatigue life are modeled by a log-normal distribution then the characteristic value for the fatigue life, n_c corresponding to the stress range, $\sigma_{a0,c}$ defined as a 5% quantile can obtained from by (Mirzaei Rafsanjani & Sørensen, 2015a):

$$P\left(\log n_c > m\log\sigma_f - m\log\sigma_{a0,c} + \frac{1}{b_n}\log s_V + \varepsilon - \log 2\right) = 0.05 \tag{3-8}$$

with a corresponding limit state equation written as (Mirzaei Rafsanjani & Sørensen, 2015a):

$$g\left(\sigma_f, m, \varepsilon, \sigma_\varepsilon\right) = m\log\sigma_f - m\log\sigma_{a0,c} + \frac{1}{b_n}\log s_V + \varepsilon - \log 2 - \log n_c \tag{3-9}$$

Here, ε, m, σ_ε and σ_f are modeled as stochastic variables as described above (Mirzaei Rafsanjani H. , et al., 2014). For given $\sigma_{a0,c}$ Equation (3-9) can be solved with respect to the characteristic fatigue life, n_c using e.g., First Order Reliability Method (Madsen, Krenk, & Lind, 1986).

Alternatively to the log-normal model for the *SN* curve a weibull model can be used, as described in the next section (Mirzaei Rafsanjani & Sørensen, 2014)

3.4. Fatigue strength modeled by a Weibull distribution

As mentioned above, the strength of wind turbine drivetrain components are subject to uncertainties and, therefore, a stochastic modeling of life distribution is needed to study the reliability of the components (Mirzaei Rafsanjani & Sørensen, 2015a). The influence of scale effects on damage modeling and fatigue life can from a theoretical basis be modeled by a Weibull mode (Madsen, Krenk, & Lind, 1986). Hence, the fatigue life can alternatively be modeled by a Weibull distribution for number of cycles to failure, N given stress range σ_{a0} written as (Mirzaei Rafsanjani & Sørensen, 2015a; Sørensen & Toft, 2010):

$$F_N\left(n\right)=1-\exp\left[-\left(\frac{n}{N\left(\sigma_{a0}\right)}\right)^{b_n}\right] \tag{3-10}$$

where b_n is a shape parameter. By substituting Equation (3-2) in Equation (3-10), the corresponding density function becomes (Mirzaei Rafsanjani & Sørensen, 2014):

$$f_N\left(n\right)=\frac{2b_n}{s_V^{1/b_n}}\left(\frac{\sigma_{a0}}{\sigma_f}\right)^m\left(\frac{2n}{s_V^{1/b_n}}\left(\frac{\sigma_{a0}}{\sigma_f}\right)^m\right)^{b_n-1}\exp\left[-\left(\frac{2n}{s_V^{1/b_n}}\left(\frac{\sigma_{a0}}{\sigma_f}\right)^m\right)^{b_n}\right] \tag{3-11}$$

The statistical parameters σ_f and m in Equation (3-11) can be estimated by the Maximum-Likelihood method with the likelihood function (Mirzaei Rafsanjani & Sørensen, 2014):

$$\begin{aligned}\ln L\left(\sigma_f,m\right)=&\sum_{i=1}^{n_F}\ln\left(\frac{2b_n}{s_V^{1/b_n}}\left(\frac{\sigma_{a0,i}}{\sigma_f}\right)^m\left(\frac{2n_i}{s_V^{1/b_n}}\left(\frac{\sigma_{a0,i}}{\sigma_f}\right)^m\right)^{b_n-1}\exp\left[-\left(\frac{2n_i}{s_V^{1/b_n}}\left(\frac{\sigma_{a0,i}}{\sigma_f}\right)^m\right)^{b_n}\right]\right)\\&+\sum_{i=1}^{n_R}\ln\left(\exp\left[-\left(\frac{2n_i}{s_V^{1/b_n}}\left(\frac{\sigma_{a0,i}}{\sigma_f}\right)^m\right)^{b_n}\right]\right)\end{aligned} \tag{3-12}$$

where n_i is the number of stress cycles to failure or run-out (no failure) with stress range equal to test number i. n_F is the number of tests where failure occurs, and n_R is the number of tests where failure does not occur after n_i stress cycles (run-outs) (Mirzaei Rafsanjani & Sørensen, 2014).

Similarly, if the fatigue life is modeled by a Weibull distribution and statistical uncertainty is accounted for, and then the characteristic value can be estimated using the following limit state equation (Mirzaei Rafsanjani & Sørensen, 2015a; Sørensen & Toft, 2010):

$$g\left(\sigma_f, m, \varepsilon, \sigma_\varepsilon\right) = \log n_c + \log 2 - \frac{1}{b_n}\log s_V + m\log\sigma_{a0,c} - m\log\sigma_f - \log\left(-\ln\left(0.95\right)\right)^{1/b_n} - \varepsilon \tag{3-13}$$

In equation (3-13), ε, m, σ_ε and σ_f model the physical/model and statistical uncertainties, respectively. As mentioned before, these parameters can be obtained from test results by using e.g. First Order Reliability Method (Mirzaei Rafsanjani & Sørensen, 2015a; Marquez-Dominguez & Sørensen, 2012).

3.5. Reliability assessment and damage accumulation model

Drivetrain components are typically exposed to complex loading conditions. Often the fatigue load is due to a range of fluctuating loads, different mean stress levels and variable frequencies. Cumulative damage theories consider the fatigue process to be one of damage accumulation until the life of the component is exhausted. As mentioned above, the cumulative damage during fatigue is often modeled by using the Palmgren-Miner rule, which assumes that the total life of a part can be estimated by adding up the percentage of life consumed by each stress level and can be written as follows if used in a deterministic code-based verification (Mirzaei Rafsanjani & Sørensen, 2015a):

$$D = \sum_i \frac{n_{i,S} T_L}{N_{0;0.05}\left(\frac{\sigma_{a0,i}}{z}, \frac{\sigma_f}{\gamma_m}\right)} \le 1 \tag{3-14}$$

where $n_{i,S}$ represents the number of cycles per year at a specific stress level $\sigma_{a0,i}$ and T_L is the design lifetime (Mirzaei Rafsanjani & Sørensen, 2015a). It is assumed that for a wind turbine component the total number of stress ranges for a given fatigue critical detail can be grouped in n_σ groups/intervals such that the number of stress ranges in group i is $n_{i,S}$ per year (Marquez-Dominguez & Sørensen, 2012). ($\sigma_{a0,i}$, $n_{i,S}$) can be obtained by rain-flow counting and can be represented by so-called 'Markov matrices' (Marquez-Dominguez & Sørensen, 2012). Further, $N_{0;0.05}\left(\frac{\sigma_{a0,i}}{z}, \frac{\sigma_f}{\gamma_m}\right)$ is the 5% quantile of the number of cycles to failure given fatigue load equal to $\sigma_{a0,i}/z$ and given the design fatigue strength σ_f/γ_m. $N_{0;0.05}$ can be obtained both without and with statistical uncertainty included. z is a design/scaling parameter, e.g. related to a cross-sectional parameter; γ_m is a partial safety factor for fatigue (Mirzaei Rafsanjani & Sørensen, 2015a).

This thesis uses the Level II method to measure the reliability of the components (Madsen, Krenk, & Lind, 1986). The design parameter z is obtained from (3-14) assuming that a fatigue partial safety factor γ_m is given. Thereby the reliability analyses become normalized in the way that the reliability is linked to the partial safety factors and it is assumed that the structure is designed to the limit though the design parameter z in the design equation (Mirzaei Rafsanjani & Sørensen, 2015a).

The corresponding limit state equation to be used in the reliability analysis is written:

$$g(t) = \Delta - \sum_i \frac{n_{i,S} t}{N_{0;0.05}\left(\frac{X_W X_{SCF} \sigma_{a0,i}}{z}, \frac{\sigma_f}{\gamma_m}\right)} \tag{3-15}$$

where t is time (in years), Δ models model uncertainty related to Miner's rule for linear damage accumulation (Marquez-Dominguez & Sørensen, 2012) (Mirzaei Rafsanjani & Sørensen, 2015a) (see equation (3-4)). The distribution function for number of cycles to failure, $N_{0;0.05}$ for given stress $\sigma_{a0,i}$ can be obtained by equations (3-9) and (3-13) for log-normal and Weibull distributed fatigue lives (Mirzaei Rafsanjani & Sørensen, 2015a).

If statistical uncertainty is included then the statistical parameters are modeled by stochastic variables (Sørensen & Toft, 2010). X_W is a stochastic variable modeling model uncertainty related to determination of fatigue loads, and X_{SCF} is a stochastic variable modeling model uncertainty related to determination of stresses given fatigue loads (Sørensen & Toft, 2014).

For wind turbines the fatigue loads are typically estimated for mean wind speeds from 4 m/s to 25 m/s and are normally represented by time series of load effects or equivalently by Markov matrices obtained by rain-flow counting (Mirzaei Rafsanjani & Sørensen, 2015a). Additionally contributions from other load cases such as stat/stop may contribute to the fatigue, but these contributions are included in the following. Hence, equation (3-14) can be written as:

$$D = \sum_{V_j} \left(\sum_i \frac{n_{i,S} T_L}{N_{0;0.05}\left(\frac{\sigma_{a0,i}}{z}, \frac{\sigma_f}{\gamma_m}\right)} \right) * P\left(V_j\right) = 1 \tag{3-16}$$

where, V_j is the mean wind speed and $P(V_j)$ is probability of occurrence of this mean wind speed, modeled by a Weibull distribution according to IEC 61400-1 (IEC 61400, 2015; Mirzaei Rafsanjani & Sørensen, 2015a). By substituting Equation (3-16) in Equation (3-15), the limit state equation can be written:

$$g(t) = \Delta - \sum_{V_j} \left(\sum_i \frac{n_{i,S} t}{N_{0;0.05}\left(\frac{X_W X_{SCF} \sigma_{a0,i}}{z}, \frac{\sigma_f}{\gamma_m}\right)} \right) * P\left(V_j\right) \tag{3-17}$$

In Equation (3-17), Δ, X_W and X_{SCF} are assumed to be log-normal distributed with mean values equal 1 and coefficients of variation COV_Δ, COV_W and COV_{SCF}, respectively, following the recommendations in e.g. (Wirsching, 1984; Sørensen & Toft, 2014). The coefficient of variations are estimated based partly subjectively, but following generally the recommendations used as basis for the material partial

safety factors in IEC 61400-1, and also considering information from e.g. (DNV-RP-C203, 2010).

Table 3-1 shows the representative stochastic model. Expected values and coefficient of variations for m and σ_f (if a weibull model is used) must be extracted from tests results as described above (Mirzaei Rafsanjani & Sørensen, 2015a). Based on Equation (3-17), the probability of failure in the time interval $[0,t]$ can be estimated by FORM/SORM techniques or simulation (Sørensen & Toft, 2010).

Table 3-1 Stochastic model (Mirzaei Rafsanjani & Sørensen, 2015a)

Variable	Definition	Distribution	Expected Value	Coefficient of Variation
Δ	Model uncertainty related to Miner's rule	LN*	1	0.2
X_{SCF}	Model uncertainty related to determination of stresses given fatigue load	LN	1	0.05
X_W	Model uncertainty related to determination of fatigue loads	LN	1	0.1
m	Statistical uncertainty	N**	Extracted from test results	
σ_f [Mpa]	Statistical uncertainty	N	Extracted from test results	

* LN: Log-normal distribution, ** N: Normal distribution

3.6. Comparison of fatigue *SN* curves by analysis of covariance

The fatigue life of wind turbine cast components is generally influenced significantly by the defects/nodules from the casting process (Shirani & Härkegård, 2014). These defects may reduce the fatigue life and they are generally distributed randomly in the components. Casting defects are one of the main reasons of low fatigue life. The fatigue life of cast iron components is often controlled by the growth of cracks initiated from defects such as shrinkage cavities, graphite nodules and gas pores (Shirani & Härkegård, 2012; Shirani & Härkegård, 2014). Further, different manufacturers apply different manufacturing processes of cast components resulting in different fatigue lives of the produced components.

In this section, the Analysis of Covariance (ANCOVA) method is used for comparing different groups / manufacturing steps of specimens from casted components. As basis for this method, the following sections will explain the general hypothesis testing and the hypothesis testing methods Analysis of Variance (ANOVA) and Analysis of Covariance (ANCOVA) and illustrate their application.

3.6.1. Hypothesis testing

Hypothesis testing is a class of statistical analysis that is widely used because it encourages systematic decision-making about problems that involve considerable uncertainty (Ayyub & McCuen, 2002). It enables inferences to be made in such a way that sample data can be combined with statistical theories. The following six steps can be used to make a statistical analysis of a hypothesis (Ayyub & McCuen, 2002):

1. Formulate hypothesis.
2. Select the appropriate statistical model that identifies the test statistic.
3. Specify the level of significance, which is a measure of risk.
4. Collect a sample of data and compute an estimate of the test statistic.
5. Define the region of rejection for the test statistic.
6. Select the appropriate hypothesis.

In the following, a brief description of steps is given, for further details, see (Ayyub & McCuen, 2002).

3.6.1.1 Formulation hypothesis

The first step is to formulate two or more hypotheses for testing. The first hypothesis is called the *null hypothesis,* denoted H_0, and is formulated as an equality (Ayyub & McCuen, 2002). For example, in the comparison of casting suppliers, the null hypothesis could be "there is no effect by casting suppliers on fatigue life". The associated, second hypothesis, which is called the alternative hypothesis, is formulated to indicate that a difference does exist (Ayyub & McCuen, 2002). The alternative hypothesis is denoted by either H_1 or H_A. The null and alternative hypothesis should be mutually exclusive (Ayyub & McCuen, 2002).

3.6.1.2 The test statistic and its sampling distribution

The test statistic is related to the statistical method that is chosen for analysis of the data. In this thesis, ANCOVA is used, but for studying ANCOVA, the ANOVA method is also introduced to receive the overall overview of the method.

3.6.1.3 The level of significance

This step involves a probabilistic framework for accepting or rejecting the null hypothesis and, subsequently, making a decision (Ayyub & McCuen, 2002). Table 3-2 shows the available situations and the potential decision involved in a hypothesis test. The decision table suggests two types of error (Ayyub & McCuen, 2002).

The level of significance, which is a primary element of the decision process in hypothesis testing, represent the probability of making a type I error and is denoted by α. The probability of making a type II error is denoted by β. The two possible incorrect decisions are not independent (Ayyub & McCuen, 2002). The level of significance should not be too low, because the probability of making a type II error

will then be increased. However, the value chosen for α is often based on convention and the availability of statistical tables, with values for α of 0.05 and 0.01 being selected frequently (Ayyub & McCuen, 2002).

Table 3-2 Decision table for Hypothesis Testing (Ayyub & McCuen, 2002)

	Situation	
Decision	**H_0 is true**	**H_0 is not true**
Accept H_0	Correct decision	Incorrect decision: type II error
Reject H_0	Incorrect decision: type I error	Correct decision

3.6.1.4 Data analysis

After obtaining necessary data, the sample is used to compute an estimate of the test statistic (Ayyub & McCuen, 2002). In the following, the fatigue life is used for data analysis.

3.6.1.5 The region of rejection

The region of rejection consists of those values of the test statistic that would be unlikely to occur when the null hypothesis is, in fact, true. Conversely, the region of acceptance consists of those values of the test statistic that would be expected when the null hypothesis is, in fact, true. Extreme values of the test statistic are least likely to occur when the null hypothesis is true. Thus, the region of rejection is usually represented by one or both tails of the distribution of the test statistic (Ayyub & McCuen, 2002). Figure 3-1 shows the expression of region of rejection graphically.

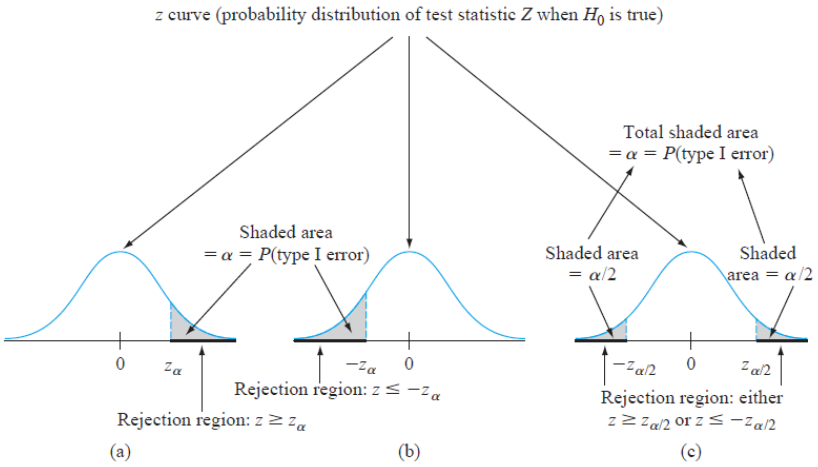

Figure 3-1 Rejection regions: (a) upper-tailed test; (b) lower-tailed test; (c) two-tailed test (Montgomery, 2008)

The critical value of the test statistic is defined as the value that separates the region of ejection from the region of the acceptance. The critical value of the test statistic depends on (Ayyub & McCuen, 2002):

1. The statement of the alternative hypothesis
2. The distribution of the test statistic
3. The level of significance
4. Characteristics of the sample or data

These four components represent the first four steps of a hypothesis test (Ayyub & McCuen, 2002).

3.6.1.6 Select the appropriate hypothesis

A decision of whether or not to accept the null hypothesis depends on a comparison of the computed value of the test statistic and the critical value. The null hypothesis is rejected when the computed value lies in the region of rejection. Rejection of the null hypothesis implies acceptance of the alternative hypothesis (Ayyub & McCuen, 2002).

3.6.2. Analysis of Variance (ANOVA)

ANalysis Of VAriance (ANOVA) is a statistical method used to analyze the differences between mean values of different groups of e.g. suppliers. In its simplest form, ANOVA provides a statistical test of whether or not the means of several groups are equal, and therefore generalizes the statistical *t*-test applied to more than two groups (Zimmerman, 1997). Doing multiple two-sample *t*-tests would result in

an increased chance of committing a type I error. Based on hypothesis testing, the null hypothesis of ANOVA is that the mean values of several groups are equal, and on the other hand, the alternative hypothesis is that the mean values are not equal (Ayyub & McCuen, 2002).

ANOVAs are useful in comparing (testing) three or more groups. A decision of whether or not to accept the null hypothesis depends on a comparison of the computed value of the test statistics and the critical values (Ayyub & McCuen, 2002). The ANOVA analysis can be performed computationally as follows (based on six steps in section 3.6.1).

Step 1: Formulation of hypothesis – If a problem involves *k* groups, the following hypotheses are appropriate for comparing *k* group means (Ayyub & McCuen, 2002):

$$\begin{aligned} &\mathrm{H}_0 : \mu_1 = \mu_2 = \ldots = \mu_k \\ &\mathrm{H}_\mathrm{A} : \text{ at least one pair of group means are not equal} \end{aligned} \tag{3-18}$$

Note that the test compares the means, but if the null hypothesis is rejected, the following five steps do not identify which pair or pairs of means are not equal.

Step 2: Define the test statistic and its distribution – The hypotheses of step 1 can be tested using the following test statistics (Ayyub & McCuen, 2002):

$$F = \frac{MS_b}{MS_w} \tag{3-19}$$

where MS_b and MS_w are the mean squares between and within variations, respectively, and F is a random variable following an F distribution with degrees of freedom of (k-1, M-k) (Ayyub & McCuen, 2002). Table 3-3 shows the calculation for ANOVA. In Table 3-3, k is the number of groups, m_j is the number of data in j-th group, $\overline{X}$ is the mean value of all data, $\overline{X_j}$ is the mean value of data in j-th group and M is the total number of data (Ayyub & McCuen, 2002).

Table 3-3 Computation Table for the Analysis of Variance Test (Ayyub & McCuen, 2002)

Source of Variation	Sum of squares	Degrees of freedom	Mean square
Between	$SS_b = \sum_{j=1}^{k} m_j \left(X_j - \overline{X} \right)^2$	k-1	$MS_b = SS_b / \left(k-1 \right)$
Within	$SS_w = \sum_{j=1}^{k} \sum_{i=1}^{m_j} \left(X_{ij} - \overline{X_j} \right)^2$	M-k	$MS_w = SS_w / \left(M-k \right)$
Total	$SS_t = \sum_{j=1}^{k} \sum_{i=1}^{m_j} \left(X_{ij} - \overline{X} \right)^2$	M-1	

Step 3: The level of significance: The level of significance is used in the same way as other tests of hypotheses (Ayyub & McCuen, 2002). Tables of the F distribution are usually available only for levels of significance of 5% and 1%.

Step 4: Collect data and compute test statistic – The data should be collected and used to compute the value of the test statistics (F) in equation (3-19). All data must be categorized according to the different groups to be compared statistically to each other (Ayyub & McCuen, 2002). If there are m_j values in the j-th group, then the total number of observations M is given by (Note that all m_j do not have to be equal):

$$M = \sum_{j=1}^{k} m_j \tag{3-20}$$

Step 5: Determine the critical value of the test statistic – The critical value of the F statistic is obtained from the F distribution. It is a function of the level of significance and the degrees of freedom. The region of rejection consists of all values of F greater than the critical F value. If the computed value of step 4 is greater than the critical value, the null hypothesis of equation (3-18) should be rejected and the alternative hypothesis of equation (3-18) accepted, for further details, see (Ayyub & McCuen, 2002).

Step 6: Make a decision – The computed and table values should be compared in order to select the appropriate hypothesis.

3.6.3. Analysis of Covariance (ANCOVA)

Similar to the analysis of variance, the analysis of covariance (ANCOVA) is used to test the null hypothesis that two or more population means are equal (Huitema, 2011). The ANCOVA always involves at least three variables: an independent variable, a dependent variable, and a covariate. The covariate is the variable likely to be correlated with the dependent variable. For application of fatigue data, these variables are as follows:

- The independent variable is the group types that we consider to compare to each other (for example casting supplier).
- The dependent variable is the fatigue life, N, and it depends on the test stress amplitude and the type of group.
- The covariate is the test stress amplitude, σ, and it is likely related with the fatigue life (the dependent variable).

The major differences between ANOVA and ANCOVA can be illustrated using a two-group experiment, cf. Figure 3-2. The major distinction between the two analyses is that in ANOVA the error term is related to the variation of log$N$ around individual group means, shown as distributions A and B, whereas the ANCOVA error term is based on variations of log$N$ scores around regression lines, distributions C and D. The effect of the smaller within-group variation associated with ANCOVA is an increase of the power of the analysis. Note that the ANOVA

distributions have a larger overlap than the ANCOVA distributions (Huitema, 2011). The analysis of covariance is a combination of the linear models employed in analysis of variance and regression (Montgomery, 2008).

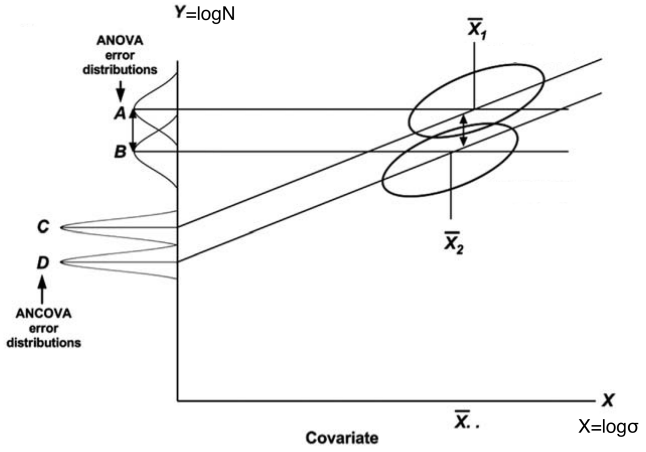

Figure 3-2 Distribution of estimated errors associated with ANOVA and ANCOVA (Huitema, 2011)

Suppose we have data from *k*-group experiments where the dependent variable is the fatigue life, the covariate variable is the test stress amplitude, and the independent is the type of group (Huitema, 2011). The starting point for ANCOVA is exactly the same as for ANOVA; the total sum of squares is computed. It is noticed that ANCOVA can be used for linear regression methods and because of that the calculation is carried out using the "logarithm of fatigue life (log*N*)" and the "logarithm of test stress amplitude (logσ)". Hence, the covariate variable (x) is logσ and dependent variable (y) is log*N*. Assuming that there is a linear relationship between the dependent variable and the covariate, we find that an appropriate statistical model is (Montgomery, 2008):

$$\log N_{ij} = \mu + \tau_j + \beta\left(\log\sigma_{ij} - \log\overline{\sigma_{..}}\right) + \varepsilon_{ij} \quad \begin{cases} i = 1,2,...,m_j \\ j = 1,2,...,k \end{cases} \tag{3-21}$$

where $\log N_{ij}$ is the i-th observation on the response variable taken under the j-th group, $\log\sigma_{ij}$ is the measurement made on the covariate variable responding to $\log N_{ij}$, $\log\overline{\sigma}_{..}$ is the mean of the $\log\sigma_{ij}$ values, μ is an overall mean, τ_j is the effect of the j-th group, β is a linear regression coefficient indicating the dependency of $\log N_{ij}$ on $\log\sigma_{ij}$, and ε_{ij} is a random error component. The null hypothesis is "the group effects is zero ", and we assume that the concomitant variable $\log N_{ij}$ is not affected by the groups (Huitema, 2011; Montgomery, 2008).

Notice from Equation (3-21), we have group effects $\{\tau_j\}$ as in a single-factor analysis of variance and a regression coefficient β as in a regression equation. The

concomitant variable in Equation (3-21) is expressed as ($\log\sigma_{ij}$ - $\log\overline{\sigma}_{..}$) instead of $\log\sigma_{ij}$ so that the parameter μ is preserved as the overall mean. The following shows the steps of ANCOVA:

Step 1. Computation of total sum of squares

The total sum of squares is obtained by:

$$S_{yy}=\sum_{j=1}^{k}\sum_{i=1}^{m_j}\left(\log N_{ij}-\log\overline{N}_{..}\right)^2=\sum_{j=1}^{k}\sum_{i=1}^{m_j}\left(\log N_{ij}\right)^2-\frac{\left(\sum_{j=1}^{k}\sum_{i=1}^{m_j}\log N_{ij}\right)^2}{M} \tag{3-22}$$

The total sum of squares results from:

1. "Type of groups" effects - these effects are independent from the stress amplitude effect.
2. Differences in fatigue life predicted from stress amplitudes and real fatigue life of component, which is called the regression effect.
3. Differences among subjects that are not due to the group's effects and cannot be predicted from the stress amplitudes (i.e. errors).

Thus, S_{yy} consists of three different effects (type of groups, stress amplitude, and error) as mentioned before. After the total sum of squares is computed, the second step is to remove the sum of squares due to the regression of $\log N$ on $\log\sigma$ from the total sum of squares.

Step 2: Computation of total residual *SS*

For further steps, the effect of regression must be decreased from total sum of square. Hence, the total residual sum of squares (SS_{res_t}) must be calculated (Huitema, 2011). According to this, the following sum of squares must be evaluated firstly:

$$\begin{aligned}S_{xy}&=\sum_{j=1}^{k}\sum_{i=1}^{m_j}\left(\log N_{ij}-\log\overline{N}_{..}\right)\left(\log\sigma_{ij}-\log\overline{\sigma}_{..}\right)\\&=\sum_{j=1}^{k}\sum_{i=1}^{m_j}\left(\log N_{ij}\right)\left(\log\sigma_{ij}\right)-\frac{\left(\sum_{j=1}^{k}\sum_{i=1}^{m_j}\log N_{ij}\right)\left(\sum_{j=1}^{k}\sum_{i=1}^{m_j}\log\sigma_{ij}\right)}{M}\end{aligned} \tag{3-23}$$

$$S_{xx}=\sum_{j=1}^{k}\sum_{i=1}^{m_j}\left(\log\sigma_{ij}-\log\overline{\sigma}_{..}\right)^2=\sum_{j=1}^{k}\sum_{i=1}^{m_j}\left(\log\sigma_{ij}\right)^2-\frac{\left(\sum_{j=1}^{k}\sum_{i=1}^{m_j}\log\sigma_{ij}\right)^2}{M} \tag{3-24}$$

Hence, the total residual sum of squares (SS_{res_t}) is calculated as

$$SS_{res_t} = S_{yy} - \left[\frac{\left(S_{xy}\right)^2}{S_{xx}}\right] \tag{3-25}$$

In Equation (3-25), the quantity $(S_{xy})^2/S_{xx}$ is the reduction in the sum of squares of log$N$ obtained through the linear regression of log$N$ on logσ. Hence, the Equation (3-25) contains only the variability due to "Type of groups" effects and the effect of the regression has been removed. The reason of this partitioning is that usually the actual value of log$N$ associated with a specific subject (group j-th) does not fall exactly on the regression line and, therefore, there is some prediction error for this subject. This prediction error is called the residual and is denoted SS_{res_t}.

Step 3: Computation of within-group sum of square

The within-group sum of squares may be obtained by computing logN^2 for each group and then summation of the results of the k separate groups. The within-group sum of square is not influenced by "Type of group" or between-group differences. The within-group sum of squares includes the regression effect and error:

$$E_{yy} = \sum_{j=1}^{k}\left[\sum_{i=1}^{m_j}\left(\log N_{ij}\right)^2 - \frac{\left(\sum_{i=1}^{m_j}\log N_{ij}\right)^2}{m_j}\right] \tag{3-26}$$

Equation (3-26) estimates the sum of squares within each group, and finally the summation of within-group sum of square of all groups is calculated. The within-group deviation cross products required in the next step are computed using the following formula:

$$E_{xy} = \sum_{j=1}^{k}\left[\sum_{i=1}^{m_j}\left(\log N_{ij}\right)\left(\log \sigma_{ij}\right) - \frac{\left(\sum_{i=1}^{m_j}\log N_{ij}\right)\left(\sum_{i=1}^{m_j}\log \sigma_{ij}\right)}{m_j}\right] \tag{3-27}$$

and sums of squares on logσ required in the following step are computed using:

$$E_{xx} = \sum_{j=1}^{k}\left[\sum_{i=1}^{m_j}\left(\log \sigma_{ij}\right)^2 - \frac{\left(\sum_{i=1}^{m_j}\log \sigma_{ij}\right)^2}{m_j}\right] \tag{3-28}$$

Hence, the within-group regression sum of squares (error of regression) is as below

$$SS_{reg_W} = \frac{\left(E_{xy}\right)^2}{E_{xx}} \tag{3-29}$$

Furthermore, the within-group regression coefficient (to be used later in adjusting the means) is

$$b_W = \frac{E_{xy}}{E_{xx}} \tag{3-30}$$

Step 4: Computation of within-group residual sum of square (or error *SS*). Because the within-group sum of squares contains variability predictable from logσ, it is necessary to remove the predictable variability in order to obtain the portion of the total residual sum of squares that is unrelated to either "Type of groups" or the regression. This is accomplished by subtracting sum of square due to predictable differences among subjects within groups (sometimes called within-group regression sum of square and is shown with SS_{reg_W}) from sum of squares within-groups. The result is called the within-group residual sum of squares (i.e., SS_{res_W}) (Huitema, 2011), which is used as "the error sum of square" in ANCOVA. Differences contributing to this sum are not predictable from logσ (using a linear rule) and are not accounted for by "Type of group" differences.

$$SS_{res_W} = E_{yy} - SS_{reg_W} \tag{3-31}$$

The experimental error variance is estimated by

$$MS_{res_W} = SS_{res_W} \Big/ \left(M - k - 1\right) \tag{3-32}$$

Step 5: Computation of adjusted effects

By subtracting the sum of squares of residual within (SS_{res_W}) from the total residual sum of squares (SS_{res_t}), the adjusted sum of square is obtained (Huitema, 2011). This quantity was described as the sum of squares due to "Type of groups effects independent of logσ" in the previous steps and is

$$SS_{AT} = SS_{res_t} - SS_{res_W} \tag{3-33}$$

Therefore, the SS_{AT} provides a sum of squares with *k*-1 degrees of freedom for testing the hypothesis of no group's effects (Montgomery, 2008).

Step 6: Computation of *F*-ratio.

Step 5 involves the partitioning of the total residual sum of squares into the sum of squares residual within (i.e., SS_{res_W}) and the adjusted sum of squares. The latter two correspond directly to within- and between-group sum of squares in a simple analysis of variance (Huitema, 2011). Thus the *F*-ratio can be obtained by dividing mean square adjusted (MS_{AT}) by mean square error (MS_{res_W}). The degrees of freedom are computed in the same way as in ANOVA except that an additional degree of

freedom is lost from the error *MS* for each covariate (or covariate polynomial) employed in the analysis. Table 3-4 shows the ANCOVA summary table, for further details see (Huitema, 2011; Montgomery, 2008).

Table 3-4 Computation Table for the Analysis of Covariance Test (Huitema, 2011)

Source of Variation	Sum of squares	Degrees of freedom	Mean square	*F*
Adjusted (AT)	SS_{AT}	k-1	$MS_{AT} = SS_{AT} \big/ \left(k-1\right)$	$MS_{AT} = MSre_{res_w}$
Error (res_w)	SS_{res_w}	M-k-1	$MS_{res_w} = SS_{res_w} \big/ \left(M-k-1\right)$	
Total residual (res_t)	SS_{res_t}	M-1	-	

If the computed value of *F* in Table 3-4 is larger than the critical value (*t*-test value with degrees of freedom from Table 3-4), the null hypothesis should be rejected and the alternative hypothesis accepted (Huitema, 2011). In this case, the null hypothesis is: H_0: The choice of groups does not affect the fatigue test results ($\tau_j = 0$). Further, to find the real position of regression line, the adjusted mean of each group must be investigated and the slopes are evaluated (for detail see related paper in appendix).

3.6.4. Comparison of casting supplier

The fatigue tests are carried out for two different casting suppliers (CS1, CS2). Table 3-5 shows the number of tests for sand casting method. The comparison between groups (suppliers) is performed. Table 3-6 shows a summary of the ANCOVA calculations.

Table 3-5 Number of test results by Test laboratories (For sand casting)

Suppliers	Broken	Run-out	Total
Supplier 1 (CS1)	688	120	808
Supplier 2 (CS2)	82	3	85
Summation	770	123	893

Table 3-6 Summary of calculation for sand casting supplier comparison

Parameter	Value	Parameter	Value
S_{yy}	621.01	SS_{res_w}	209.86
SS_{res_t}	220.95	SS_{AT}	11.08
SS_{reg_w}	403.95	b_w	-8.76

The value of b_w shows that the stress amplitude and fatigue life are negatively correlated. First it is tested whether or not the choice of casting suppliers does affect the fatigue test results. The null hypothesis is:

H_0: The choice of casting supplier does not affect the fatigue test results.

The *F*-ratio is calculated according to Table 3-4. The study involves one covariate, two groups and 893 test results. The *F*-ratio calculation is summarized in Table 3-7.

Table 3-7 Computation Table for the casting supplier comparison

Source of Variation	Sum of squares	Degrees of freedom	Mean square	*F*
Adjusted (AT)	11.08	1	11.08	46.17
Error (res_w)	209.86	890	0.24	-
Total residual (res_t)	220.95	891	-	-

The obtained *F* is then compared with the critical value of *F* with 1 and 890 degrees of freedom and level of significance 5%; $F_{(0.05,\ 1,\ 890)}$ is 3.85, and the null hypothesis of "The choice of casting supplier does not affect the fatigue test results" is rejected (Note that if level of significance had been 1%, then critical value would be 6.66 and the null hypothesis is still rejected). Next, the homogeneity of slopes of regression lines is considered (for details see related paper I appendix).

Figure 3-3 (from paper 2) shows the results for the regression lines. The fatigue lives from "CS1" are larger than the fatigue lives of the other group and the groups have the same slope. It is noted that the test data points and the name of casting suppliers are not shown due to confidentiality.

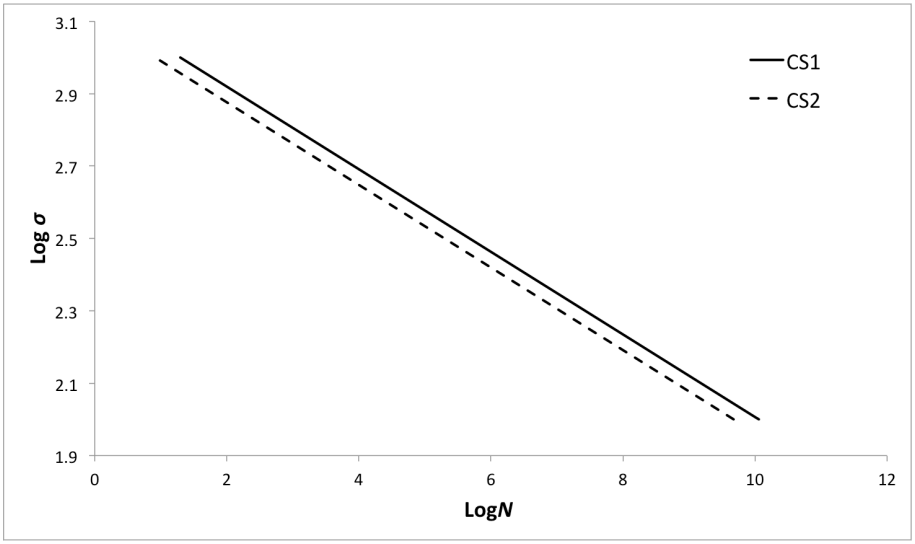

Figure 3-3 Comparison of "casting suppliers" on logarithmic scale

CHAPTER 4. STOCHASTIC MODEL OF DEFECT DISTRIBUTION

This section describes the stochastic model and statistical analysis of nodules/defects in nodular cast irons. The cast iron samples were cut out as standard fatigue samples with diameters of 6 mm (ASTM E466-07, 2007) and tomographcally scanned at DTU, Department of Wind Energy (RISØ campus). The samples are from two different casting methods: sand casting and chill casting. Using the AVIZO 3D software for materials science, it is possible to obtain the center position of all identified nodules, and geometrical parameters of the nodules (FEI.com, 2015). In this chapter a statistical analysis of nodules in cast iron is presented.

4.1. Defects/Nodules in ductile cast iron

The common defining characteristic of ductile cast iron (nodular cast iron) is the shape of the graphite nodules (for details see section 1.2 in Chapter 1) (Shirani & Härkegård, 2014). In ductile cast iron, the graphite 'particles' has the form of nodules rather than flakes as in grey iron (Ecob, 2005; Shirani & Härkegård, 2014). Whereas sharp graphite flakes creates stress concentration points within the metal matrix, rounded nodules inhibit the creation of cracks, thus providing an enhanced ductility. Defects may be divided into two basic categories (Shirani & Härkegård, 2014):

- Those related to nodule shape and size, such as compacted graphite structures, exploded and chunky graphite, graphite floatation, spiky graphite and nodule alignment (Shirani & Härkegård, 2014).
- Those related to inclusions/abnormalities, such as flake graphite, slag inclusions, carbides, gas pores and shrinkage cavities (Shirani & Härkegård, 2014).

These defects are explained in more detail in Chapter 1. In this thesis, the main focus is on the nodules shape and size. Nodules are generally characterized by three parameters "Equivalent Size", " Sphericity" and " Aspect Ratio" (Shirani & Härkegård, 2012). The "Equivalent Size" of a nodule is the diameter of a sphere with the same volume as the considered nodule. The "Sphericity" of a nodule is the ratio of the surface area of a sphere with the same volume as the given nodule to the surface area of the nodule obtained by scans (Shirani & Härkegård, 2012). Sphericity is 1 for a perfect sphere and close to 0 for very tortuous shape (Buffiere, Savelli, Jouneau, Maire, & Fougeres, 2001). The "Aspect Ratio" of a nodule is the ratio of minimum to the maximum dimension of the bounding box encapsulating the nodule (Shirani & Härkegård, 2012).

Niimi et al. studied the fatigue strength of nodular cast iron, focusing on the size of graphite nodules (Niimi, Ohashi, Komatsu, & Hibino, 1971). According to their results, metal die cast iron[1] has the smallest nodule sizes and the highest fatigue strength. Niimi also adopted the average size of nodules as the representative nodule size.

Further, Endo carried out experiments where the fatigue strength of nodular cast iron specimens containing nodules is compared with those which were electropolished in order to remove nodules at the specimen surface (Murakami, 2002). Thus, the nodules of the latter specimens became vacant pores (Endo, 1989). Endo tested two different nodular cast irons (called as FCD60 and FCD70). The nodularity are 84% for both FCD60 and FCD70 (Murakami, 2002). Based on his results, there are no distinct differences between the fatigue strengths of non electropolished specimens and those of electropolished specimens. Therefore, as far as the materials used by Endo are concerned, the contribution of graphite nodules to improvement of fatigue strength is negligible, and a nodule can be regarded as equivalent to a hole (Murakami, 2002). That means the nodules and similar holes could affect the fatigue strength in a same way and the the existance of big nodules / voids reduce th fatigue life of component.

From the above discussion and (Murakami, 2002), the domain occupied by nodules can be regarded as equivalent to a hole, or a small defect, without a nodule. This assumption is applied in the following since in 3D X-ray tomography scans, the differences of nodules and voids inside of material is hard to distinguish.

Determination of nodule size distribution and the number of nodules per volume are a prerequisite for modeling fatigue life scatter of the components. Nodule distributions can be obtained from XCT (3D X-ray Computed Tomography) scans (Shirani & Härkegård, 2012) which in this thesis are performed at DTU, Wind Energy Department (at RISØ campus).

3D X-ray Computed Tomography (XCT) is a powerful nondestructive examination (NDE) technique for producing two dimensional and three dimensional images of an object (Shirani & Härkegård, 2012). Characteristics of the internal structure of an object such as defects size, shape and position are readily available from XCT. These parameters can be used in conjunction with fatigue crack growth analysis to predict the fatigue life of the component (Shirani & Härkegård, 2012).

Murakami (Murakami, 2002) showed that the most relevant parameter to the model nodule size is the square root of the area of a nodule. Thus, in this research, the square root of the nodule area perpendicular to the maximum principal stress axis (z- axis in Figure 4-1) is used to characterize nodule size. Statistical analysis of the data showed that the generalized extreme value (GEV) distribution is the best fit to

[1] Die casting is a metal casting process that is characterized by forcing molten metal under high pressure into a mold cavity (wikipedia.org)

the square root of the nodules area projected along the specimen axis. Its cumulative distribution function is given by

$$F\left(x;\mu,\sigma,\xi\right)=\exp\left\{-\left[1+\xi\left(\frac{x-\mu}{\sigma}\right)\right]^{-1/\xi}\right\} \tag{4-1}$$

where μ, σ and ζ are the location, scale and shape parameters, respectively. The GEV distribution can be divided into three types depending on the shape parameter ζ, which defines the upper tail behavior of the distribution:

- Gumbel distribution (Type I) ($\zeta = 0$)

$$F_{I}\left(x;\mu,\sigma\right)=\exp\left\{-\exp\left[-\frac{x-\mu}{\sigma}\right]\right\} \tag{4-2}$$

- Frechet distribution (Type II) ($\zeta = \alpha^{-1} > 0$)

$$F_{II}\left(x;\mu,\sigma,\xi\right)=\begin{cases}0 & x\le\mu\\ \exp\left\{-\left(\frac{x-\mu}{\sigma}\right)^{-1/\xi}\right\} & x>\mu\end{cases} \tag{4-3}$$

- Reversed Weibull distribution (Type III) ($\zeta = -\alpha^{-1} < 0$)

$$F_{III}\left(x;\mu,\sigma,\xi\right)=\begin{cases}\exp\left\{-\left(-\frac{x-\mu}{\sigma}\right)^{-1/\xi}\right\} & x<\mu\\ 1 & x\ge\mu\end{cases} \tag{4-4}$$

Distribution Type I contains a double exponential form whereas Type II and III have single exponential forms. Distribution equations (4-2) and (4-3) focus on maximum values of a data set, whereas equation (4-4) focuses on the minima values. When dealing with maxima values and Weibull distributions, equation (4-4) can be adjusted by replacing x by $-x$ and subtracting 1 from F_{III}. This leads to the following Weibull distribution that focuses on maxima values ($x > \mu$) (Ambuhl, 2015):

$$F\left(x;\mu,\sigma,\xi\right)=1-\exp\left\{-\left(\frac{x-\mu}{\sigma}\right)^{-1/\xi}\right\} \tag{4-5}$$

Which distribution type fits best to the considered data set needs to be checked by e.g. a Q-Q plot where the theoretical values and the sample values are compared. In the following, the test setup and the statistical analysis of the experiments are explained.

4.2. Introduction to test set-up

The samples scanned in this project are from two different casting processes (Sand casting and Chill casting). In this section, the experimental procedure is explained.

4.2.1. Material and specimen

The material under investigation is EN-GJS-400-18 ductile cast iron. Fatigue specimens with 6 mm diameter were machined based on (ASTM E466-07, 2007). In Figure 4-1 and Figure 4-2, the configuration of samples and the geometrical coordination that will be used in this thesis is shown (for further detail; see (ASTM E466-07, 2007)). From each casting methods, 4 samples are chosen for X-ray tomography scanning followed by fatigue testing.

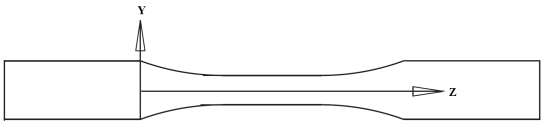

Figure 4-1 The fatigue test specimen geometrical coordination

Figure 4-2 The fatigue test sample

4.2.2. 3D tomography

The X-ray tomography scannings were performed at a ZEISS Xradia 520 Versa (located at DTU, Wind Energy Department, RISØ campus). The tomography data was reconstructed by a standard filtered back-projection algorithm to form 3D density maps from which the 3D distribution of the nodules were obtained in selected fatigue samples (Figure 4-3 and Figure 4-4). The X-ray energy was 160 kV and the parameters were set such that it is possible to detect nodules with

dimensions larger than 10 µm. The voxel size in the reconstructed volumes were 10 µm. The scanned volume of each specimen was about 650 – 700 mm^3.

Figure 4-3 ZEISS Xradia 520 Versa

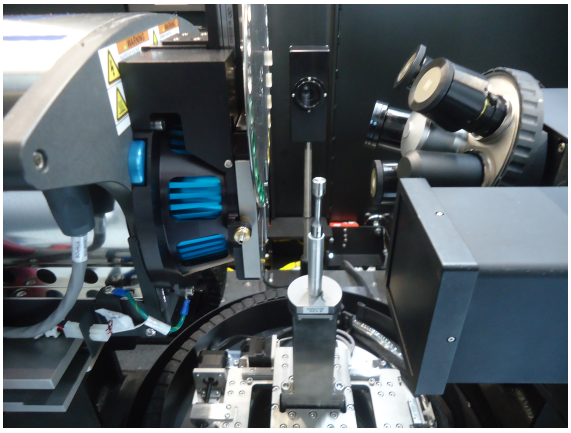

Figure 4-4 The configuration of samples inside of 3D tomography instrument

4.2.3. Analysis of scanned samples

The AVIZO 9 3D software for materials science was used for three-dimensional visualization and analysis of 3D scans. By using this software, it is possible to obtain the volume, equivalent diameter, surface area, projected area perpendicular to z-axis, center position of nodule, sphericity and the size of the bounding box encapsulating the nodule for each nodules inside of specimen. Figure 4-5 shows these parameters; from (Shirani & Härkegård, 2012). Lists of nodules associated with the highest volume for each specimen are given in Appendix A. As mentioned above, the projected area of nodules along the specimen axis, PZ, was used as the nodule area and the nodules were assumed to be circular, i.e. the nodule radius is estimated by (Shirani & Härkegård, 2012):

$$a = \sqrt{\frac{PZ}{\pi}} \tag{4-6}$$

Finally, all of the detected nodules are used to find out the GEV parameters. Figure 4-6 shows a view of nodules detected by a 3D scan in an example for a chill casting specimen.

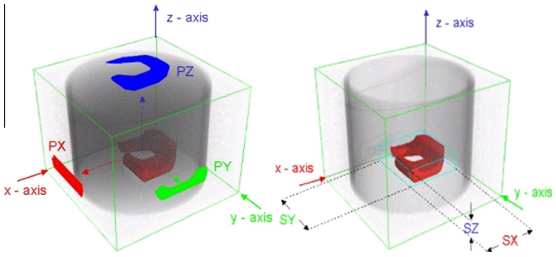

Figure 4-5 Some of the characteristic parameters that can be extract from processing of the tomographic reconstructions; from (Shirani & Härkegård, 2012)

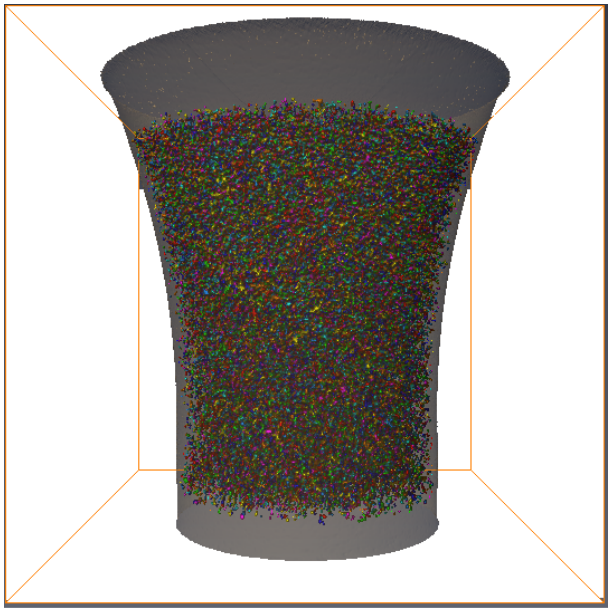

Figure 4-6 Nodules detected by 3D scanner in fatigue specimen

Furthermore, Figure 4-7 shows a slice through tomographic reconstructions of two samples; one produced by sand casting and one by chill casting. Based on these figures, it is seen that the sand casting specimens have less nodules but the size of the nodules are tremendously bigger than for chill casting specimens.

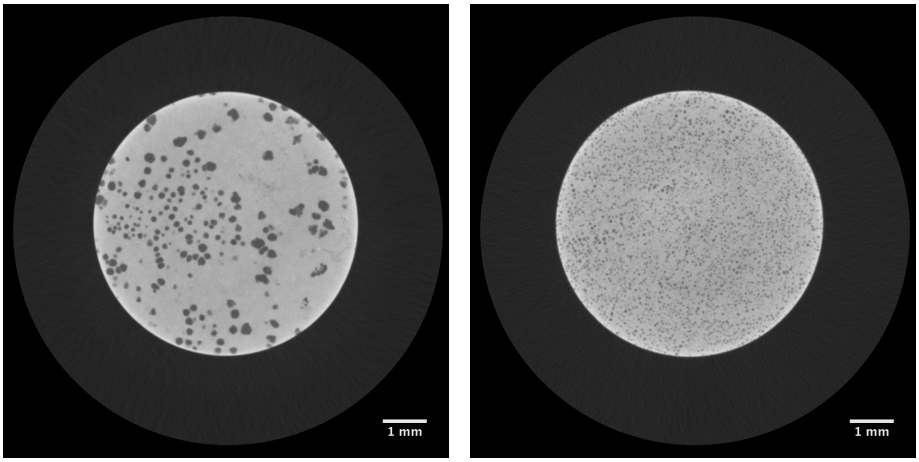

Figure 4-7 A virtual slice through two tomographical reconstructions of cast iron (left:Sand Casting; Right: Chill casting)

4.2.4. Fatigue test procedure

Constant amplitude axial fatigue tests were conducted on cylindrical specimens in ambient air according to standard ASTM E466-7 at R = -1 (ASTM E466-07, 2007). The specimens were cyclically loaded using a sinusoidal signal at 30 Hz. The specimens were tested until final fracture, or at least 1 million cycles. In Table 4-1, the list of specimens and the test characteristic are shown.

Table 4-1 Test information for fatigue samples

Speciemn #	Max Load [kN]	Cycles to failure	Casting type
269-1	8.00	3,781	Sand
269-19	7.00	11,715	Sand
308-8	10.50	29,886	Sand
338-13	5.00	596,781	Sand
626-02	8.00	38,680	Chill
656-1	9.00	8,133	Chill
656-4	9.00	7,369	Chill
656-13	9.00	1,176	Chill

The specimens were chosen from several numbers of samples. These samples were used to estimate a *SN* curve representing the two casting methods (Sand casting and

chill casting); for further details see (Mirzaei Rafsanjani H. , et al., 2014). The number of test data used to estimate the *SN* curves is listed in Table 4-2.

Table 4-2 The number of Fatigue samples that used to extract SN curve

Manufacturing Method	Broken	Run-out
Sand Casting	713	114
Chill Casting	302	107

The equations (3-10) and (3-12) are used for estimation of the parameters for Weibull models. The results of the statistical analyses using the Weibull distribution are shown in Table 4-3. The Figure 4-8 shows the fatigue lives of specimens based on the data from Table 4-1. The number of data in Figure 4-1 are vey low and it isdifficult to draw conclusion but, as could be expect, the higher stress amplitude would lead to lower fatigue life in components.

Table 4-3 Estimated statistical parameters from tests with Weibull distribtuions

Manufacturing Method	σ_f[Mpa]	m	b_n
Sand Casting	1260.84	10.44	0.9
Chill Casting	952.21	19.21	0.76

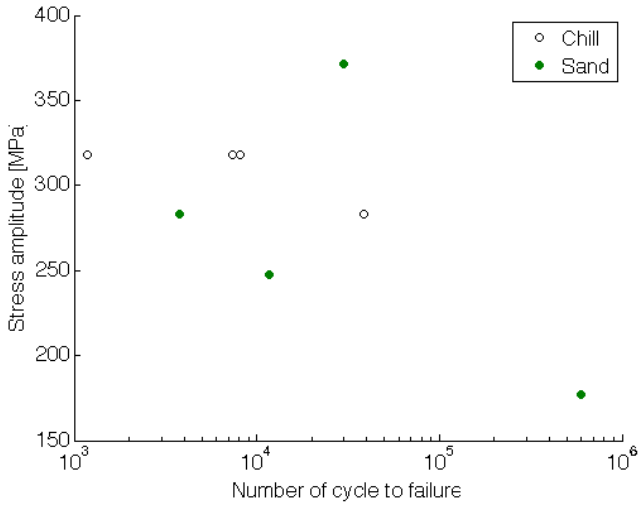

Figure 4-8 Fatigue life scatter of fatigue test specimens (Sand casting)

4.3. General statistical analysis of sand casting specimens

The total number of detected nodules in the sand casting specimens, the total volume and number of detected nodules per volume are listed in Table 4-4. Further, the main statistical descriptions of the nodules are listed in Appendix B. The GEV distribution parameters, for each specimen, are listed in Table 4-5 (see equation (4-1)). Note, all the nodules are considered as basis for the parameters in Table 4-5.

Table 4-4 The number of nodules and total volume for Sand Casting Specimens

Specimen ID	Number of nodules	Total Volume [mm^3]	Nodules per volume
269-1	20730	711.52	26.18
269-19	26663	654.06	36.27
308-8	22195	646.63	30.19
338-13	38069	671.92	51.78

Table 4-5 The GEV distribution parameters for each specimen (Sand Casting)

Specimen Number	269-1	269-19	308-8	338-13
Shape parameter, ζ	-0.112	-0.080	-0.142	-0.061
Scale parameter, σ (mm)	0.010	0.008	0.010	0.007
Location parameter, μ (mm)	0.024	0.021	0.022	0.018

According to Table 4-5, the shape parameters are less than zero and consequently, the Type III GEV (reverse weibull distribution) could be the fitted distribution. To compare the fit of GEV and Weibull distributions, the qq-plot of both distributions are shown in the following figures for each specimen. It is seen that the best fits are obtained by the Weibull distribution, especially in the upper, most important tail.

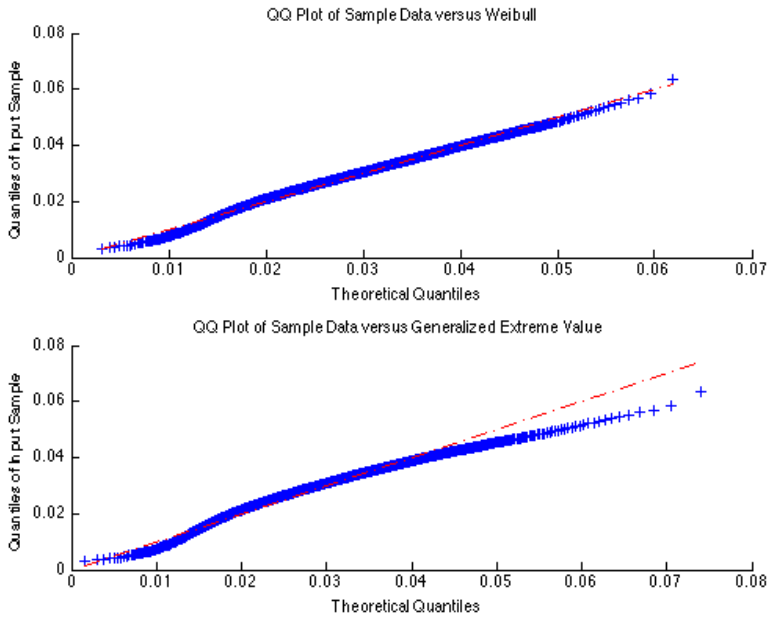

Figure 4-9 qq-plots of GEV and Weibull distributions for all defects for specimen 269-1

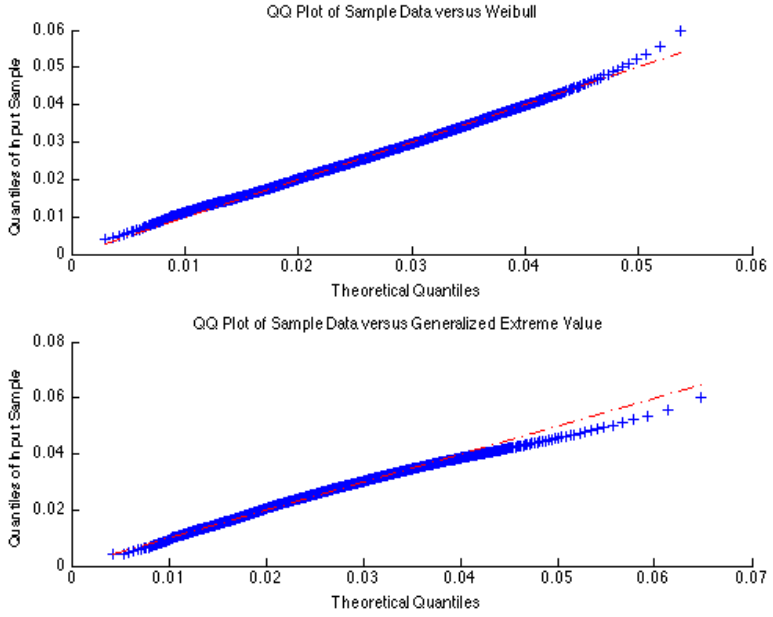

Figure 4-10 qq-plots of GEV and Weibull distributions for all defects for specimen 269-19

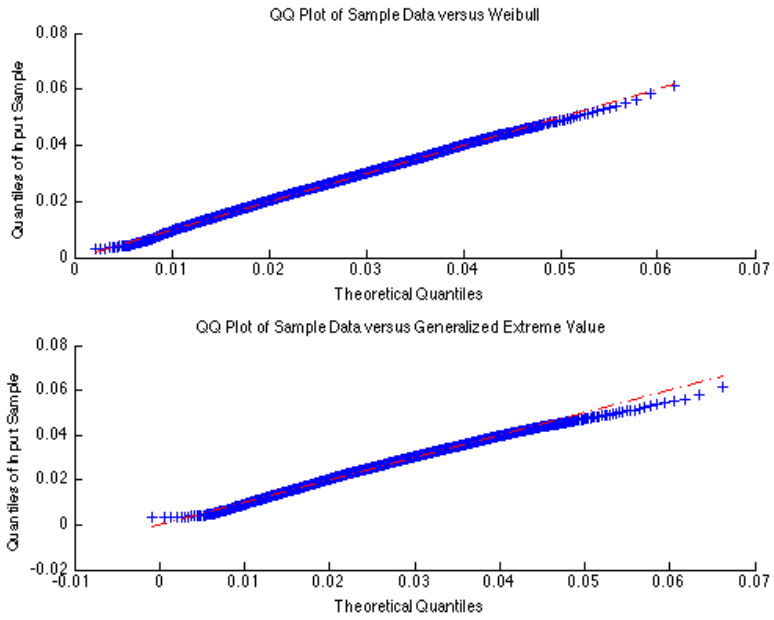

Figure 4-11 qq-plots of GEV and Weibull distributions for all defects for specimen 308-8

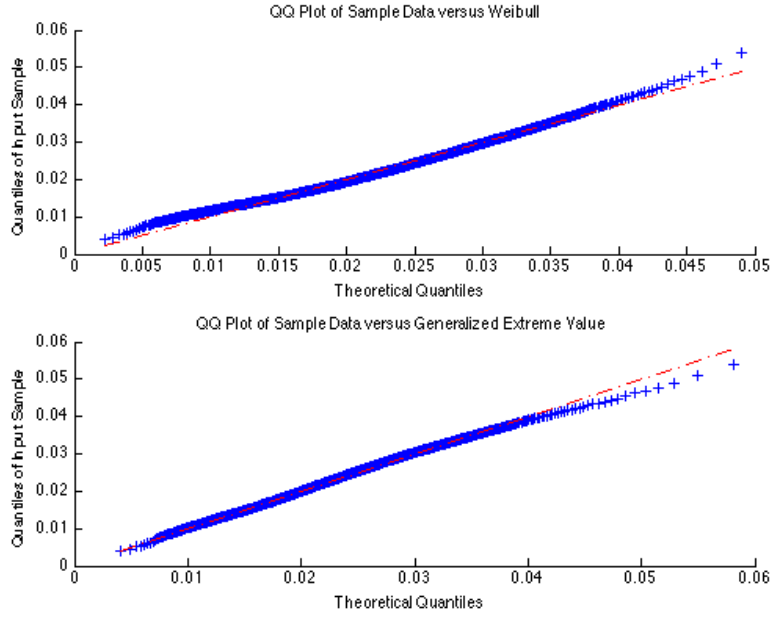

Figure 4-12 qq-plots of GEV and Weibull distributions for all defects for specimen 338-13

Furthermore, the empirical CDF (Cumulative Density Function) is shown in the following figures for all specimens. In these figures, the blue line is the empirical and the red line is the fitted GEV and the black line is the Weibull fit.

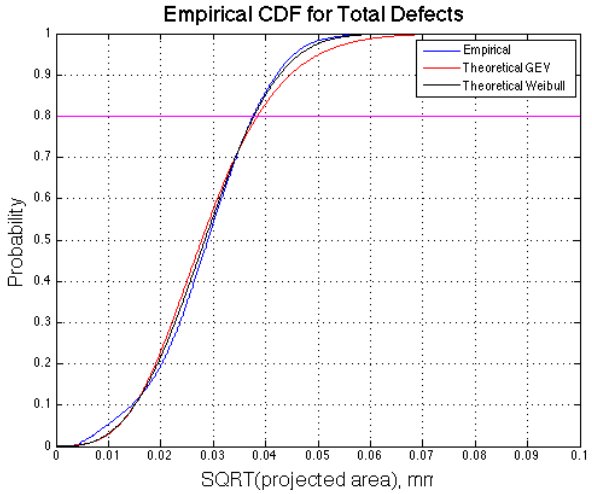

Figure 4-13 The empirical CDF of all nodules for specimen 269-1

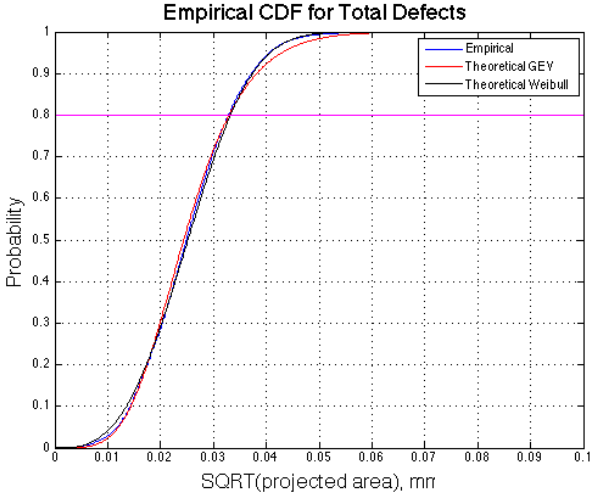

Figure 4-14 The empirical CDF of all nodules for specimen 269-19

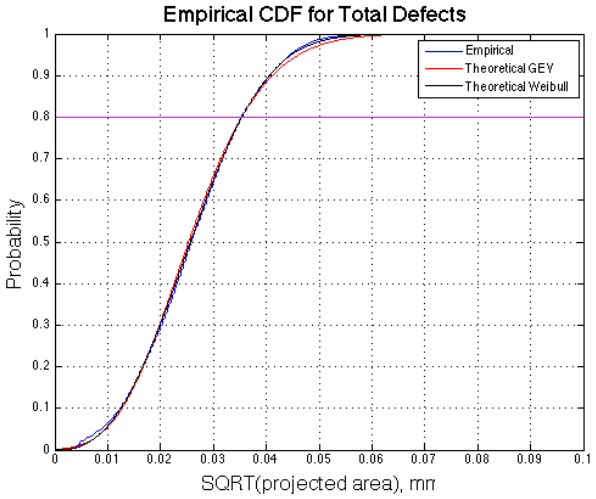

Figure 4-15 The empirical CDF of all nodules for specimen 308-8

The "magenta line" shows the 80% quantile for each empirical CDF. In the following, the data are filtered based on the probability; that means that only the largest nodules are considered. Each category is labeled as PSXX where XX stands for the probability level that is considered. For example, PS80 stands for nodules above the 80% quantile, i.e. only the 20% largest nodules are considered in category of PS80. Based on this labeling, we consider PS80, PS85, PS90, PS95, PS96, PS97, PS98 and PS99.

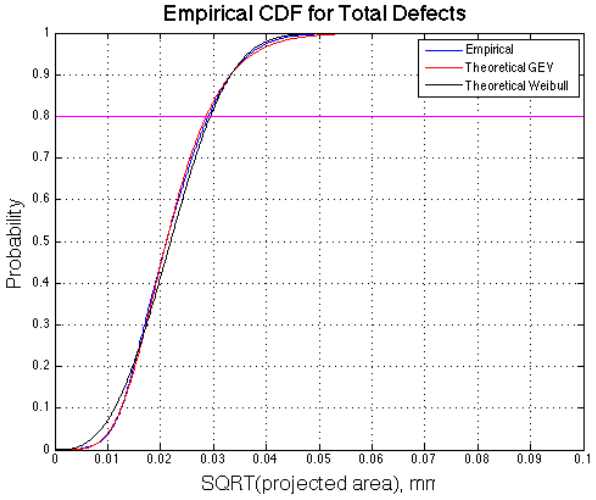

Figure 4-16 The empirical CDF of all nodules for specimen 338-13

Like Table 4-5, the GEV distribution parameters for each category for each specimen are estimated and are listed in Appendix C. In specimen 269-1, the number of nodules for group PS99 is less than 30, and therefore the parameters are not estimated (due to too high statistical uncertainty).

Moreover, in Appendix D, the qq-plots for nodule sizes for the different specimens (for PS95) based on the GEV and Weibull distributions are shown. From the figures in Appendix D, it is seen that generally the GEV distribution fit better than Weibull distribution.

Furthermore, the evaluation of the "Sphericity" versus "Equivalent Size" for each specimen is described in Appendix E. Generally, there is a slight tendency that when the Equivalent size increases, the sphericity decreases. Moreover, plots of the "Aspect Ratio" vs. "Equivalent Size" are shown for each specimen in Appendix F. Based on the figures in Appendix F, there is no indication of a relation/correlation between "Aspect Ratio" and " Equivalent Size".

4.4. Statistical analyses based on division in sub-volume for sand casting

In this section, the total volume is divided in 2 and 4 sub-volumes (each with approximately the same volume). The statistical parameters are estimated in each volume and are compared to each other.

4.4.1. Statistical analyses for 2 sub-volumes

In this section, the total volume is divided in two equal sub-volumes. Further, this analysis is carried out for all different categories of "PS80, PS85, … , PS99" for all specimens.

4.4.1.1 Statistical analyses for specimen 269-1

The numbers of nodules detected are listed in Table 4-6. In this specimen, the PS99 is not considered, because the number of nodules for this specimen in the category PS99 is less than 30. Note, the geometrical position of nodules in sub-volume 1 along z-axis must be lower than -27.29 and similarly, the geometrical position of the nodules in sub-volume 2 along z-axis must be higher than -27.29 (the locations of nodules are evaluated based on coordinate system of scanning set-up) (see Appendix A).

Table 4-6 The number of nodules for components divided in 2 sub-volumes (specimen 269-1)

	PS80	**PS85**	**PS90**	**PS95**	**PS96**	**PS97**	**PS98**
Sub-volume 1	1861	1200	637	170	121	65	31
Sub-volume 2	1858	1244	610	172	121	71	34

Based on the categories in Table 4-6, the mean values of nodule sizes for each sub-volume (for each group PS80, PS85, etc.) are shown in Figure 4-17. It is seen that the mean volumes of nodule size do not change significantly when comparing the two sub-volumes, but as expected the mean value increases with the PS-quantile. Note that when the number of data is less than 30 (PS99), the difference in mean values is obvious but in other cases the differences of mean values are not significant (moreover, the t-test or ANOVA can be used to compare the difference of mean values).

In addition, the standard deviations of nodule sizes for each sub-volume (for each thresholds PS80, PS85, etc.) are shown in Figure 4-18. According to Figure 4-18, due to the decrease in number of data, statistical uncertainties increase and this can explain the difference in the standard deviations.

4.4.1.2 Statistical analyses for specimen 269-19

The number of nodules that is detected is listed in Table 4-7. Like in the previous section, the mean values of nodule sizes for each sub-volume are shown in Figure 4-19. It is seen that the mean values of nodule sizes for thresholds less than PS90 do not change significantly but for thresholds PS95, PS96, …, PS99 the difference in mean values is significant. By reviewing the data, it is concluded that 8 out of the 10 largest nodules are located in sub-volume 2 and this could affect the mean value in the Figure 4-19 (moreover, the t-test or ANOVA may be used to compare the difference in mean values).

Futhermore, the standard deviations of nodule sizes for each sub-volume (for each thresholds PS80, PS 85, etc.) are shown in Figure 4-20. According to this, due to the decrease in number of data, statistical uncertainties increase and this can explain the difference of standard deviations.

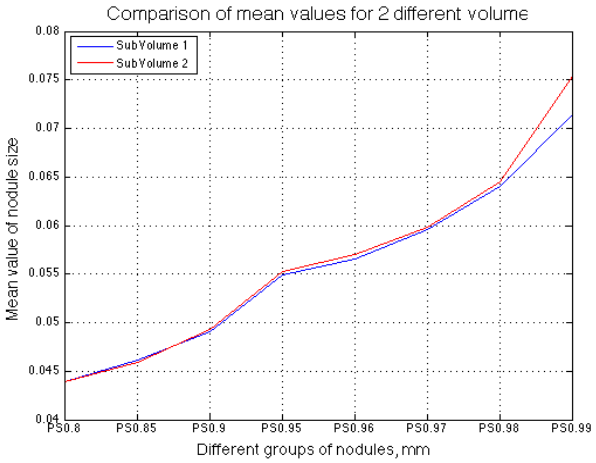

Figure 4-17 The comparison of mean values for each volume based on different categories for specimen 269-1

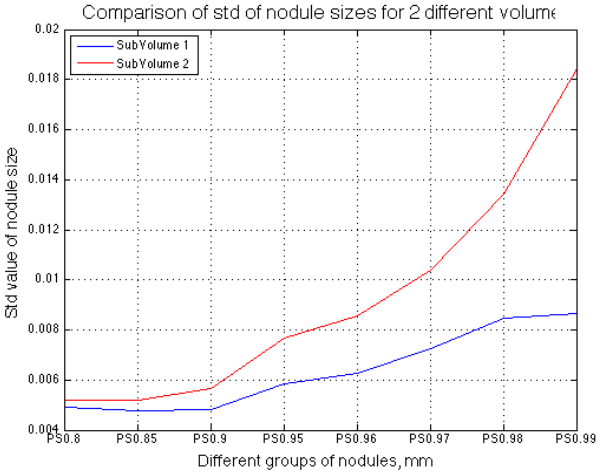

Figure 4-18 The comparison of standard deviation for each volume based on different categories for specimen 269-1

Table 4-7 The number of nodules for components divided in 2 sub-volumes (specimen 269-19)

	PS80	**PS85**	**PS90**	**PS95**	**PS96**	**PS97**	**PS98**	**PS99**
Sub-volume 1	2915	2105	1242	437	321	217	121	50
Sub-volume 2	2337	1624	952	338	244	160	99	51

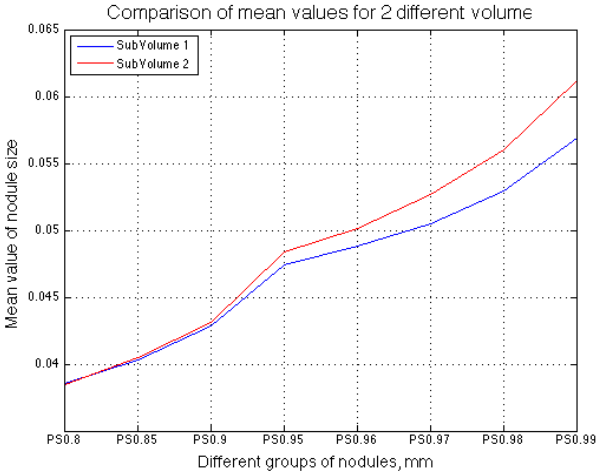

Figure 4-19 The comparison of mean values for each volume based on different categories for specimen 269-19

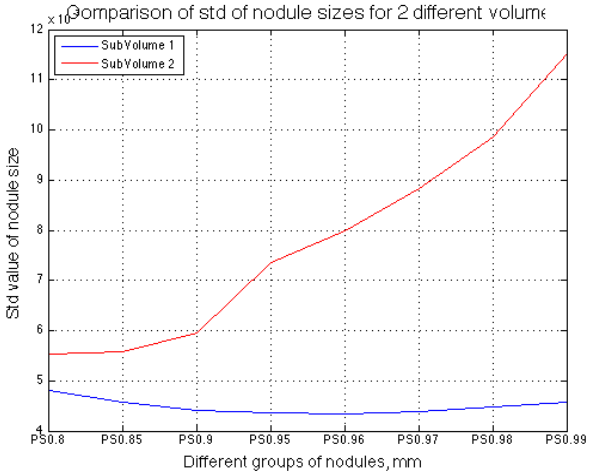

Figure 4-20 The comparison of standard deviation for each volume based on different categories for specimen 269-19

4.4.1.3 Statistical analyses for specimen 308-8

The number of nodules that is detected is listed in Table 4-8. Like in previous sections, the mean values of nodule sizes for each sub-volume shown in Figure 4-21, are not significantly different. Futhermore, the standard deviations of nodule sizes for each sub-volume (for each thresholds PS80, PS 85, etc.) are shown in Figure 4-22. According to this, the standard deviations are significantly different and similar to the other specimens.

Table 4-8 The number of nodules for components divided in 2 sub-volumes (specimen 308-8)

	PS80	**PS85**	**PS90**	**PS95**	**PS96**	**PS97**	**PS98**	**PS99**
Sub-volume 1	2155	1557	944	316	228	124	66	24
Sub-volume 2	2241	1713	1117	467	341	214	122	48

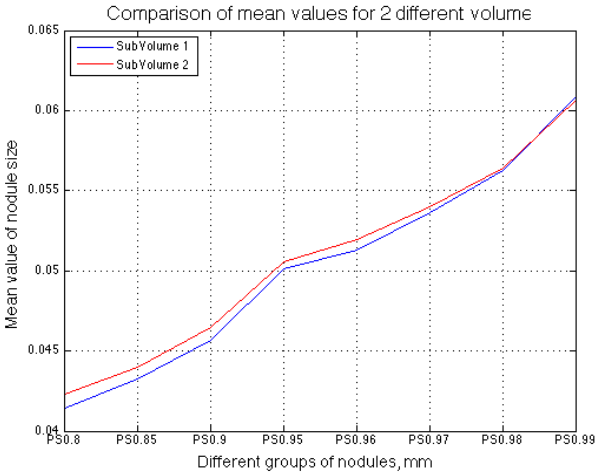

Figure 4-21 The comparison of mean values for each volume based on different categories for specimen 308-8

4.4.1.4 Statistical analyses for specimen 338-13

The number of nodules that is detected is listed in Table 4-9. Like in previous sections, the mean values of nodule sizes for each sub-volume shown in Figure 4-23, are not significantly different. Futhermore, the standard deviations of nodule sizes for each sub-volume (for each thresholds PS80, PS 85, etc.) are shown in Figure 4-24. According to this, the standard deviaion is significantly different as above.

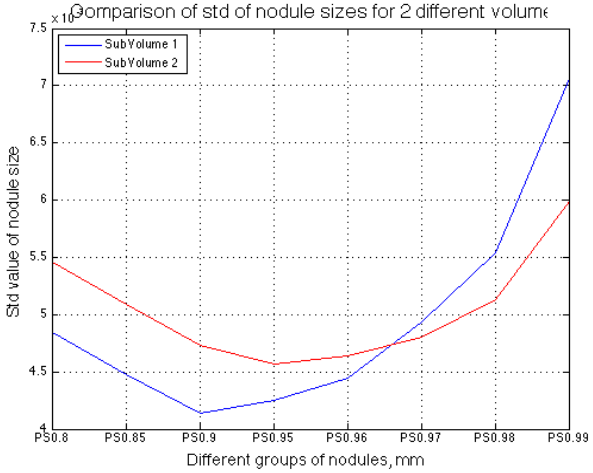

Figure 4-22 The comparison of standard deviation for each volume based on different categories for specimen 308-8

Table 4-9 The number of nodules for components divided in 2 sub-volumes (specimen 338-13)

	PS80	**PS85**	**PS90**	**PS95**	**PS96**	**PS97**	**PS98**	**PS99**
Sub-volume 1	3779	2744	1685	761	580	400	217	84
Sub-volume 2	4300	3257	2079	909	710	477	267	111

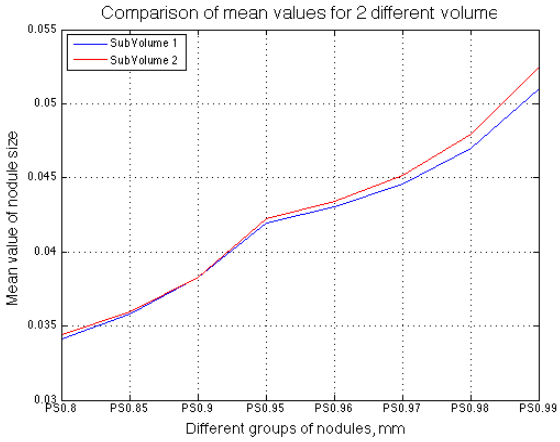

Figure 4-23 The comparison of mean values for each volume based on different categories for specimen 338-13

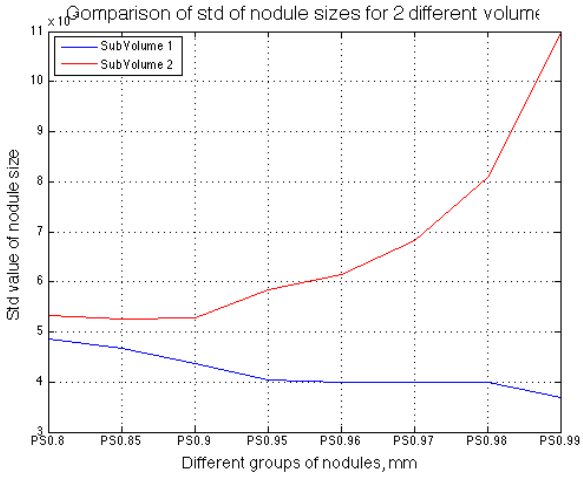

Figure 4-24 The comparison of standard deviation for each volume based on different categories for specimen 338-13

4.4.2. Statistical analyses for 4 sub-volumes

In addition, the total volume is also divided into four sub-volumes. Like in previous section, the analysis is carried out for all specimens for all different thresholds of "PS80, PS 85, …, PS99".

4.4.2.1 Statistical analyses for specimen 269-1

The number of nodules that is detected is listed in Table 4-10. Note, that if the number of nodules in the groups PS97, PS98 and PS99 is less than 30 and they are not considered for statistical analysis. Like the 2 sub-volume section, the mean value of the nodule sizes based on projected surface for each sub-volume is shown in Figure 4-25. According to Figure 4-25, PS98 has a low number of data (especially in sub-volume 2) and consequently the mean value of this group is different compared to the other sub-volumes. Moreover, when the number of data is less than 30 (PS98), the difference in mean values is obvious but in other cases the differences of mean values are not significant. In addition, the standard deviation of nodule sizes is shown in Figure 4-26, indicating similar behavior as above.

Table 4-10 The number of nodules for components divided in 4 sub-volumes (specimen 269-1)

	PS80	**PS85**	**PS90**	**PS95**	**PS96**	**PS97**	**PS98**
Sub-volume 1	1069	713	385	105	76	42	23
Sub-volume 2	792	487	252	65	45	23	8
Sub-volume 3	861	583	308	94	69	44	21
Sub-volume 4	997	661	302	78	52	26	13

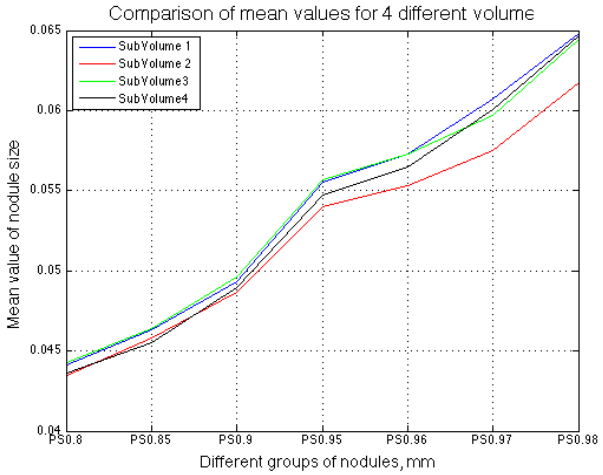

Figure 4-25 The comparison of mean values for each volume based on different categories for specimen 269-1 (4 sub-volumes)

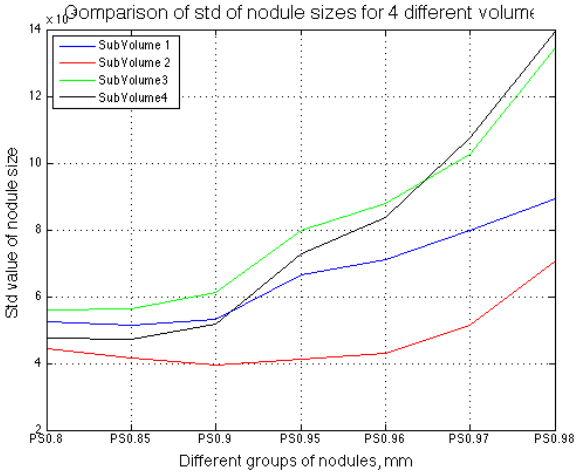

Figure 4-26 The comparison of standard deviations for each volume based on different categories for specimen 269-1 (4 sub-volumes)

4.4.2.2 Statistical analyses for specimen 269-19

The statistical analysis is carried out as in above sections. The number of nodules that is detected is listed in Table 4-11 with mean values shown in Figure 4-27 and the standard deviations are shown in Figure 4-28. It is seen that the difference in mean values increase when the number of data decrease.

Table 4-11 The number of nodules in specimen 269-19 divided in 4 sub-volumes

	PS80	**PS85**	**PS90**	**PS95**	**PS96**	**PS97**	**PS98**	**PS99**
Sub-volume 1	1595	1162	688	230	167	113	59	26
Sub-volume 2	1320	943	554	207	154	104	62	24
Sub-volume 3	1056	754	444	182	138	93	62	37
Sub-volume 4	1281	870	508	156	106	67	37	14

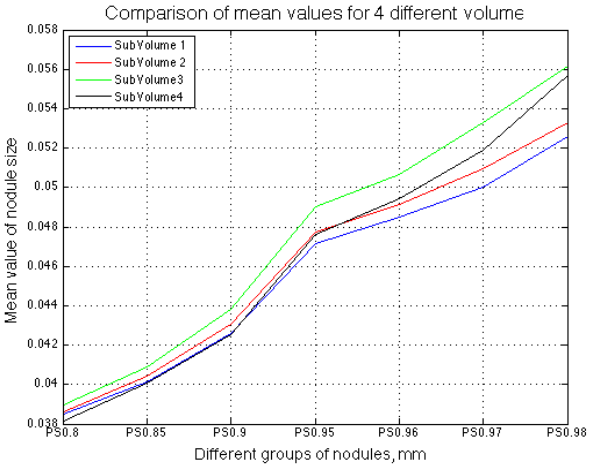

Figure 4-27 The comparison of mean values for each volume based on different categories for specimen 269-19 (4 sub-volume)

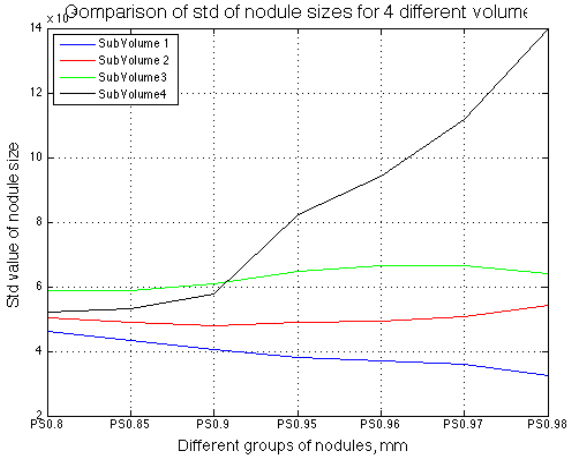

Figure 4-28 The comparison of standard deviation values for each volume based on different categories for specimen 269-19 (4 sub-volume)

4.4.2.3 Statistical analyses for specimen 308-8

The number of nodules detected is listed in Table 4-12. The number of nodules in sub-volumes PS98 and PS99 are less than 30 and are therefore not considered for the statistical analysis.

Table 4-12 The number of nodules in specimen 308-8 divided in 4 sub-volumes

	PS80	**PS85**	**PS90**	**PS95**	**PS96**	**PS97**	**PS98**	**PS99**
Sub-volume 1	1103	753	443	133	97	53	27	7
Sub-volume 2	1052	804	501	183	131	71	39	17
Sub-volume 3	1069	806	503	201	144	86	44	15
Sub-volume 4	1172	907	614	266	197	128	78	33

The mean values are shown in Figure 4-29. It is seen that the mean value of sub-volume 4 is larger than all the others and this is likely due to the largest nodules located in this sub-volume.

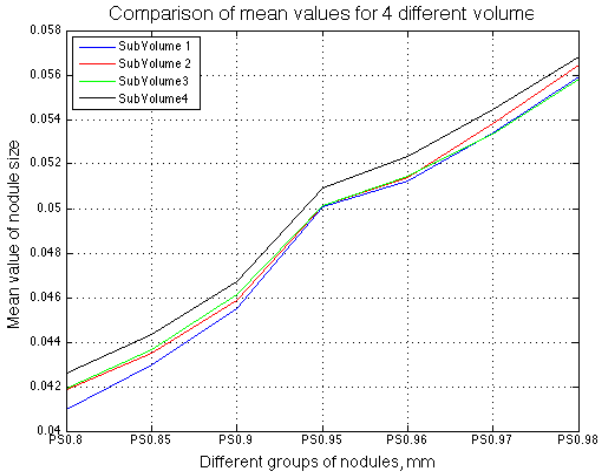

Figure 4-29 The comparison of mean values for each volume based on different categories for specimen 308-8 (4 sub-volume)

Furthermore, the standard deviation of nodule sizes are shown in Figure 4-30 indicating similar behavior as above.

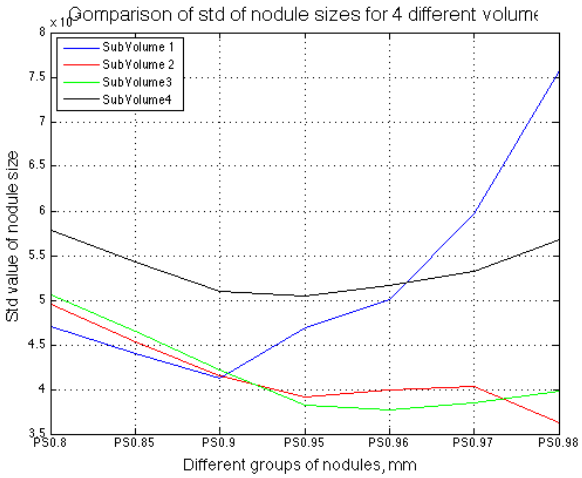

Figure 4-30 The comparison of the standard deviation values for each volume based on different categories for specimen 308-8 (4 sub-volume)

4.4.2.4 Statistical analyses for specimen 338-13

The number of nodules detected is shown in Table 4-13. In Figure 4-31, the mean values of the nodule sizes are shown. It is seen that the mean values of sub-volume 3 are higher than all the others and also that the other sub-volumes are not significantly different. In addition, the standard deviation is shown in Figure 4-32. A similar behaviour as above is observed.

Table 4-13 The number of nodules for specimen 338-13 divided in 4 sub-volumes

	PS80	**PS85**	**PS90**	**PS95**	**PS96**	**PS97**	**PS98**	**PS99**
Sub-volume 1	1986	1427	898	390	289	193	109	39
Sub-volume 2	1793	1317	787	371	291	207	108	451
Sub-volume 3	1874	1428	896	415	330	233	129	57
Sub-volume 4	2426	1829	1183	494	380	244	138	54

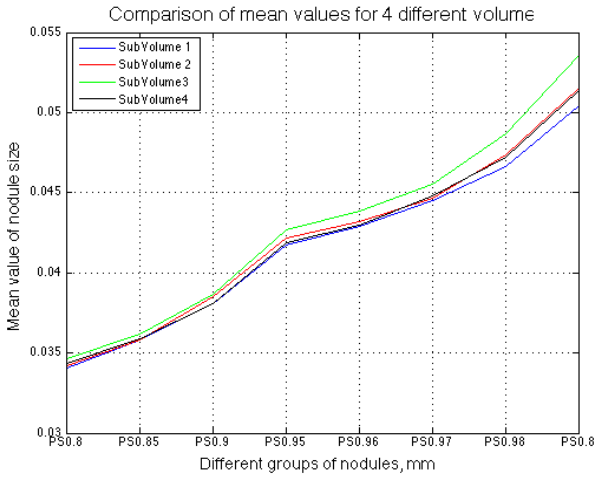

Figure 4-31 Comparison of mean values for each volume based on different categories for specimen 338-13 (4 sub-volume)

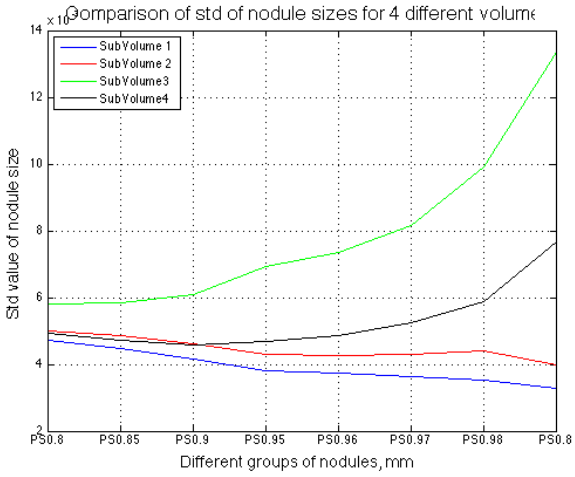

Figure 4-32 Comparison of standard deviation values for each volume based on different categories for specimen 338-13 (4 sub-volume)

4.5. Statistical analysis of chill casting specimens

The statistical analysis is carried out for chill casting samples as for the sand casting specimens. The total number of detected nodules in chill casting specimens, the total volume and number of detected nodules per volume are listed in Table 4-14. Further, the main statistical descriptions of the nodules of specimens are listed in

Appendix B. The GEV distribution parameters for each specimen are listed in Table 4-15 considering all nodules.

Table 4-14 The number of nodules and total volume for Chill Casting Specimens

Specimen ID	Number of nodules	Total Volume [mm^3]	Nodules per volume
626-2	222528	657.94	302.70
656-1	184674	640.75	272.15
656-4	225415	697.38	284.73
656-13	220608	642.25	325.10

Table 4-15 The GEV distribution parameters for each specimen (Chill Casting)

Specimen Number	**626-2**	**656-1**	**656-4**	**656-13**
Shape parameter, ζ	-0.039	-0.053	-0.051	-0.047
Scale parameter, σ (mm)	0.002	0.003	0.003	0.002
Location parameter, μ (mm)	0.008	0.009	0.009	0.009

To compare the GEV and Weibull fits, qq-plot of both distributions are shown in the following figures for each specimen. It is seen that the best fits are obtained by the GEV distribution, especially in the upper tail. It is noted that these results are not similar to those for Sand casting components where the best fits are obtained with the Weibull distribution.

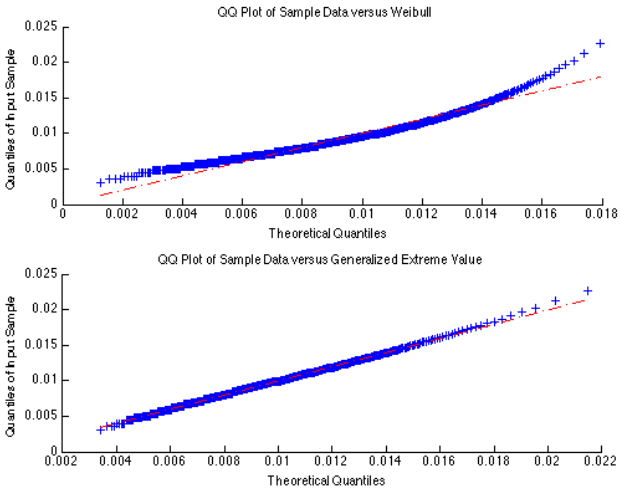

Figure 4-33 qq-plots of GEV and Weibull distributions for all defects for specimen 626-2

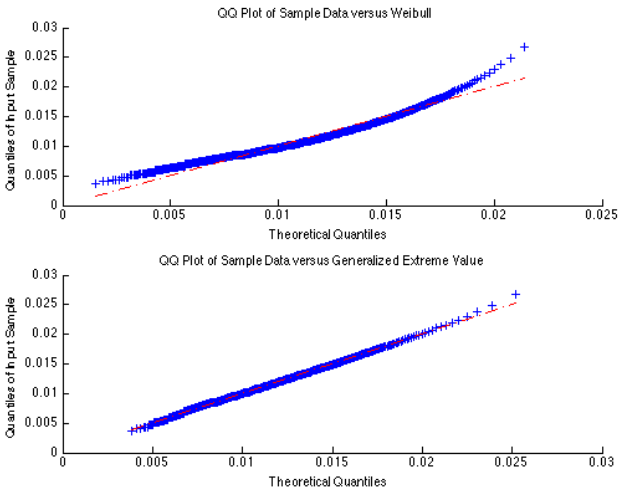

Figure 4-34 qq-plots of GEV and Weibull distributions for all defects for specimen 656-1

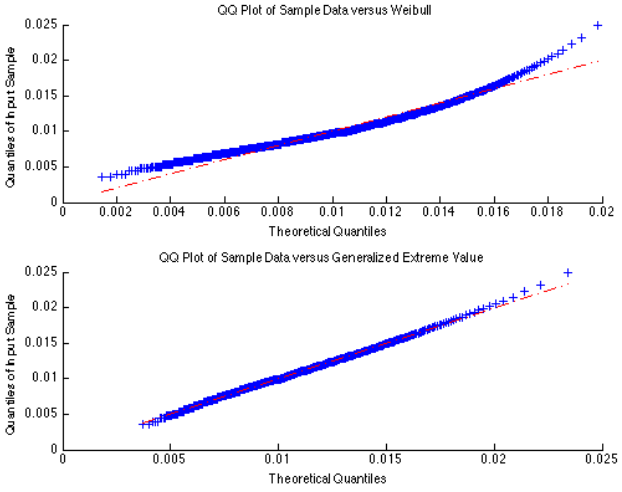

Figure 4-35 qq-plots of GEV and Weibull distributions for all defects for specimen 656-4

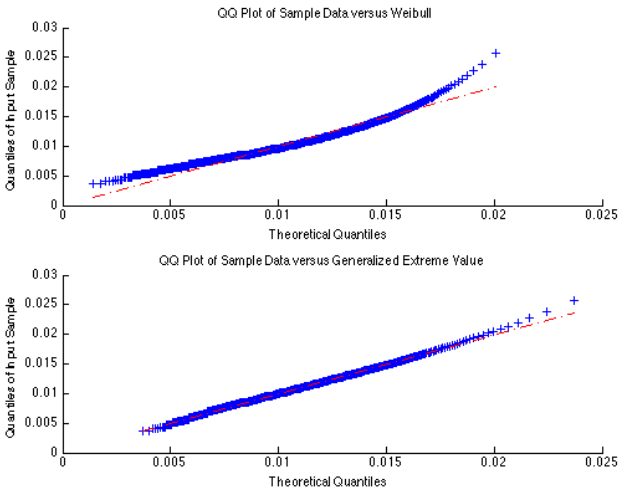

Figure 4-36 qq-plots of GEV and Weibull distributions for all defects for specimen 656-13

According to Table 4-5, the shape parameters are less than zero indicating that the best fits are obtained with the Type III GEV (reverse Weibull distribution). To compare the fits of GEV and Weibull, qq-plots of both distributions are shown in the following figures for each specimen. It is seen that the best fits are obtained by the reverse Weibull distribution, especially in the upper tail. Furthermore, the empirical CDFs (Cumulative Density Function) are shown in the following figures for all specimens. In these figures, the blue line is the empirical and the red line is the fitted GEV and the black line is Weibull fit.

The GEV distribution parameters for each category for each specimen are estimated and are listed in Appendix C. Moreover, in Appendix D, the qq-plots for nodule sizes for the different specimens (for PS999) based on the GEV and Weibull distributions are shown. From the figures in Appendix D, it is seen that generally the GEV distribution fits better than the Weibull distribution.

Like Sand Casting specimens, the evaluation of the "Sphericity" versus "Equivalent Size" for each specimen is described in Appendix E. Generally, there is a slight tendency that when the Equivalent size increases, the sphericity decreases, and this negative correlation is more clear for Chill casting specimens compare to Sand casting specimens. Moreover, plots of the "Aspect Ratio" vs. "Equivalent Size" are shown for each specimen in Appendix F. Based on the figures in Appendix F no correlation is indicated between the "Aspect Ratio" and the "Equivalent Size".

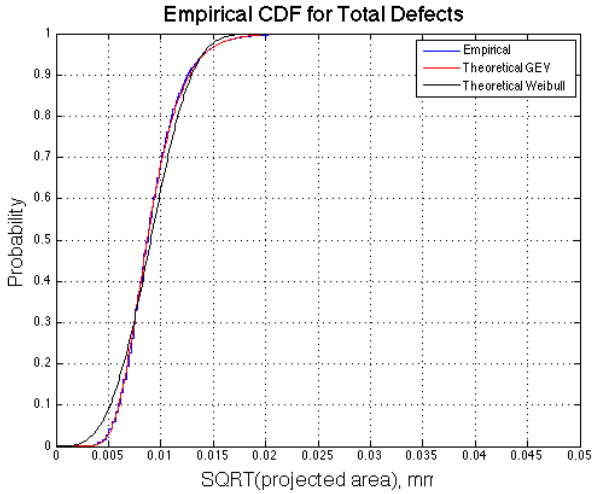

Figure 4-37 The empirical CDF of all nodules for specimen 626-2

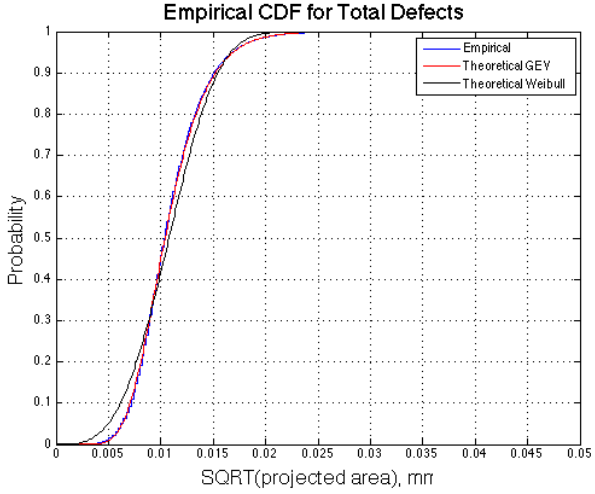

Figure 4-38 The empirical CDF of all nodules for specimen 656-1

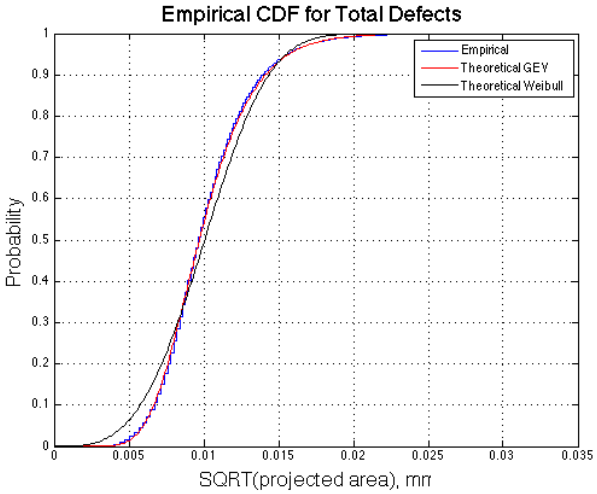

Figure 4-39 The empirical CDF of all nodules for specimen 656-4

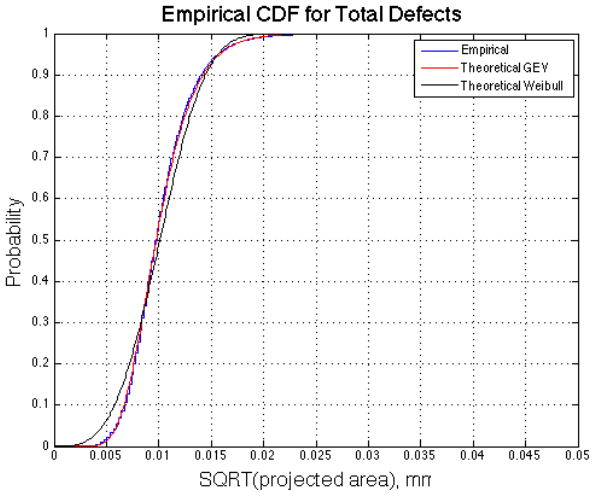

Figure 4-40 The empirical CDF of all nodules for specimen 656-13

4.6. Statistical analyses based on division in sub-volume for chill casting

Like in section 4.4, the total volume is divided in 2 and 4 sub-volume (each with approximately the same volume) and the statistical parameters are estimated in each volume and compared to each other.

4.6.1. Statistical analyses for 2 sub-volumes

The total volume is divided in two equal sub-volumes. Further, this analysis is carried for all different categories of "PS97, PS98, … , PS999" for all specimens.

4.6.1.1 Statistical analyses for specimen 626-2

The number of nodules detected is listed in Table 4-16.

Table 4-16 The number of nodules in specimen 626-2 divided in 2 sub-volumes

	PS97	**PS98**	**PS99**	**PS995**	**PS996**	**PS997**	**PS998**	**PS999**
Sub-volume 1	3230	2272	1163	608	496	359	250	141
Sub-volume 2	3343	2409	1349	755	640	542	410	259

Likewise, the mean values and standard deviations of the nodule sizes for each sub-volume (for each threshold) are shown in Figure 4-41 and Figure 4-42, respectively. It is seen that the mean volumes of nodule size do not change significantly when comparing the two sub-volumes, but of course the mean value increases with the PS-quantile. Further, due to the decrease in number of data, statistical uncertainties increase and this can explain the difference of standard deviations.

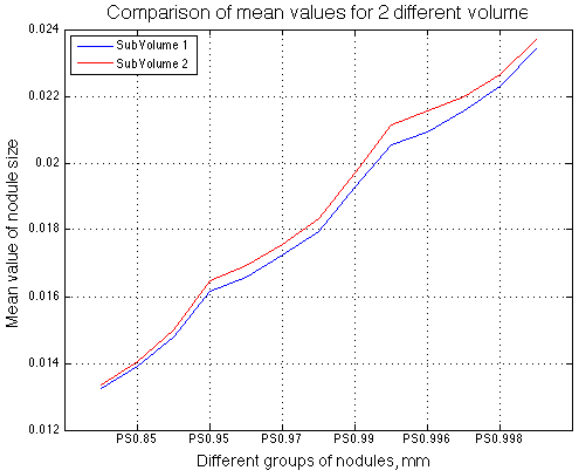

Figure 4-41 The comparison of mean values for each volume based on different categories for specimen 626-2

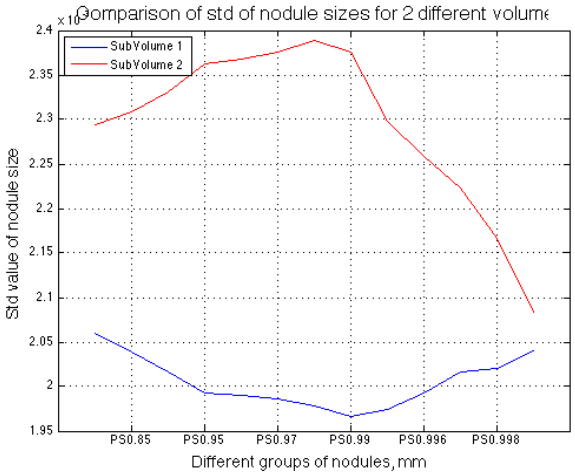

Figure 4-42 The comparison of standard deviation for each volume based on different categories for specimen 626-2

4.6.1.2 Statistical analyses for specimen 656-1

The number of nodules detected is listed in Table 4-17. Like in previous sections, the mean values and standard deviations of nodule sizes for each sub-volume are shown in Figure 4-43 and Figure 4-44, respectively. It is seen that the mean of nodule size for thresholds less than PS99 do not change significantly but for thresholds PS995, PS996, …, PS999, the difference of mean values is significant. By reviewing the data, it is concluded that 8 out of the 10 largest nodules are located in sub-volume 2 and this could affect the mean values in the Figure 4-43 (moreover, the t-test or ANOVA can be used to compare the difference of mean values). Aain no specific trend for standard deviations is observed.

Table 4-17 The number of nodules for components divided in 2 sub-volumes (specimen 656-1)

	PS97	**PS98**	**PS99**	**PS995**	**PS996**	**PS997**	**PS998**	**PS999**
Sub-volume 1	2625	1751	916	502	405	314	225	136
Sub-volume 2	2899	2003	1042	570	481	394	283	173

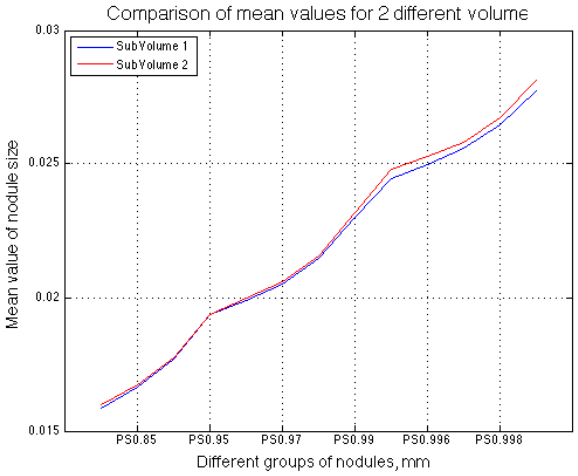

Figure 4-43 The comparison of mean values for each volume based on different categories for specimen 656-1

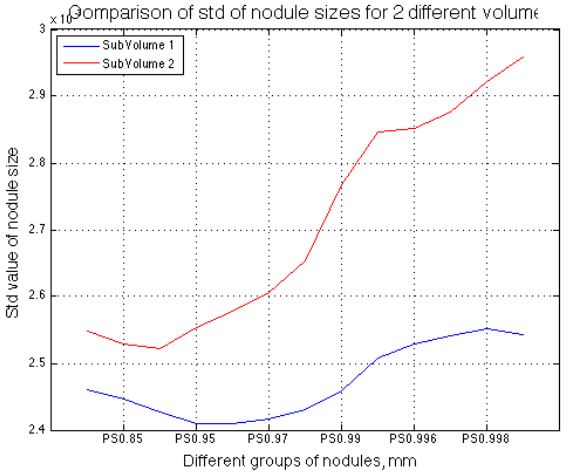

Figure 4-44 The comparison of standard deviation for each volume based on different categories for specimen 656-1

4.6.1.3 Statistical analyses for specimen 656-4

The number of nodules detected is listed in Table 4-18. As in previous sections, the mean values and standard deviations of nodule sizes for each sub-volume are shown in Figure 4-45 and Figure 4-46, respectively. It is seen that the mean of nodule size do not change significantly and there is no specific trend for standard deviations.

Table 4-18 The number of nodules for components divided in 2 sub-volumes (specimen 656-4)

	PS97	**PS98**	**PS99**	**PS995**	**PS996**	**PS997**	**PS998**	**PS999**
Sub-volume 1	3404	2322	1207	651	531	382	287	162
Sub-volume 2	3273	2307	1347	770	663	546	409	241

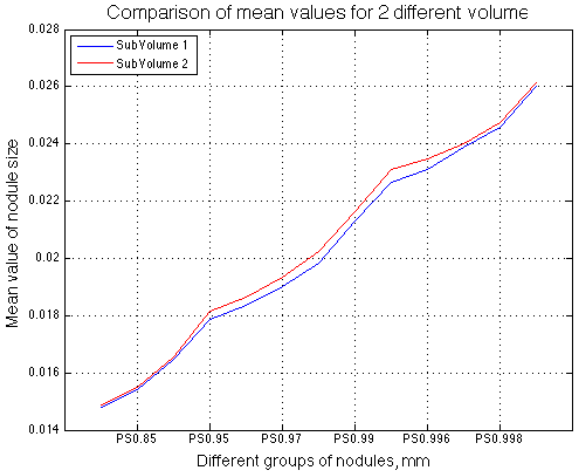

Figure 4-45 The comparison of mean values for each volume based on different categories for specimen 656-4

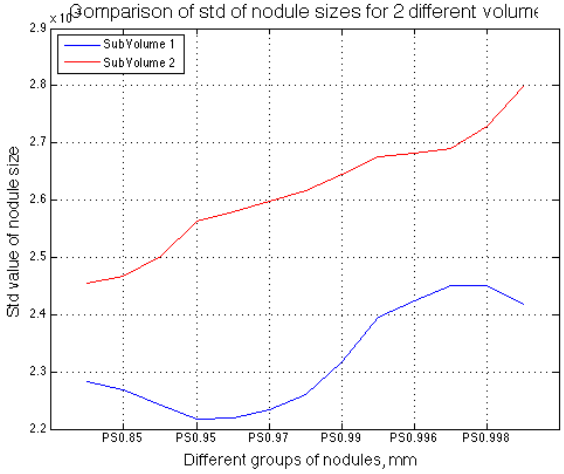

Figure 4-46 The comparison of standard deviation for each volume based on different categories for specimen 656-4

4.6.1.4 Statistical analyses for specimen 656-13

The number of nodules detected is listed in Table 4-19. The mean values and standard deviations of nodule sizes for each sub-volume are shown in Figure 4-47 and Figure 4-48, respectively. It is seen that the mean of nodule sizes for each sub-volume are not significantly different and that the standard deviations are significantly different.

Table 4-19 The number of nodules for components divided in 2 sub-volumes (specimen 656-13)

	PS97	**PS98**	**PS99**	**PS995**	**PS996**	**PS997**	**PS998**	**PS999**
Sub-volume 1	3350	2270	1260	701	606	479	352	201
Sub-volume 2	3139	2171	1261	737	647	525	405	264

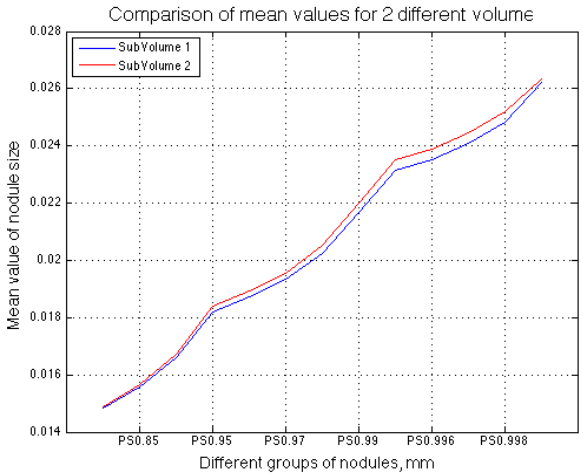

Figure 4-47 The comparison of mean values for each volume based on different categories for specimen 656-13

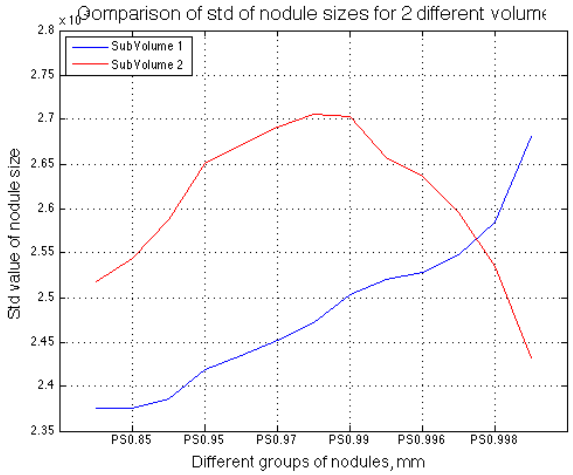

Figure 4-48 The comparison of standard deviation for each volume based on different categories for specimen 656-13

4.6.2. Statistical analyses for 4 sub-volumes

In this section, the total volume is divided in four sub-volumes. In following, the results for all chill casting specimen are explained.

4.6.2.1 Statistical analyses for specimen 626-2

The number of nodules detected is shown in Table 4-20. As for the 2 sub-volume section, the mean value and standard deviation of nodule sizes for each sub-volume are shown in Figure 4-49 and Figure 4-50, respectively. According to this figure, the trends of mean values are similar to previous cases and furthermore, the standard deviations are significantly different too.

Table 4-20 The number of nodules for components divided in 4 sub-volumes (specimen 626-2)

	PS97	**PS98**	**PS99**	**PS995**	**PS996**	**PS997**	**PS998**	**PS999**
Sub-volume 1	1111	720	315	137	110	73	49	28
Sub-volume 2	2119	1552	848	471	386	286	201	113
Sub-volume 3	2514	1925	1158	689	593	511	391	248
Sub-volume 4	829	484	191	66	47	31	19	11

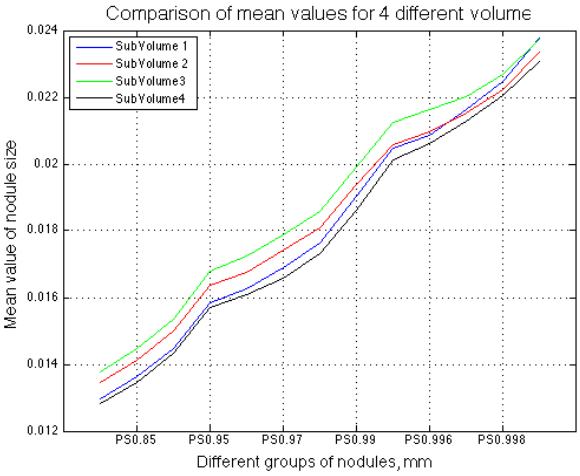

Figure 4-49 The comparison of mean values for each volume based on different categories for specimen 626-2 (4 sub-volumes)

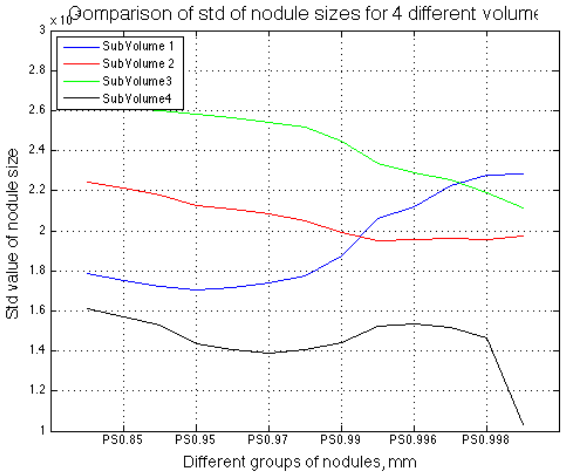

Figure 4-50 The comparison of standard deviation for each volume based on different categories for specimen 626-2 (4 sub-volumes)

4.6.2.2 Statistical analyses for specimen 656-1

The number of nodules is listed in Table 4-21 and the mean value is shown in Figure 4-51. It is seen that the difference in mean values increases when then number of data decrease. Furthermore, the standard deviations are shown in Figure 4-52. Hence, due to the decrease of the number of data, statistical uncertinties increase and the difference in standard deviations increase.

Table 4-21 The number of nodules for components divided in 4 sub-volumes (specimen 656-1)

	PS97	**PS98**	**PS99**	**PS995**	**PS996**	**PS997**	**PS998**	**PS999**
Sub-volume 1	1107	695	332	173	131	93	63	33
Sub-volume 2	1518	1056	584	329	274	221	162	103
Sub-volume 3	1760	1224	671	405	351	292	215	143
Sub-volume 4	1139	779	371	165	130	102	68	30

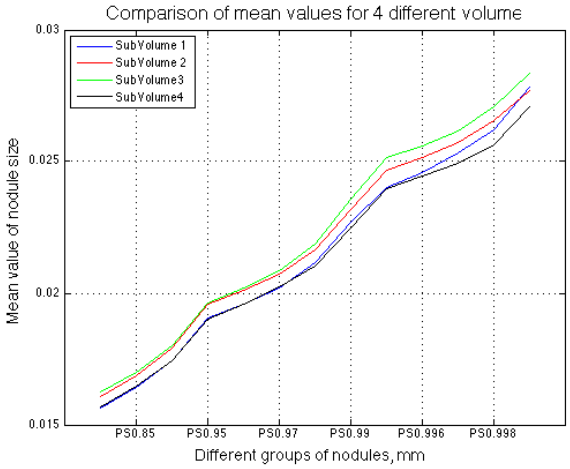

Figure 4-51 The comparison of mean values for each volume based on different categories for specimen 656-1 (4 sub-volumes)

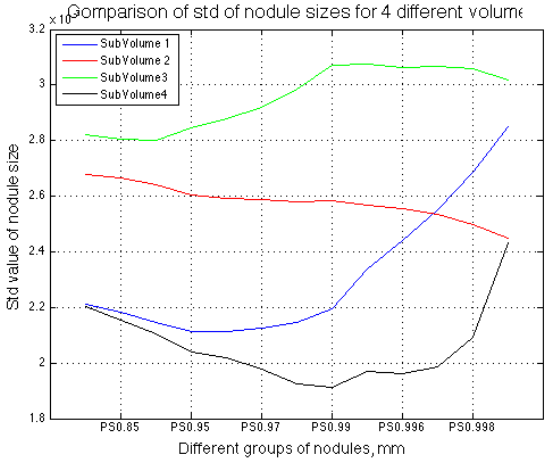

Figure 4-52 The comparison of standard deviation for each volume based on different categories for specimen 656-1 (4 sub-volumes)

4.6.2.3 Statistical analyses for specimen 656-4

The number of nodules is listed in Table 4-22 and the mean values are shown in Figure 4-53 with trends as in previous sections. Furthermore, the standard deviations are shown in Figure 4-54. Hence, due to the decrease of the number of data, statistical uncertainties increase and the difference in standard deviations increase.

Table 4-22 The number of nodules for components divided in 4 sub-volumes (specimen 656-4)

	PS97	**PS98**	**PS99**	**PS995**	**PS996**	**PS997**	**PS998**	**PS999**
Sub-volume 1	1349	856	403	181	137	96	68	29
Sub-volume 2	2055	1466	804	470	394	286	219	133
Sub-volume 3	2296	1719	1094	648	572	477	368	220
Sub-volume 4	977	588	253	122	91	69	41	21

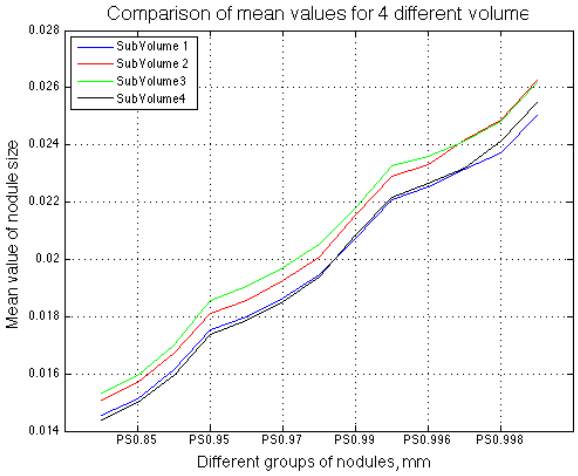

Figure 4-53 The comparison of mean values for each volume based on different categories for specimen 656-4 (4 sub-volumes)

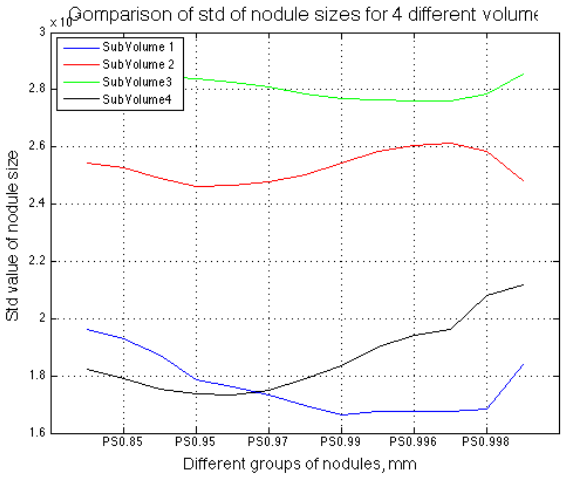

Figure 4-54 The comparison of standard deviation for each volume based on different categories for specimen 656-4 (4 sub-volumes)

4.6.2.4 Statistical analyses for specimen 656-13

The number of nodules is listed in Table 4-23 and the mean values are shown in Figure 4-55 with similar trends as above.

Table 4-23 The number of nodules for components divided in 4 sub-volumes (specimen 656-13)

	PS97	**PS98**	**PS99**	**PS995**	**PS996**	**PS997**	**PS998**	**PS999**
Sub-volume 1	1124	678	299	144	109	79	50	21
Sub-volume 2	2226	1592	961	557	497	400	302	180
Sub-volume 3	2346	1749	1097	661	583	480	376	250
Sub-volume 4	793	422	164	76	64	45	29	14

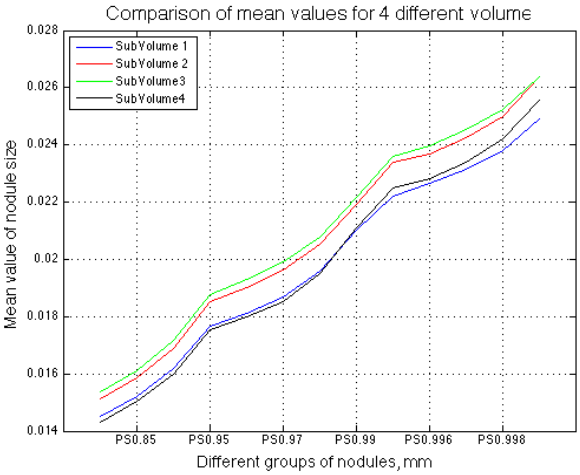

Figure 4-55 The comparison of mean values for each volume based on different categories for specimen 656-13 (4 sub-volumes)

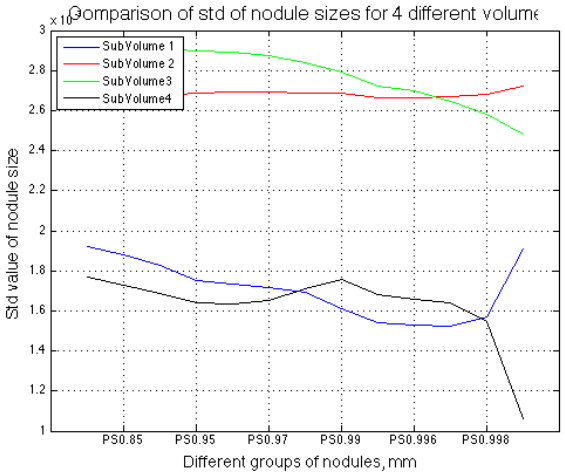

Figure 4-56 The comparison of standard deviation for each volume based on different categories for specimen 656-4 (4 sub-volumes)

Based on the statistical analysis, it is concluded that the mean values of nodule sizes for both sand casting and chill casting do not change significantly with volume. Hence, by scanning of only one part of a component, the mean value of nodules sizes could be expanded to the whole component, indicating a uniform, statistically homogeneous distribution of defects. Note, that this seems not to be the case for the

standard deviations, but probably this is due to larger statistical uncertainties in the estimate of the standard deviations.

Furthermore, the GEV distribution could be used to model the nodules sizes when maximum values considered for both sand casting and chill casting.

CHAPTER 5. EFFECTS OF DEFECTS

The relibility of casted components for wind turbines is generally highly dependent on defects introuced during manufacturing process. In this section a stochastic model is proposed for modelling of effects of defects/nodules including their influence on the fatigue life (Mirzaei Rafsanjani & Sørensen, 2015b). Basically, the nodules are assumed to be distributed randomly by a Poisson process where the defects form clusters consist of a parent defect and related defects around the parent defect. The fatigue life is dependent on the number, type, location and size of the defects in the component and is therefore quite uncertain and needs to be described by stochastic models (Mirzaei Rafsanjani & Sørensen, 2015b).

5.1. Defects/Nodules distribution model

Manufacturing of casted components often leads to some (small) defects that are distributed randomly in the volume of the components (Mirzaei Rafsanjani & Sørensen, 2015c). These defects are different according their size, type, orientation and etc. and influence on the load-bearing capacity of the components, see (Toft, Branner, Berring, & Sørensen, 2011) for a correspond model for defects in blades. Hence, an important factor affecting the strength of component is the presence of defects/nodules from processing and/or manufacturing (Mirzaei Rafsanjani & Sørensen, 2015b).

An important challenge related to materials containing nodules is to model the occurrence of nodules in the component volume (Mirzaei Rafsanjani & Sørensen, 2015b). In some cases, clustering of nodules is important and strongly influences the probability of failure. Clustering of two or more nodules within a small volume often decrease critically the load-bearing capacity and increases the stress concentration (Mirzaei Rafsanjani & Sørensen, 2015b). Hence, the number of nodules in each volume and the size / dimension of the nodules should be modeled according to their size, type, orientation and etc (Mirzaei Rafsanjani & Sørensen, 2015b).

In order to determine the probability of fracture failure, all initiating defects are divided into categories depending on their type (Todinov, 2000). In the categories, each nodule, according to its size, shape, and orientation etc., is characterized by the number of load cycles to failure at a specific local fatigue stress amplitude (Mirzaei Rafsanjani & Sørensen, 2015b). Each type of nodule i is thus characterized by a cumulative distribution function for the number of fatigue load cycles to failure, $F_{N,i}(n, R, \sigma)$, modeling the probability that fatigue failure does not occur within n load cycles with fatigue stress amplitude equal to σ and a given R-ratio (ratio of the minimum stress experienced during a cycle to the maximum stress experienced during a cycle), (Todinov, 2000; Mirzaei Rafsanjani & Sørensen, 2015b).

Hence, suppose that in a specimen with volume V_T, M types of defects exist (Mirzaei Rafsanjani & Sørensen, 2015b). It is important to emphasize that the nucleation of fatigue cracks in the groups of defects are assumed as statistically independent events. In other words, a fatigue crack in a particular group is not affected by fatigue crack in other groups (Mirzaei Rafsanjani & Sørensen, 2015b). Therefore, the nodules can be categorized in M groups of nodules such that the size, type and orientation etc. of nodules in each group are very close to each other. It is noted that each type of defects is assumed to be characterized by a cumulative distribution function $F_{N,i}(n, R, \sigma)$ for the number of load cycles to failure, see below (Mirzaei Rafsanjani & Sørensen, 2014).

Furthermore, it is assumed that the number of nodules of group j can be modeled by a multi-dimensional Poisson process (Mirzaei Rafsanjani & Sørensen, 2015b). Thus, if D is any region in the multi-dimensional space and $N(D)$ is the number of nodules in D, then (Mirzaei Rafsanjani & Sørensen, 2014)

$$P\left(N\left(D\right)=k\right)=\frac{\left(\lambda\left|D\right|\right)^{k}e^{-\lambda|D|}}{k!} \tag{5-1}$$

is the probability that the number of nodules in D is k. Equivalently, the density function of the number of nodules in group j in volume V of component is (Ravi Chandran & Jha, 2005):

$$P\left(k\right)=\frac{\left(\lambda_j V\right)^{k}e^{-\lambda_j V}}{k!} \tag{5-2}$$

where λ_j is the average number of nodules of group j (there is M different groups of nodules). The probability of occurrence of the number of nodules in different parts of the specimen can now be assessed using the Poisson model (Mirzaei Rafsanjani & Sørensen, 2014). Equations (5-1) and (5-2) are the general equations for modeling the nodule distribution of the j-th group of nodules (Mirzaei Rafsanjani & Sørensen, 2015b).

In the next step, the whole component is modeled. Suppose, that in a specimen with volume V_T, a smaller sub-volume $\mathrm{d}V_i$ is stressed to a stress amplitude $\sigma_{i,j}$ which is assumed to be uniform inside the sub-volume $\mathrm{d}V_i$, it is assumed that (Mirzaei Rafsanjani & Sørensen, 2015b)

$$V_T=\sum_{i=1}^{N_V}dV_i \tag{5-3}$$

where N_V is the number of sub-volumes $\mathrm{d}V_i$ in volume V_T. Fatigue cracks are assumed to initiate from surface cracks / nodules or from sub-surface (embedded) cracks / nodules. Sub-volume $\mathrm{d}V_i$ in Equation (5-3) is rewritten as (Ravi Chandran & Jha, 2005):

$$dV_i=\left(A_i+dA_i\right)dl \tag{5-4}$$

where, A_i is interior area of each smaller volume and dA_i is the area of the surface rim of a certain width wrapping around A_i such that the total cross-sectional area of the sample is A_i+dA_i, (Mirzaei Rafsanjani & Sørensen, 2015c)see Figure 5-1.

Whether a specimen fails by internal or surface crack initiation is related to whether there is a cluster of nodules at that location (Ravi Chandran & Jha, 2005).

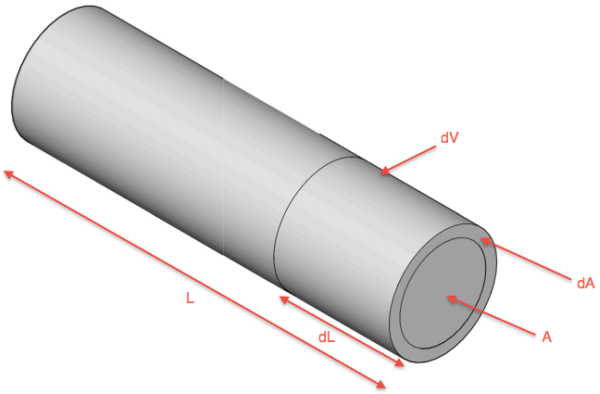

Figure 5-1 The model segment of specimen volume

In this context, three cases are considered (Ravi Chandran & Jha, 2005):

- If there is a finite probability that there are cluster nodules in the interior and no cluster nodules in the surface rim volume, implying the specimens to fail only by internal crack initiation (Ravi Chandran & Jha, 2005).
- If there is a finite probability that there are cluster nodules in the surface rim region and no cluster nodule in the interior, implying the specimens to fail only by surface crack initiation (Ravi Chandran & Jha, 2005).
- If cluster nodules exist both in the interior as well as in the surface rim volumes, then, the specimen is likely to fail by surface crack initiation only, because it is known that fatigue crack initiation at surface typically is accelerated by the air environment (Ravi Chandran & Jha, 2005).

The probability of occurrence of interior nodules, $P_{int,j}$, is the probability that one or more nodules from group j in A_i with no such nodules present in dA_i (Mirzaei Rafsanjani & Sørensen, 2015b). This can be written on the basis of Equations (5-2) and (5-4) as

$$P_{\text{int},i,j}\left(k\right)=\frac{\left(\lambda_j\left(A_i dl\right)\right)^k e^{-\lambda_j\left(A_i dl\right)}}{k!}e^{-\lambda_j\left(dA_i dl\right)} \tag{5-5}$$

Similarly, the probability of occurrence of surface nodules, $P_{surf,j}$, is equal to the probability that at least one or more nodule from group *j* will occur in dA_i regardless of a nodule from group *j* being absent or present in the interior area A_i (Mirzaei Rafsanjani & Sørensen, 2015c). In other words, the occurrence of a nodule in the interior does not matter as long as one surface nodule is present, since it will preferentially initiate a critical fatigue crack which is more critical than a nodule in A_i due to environmental effects (Ravi Chandran & Jha, 2005). The probability of surface-crack initiation is then given by the probability of presence of one or more nodules in dA_i (Ravi Chandran & Jha, 2005)

$$P_{surf,i,j}\left(k\right)=\frac{\left(\lambda_j\left(dA_i dl\right)\right)^k e^{-\lambda_j\left(dA_i dl\right)}}{k!} \tag{5-6}$$

In the following, the probability of fatigue failure of component due to existence of nodules will be modeled.

5.2. Probability of fatigue failure

In the previous section, the nodule location in the volume V_T is modeled by a Poisson model. The volume V_T is modeled as a "series system" of sub-volumes $\mathrm{d}V_i$. Hence, failure in any of the sub-volumes $\mathrm{d}V_i$ is assumed (conservatively) to result in 'collapse' in whole volume. The probability of failure of each sub-volume $\mathrm{d}V_i$ is denoted $P_{f,i}$ (Mirzaei Rafsanjani & Sørensen, 2015c). The probability $P_{f,i}$ is dependent on (Mirzaei Rafsanjani & Sørensen, 2015c)

- Probability of existence of nodules in sub-volume $\mathrm{d}V_i$.
- Probability of fatigue failure if nodules exist in sub-volume $\mathrm{d}V_i$.

As mentioned above, the nodules are categorized in *M* groups. For each one of these groups, the probability of failure is to be evaluated. Hence, the probability of failure of each sub-volume $\mathrm{d}V_i$ is written (Mirzaei Rafsanjani & Sørensen, 2015b)

$$P_{f,i}=\sum_{j=1}^{M}\Big[P\left(\text{defect of j-th group exist in } dV_i\right) \times P\left(\text{fatigue failure}\middle|\text{defect from j-th type/size exist}\right)\Big] \tag{5-7}$$

Equation (5-7) is applied for both interior and surface nodules and in each sub-volume $\mathrm{d}V_i$. As described above, it is assumed that the nodules follow a homogeneous Poisson process in the sub-volume $\mathrm{d}V_i$ (Mirzaei Rafsanjani & Sørensen, 2015c).The distribution function for the number of fatigue load cycles to failure given a nodule of group *j* in sub-volume *i*, $F_{N,i}(n, R, \sigma)$ is assumed to follow a Weibull distribution (Fjeldstad, Wormsen, & Härkegård, 2010). The Weibll distribution for fatigue life is explained in section 3.4.

$$F_{N,j}\left(n,R,\sigma_{i,j}\right)=1-\exp\left[-\left(\frac{n}{N_j(R,\sigma_{i,j})}\right)^{b_{n,j}}\right] \tag{5-8}$$

where $N_j(R, \sigma_{i,j})$ and $b_{n,j}$ are the shape and scale parameters of Weibull distribution. It is noted that these parameters are subject to statistical uncertainties, if modeled on the basis of test data and should be evaluated by statistical analysis methods such as Maximum Likelihood Method or Bootstrapping using available data sets (Mirzaei Rafsanjani & Sørensen, 2015a). n is the actual number of cycles in the lifetime [0, T_L] with stress range $\sigma_{i,j}$ and T_L is life time of the component:

$$n=\nu * T_L \tag{5-9}$$

where ν is the number of load cycles with the stress range $\sigma_{i,j}$ per year (Mirzaei Rafsanjani & Sørensen, 2015b).

Three cases are considered:

1. Fatigue test results are available for test specimens with defects/nodules that fulfil certain quality control requirements implying that some (relatively well defined, controlled) defects/nodules of various sizes and shapes will be present. A stochastic model for the fatigue life representative for sub-volume $\mathrm{d}V_i$ is given by the distribution function $F_N(n, R, \sigma_i)$ assuming that the sub-volume is subjected to a constant fatigue load represented by the fatigue stress σ_i.
2. Fatigue test results are available for test specimens with defects/nodules divided in M groups such that based on the fatigue tests stochastic models for the fatigue life can be obtained for sub-volumes $\mathrm{d}V_i$ for each group, j and given by the distribution function $F_{Nj}(n, R, \sigma_i)$.
3. Detailed fatigue test results are available for test specimens with only one (important / critical) defect/nodule in each of the groups $j = 1, \ldots, M$ such that stochastic models for the fatigue life can be obtained and given by the distribution function $F_{Nj,I}(n, R, \sigma_i)$ (Mirzaei Rafsanjani & Sørensen, 2015a).

Failure of a structural element of volume V_T subdivided in N_V sub-volumes is assumed to be modeled as a "series system" of independent failure events in sub-volumes $\mathrm{d}V_i$.

For case 1 the probability of failure is obtained by

$$P_f\left(n,R,Q\right)=1-\prod_{i=1}^{N_V}\left(1-P_{f,i}\left(n,R,\sigma_i\right)\right)=1-\prod_{i=1}^{N_V}F_N\left(n,R,\sigma_i\right) \tag{5-10}$$

where σ_i is the fatigue stress in sub-volume i due to the fatigue load Q.

For case 2 the probability of failure is obtained by (Mirzaei Rafsanjani & Sørensen, 2015b)

$$P_f(n,R,Q) = 1 - \prod_{i=1}^{N_V} \left(1 - P_{f,i}(n,R,\sigma_i)\right) \tag{5-11}$$

with

$$P_{f,i}(n,R,\sigma_i) = 1 - p_i^0(n,R,\sigma_i) = 1 - \prod_{j=1}^{M} p_{i,j}^0(n,R,\sigma_i) \tag{5-12}$$

where $p_i^0(n,R,\sigma_i)$ is the probability of no fatigue failure in sub-volume *i* and $p_{i,j}^0(n,R,\sigma_i)$ is the probability of no failure in sub-volume *i* due to group *j* defects (assuming statistically independence between the groups). Finally (Mirzaei Rafsanjani & Sørensen, 2015b),

$$p_{i,j}^0(n,R,\sigma_i) = 1 - F_{N,j}(n,R,\sigma_i).$$

For case 3 the probability of failure is obtained by the same model as for case 2 but with (Mirzaei Rafsanjani & Sørensen, 2015b)

$$p_{i,j}^0(n,R,\sigma_i) = \sum_r p_{i,j,r}^0(n,R,\sigma_i) \tag{5-13}$$

where the summation is over the number *r* of defects in the sub-volume for each group of defects. $p_{i,j,r}^0(n,R,\sigma_i)$ is the probability of no fatigue failure in sub-volume *i* due to group *j* defects and with exactly *r* defects/nodules (Mirzaei Rafsanjani & Sørensen, 2015b) (Mirzaei Rafsanjani & Sørensen, 2015c). It is assumed that the failure events due to different defects are statistically independent. If *m* defects/nodules are interior defects/nodules in sub-volume dV_i, and *r*-*m* nodules are surface nodules then (Mirzaei Rafsanjani & Sørensen, 2015b)

$$\begin{aligned} p_{i,j}^0(n,R,\sigma_i) = & \sum_{k=1}^{m} P_{\text{int},i,j}(k) \times \left[1 - F_{N,j,1,\text{int}}\left((n,R,\sigma_i)\right)\right]^k + \\ & \sum_{k=1}^{r-m} P_{surf,i,j}(k) \times \left[1 - F_{N,j,1,surf}\left((n,R,\sigma_i)\right)\right]^k \end{aligned} \tag{5-14}$$

where

$P_{\text{int},i,j}(k)$ is the probability of exactly *k* interior defects

$P_{surf,i,j}(k)$ is the probability of exactly *k* surface defects

$F_{N,j,1,\text{int}}\left((n,R,\sigma_i)\right)$ is the distribution function for fatigue failure given interior defects

$F_{N,j,1,surf}\left((n,R,\sigma_i)\right)$ is the distribution function for fatigue failure given surface defects

The probability of failure $P_f(n,R,Q)$ is a function of the

- The applied fatigue load *Q*

- Time t since the number of fatigue load cycles can be written as $n=v*t$ where v is number of cycles per time unit (typically one year) (Mirzaei Rafsanjani & Sørensen, 2015b)

In addition to the uncertainty related to number and type of defects/nodules and the fatigue life given defects/nodules, also uncertainty related to the fatigue loads has to be accounted for. This uncertainty can be modelled as random variables, X_W and X_{SCF} multiplied to the fatigue load, following the approach used as background for calibrating safety factors for the IEC 61400-1 standard, see e.g. (Sørensen & Toft, 2014). The total probability of failure accounting for these additional uncertainties can e.g. be obtained by simulation or a nested FORM approach (Sørensen & Toft, 2014).

In the above models the size, type, orientation of nodules are considered independent, but when there are clusters of nodules in the components, the distance between the nodules play an important role and should be introduced in the models, e.g. following the models in (Toft, Branner, Berring, & Sørensen, 2011).

5.3. Analysis of data for sand casting samples

In this section, the probability of failure is estimated for the fatigue specimens mentioned in Table 4-1 (Sand casting specimens). The Weibull distribution (Equation (3-10)) is used to model the probability distribution for fatigue failure for the specmiens. Since the data of Table 4-1 are for various stress amplitudes, the basquin equation is used to convert the estimated fatigue lifes to the same stress level (in this case, the max load equal to 7 kN is chosen). Hence, the basquin equation as below is used (Note that σ_f and m are extracted from Table 4-3)

$$\sigma_a \left(2N\right)^{\frac{1}{m}} = \sigma_f \tag{5-15}$$

By using this equation, the data of Table 4-1 is converted to the data in Table 5-1. Based on these data and Appendix A, Figure 5-2 is extracted showing the number of cycles to failure for each specimen compared to the largest nodule volumes. According to Figure 5-2, the specimen with smallest nodule (specimen 308-8) has the largest number of cycles to failure. Note, this can not be used as a rule for fatigue life assessent because the fatigue life is not only related to the size of the nodules but also other parameters such as shape, orientation etc. In following, each specimen is considered seperately.

Table 5-1 Converted faitgue life of sand casting specimen by basquin equation

Speciemn #	New Max Load [kN]	Cycles to failure
269-1	7.00	15242
269-19	7.00	11715
308-8	7.00	2059968
338-13	7.00	17793

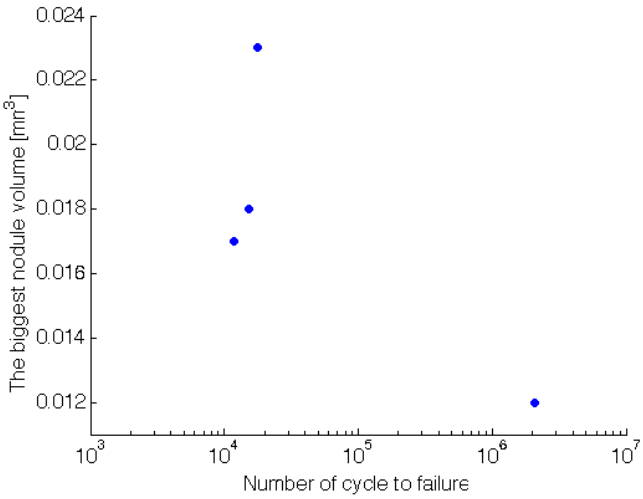

Figure 5-2 The number of cycles compare to nodule size for sand casting specimens

5.3.1. Specimen 269-1 (Sand casting)

By using the methodology presented above, the probability of failure of the specimen is estimated based on the nodules distribution. Based on the data, the most probable sub-volumes to cause failure are listed in Table 5-2 (as a function of the position on the z-axis).

In Figure 5-3, the distribution of nodules and the probability of failure (at 100,000 cycles) in each sub-volume are shown. The largest probability of failure is in the sub-volume with z-value between -23 and -25. According to Appendix A, the largest nodule location along z-axis is not btween -23 and -25 and it is not located in this sub-volume, and only the 3rd and 6th largest nodules (based on the nodule volumes listed in Appendix A) are located in this sub-volume and they are very close to each other. In Figure 5-4, the mentioned nodules are shown and it is seen that there are also many other nodules very close to largest nodules and this could further contribute to the high probability of failure in this section.

Table 5-2 The most probable fracture volumes based on threshold PS98 of specimen 269-1

	#1 most critical sub-volume	2# most critical sub-volume	#3 most critical sub-volume
z-value	-25 , -23	-37 , -35	-21 , -19

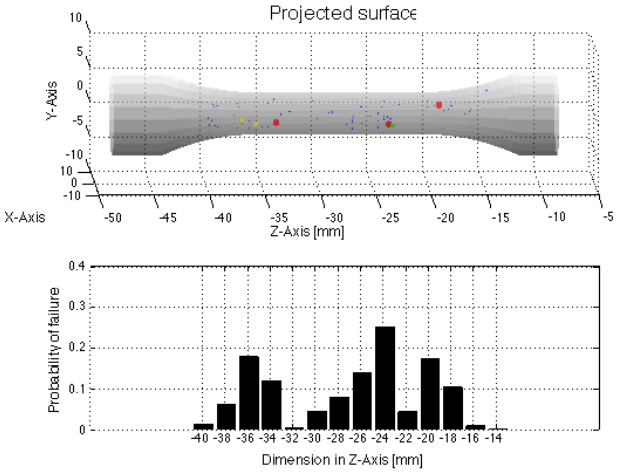

Figure 5-3 The probability of failure based on volume divisions for specimen 269-1

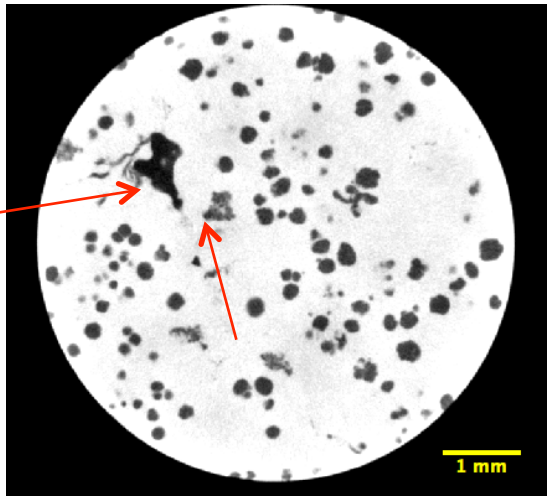

Figure 5-4 The predicted fracture surface of specimen 269-1

5.3.2. Specimen 269-19 (Sand casting)

As in the previous subsection, the probability of failure of specimen 269-19 is estimated based on the nodule distribution. The most probable sub-volumes to fail are listed in Table 5-3 (with z-values being the geometrical z-axis).

Table 5-3 The most probable fracture volumes based on threshold PS99 of specimen 269-19

	#1 most critical sub-volume	**2# most critical sub-volume**	**#3 most critical sub-volume**
z-value	-28 , -26	-30 , -28	-34 , -32

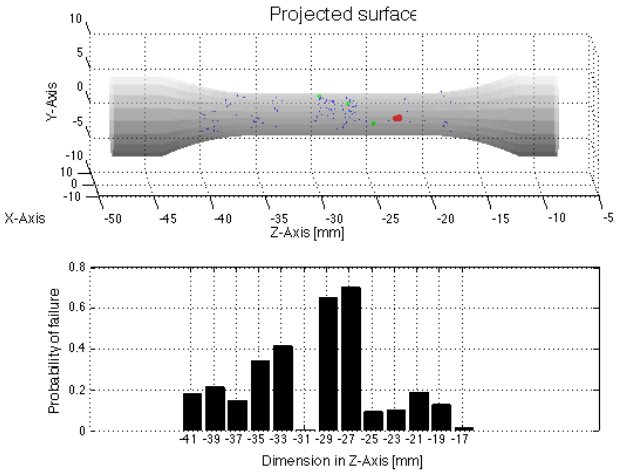

Figure 5-5 The probability of failure based on volume divisions for specimen 269-19

In Figure 5-5, the distribution of nodules and the probability of failure in each sub-volume section are shown. The probability of failure is estimated for 100,000 cycles. According to Appendix A, the largest nodules location along z-axis is between -22 and -24, but the probability of failure in sub-volume (with z-value between -22 and -24) is smaller than the probability of failure of the sub-volumes with z-value between "-26 , -28" and "-28 , -30".

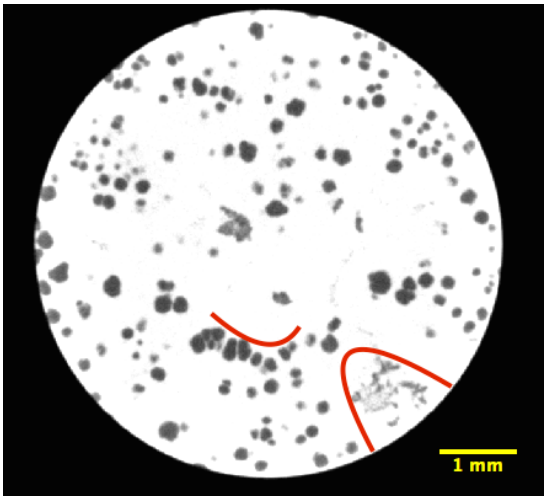

Figure 5-6 The predicted fracture surface of specimen 269-19

By reveiwing the nodule sizes, it is seen that the number of nodules in the most critical sub-volumes are largest than in the other sub-volumes and the reason of the large failure probability could be the cluster of nodules in the surface area and in addition also the largest nodules locatd in the interior of the specimen. In Figure 5-6 is shown the section of sub-volume between z-values "-28, -30" and the configuration of nodules.

5.3.3. Specimen 308-8 (Sand casting)

Like in previous sections, the probability of failure of this specimen is estimated based on the nodule distribution. Based on the data, the most probable volumes to fail are listed in Table 5-4.

Table 5-4 The most probable fracture volumes based on threshold PS99 of specimen 308-8

	#1 most critical	**2# most critical**	**#3 most critical**
z-value	-21 , -19	-19 , -17	-17 , -15

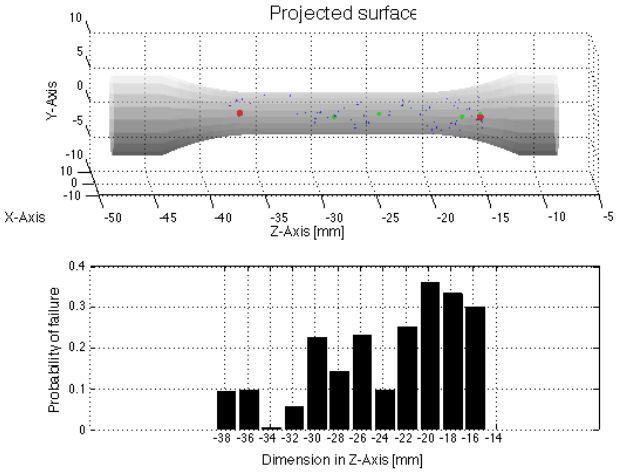

Figure 5-7 The probability of failure based on volume divisions for specimen 308-8

In Figure 5-7 is shown the distribution of nodules and the probability of failure in each sub-volume section. The probability of failure is estimated for 100,000 cycles. Based on the nodule distribution, again the reason of the largest failure probability could be the cluster of nodules in the surface area. In Figure 5-8 the configuration of the nodules is shown. The reason could be existance of large defect in the surface rim of component. By reviewing the data of mentioned nodule, the length of bounding box in z direction is more than one, and this means this defect is extended in the z direction (which is perpendicuar to the image surface). Hence, a slice of defect is shown in Figure 5-8 for illustration.

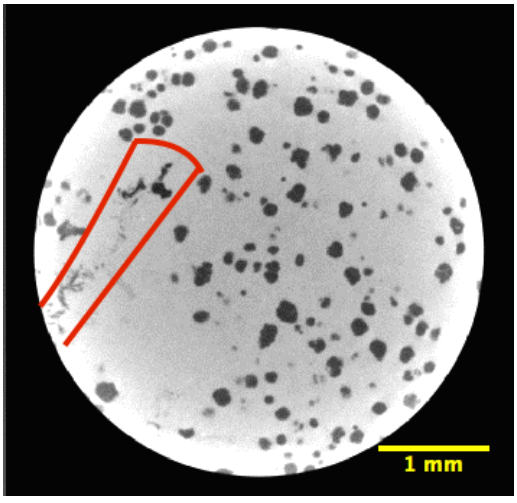

Figure 5-8 The predicted fracture surface of specimen 308-8

5.3.4. Specimen 338-13 (Sand casting)

Like in the previous sections, the probability of failure of this specimen is estimated based on the nodule distribution. Based on the data, the most probable volumes to fail are listed in Table 5-5.

Table 5-5 The most probable fracture volumes based on threshold PS99 of specimen 338-13

	#1 most critical	2# most critical	#3 most critical
z-value	-22 , -20	-28 , -26	-32 , -30

In Figure 5-9, the distribution of nodules and the probability of failure in each volume sections are shown. The probability of failure is estimated for 100,000 cycles. Based on the nodule distribtuion, the reason of the largest failure probability is that the largest nodule is located very close to 3rd rank nodule and both of them are surface defects. In Figure 5-10 configuration of nodules is shown.

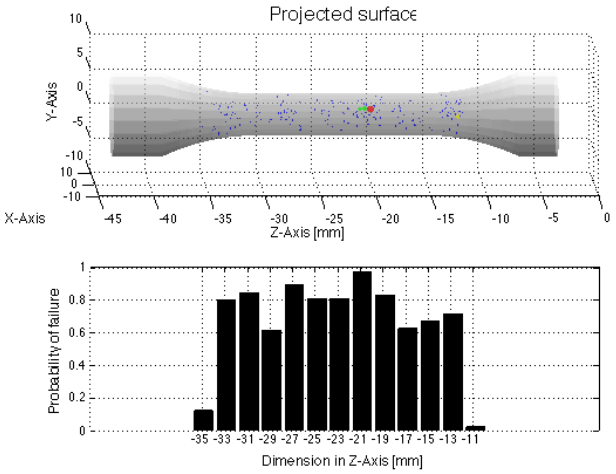

Figure 5-9 The probability of failure based on volume divisions for specimen 338-13

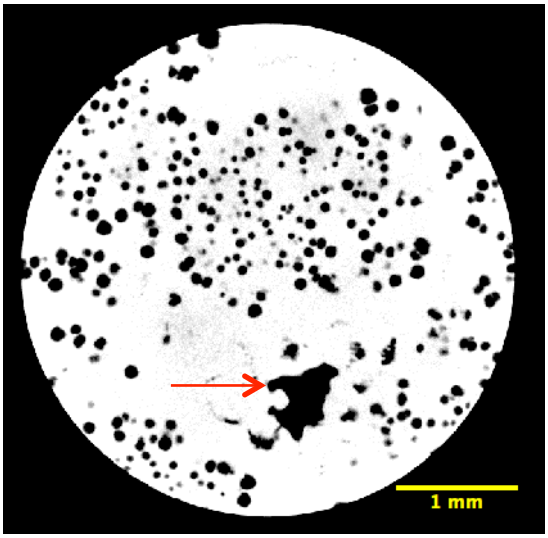

Figure 5-10 The predicted fracture surface of specimen 338-13

5.4. Analysis of data for chill casting samples

Like in previous sections, the data of Table 4-1 for chill casted specimens are convered to the data in Table 5-6. Based on these data and Appendix A, Figure 5-11 is obtained showing the number of cycles to failure for each specimen compared to the largest nodule volumes. Based on this figure, there is no specfic relation between nodule size and fatigue life as for the sand casting results. However it is noted that the fatigue life is not only related to the size of the nodules but also to other parameters such as shape, orientation.

Table 5-6 Converted faitgue life of chill casting specimen by basquin equation

Speciemn #	New Max Load [kN]	Cycles to failure
626-2	9.00	4026
656-1	9.00	8133
656-4	9.00	7369
656-13	9.00	1176

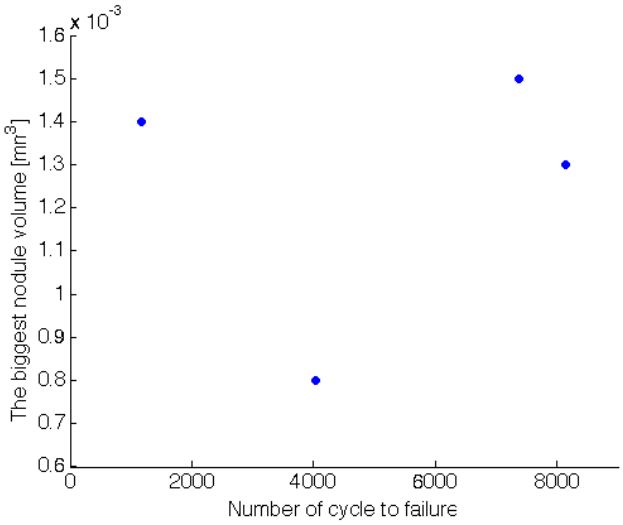

Figure 5-11 Number of cycles to failure compared to nodule size for chill casted specimens

5.4.1. Specimen 626-2 (Chill casting)

Like for sand casting specimens, the probability of failure for each specimen is estimated based on the nodule distribution. Based on the data, the most probable volumes to failure are listed in Table 5-7.

Table 5-7 The most probable fracture volumes based on threshold PS999 of specimen 626-2

	#1 most critical	**2# most critical**	**#3 most critical**
z-value	-24 , -22	-26 , -24	-28 , -26

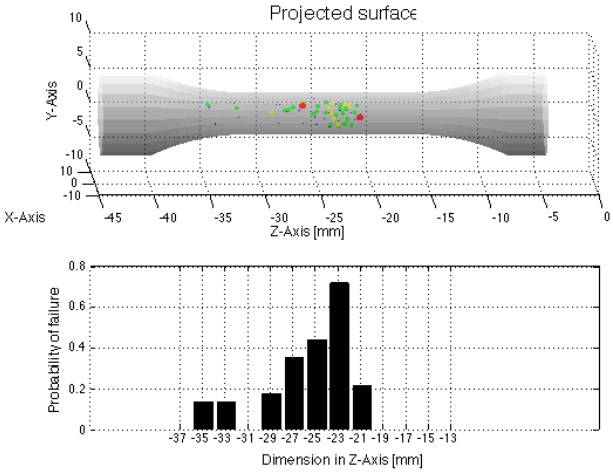

Figure 5-12 The probability of failure based on volume divisions for specimen 626-2

In Figure 5-13, the distribution of nodules and the probability of failure in each volume section are shown. The probability of failure is estimated for 100,000 cycles. Based on the nodule distribution, it is seen that the differences in nodule sizes are not significant and fatigue failure of chill casting specimens are not like sand casting specimen highly related to the nodule sizes. In chill casting samples, the nodules are smaller but the number of nodules is higher. Failure of chill casting specimens seems to be more related to the relative number of nodules in each sub-volumes.

By reviewing the data, it is seen that the most probable sub-volumes to fail, in Figure 5-12, are sub-volumes with the highest number of nodules. this also indicates that clustering of nodules in the surface area is important.

In this specimen devided in 13 sub-volumes 400 nodules are detected with threshold PS999. In Table 5-8, the percentage of number of nodules (out of total number of nodules with threshholds PS999) is listed for the most probable sub-volumes. The remaining sub-volumes (10 sub-volumes) have less than 25% of the total number of nodules.

Table 5-8 The percentage of nodule counts for probable fracture volumes of specimen 626-2

	#1 most critical	**2# most critical**	**#3 most critical**
z-vaue	-24 , -22	-26 , -24	-28 , -26
Percentage of nodule count	35%	24%	16%

5.4.2. Specimen 656-1 (Chill casting)

Like in previous sections, the probability of failure of this specimen is estimated based on the nodule distribution. Based on the data, the most probable volumes to fail are listed in Table 5-9.

Table 5-9 The most probable fracture volumes based on threshold PS999 of specimen 656-1

	#1 most critical	2# most critical	#3 most critical
z-value	-27 , -25	-29 , -27	-25 , -23

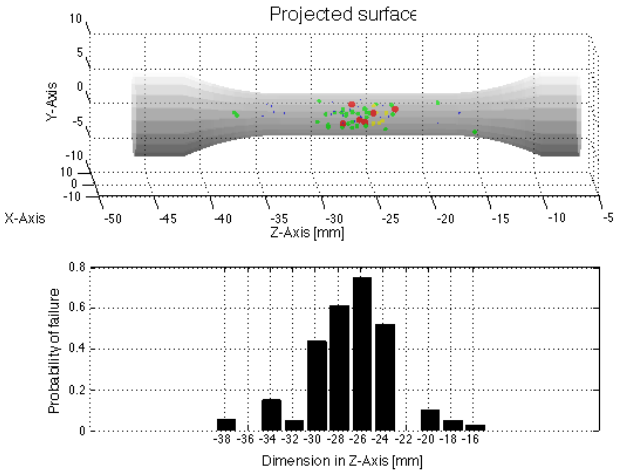

Figure 5-13 The probability of failure based on volume divisions for specimen 656-1

In Figure 5-13, the distribution of nodules and the probability of failure in each volume section are shown. The probability of failure is estimated for 100,000 cycles. Based on the nodule distribtuion, the largest nodules are located very close to each other between sub-volumes with z-values -27 and -25. Further in Table 5-10, the percentage of nodules (threshold PS999) is listed for the most probable sub-volumes (Note, the total number of nodules for threshold PS999 is 309). Like in previous specimens, the sub-volumes with high number of nodules are the most probable sub-volumes to fail. This indicates that the number of nodules play an important role for the reliability of chill casting specimens.

Table 5-10 The percentage of nodule counts for probable fracture volumes of specimen 656-1

	#1 most critical	2# most critical	#3 most critical
z-vaue	-27 , -25	-29 , -27	-25 , -23
Percentage of nodule count	25%	21%	20%

5.4.3. Specimen 656-4 (Chill casting)

The probability of failure of this specimen is estimated based on the nodule distribution. Based on the data, the most probable volumes to fail are listed in Table 5-11.

Table 5-11 The most probable fracture volumes based on threshold PS999 of specimen 656-4

	#1 most critical	2# most critical	#3 most critical
z-value	-26 , -24	-28 , -26	-30 , -28

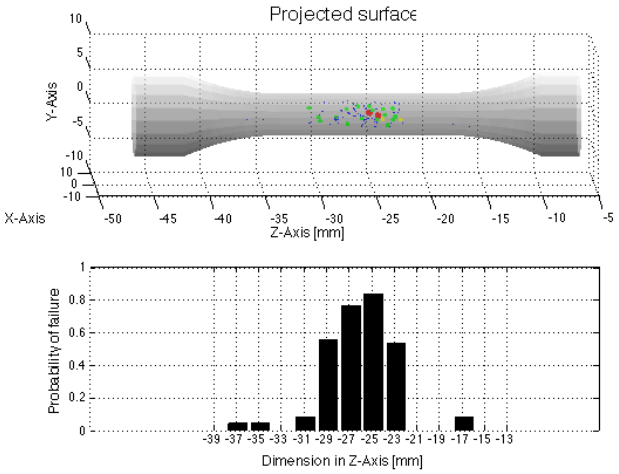

Figure 5-14 The probability of failure based on volume divisions for specimen 656-4

In Figure 5-14 the distribution of nodules and the probability of failure in each volume section are shown. The probability of failure is estimated for 100,000 cycles. Based on the nodule distribtuion, the largest nodules are located very close to each other between sub-volumes with z-values -26 and -24 and this could be the

reason of the large failure probability. Further in Table 5-12, the percentage of number of nodules (for threshold PS999) is listed for the most probable sub-volumes (Note, the total number of nodules for threshold PS999 is 403). Like in previous specimen, the sub-volumes with the largest number of nodules are the most probable sub-volume to fail.

Table 5-12 The percentage of nodule counts for probable fracture volumes of specimen 656-4

	#1 most critical	**2# most critical**	**#3 most critical**
z-vaue	-26 , -24	-28 , -26	-30 , -28
Percentage of nodule count	29%	22%	18%

5.4.4. Specimen 656-13 (Chill casting)

The probability of failure of this specimen is estimated based on the nodule distribution. Based on the data, the most probable volumes to fail are listed in Table 5-13.

Table 5-13 The most probable fracture volumes for threshold PS999 of specimen 656-13

	#1 most critical	**2# most critical**	**#3 most critical**
z-value	-29 , -27	-27 , -25	-25 , -23

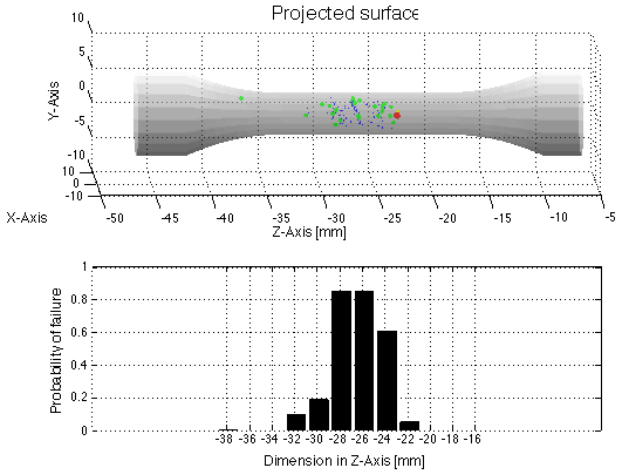

Figure 5-15 The probability of failure based on volume divisions for specimen 656-13

In Figure 5-15, the distribution of nodules and the probability of failure in each volume section are shown. The probability of failure is estimated for100,000 cycles. Based on the nodule distribtuion, the largest nodules are located very close to each other and the highest number of nodules are located in this sub-volume (see Table 5-14).

Table 5-14 The percentage of nodule counts for probable fracture volumes of specimen 656-13

	#1 most critical	**2# most critical**	**#3 most critical**
z-vaue	-29 , -27	-27 , -25	-25 , -23
Percentage of nodule count	29%	28%	22%

CHAPTER 6. RELIABILITY ASSESSMENT OF CAST COMPONENTS

The reliability of a component can be defined as the probability that the component under consideration has a proper performance throughout its lifetime. (Mirzaei Rafsanjani & Sørensen, 2015a; Sørensen J. D., 2011) Structural reliability methods can be used to estimate the probability of failure / reliability which next can be used for decision-making, e.g., with respect to design or planning of inspections, maintenance and repair (Mirzaei Rafsanjani & Sørensen, 2015a; Ambühl, Kramer, & Sørensen, 2016; Sørensen & Toft, 2010).

The reliability estimated as a measure of the safety of a structure can be used in a decision process (for example Markov decision process) (Byon & Ding, 2010) (Sørensen J. D., 2011). A lower level of the acceptable reliability can be used as a constraint in a reliability-based optimal design problem (Sørensen J. D., 2011). The lower level of the reliability can be obtained by analyzing similar structures designed after current design practice or it can be determined as the reliability level giving the largest utility (benefits-costs) when solving a decision problem where all possible costs and benefits in the expected lifetime of the structure are taken into account (Sørensen & Toft, 2010). Further, the reliability and failure rate of components can be used for decision-making for maintenance plans (Byon, Ntaimo, & Ding, 2010).

Drivetrain components are typically exposed to complex loading conditions (Campbell, 2008). Often the fatigue load is due to a range of fluctuating loads, different mean stress levels and variable frequencies (Mirzaei Rafsanjani & Sørensen, 2015a). Based on (ISO 2394, 2015), the *SN* curve approach is often used for design with respect to fatigue and combines all three phases of the fatigue mechanism and is completely based on experiments. A number of test specimens are subjected to a series of constant amplitude load cycles until failure. The *SN* curve might depend on the mean stress level. In order to deal with realistic variable amplitude loading on a structure, a damage accumulative rule has to be applied. Cumulative damage during fatigue is often modeled by using the Palmgren-Miner rule, which assumes that the total life of a part can be estimated by adding up the percentage of life consumed by each stress level (Mirzaei Rafsanjani & Sørensen, 2015a).

Further, reliability assessment requires development of stochastic models that account for the uncertainties both in the fatigue strength of the materials and loads. Therefore, a stochastic fatigue model to assess the reliability is needed. This model can be used to assess the reliability for both sand casting samples and chill casting samples (Mirzaei Rafsanjani & Sørensen, 2015a). This chapter describes a statistical analysis of test data from fatigue tests of casting methods, firstly. The statistical

analysis is performed using the Maximum-Likelihood Method (MLM) (Mirzaei Rafsanjani & Sørensen, 2015a). The statistical analysis is based on the number of cycles to failure, and tests with run-outs (no failure) are also taken into account. Next, the statistical model is used for reliability assessment of each casting component (Marquez-Dominguez & Sørensen, 2012).

6.1. Statistical analysis of strength distribtuion

6.1.1. Sand casting samples

In this section, the Log-Normal distribution (Equation (3-5)) and the Weibull distribution (Equation (3-10)) are used to model the fatigue strength distribution based on *SN* curves. As mentioned above, the Maximum-Likelihood Method is used to estimate the parameters (Sørensen J. D., 2011). Note, that run-out data are also considered in the estimation of the parameters (for further detail, see sections 3.3 and 3.4). The estimated parameters for sand casting samples are shown in Table 6-1.

Table 6-1 Estimated statistical parameters from sand casting samples

Distribution	σ_f[Mpa]		m		σ_ε	
	mean	*Std dev*	*mean*	*Std dev*	*mean*	*Std dev*
LogNormal	1333.91	5.12	9.61	0.3	0.56	0.00
Weibull	1260.84	5.11	10.44	0.01	0.44	0.01

The correlation matrices for the statistical uncertainties related to each distribution are estimated by Equation (3-7). The correlation matrix for the LogNormal distribution is shown in equation (6-1) and for Weibull distribution it is shown in equation (6-2). It is seen that σ_f and m are highly negative correlated. The number of fatigue samples that is used is 825 samples. The estimated values will be used for reliability assessment in the following.

$$C_{Sand,LN} = \begin{bmatrix} 1 & -0.52 & -0.14 \\ -0.52 & 1 & -0.14 \\ -0.14 & -0.14 & 1 \end{bmatrix} \tag{6-1}$$

$$C_{Sand,W} = \begin{bmatrix} 1 & -0.14 & -0.32 \\ -0.14 & 1 & 0.4 \\ -0.32 & 0.4 & 1 \end{bmatrix} \tag{6-2}$$

6.1.2. Chill casting samples

Like for sand casting samples, the Log-Normal distribution and the Weibull distribution are used to model the fatigue strength distribution based on the *SN* curve (Sørensen J. D., 2011). Note, that run-out data are also considered here. The estimated parameters for chill casting samples are shown in Table 6-2. Further, the correlation matrix for the LogNormal distribution is shown in equation (6-3) and for the Weibull distribution it is shown in equation (6-4). It is seen again that σ_f and m are highly negative correlated. The number of fatigue samples that used is 409 samples. The estimated values will be used for reliability assessment in the following.

Table 6-2 Estimated statistical parameters from chill casting samples

Distribution	σ_f[Mpa]		m		σ_ε	
	mean	*Std dev*	*mean*	*Std dev*	*mean*	*Std dev*
LogNormal	1097.74	5.34	15.45	0.07	0.628	0.01
Weibull	952.21	5.11	19.21	0.02	0.593	0.01

$$C_{Chill,LN} = \begin{bmatrix} 1 & -0.22 & -0.10 \\ -0.22 & 1 & -0.06 \\ -0.10 & -0.06 & 1 \end{bmatrix} \quad (6\text{-}3)$$

$$C_{Chill,W} = \begin{bmatrix} 1 & -0.29 & -0.14 \\ -0.29 & 1 & -0.02 \\ -0.14 & -0.02 & 1 \end{bmatrix} \quad (6\text{-}4)$$

This statistical analysis should be considered as an example so that the same procedure can be applied and even updated if more data become available. In Figure 6-1, the *SN* curves for both sand casting methods (based on LogNormal and Weibull distributions) are shown. Note that due to confidentiality, the numbers of tables was not shown. The results show only a small difference between the curves for the LogNormal and Weibull disribution and also that the specimens with “Chill casting” manufacturing have higher fatigue strengths compare to “Sand Casting” manufacturing.

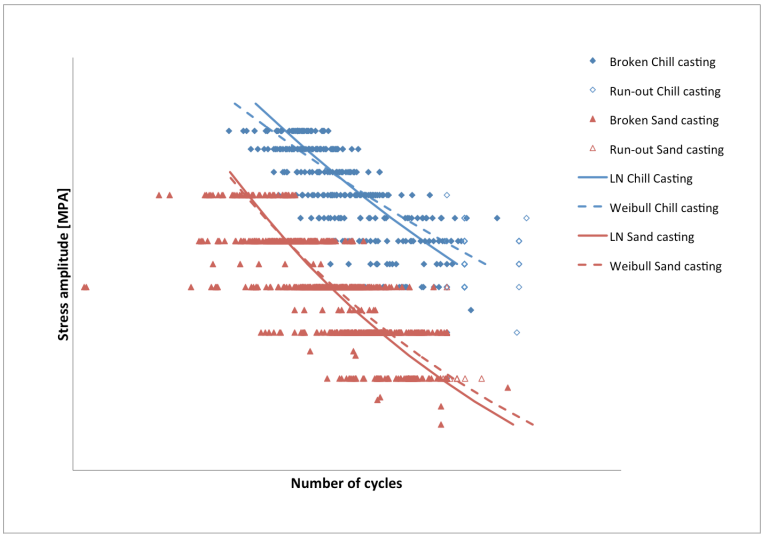

Figure 6-1 Comparison of "Sand Casting" and "Chill Casting"

6.2. Stochastic model and reliability assessment

In this section, an illustrative example is shown in order to describe a reliability assessment for fatigue failure in combination with Miner's rule. Hence, the equations described in section 3.5 are used. According to this, the following limit state equation is used (for further details see section 3.5)

$$g(t) = \Delta - \sum_{V_j} \left(\sum_i \frac{n_{i,S} t}{N_{0;0.05}\left(\frac{X_W X_{SCF} \sigma_{a0.i}}{z}, \frac{\sigma_f}{\gamma_m} \right)} \right) * P(V_j) \tag{6-5}$$

where X_W is a stochastic variable modeling model uncertainty related to determination of fatigue loads and X_{SCF} is a stochastic variable modeling model uncertainty related to determination of stresses given fatigue loads (Sørensen J. D., 2011; Marquez-Dominguez & Sørensen, 2012; Mirzaei Rafsanjani & Sørensen, 2015a). In addition, Δ models model uncertainty related to Miner's rule for linear damage accumulation (Mirzaei Rafsanjani & Sørensen, 2015a).

Further, V_j is the mean wind speed and $P(V_j)$ is probability of occurrence of this mean wind speed, modeled by a Weibull distribution according to IEC 61400-1 (IEC 61400, 2015; Mirzaei Rafsanjani & Sørensen, 2015a). For wind turbines, the fatigue loads are typically estimated for mean wind speeds from 3 m/s to 25 m/s and are normally represented by time series of load effects or equivalently by Markov matrices obtained by rain-flow counting (Mirzaei Rafsanjani & Sørensen, 2015a). In

the following, the loads are extracted from simulated loads for a main shaft of the 5 MW NREL reference wind turbine for each mean wind speed V_j. The hub diameter is 3 meter and the rotor has a diameter of 126 meter. The hub height is 90 meter, the cut-in and cut-out wind speeds are 3 m/s and 25 m/s, respectively. Further information can be found in (Jonkman, Butterfield, Musial, & Scott, 2009) (Mirzaei Rafsanjani & Sørensen, 2015a).

In Equation (6-5), Δ, X_W and X_{SCF} are assumed to be log-normal distributed with mean values equal 1 and coefficients of variation COV_Δ, COV_W and COV_{SCF}, respectively (Mirzaei Rafsanjani & Sørensen, 2015a). The coefficient of variations are estimated based partly subjectively, but following generally the recommendations used as basis for the material partial safety factors in IEC 61400-1, and also considering information from e.g., (DNV-RP-C203, 2010) (Mirzaei Rafsanjani & Sørensen, 2015a). The importance of the choices of the coefficient of variations is investigated by sensitivity analyses. It is noted that the reliability level obtained is in accordance with the target reliability corresponding to an annual probability failure of the order 5×10^{-4} (annual reliability index 3.3) (IEC 61400, 2015; Mirzaei Rafsanjani & Sørensen, 2015a).

Based on Equation (6-5), the probability of failure in the time interval $[0,t]$ is estimated by FORM/SORM techniques or simulation (Madsen, Krenk, & Lind, 1986). The reliability index, $\beta(t)$ corresponding to the accumulated probability of failure $P_F(t)$ is defined by (Mirzaei Rafsanjani & Sørensen, 2015a) (Sørensen J. D., 2011):

$$\beta(t) = -\Phi^{-1}(P_F(t)) \tag{6-6}$$

where $\Phi(\ )$ is the standardized normal distribution function. The annual probability of failure conditioned on survival up to time t is obtained from: (Mirzaei Rafsanjani & Sørensen, 2015a) (Marquez-Dominguez & Sørensen, 2012)

$$\Delta P_F(t) = \left(P_F(t-\Delta t) - P_F(t)\right)/\Delta t/\left(1-P_F(t)\right) \tag{6-7}$$

where Δt is a time increment, typically 1 year. The reliability index, $\Delta\beta$ corresponding to the probability ΔP_F is denoted the annual reliability index when Δt = 1 year (Mirzaei Rafsanjani & Sørensen, 2015a).

In the following, the annual reliability index for Sand casting are estimated using the two distributions (LogNormal and Weibull distributions). Further, the design fatigue life is assumed equal to 25 years. The stochastic model is shown in Table 6-3.

The reference for the example values of COV_W and COV_{SCF} is (Sørensen & Toft, 2014). The partial safety factor for the fatigue strength is chosen to correspond to a safe life design and is chosen to γ_m = 1,25 (Sørensen & Toft, 2014; IEC 61400, 2015). Hence, the reliability index is estimated by equation (6-5).

Table 6-3 Stochastic model for fatigue of casted specimens (Sørensen & Toft, 2014).

Variable	Definition	Distribution	Expected Value	Coefficient of Variation
Δ	Model uncertainty related to Miner's rule	LN*	1	0.3
X_{SCF}	Model uncertainty related to determination of stresses given fatigue load	LN	1	0.05
X_W	Model uncertainty related to determination of fatigue loads	LN	1	0.10
m	Statistical uncertainty	N**	Extracted from test results	
σ_f [Mpa]	Statistical uncertainty	N	Extracted from test results	

First, the sensitivity of the reliability with respect to the uncertainty level of X_W is investigated with the partial safety factor equal to 1,25 (Mirzaei Rafsanjani & Sørensen, 2015a). Based on Appendix G, COV_{SCF} is chosen to 0,05. For sensitivity analysis, values of COV_W between 0,10 and 0,20 are used to estimate the reliability index. The result is shown in Figure 6-2. It is seen that when the uncertainty related to the fatigue loads increases, then the reliability index (as expected) decreases (Mirzaei Rafsanjani & Sørensen, 2015a).

Further, it is seen that the reliability index estimated by the LogNormal distribution is generally higher than reliability index estimated by the Weibull distribution (Mirzaei Rafsanjani & Sørensen, 2015a). It is seen that the reliability index is quite sensitive to the coefficient of variation of X_W. Moreover, the influence of variation of COV_W is estimated when the X_{SCF} equal to 0,10, see Figure 6-3. Based on these figures, the trends of the reliability index are very similar to each other. Note that when the value of COV_{SCF} increase, the difference between LogNormal and Weibull increases.

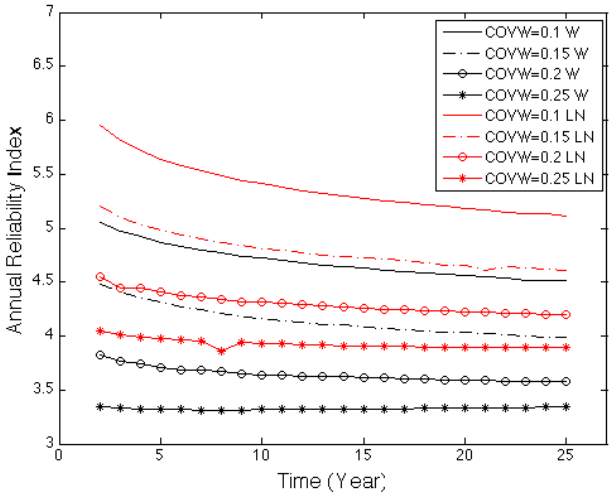

Figure 6-2 Annual reliability index for different X_W (X_{SCF} = 0.05)

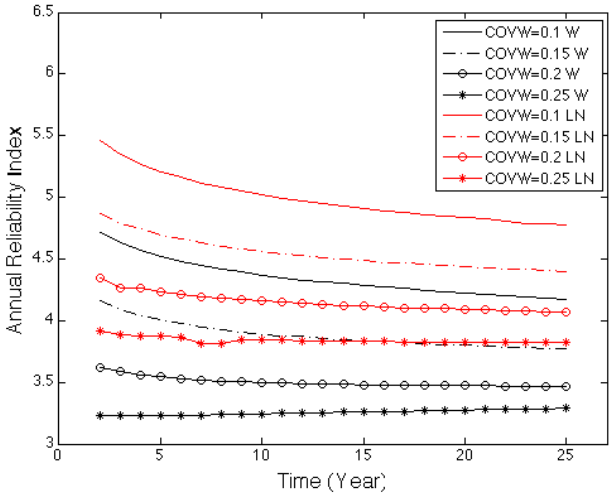

Figure 6-3 Annual reliability index for different X_W (X_{SCF} = 0.10)

Furthermore, the sensitivity of the reliability with respect to the uncertainty level of X_{SCF} is investigated. Based on Appendix G, the coefficient of variation of X_W equal to 0,10 is chosen. For sensitivity analysis, the coefficients of variation of X_{SCF} between 0,00 and 0,20 are used. The results are shown in Figure 6-4. The results is (as expected) similar to those obtained for X_W.

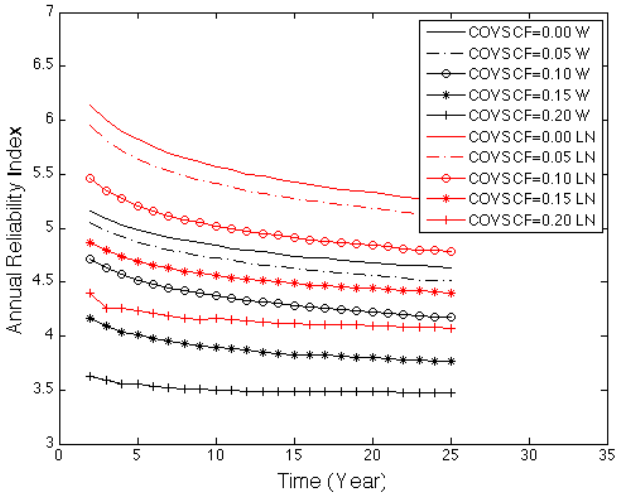

Figure 6-4 Annual reliability index for different X_{SCF} (X_W = 0.10)

Moreover, the influence of different values of COV_{SCF} is estimated when the X_W equal to 0,15, see Figure 6-5. Based on these figures, the trends of the reliability index are very similar to each other. It is seen also that the reliability index by LogNormal is much higher than by the Weibull distribution.

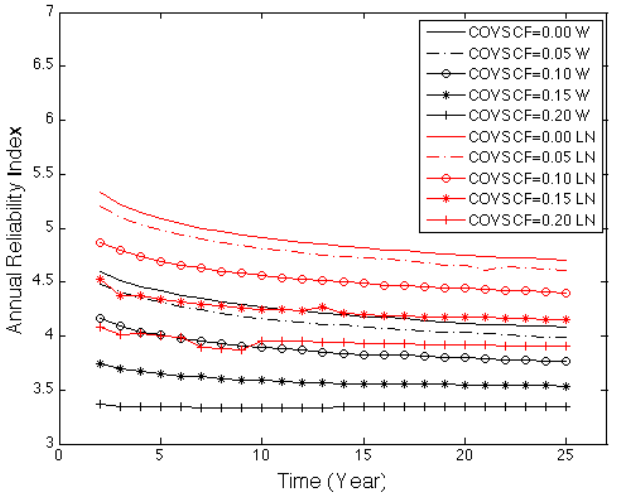

Figure 6-5 Annual reliability index for different X_{SCF} (X_W = 0.15)

CHAPTER 7. CONCULSION AND FUTURE WORKS

7.1. Conclusion

Nowadays, reliability of wind turbine drivetrain components is very important for wind turbine manufacturers and owners (Mirzaei Rafsanjani & Sørensen, 2015a). Offshore wind turbines are large structures exposed to wave excitations, highly dynamic wind loads influenced by the wind turbine control system and wakes from other wind turbines (Mirzaei Rafsanjani & Sørensen, 2014). Therefore, most components in a wind turbine experience highly dynamic and time-varying loads. These components may fail due to wear or fatigue and this can lead to unplanned shut down and repairs (Mirzaei Rafsanjani & Sørensen, 2015c). In order to decrease the maintenance costs, the fatigue failure of drivetrain component must be considered and reliability assessment of component must be done according to the most related uncertainties that could be arise during the design life of components.

The probabilistic model must be made in order to reach a certain structural level defined in accordance with the consequences in case of structural failure can be reached using so-called probabilistic reliability methods. Threfore, FORM (First Order Reliability Methods) techniques or Monte Carlo simulations can be applied to estimate the structural reliability index and the probability of failure of a certain design (Sørensen J. D., 2011).

In this thesis, different stochastic models for fatigue failure of casted steel components in wind turbine drivetrain components are considered. Firstly, the fatigue life is modeled and various uncertainties that affect the stochastic models of failure are described. These uncertainties include model and statistical uncertainties. The basic uncertainty of the fatigue life is modeled by two distribution models, namely log-normal and Weibull distribution. It is described how the statistical parameters can be derived including the statistical uncertainties. Next, characteristic SN-curves are derived using structural reliability techniques (Mirzaei Rafsanjani & Sørensen, 2015a).

A set of test data is used to illustrate the procedure to rationally model the uncertainties and next to estimate the reliability for generic cases. The results indicate that the characteristic SN-curves are almost the same using the Weibull and log-normal models, but the reliability obtained by the log-normal distribution model is generally higher than reliability index obtained using the Weibull distribution model. Further, the uncertainty of the load model is seen to influence the reliability level significantly (Mirzaei Rafsanjani & Sørensen, 2015a).

Furthermore, the 3D tomography of casting ssamples of wind turbine components are used to study the distribution of nodules and also study the effect of nodules distribution of fatigue life of component. The GEV 3-parameter distribution is used to study the nodules configuration in fatigue samples from two diffirent casting methods (Sand casting and chill casting). Furthemore, the distribution of nodules in various voulmes of each samples compare to each to find out that the nodules are distributed homogeneously in volume of samples or not.

In addition, in this thesis is presented generic models for estimation of the probability of fatigue failure due to manufacturing nodules in casted components (Mirzaei Rafsanjani & Sørensen, 2015b). The nodules are categorized in different groups according to their size, type, orientation and etc. For each group, a Poisson distribution is used to model the distribution of nodules. Further, the nodules are divided in two sub-groups of interior and surface nodules. The based on configuration of nodules in each specimen, the probability of failure (based on nodules distribbution) is modeled. The probability of failure is a function of i) existence of nodule(s), ii) the conditional probability of failure due to existence of nodule(s). In this model, the interior and surface nodules are separated from each other. The model accounts for cluster of nodules. To model the probability of failure for whole component, the probability of failure is estimated in smaller sub-volumes firstly and for each sub-volume, the probability of failure is modeled. As the component volume is assumed to be considered as a series system of sub-volumes, the probability of failure of the whole components can be estimated according to a series systems probability of failure models (Mirzaei Rafsanjani & Sørensen, 2015c) (Mirzaei Rafsanjani & Sørensen, 2015b).

Finally, the set of test data is used to illustrate the procedure to rationally model the uncertainties and next to estimate the reliability for generic cases (Mirzaei Rafsanjani & Sørensen, 2014). Further, the sensitivity analysis for model uncertainties ("related to determination of stresses given fatigue load" and related to determination of fatigue loads"), are considered. The sensitivity analysis is done for both LogNormal ad Weibull distribtuions.

7.2. Future work

In this work, the focus is on the cast components of wind turbine drivetrain but the considered methodologies could be used for other compoents of wind turbine that have same material characteristics. Moreover, the geometry side effect could be considered more detailed. This thesis mainly focus on reliability assessment based on *SN* curve but in parallel the damage mechanic rules such as Paris law could be extended to estimate the fatigue failure and reliability assessment. Furthermore, it could be valuable to use more data sets for evaluations of undefined parameters to reduce the statistical uncertainties.

The methodologies could be used for operation and maintenance considerations, risk considerations and Cost-optimal reliability based design. Therefore, the

methodlogies could be used for introduction of probabilistic models for time to failure and RUL (Remaining Useful Life). These probabilistic models can be used for planning of O&M and consequently the O&M costs may be decreased.

Furthermore, information from condition monitoring and structural health monitoring could be introduced to optimize inspection intervals as well as replacements of components. Moreover, the uncertainties related to estimation of loads should and the various uncertainties such as statistical, model and measurement uncertainties have to be included in the limit state equations.

This thesis focuses on fatigue assessments of cast compoennts and another important structural component (or drivetrain components) where fatigue/damage accumulation is of importance should also be considered. Moreover, the composite material are used vastly in wind turbine industries and fatigue failure of composite material should also be considered.

Moreover, the uncertainties related to evaluation of loads must be considered and the different uncertainties such as statistical, model and measurement uncertaintiess must be included in limit state equation. Further, for each one of the load uncertainties the sensitivity analysis must be done to figure out the most critical uncertainty and planning to reduce the effect of that on reliability index.

BIBLIOGRAPHY

(u.d.). Hentet fra http://www.fei.com/software/avizo-3d/

(2015). Hentet fra FEI.com: http://www.fei.com/software/avizo-3d/

Ackermann, T. (2012). *Wind power in power systems.* Chichester: John Wiley & Sons.

Ambühl, S., Kramer, K., & Sørensen, J. (2016). Structural Reliability of Plain Bearings for Wave Energy Converter Applications . *Energies , 9* (118).

Ambuhl, S. (2015). *Reliability of wave energy converters.* PhD Thesis, Aalborg University, Department of Civil Engineering.

ASTM E466-07. (2007). *Standard practice for conducting force controlled constant amplitude axial fatigue tests of metallic materials.* ASTM International.

Ayyub, B. M., & McCuen, R. H. (2002). *Probability, Statistics, and Reliability for Engineers and Scientists* (2nd Edition udg.). CRC Press.

Berns, H., & Thesen, W. (2008). *Ferrous Materials.* Berlin: Springer.

Buffiere, J., Savelli, S., Jouneau, P., Maire, E., & Fougeres, R. (2001). Experimental study of porosity and its relation to fatigue mechanisms of model Al-Si7-Mg0.3 cast Al alloys. *Materials Science and Engineering: A , 316*, 115-126.

Byon, E., & Ding, Y. (2010). Season-dependent condition-based maintenance for a wind turbine using a partially observed Markov decision process. *Power Systems, IEEE Transactions , 25* (4), 1823-1834.

Byon, E., Ntaimo, L., & Ding, Y. (2010). Optimal maintenance strategies for wind turbine systems under stochastic weather conditions. *Reliability, IEEE Transactions , 59* (2), 393-404.

Campbell, F. C. (2008). *Elements of metallurgy and engineering alloys.* ASM International.

DNV-RP-C203. (2010). *Fatigue design of offshore steel structures.* Høvik, Norway.

Dong, W., Xing, Y., Moan, T., & Gao, Z. (2013). Time domain.based gear contact fatigue analysis of a wind turbine drivetrain under dynamic conditions. *International Journal of Fatigue , 48*, 133-146.

Dong, W., Xing, Y., Moan, T., & Gao, Z. (2013). Time domain-based gear contact fatigue analysis of a wind turbine drivetrain under dynamic conditions. *International Journal of Fatigue , 48*, 133-146.

Ecob, C. (2005). *A review of common metallurgical defects in ductile cast iron.* Elkam AS, Foundry Product Division.

EN 1990. (2002). *Eurocode - Basic of structural design.* European Committee for Standardization.

Endo, M. (1989). Effects of graphite shape, size and distribution on the fatigue strength of spheroidal graphite cast irons. *Journal of the Society of Materials Science (Japan) , 38* (433), 1139-1144.

fei.com. (u.d.). Hentet fra http://www.fei.com/software/avizo-3d-for-materials-science/

Fjeldstad, A., Wormsen, A., & Härkegård, G. (2010). Simulation of fatigue crack growth in components with random defects. *Engineering Fracture Mechanics , 75*, 1184-1203.

Gasch, R., & Twele, J. (2011). *Wind power plants: fundamentals, design, construction and operation* (2nd Edition udg.). Berlin: Springer.

Hau, E. (2006). *Wind turbines: Fundamentals, Technologies, Application, Economics* (2nd Edition udg.). New York, USA: Springer.

Horenbeek, A., Ostaeyen, J., Duflou, J., & Pintelon, L. (2013). Quantifying the added value of an imperfectly performing condition monitoring system - Application to a wind turbine gearbox. *Reliability Engineering and System Safety , 111*, 45-57.

Huitema, B. (2011). *The analysis of covariance and alternatives statistical methods for experiments, quasi-experiments, and single-case studies.* John Wiley & Sons.

IEC 61400. (2015). *Wind Turbine- Part 1: Design Requirements.* Geneva.

ISO 19902. (2007). *Petroleum and natural gas industries - Fixed steel offshore structures.*

ISO 2394. (1998). *General principles on reliability of structures.* International Organization for Standadization (ISO).

ISO 2394. (2015). *General principles on reliability of structures.* International Organization for Standadization (ISO).

JCSS. (2001). *Probabilistic Model Code.* Joint Committee on Structural Safety.

Jonkman, J., Butterfield, S., Musial, W., & Scott, G. (2009). *Definition of a 5-MW reference wind turbine for offshore system development.* Technical Report, NREL.

Källboma, R., Hambergb, K., Wesséncc, M., & Björkegrena, L. (2005). On the solidification sequence of ductile iron castings containing chunky graphite. *Materials Science and Engineering: A , 413-414*, 346–351.

Lindley, D. (1976). *Introduction to Probability and Statistics from a Bayesian Viewpoint.* Cambridge, UK: Cambridge University Press.

Link, H., LaCava, W., Van Dam, J., McNiff, B., Sheng, S., Wallen, R., et al. (2011). *Gearbox reliability collaborative project report: Findings from phase 1 and 2 testing.* Technical Report, National Renewable Energy Laboratory, Golden, CO.

Liu, W., Zhang, W., Han, J., & Wang, G. (2012). A new turbine fault diagnosis method based on the local mean decomposition. *Renewable Energy , 48*, 411-415.

Madsen, H. O., Krenk, S., & Lind, N. C. (1986). *Methods of structural safety.* Englewood cliffs, NY, USA: Prentice-Hall.

Manwell, J. F., McGowan, J. G., & Rogers, A. L. (2009). *Wind energy explained: Theory, Design and Application.* Chippenham, Wiltshire: John Wiley & Sons.

Marquez-Dominguez, S., & Sørensen, J. D. (2012). Fatigue Reliability and Calibration of Fatigue Design Factors for Offshore Wind Turbines. *Energies , 5* (6), 1816-1834.

Melchers, R. E. (1999). *Structural reliability analysis and prediction* (2nd Edition udg.). Chichester: John Wiley and Sons.

Mirzaei Rafsanjani, H., & Sørensen, J. D. (2015c). Effect of Defects Distribution on Fatigue Life of Wind Turbine Components. *Procedia IUTAM , 13*, 144-150.

Mirzaei Rafsanjani, H., & Sørensen, J. D. (2015b). Fatigue Reliability of Casted Wind Turbine Components Due to Defects. *12th International Conference on Applications of Statistics and Probability in Civil Engineering, ICASP12.* Vancouver, Canada.

Mirzaei Rafsanjani, H., & Sørensen, J. D. (2015a). Reliability analysis of fatigue failure of cast components for wind turbine. *Energies , 8*, 2908-2923.

Mirzaei Rafsanjani, H., & Sørensen, J. D. (2014). Stochastic models of defects in wind turbine drivetrain components. (M. Papadrakakis, & G. Stefanou, Red.) *Multiscale modeling and uncertainty quantification of materials and structures* , 287-298.

Mirzaei Rafsanjani, H., Sørensen, J. D., Krishnendu, M., Fæster, Søren, Sturlason, et al. (2014). Statistical analysis of manufacturing defects on fatigue life of wind turbine casted component. *International Conference on Safety & Reliability of Ships, Offshore & Subsea Structures.* Glasgow, UK: ASRANET Ltd.

Moan, T. (2008). *Structural risk and reliability analysis.* The Norwegian University of Science and Technology, Department of Marine Technology, Trondheim.

Montgomery, D. (2008). *Design and analysis of experiments.* John Wiley & Sons.

Murakami, Y. (2002). *Metal fatigue: effects of small defects and nonmetallic inclusions.* Oxford: Elsevier.

Nørskov, J. (6. January 2015). *Vindmøller slog rekord i 2014.* Hentede 6. January 2015 fra Energinet.dk: http://energinet.dk/DA/El/Nyheder/Sider/Vindmoeller-slog-rekord-i-2014.aspx

Nielsen, J. S. (2013). *Risk-based operation and maintenance of offshore wind turbines.* PhD Thesis, Aalborg University, Civil Engineering Departement.

Niimi, I., Ohashi, M., Komatsu, Y., & Hibino, Y. (1971). Influence of graphite nodules on the fatigue strength of S.G. cast iron. *IMONO (J. Cast. Inst. Jpn.) , 43* (2), 101-107.

Oyague, F. (2009). *Gearbox modeling and load simulation of a baseline 750-kW wind turbine using state-of-the-art simulation codes.* National Renewable Energy Laboratory. Golden: NREL.

Radzikowska, J. M. (2004). Metallography and microstructures of cast iron. I *ASM Handbook* (s. 565-587). Materials Par, OH, USA: ASM International.

Ravi Chandran, K. S., & Jha, S. K. (2005). Duality of the S-N fatigue curve caused by competing failure modes in a titanium alloy and the roleof Poisson defect statistics. *Acta Materialia , 53*, 1867-1881.

Rothbart, H. A., & Brown, T. H. (2006). *Mechanical Design Handbook* (2nd Edition udg.). New York: McGraw-Hill.

Sørensen, J. D. (2011). *Notes in structural reliability theory - and risk analysis.* Aalborg University, Aalborg.

Sørensen, J. D., & Toft, H. S. (2010). Probabilistic Design of Wind Turbines. *Energies , 3*, 241-257.

Sørensen, J. D., & Toft, H. S. (2014). *Safety factors - IEC 61400-1 ed. 4 - background document.* DTU Wind Energy.

Sørensen, J. (2015). Reliability Assessment of Wind Turbines. *2th International Conference on Applications of Statistics and Probability in Civil Engineering, ICASP12, July 12-15.* Vancouver, Canada.

Saleh, M. S., El-Betar, A. A., & El-Assal, A. M. (2014). Review of Modeling and Simulation Technologies Application to Wind Turbines Drive Train. *Journal on Today's Ideas - Tomorrow's Technologies , 2* (2), 117-131.

Schittkowski, K. (1986). NLPQL: A fortran subroutine solving constrained nonlinear programming problems. *Annals of Operations Research , 5*, 485-500.

Sheng, S., & Veers, P. (2011). Wind turbine drivetrain condition monitoring - an overview. *Mechanical Failures Prevention Group: Applied Systems Health Management Conference.* Virginia Beach.

Shirani, M., & Härkegård, G. (2014). A review on fatigue design of heavy section EN-GJS-400-18-LT ductile iron wind turbine castings. *Energy Equipment and Systems , 2*, 5-24.

Shirani, M., & Härkegård, G. (2012). Damage tolerant design of cast components based on defects detected by 3D X-ray computed tomography. *International Journal of Fatigue , 41*, 188-198.

Shirani, M., & Härkegård, G. (2011). Fatigue life distribution and size effect in ductile cast iron for wind turbine components. *Engineering Failure Analysis , 18*, 12-24.

Singh, B., & Agarwal, M. K. (2011). Research of cast iron in acidic medium in the industrial field as component in acid pickling. *International Journal of Research in Science and Technology , 1* (1).

Soua, S., Lieshout, P., Perera, A., Gan, T., & Bridge, B. (2013). Determination of the combined vibrational and acoustic emission signature of a wind turbine gearbox and generator shaft in service as a pre-requisite for effective condition monitoring. *Renewable Energy , 51*, 175-181.

The Guardian. (26. March 2012). Denmark aims to get 50% of all electricity from wind power.

Todinov, M. T. (2006). Equations and a fast algorithm for determining the probability of failure initiated by flaws. *International Journal of Solids and Structures , 43*, 5182-5195.

Todinov, M. T. (2000). Probability of fracture initiated by defects. *Materials Science and Engineering , A276*, 39-47.

Toft, H. S., Branner, K., Berring, P., & Sørensen, J. D. (2011). Defect distribution and reliability assesment of wind turbine blades. *Engineering Structures , 33*, 171-180.

Vittrup, C. (15. January 2014). *2013 was a record-setting year for Danish wind power.* Hentede 15. January 2014 fra Energinet.dk: http://energinet.dk/EN/El/Nyheder/Sider/2013-var-et-rekordaar-for-dansk-vindkraft.aspx

wikipedia.org. (u.d.). Hentet fra http://www.plagscan.com/highlight?doc=9231359&source=60&cite=0#jump

Wirsching, P. (1984). Fatigue reliability for offshore structures. *Journal of Structural Engineering (ASCE) , 10*, 2340-2356.

Zimmerman, D. (1997). Teacher's corner: A note on interpretation of the paired samples t test. *Journal of Educational and Behavioral Statistics , 22* (3), 349-360.

A PAPER 1

Title: Reliability of analysis of fatigue failure of cast components for wind turbines.

Authors: Hesam Mirzaei Rafsanjani, John Dalsgaard Sørensen

Journal: Energies, 8(4), 2908-2923

Year: 2015

Energies **2015**, *8*, 2908-2923; doi:10.3390/en8042908

OPEN ACCESS

energies

ISSN 1996-1073

www.mdpi.com/journal/energies

Article

Reliability Analysis of Fatigue Failure of Cast Components for Wind Turbines

Hesam Mirzaei Rafsanjani * and John Dalsgaard Sørensen

Department of Civil Engineering, Aalborg University, Aalborg 9200, Denmark;
E-Mail: jds@civil.aau.dk

* Author to whom correspondence should be addressed; E-Mail: hmr@civil.aau.dk;
Tel.: +45-9940-8557.

Academic Editor: Frede Blaabjerg

Received: 23 December 2014 / Accepted: 7 April 2015 / Published: 15 April 2015

Abstract: Fatigue failure is one of the main failure modes for wind turbine drivetrain components made of cast iron. The wind turbine drivetrain consists of a variety of heavily loaded components, like the main shaft, the main bearings, the gearbox and the generator. The failure of each component will lead to substantial economic losses such as cost of lost energy production and cost of repairs. During the design lifetime, the drivetrain components are exposed to variable loads from winds and waves and other sources of loads that are uncertain and have to be modeled as stochastic variables. The types of loads are different for offshore and onshore wind turbines. Moreover, uncertainties about the fatigue strength play an important role in modeling and assessment of the reliability of the components. In this paper, a generic stochastic model for fatigue failure of cast iron components based on fatigue test data and a limit state equation for fatigue failure based on the SN-curve approach and Miner's rule is presented. The statistical analysis of the fatigue data is performed using the Maximum Likelihood Method which also gives an estimate of the statistical uncertainties. Finally, illustrative examples are presented with reliability analyses depending on various stochastic models and partial safety factors.

Keywords: wind turbine; drivetrain; fatigue; stochastic model; reliability analysis

---

1. Introduction

Wind energy is a rapid growing industry in the renewable energy sector with large the potential to contribute significantly to future energy production. A main focus for wind turbine manufacturers and operators is how to increase the reliability of wind turbines and to decrease their cost. Hence, cheaper and more efficient wind turbine components have to be developed to have an optimal balance between initial costs related to required reliability level on the one hand and the cost of operation and maintenance on the other hand. In order to perform this optimization, it is important to be able to estimate the reliability of the components.

Wind turbines, depending on whether placed in offshore or onshore locations, are exposed to wave excitations, highly dynamic wind loads and the wakes from other wind turbines. Therefore, most components in a wind turbine experience highly dynamic and time-varying loads. These components may fail due to wear or fatigue and this can lead to unplanned shutdown repairs that are very costly. The design of mechanical components in the wind turbine drivetrain by deterministic methods using safety factors is generally unable to account for the many uncertainties. Thus, a reliability assessment should be based on probabilistic methods where stochastic modeling of failures is performed.

The most common drivetrain configuration consists of the main shaft, the main bearings, the gearbox and the generator, see [1]. Modeling of the reliability of drivetrain component failures is important for predicting the expected time-to-failure which is an important indicator to be used in planning of operation and maintenance. In order to estimate the probability of failure of the drivetrain components careful modeling of the aleatory (physical) and epistemic (model, statistical and measurement) uncertainties has to be performed, see e.g., [2,3].

The reliability of wind turbine gearboxes has been studied in a number of research projects, e.g., the Gearbox Reliability Collaboration (GRC) project at the U.S. National Renewable Energy Laboratory (NREL) [4]. This includes important research areas on fault diagnosis and condition monitoring. Several methods have been investigated, such as vibration and acoustic emissions [5] and local mean decomposition [6]. Some studies on probabilistic modeling of failures in wind turbine drivetrain components have been carried out, e.g., [7,8] but without a detailed stochastic modeling of the uncertainties related to the parameters in the limit state equations modeling each failure mode.

This paper focuses on probabilistic models and the stochastic modeling of fatigue lives in the wind turbine drivetrain using structural reliability methods, see [9], allowing a rational modeling of all uncertainties. An important aspect in modeling fatigue failure of large cast steel components is to take into account scale effects. Two approaches are considered in this paper for stochastic modeling of the fatigue life including scale effects. One method is based on the classical Weibull approach and the other on application of a log-normal distribution as done, e.g., for the fatigue life of welded steel details. The statistical parameters in both models are estimated and applied in reliability assessments.

2. Wind Turbine Drivetrain

The drivetrain of a wind turbine converts the low-speed, high-torque rotation of the turbine's rotor (blades and hub assembly) into electrical energy. The most common drivetrain configuration consists

of the main shaft, the main bearings, the gearbox and the generator, see [1] and [10]. Typically, all individual components of the drivetrain are mounted onto the bedplate (Figure 1).

The main bearing, the main shaft and the gearbox have the highest downtime in case of failures, see e.g., [2,11]. Cyclic and variable loads excite these components during their service life and consequently fatigue is one of the main sources of failure of these components.

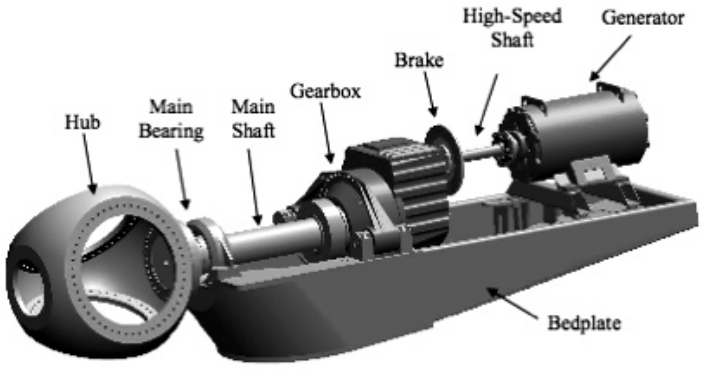

Figure 1. Modular configuration of wind turbine drivetrain components [10].

The current fatigue design is based on the life design approach [8]. In the safe life design, fatigue testing is carried out on baseline material to produce *SN* curves. However, the fatigue strength is highly uncertain and statistical uncertainties due to a limited number of tests can be important to include in modeling the fatigue strength. Moreover, model uncertainties related to e.g., application of the Miner rule for fatigue damage accumulation should be included in the probabilistic model.

3. Fatigue Strength Modeled by a Log-Normal Distribution

Fatigue failures typically occur due to the application of fluctuating stresses much lower than the stress required to cause failure during a single application of the stress. The fatigue life is the number of cycles to failure at a specified stress level, while the fatigue strength is the stress level below which failure does not occur for the given number of cycles. As the applied stress level decreases, the number of cycles to failure increases. The fatigue strength of metals is often assumed to follow the Basquin equation (the equation is based on fully reversed fatigue ($R = -1$), and the mean value is zero) [12]:

$$\sigma_a = \sigma_f (2N)^{-\frac{1}{m}} \tag{1}$$

where σ_a is the alternating stress amplitude, σ_f is the fatigue strength coefficient, N is the number of load cycle, and $1/m$ is the fatigue strength exponent.

The probability of failure increases when the volume of the component increases due to scale effects and because the probability of finding a critical micro-crack increases [8]. Thus the geometrical size effect affects the resistance of materials against fatigue failure. Hence, σ_a is affected by geometrical size effects and can be modeled by the following equation, see e.g., [8]. According to this Equation (1) can be written as [13]:

$$N = \frac{1}{2}\left(\frac{\sigma_{a0}}{\sigma_f}\right)^{-m}\left(\frac{V}{V_0}\right)^{\frac{1}{b_n}} = \frac{1}{2}\left(\frac{\sigma_{a0}}{\sigma_f}\right)^{-m} s_V^{\frac{1}{b_n}} \tag{2}$$

where V_0 is the reference volume and σ_{a0} is the alternative fatigue strength amplitude corresponding to reference volume of V_0. The exponent b_n determines the effect of the specimen size on the fatigue life and V is the volume of component. In a log-log format Equation (2) is linear and can be rewritten introducing an uncertainty term ε, see [13]:

$$\log N = m\log\sigma_f - m\log\sigma_{a0} + \frac{1}{b_n}\log s_V - \log(2) + \varepsilon \tag{3}$$

where ε is assumed to be normal distributed with mean value = 0 and standard deviation = σ_ε. ε models the scatter in fatigue life and can be considered here to cover both physical and model uncertainties related to imperfect knowledge or idealizations of the mathematical models used or uncertainty related to the choice of probability distribution types for the stochastic variables. It is noted that the test data applied in the example below do not allow a bilinear *SN* curve to be fitted; but the above model can easily be extended to model a bi-linear *SN* curve and a lower threshold.

The parameters in (3) can be estimated using available test data. In this paper, test data extracted from Shirani [14] are used to exemplify the procedure for the stochastic modeling. Assuming that the Shirani data are representative the results of the statistical analysis can also be used to assess the reliability level for drivetrain components and to calibrate safety factors, see below.

In the following, the Maximum Likelihood Method is used for the statistical analysis. The log-likelihood function as a function of the statistical parameters σ_f, m, and σ_ε to be estimated is written as follows accounting both for tests results where failure occurs and test results where failure does not occur (run-outs) (note, the uncertainty related to σ_f and m model statistical uncertainties and ε models model uncertainty):

$$\begin{aligned} L(\sigma_f, m, \sigma_s) &= \prod_{i=1}^{n_F} P\left[\log n_i = m\log\sigma_f - m\log\sigma_{a0,i} + \frac{1}{b_n}\log s_V + \varepsilon - \log 2\right] \\ &\times \prod_{i=1}^{n_R} P\left[\log n_i \rangle m\log\sigma_f - m\log\sigma_{a0,i} + \frac{1}{b_n}\log s_V + \varepsilon - \log 2\right] \end{aligned} \tag{4}$$

where n_i is the number of stress cycles to failure or run-out (no failure) with stress range equal to $\sigma_{a0,i}$ in test number i. n_F is the number of tests where failure occurs, and n_R is the number of tests where failure does not occur after n_i stress cycles (run-outs). $n = n_F + n_R$ is the total number of tests. σ_f, m, and σ_ε are estimated solving the optimization problem: max $L(\sigma_f, m, \sigma_\varepsilon)$. This can be done using a standard nonlinear optimizer, e.g., the NLPQL algorithm, see [15].

Since the parameters σ_f, m and σ_ε are estimated by the maximum-likelihood technique, they become asymptotically (number of data should be larger than 25–30) normally distributed stochastic variables with expected values equal to maximum-likelihood estimates and covariance matrix equal to, see [16]:

$$C_{\sigma_f,m,\sigma_\tau} = \left[-H_{\sigma_f,m,\sigma_\tau}\right]^{-1} = \begin{bmatrix} \sigma^2_{\sigma_f} & \rho_{\sigma_f,m}\sigma_{\sigma_f}\sigma_m & \rho_{\sigma_f,\sigma_\tau}\sigma_{\sigma_f}\sigma_{\sigma_\tau} \\ \rho_{\sigma_f,m}\sigma_{\sigma_f}\sigma_m & \sigma^2_m & \rho_{m,\sigma_\tau}\sigma_m\sigma_{\sigma_\tau} \\ \rho_{\sigma_f,\sigma_\tau}\sigma_{\sigma_f}\sigma_{\sigma_\tau} & \rho_{m,\sigma_\tau}\sigma_m\sigma_{\sigma_\tau} & \sigma^2_{\sigma_\tau} \end{bmatrix} \tag{5}$$

where $H_{\sigma_f,m,\sigma_\tau}$ is the Hessian matrix with second-order derivatives of the log-likelihood function. σ_{σ_f}, σ_m and σ_{σ_τ} denote the standard deviation of σ_f, m and σ_ε respectively and $\rho_{\cdot,\cdot}$ indicates correlation coefficients. Alternatively to the log-normal model for the *SN* curve a Weibull model can be used, as described in the next section.

4. Fatigue Strength Modeled by a Weibull Distribution

As mentioned above, the strength of wind turbine drivetrain components are subject to uncertainties and therefore a stochastic modeling of life distribution is needed to study the reliability of the components. The influence of scale effects on damage modeling and fatigue life can from a theoretical basis be modeled by a Weibull mode, see e.g., [9]. Hence, the fatigue life can be modeled by a Weibull distribution for number of cycles to failure, N given stress range σ_{a0} is written as:

$$F_N(n) = 1 - \exp\left[-\left(\frac{n}{N(\sigma_{a0})}\right)^{b_n}\right] \tag{6}$$

where b_n is a shape parameter. By substituting Equation (2) in Equation (6), the corresponding density function becomes [13]:

$$f_N(n) = \frac{2b_n}{S_V^{1/b_n}}\left(\frac{\sigma_{a0}}{\sigma_f}\right)^m\left(\frac{2n}{S_V^{1/b_n}}\left(\frac{\sigma_{a0}}{\sigma_f}\right)^m\right)^{b_n-1}\exp\left[-\left(\frac{2n}{S_V^{1/b_n}}\left(\frac{\sigma_{a0}}{\sigma_f}\right)^m\right)^{b_n}\right] \tag{7}$$

The statistical parameters σ_f and m in Equation (7) can be estimated by the maximum-likelihood method with the likelihood function:

$$\begin{aligned}\ln L(\sigma_f, m) = \ln\left(\prod_{i=1}^{n} f_N(n_i)\right) = \sum_{i=1}^{n_F}\ln\left(\frac{2b_n}{S_V^{1/b_n}}\left(\frac{\sigma_{a0,i}}{\sigma_f}\right)^m\left(\frac{2n_i}{S_V^{1/b_n}}\left(\frac{\sigma_{a0,i}}{\sigma_f}\right)^m\right)^{b_n-1}\exp\left[-\left(\frac{2n_i}{S_V^{1/b_n}}\left(\frac{\sigma_{a0,i}}{\sigma_f}\right)^m\right)^{b_n}\right]\right)\\ + \sum_{i=1}^{n_R}\ln\left(\exp\left[-\left(\frac{2n_i}{S_V^{1/b_n}}\left(\frac{\sigma_{a0,i}}{\sigma_f}\right)^m\right)^{b_n}\right]\right)\end{aligned} \tag{8}$$

where n_i, n_F, n_R and n are introduced in previous section and they are obtained solving the optimization problem max $L(\sigma_f, m)$, see above.

5. Characteristic Values

In deterministic approaches, code-based design safety is introduced though application of deterministic values in terms of characteristic values and safety factors to obtain design values of both loads and strengths. In the following a probabilistic basis is used to estimate the characteristic values by modeling of physical, measurement, statistical and model uncertainties.

If statistical uncertainty is not taken into account then corresponding to a stress range, $\sigma_{a0,c}$ a characteristic value of the fatigue life, n_c defined as the 5% quantile can be estimated directly from the distribution function of the fatigue life.

If statistical uncertainty is to be taken into account and the physical/model uncertainties for the fatigue life are modeled by a log-normal distribution then the characteristic value for the fatigue life, n_c corresponding to the stress range, $\sigma_{a0,c}$ defined as a 5% quantile can obtained from by:

$$P\left(\log n_c \rangle m\log\sigma_f - m\log\sigma_{a0,c} + \frac{1}{b_n}\log s_V + \varepsilon - \log 2\right) = 0.05 \tag{9}$$

with a corresponding limit state equation written as:

$$g\left(\sigma_f, m, \varepsilon, \sigma_\varepsilon\right) = m\log\sigma_f - m\log\sigma_{a0,c} + \frac{1}{b_n}\log s_V + \varepsilon - \log 2 - \log n_c \tag{10}$$

Here, ε, m, σ_ε and σ_f are modeled as stochastic variables as described above. For given $\sigma_{a0,c}$ Equation (10) can be solved with respect to the characteristic fatigue life, n_c using e.g., First Order Reliability Methods (FORM, see [9]).

Similarly, if the fatigue life is modeled by a Weibull distribution and statistical uncertainty is accounted for, and then the characteristic value can be estimated using the following limit state equation:

$$g\left(\sigma_f, m, \varepsilon, \sigma_\varepsilon\right) = \log n_c + \log 2 - \frac{1}{b_n}\log s_V + m\log\sigma_{a0,c} - m\log\sigma_f - \log\left(-\ln\left(0.95\right)\right)^{1/b_n} - \varepsilon \tag{11}$$

In equation (11), ε, σ_ε, m and σ_f model the physical/model and statistical uncertainties, respectively. As mentioned before, these parameters can be obtained from test results.

6. Reliability Analysis

Reliability of a component can be defined as the probability that the component under consideration has a proper performance throughout its lifetime. Structural reliability methods can be used to estimate the probability of failure/reliability which next can be used for decision-making, e.g., with respect to design or planning of inspections, maintenance and repair.

The reliability estimated as a measure of the safety of a structure can be used in a decision process (for example Markov decision process [17]). A lower level of the acceptable reliability can be used as a constraint in a reliability-based optimal design problem. The lower level of the reliability can be obtained by analyzing similar structures designed after current design practice or it can be determined as the reliability level giving the largest utility (benefits-costs) when solving a decision problem where all possible costs and benefits in the expected lifetime of the structure are taken into account. Further, the reliability and failure rate of components can be used for decision making for maintenance plans [18].

Drivetrain components are typically exposed to complex loading conditions, [12]. Often the fatigue load is due to a range of fluctuating loads, different mean stress levels and variable frequencies. Cumulative damage theories consider the fatigue process to be one of damage accumulation until the life of the component is exhausted. Cumulative damage during fatigue is often modeled by using the

Palmgren-Miner rule, which assumes that the total life of a part can be estimated by adding up the percentage of life consumed by each stress level [12] and can be written as follows if used in a deterministic code-based verification:

$$D = \sum_i \frac{n_{i,S} T_L}{N_{0;0.05}\left(\frac{\sigma_{a0,i}}{z}, \frac{\sigma_f}{\gamma_m}\right)} = 1 \tag{12}$$

where $n_{i,S}$ represent the number of cycles per year at a specific stress level $\sigma_{a0,i}$ and T_L is the design lifetime. It is assumed that for a wind turbine component the total number of stress ranges for a given fatigue critical detail can be grouped in n_σ groups/intervals such that the number of stress ranges in group i is $n_{i,S}$ per year. ($\sigma_{a0,i}$, $n_{i,S}$) can be obtained by rain-flow counting and can be represented by so-called 'Markov matrices'. Further, $N_{0;0.05}\left(\frac{\sigma_{a0,i}}{z}, \frac{\sigma_f}{\gamma_m}\right)$ is the 5% quantile of the number of cycles to failure given fatigue load equal to $\sigma_{a0,i}/z$ and given the design fatigue strength σ_f/γ_m. $N_{0;0.05}$ can be obtained both without and with statistical uncertainty included. z is a design / scaling parameter, e.g., related to a cross-sectional parameter; γ_m is a partial safety factor for fatigue.

In this paper, the Level II method is used to measure the reliability of the components [9]. The design parameter z is obtained from (12) assuming that a fatigue partial safety factor γ_m is given. Thereby the reliability analyses become normalized in the way that the reliability is linked to the partial safety factors and it is assumed that the structure is designed to the limit though the design parameter z in the design equation. The corresponding limit state equation to be used in the reliability analysis is written:

$$g(t) = \Delta - \sum_i \frac{n_{i,S} t}{N_{0;0.05}\left(\frac{X_W X_{SCF} \sigma_{a0,i}}{z}, \sigma_f\right)} \tag{13}$$

where t is time (in years), Δ models model uncertainty related to Miner's rule for linear damage accumulation. The distribution function for number of cycles to failure, $N_{0;0.05}$ for given stress $\sigma_{a,i}$ can be obtained by equations (10) and (11) for log-normal and Weibull distributed fatigue lives. If statistical uncertainty is included then the statistical parameters are modeled by stochastic variables. X_W is a stochastic variable modeling model uncertainty related to determination of fatigue loads and X_{SCF} is a stochastic variable modeling model uncertainty related to determination of stresses given fatigue loads. For wind turbines the fatigue loads are typically estimated for mean wind speeds from 4 m/s to 25 m/s and are normally represented by time series of load effects or equivalently by Markov matrices obtained by rain-flow counting. In the example below these loads are extracted from simulated loads for the main shaft of a 5 MW wind turbine for each mean wind speed V_j. The hub diameter is 3 meter and the rotor has a diameter of 126 meter. The hub height is 90 meter. The cut-in and cut-out wind speeds are 3 m/s and 25 m/s, respectively. Further information can be found in reference [19].

Based on the geometry of the component (main shaft) and the load matrices, the stress amplitudes have been calculated. The calculated values are not fully reversed stress amplitude. Hence, the Goodman equation is used to find the effective fully reversed stress amplitudes for each mean speed.

Equation (12) is thus rewritten:

$$D = \sum_{V_j} \left(\sum_i \frac{n_{i,S,j} T_L}{N_{0;0.05}\left(\frac{\sigma_{a0,i,j}}{z}, \frac{\sigma_f}{\gamma_m} \right)} \right) * P\left(V_j\right) = 1 \tag{14}$$

where, V_j is the mean wind speed and $P(V_j)$ is probability of occurrence of this mean wind speed, modelled by a Weibull distribution according to IEC 61400-1 [20]. In the example below, the scale and shape parameters of Weibull distribution have been chosen to 11.48 [m/s] and 1.75, respectively [21]. By substituting Equation (14) in Equation (13), the limit state equation can be written:

$$g(t) = \Delta - \sum_{V_j} \left(\sum_i \frac{n_{i,S,j} t}{N_{0;0.05}\left(\frac{X_W X_{SCF} \sigma_{a0,i,j}}{z}, \sigma_f \right)} \right) * P\left(V_j\right) \tag{15}$$

In Equation (15), Δ, X_W and X_{SCF} are assumed to be log-normal distributed with mean values equal 1 and coefficients of variation COV_Δ, COV_W and COV_{SCF}, respectively, following the recommendations in [22]. The coefficient of variations are estimated based partly subjectively, but following generally the recommendations used as basis for the material partial safety factors in IEC 61400-1, and also considering information from e.g., DNV-RP-C203 [23] although this is not directly related to the fatigue problem considered in this paper. The importance of the choices of the coefficient of variations is investigated by sensitivity analyses. It is noted that the reliability level obtained is in accordance with the target reliability corresponding to an annual probability of failure of the order 5×10^{-4} (annual reliability index: 3.3) [20].

Table 1 shows the representative stochastic model. Expected values and coefficient of variations for m and σ_f are extracted from tests results as described above. Based on Equation (15), the probability of failure in the time interval $[0,t]$ can be estimated by FORM/SORM techniques or simulation, see e.g., [9]. The reliability index, $\beta(t)$ corresponding to the accumulated probability of failure $P_F(t)$ is defined by:

$$\beta\left(t\right) = -\Phi^{-1}\left(P_F\left(t\right)\right) \tag{16}$$

where $\Phi(\ )$ is the standardized normal distribution function. The annual probability of failure conditioned on survival up to time t is obtained from:

$$\Delta P_F\left(t\right) = \left(P_F\left(t - \Delta t\right) - P_F\left(t\right)\right) / \Delta t / \left(1 - P_F\left(t\right)\right) \tag{17}$$

where Δt is a time increment, typically 1 year. The reliability index, $\Delta\beta$ corresponding to the probability ΔP_F is denoted the annual reliability index when Δt = 1 year.

Table 1. Stochastic model.

Variable	Definition	Distribution	Expected Value	Coefficient of variation
Δ	Model uncertainty related to Miner's rule	LN *	1	0.2
X_{SCF}	Model uncertainty related to determination of stresses given fatigue load	LN	1	0.05
X_W	Model uncertainty related to determination of fatigue loads	LN	1	0.1
m	Statistical uncertainty	N **	Extracted from test results	
σ_f [MPa]	Statistical uncertainty	N	Extracted from test results	

* LN: Log-normal distribution; ** N: Normal distribution.

7. Results

As mentioned above the test data by Shirani [14] will be used to illustrate the above statistical analysis and reliability assessment for wind turbine drivetrain components. The test data follows the specifications listed in Table 2. Two series of specimens were machined from T95 block (the cast block dimensions were 750 mm × 200 mm × 95 mm), and T150 block (the cast block dimensions were 150 mm × 300 mm × 150 mm), specimens with 21 mm diameter. Specimens were tested at load ratios $R = -1$ (with R defined by $R = \frac{\sigma_{\min}}{\sigma_{\max}} = \frac{\sigma_m - \sigma_a}{\sigma_m + \sigma_a}$) [14].

Table 2. The test plan [14].

Material	Load Ratio	Specimen [mm]	Number of specimens	Test frequency [Hz]
T95	−1	Ø21	12	10
T150	−1	Ø21	18	10

The statistical analysis is performed following the methodology described in section 3 and 4 for estimation of the parameters in the log-normal and Weibull models. The results using the log-normal distribution model (Equations (6) and (7)) are shown in Table 3.

Table 3. Estimated statistical parameters from tests with log-normal model for fatigue life.

Test	σ_f [MPa]		m		σ_ε	
	Mean	*Std dev*	*mean*	*Std dev*	*mean*	*Std dev*
D21 T95 R = −1	941	50.5	9.4	0.33	0.25	0.01
D21 T150 R = −1	697	67.9	10.7	0.83	0.23	0.04

As mentioned in Table 2, the tests "D21 T95 R = −1" and "D21 T150 R = −1" are done with the same frequency and the same load ratio. Hence, these two tests can be used to study the changes of volume/size effects on the fatigue strength. Moreover, the correlation matrixes of the statistical parameters for these two tests are shown below for illustration.

$$\text{Correlation matrix} = \begin{bmatrix} \sigma_{\sigma_f}^2 & \rho_{\sigma_f,m}\sigma_{\sigma_f}\sigma_m & \rho_{\sigma_f,\sigma_\varepsilon}\sigma_{\sigma_f}\sigma_{\sigma_\varepsilon} \\ \rho_{\sigma_f,m}\sigma_{\sigma_f}\sigma_m & \sigma_m^2 & \rho_{m,\sigma_\varepsilon}\sigma_m\sigma_{\sigma_\varepsilon} \\ \rho_{\sigma_f,\sigma_\varepsilon}\sigma_{\sigma_f}\sigma_{\sigma_\varepsilon} & \rho_{m,\sigma_\varepsilon}\sigma_m\sigma_{\sigma_\varepsilon} & \sigma_{\sigma_\varepsilon}^2 \end{bmatrix} = \begin{bmatrix} 1 & -0.96 & 0.21 \\ -0.96 & 1 & -0.17 \\ 0.21 & -0.17 & 1 \end{bmatrix} \quad \text{Test D21 T95 R= } -1$$

$$\text{Correlation matrix} = \begin{bmatrix} \sigma_{\sigma_f}^2 & \rho_{\sigma_f,m}\sigma_{\sigma_f}\sigma_m & \rho_{\sigma_f,\sigma_\varepsilon}\sigma_{\sigma_f}\sigma_{\sigma_\varepsilon} \\ \rho_{\sigma_f,m}\sigma_{\sigma_f}\sigma_m & \sigma_m^2 & \rho_{m,\sigma_\varepsilon}\sigma_m\sigma_{\sigma_\varepsilon} \\ \rho_{\sigma_f,\sigma_\varepsilon}\sigma_{\sigma_f}\sigma_{\sigma_\varepsilon} & \rho_{m,\sigma_\varepsilon}\sigma_m\sigma_{\sigma_\varepsilon} & \sigma_{\sigma_\varepsilon}^2 \end{bmatrix} = \begin{bmatrix} 1 & -0.99 & 0.07 \\ -0.99 & 1 & -0.06 \\ 0.07 & -0.06 & 1 \end{bmatrix} \quad \text{Test D21 T150 R= } -1$$

It is seen that σ_f and m are highly negative correlated (as expected). Next, the statistical uncertainties of fitted parameters using the Weibull distribution to model the fatigue life are extracted using the Maximum Likelihood Method. The results are shown in Table 4.

Table 4. Estimated statistical parameters from tests with Weibull model for fatigue life.

Test	σ_f [MPa]		m	
	mean	***Std dev***	***mean***	***Std dev***
D21 T95 R = −1	979	8.18	9.2	0.05
D21 T150 R = −1	686	5.76	10.9	0.07

Figures 2 and 3 show the mean and characteristic *SN* curves with log-normal and Weibull distributions for the fatigue life for tests "D21 T95 R = −1" and "D21 T150 R = −1" and with statistical uncertainties included. The figures show that the difference between the Weibull and log-normal models is small.

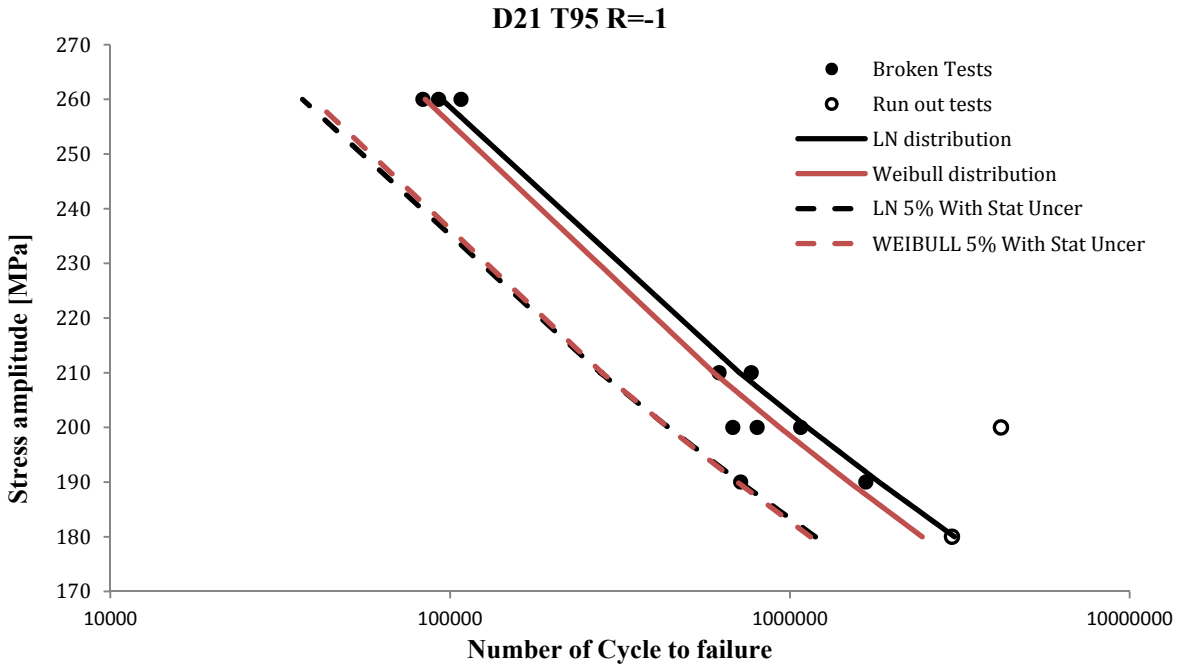

Figure 2. *SN* data for test D21 T95 R = −1 with fitted mean and characteristic *SN* curves.

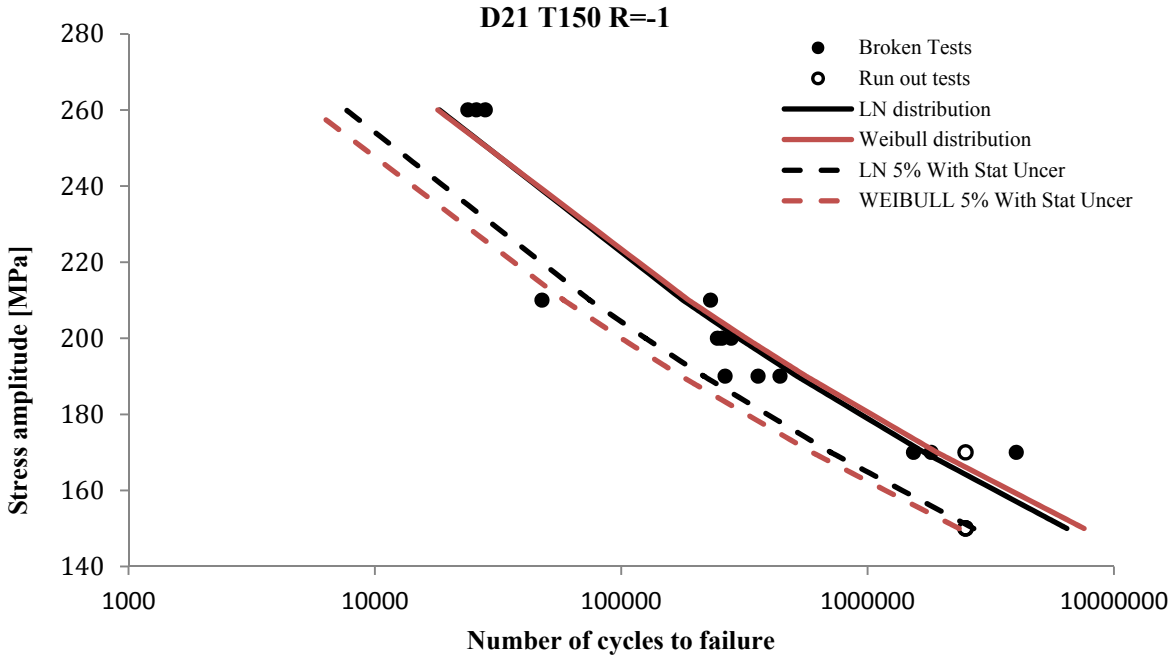

Figure 3. *SN* data for test D21 T150 R = −1 with fitted mean and characteristic *SN* curves.

Next, using these estimated statistical parameters, the annual reliability index is estimated. First, the reliability index is determined with the partial safety factor, γ_m varying between 1.5 and 2, see Figures 4 and 5. It is seen that the Weibull distribution model has the lowest sensitivity with respect to changes of the partial safety factor when compared to log-normal distribution model. The target reliability level for wind turbines is typically in the interval from 3.1 to 3.8 for the annual reliability index corresponding to annual probabilities of failure between 10^{-4} and 10^{-3}. From Figure 4, it is seen as expected that when the partial safety factor increases, the reliability index increases.

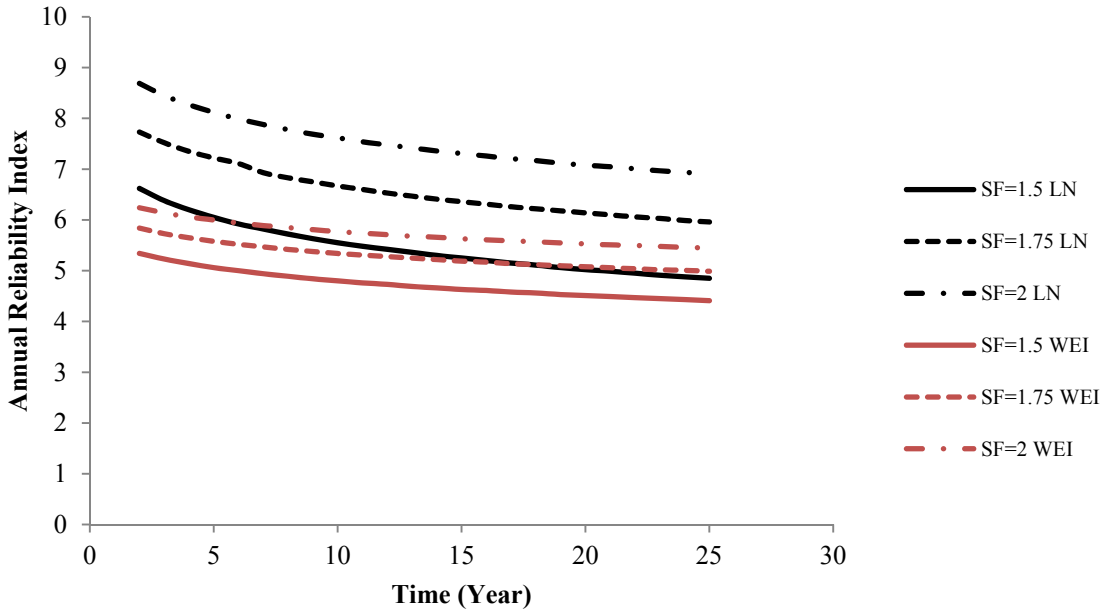

Figure 4. Annual reliability index for partial safety factor γ_m = 1.5, 1.75 and 2.0 using the Weibull and log-normal models. Test D21 T95 R = −1.

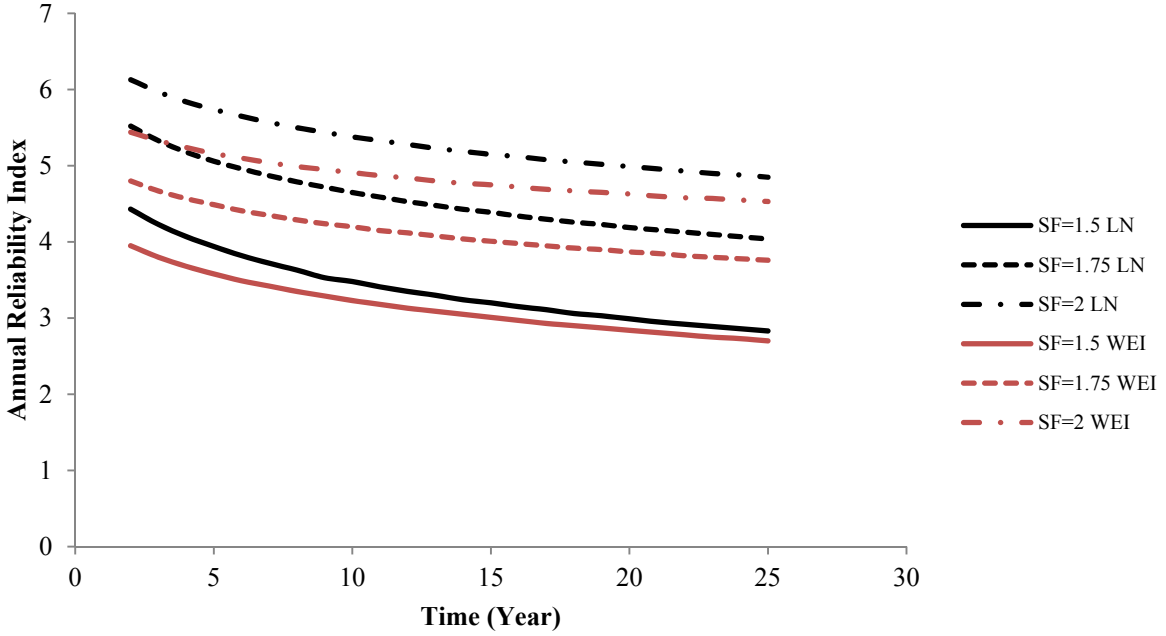

Figure 5. Annual reliability index for partial safety factor γ_m = 1.5, 1.75 and 2.0 using the Weibull and log-normal models. Test D21 T150 R = −1.

Next, the sensitivity of the reliability with respect to the uncertainty level of X_W and X_{SCF} is investigated. The partial safety factor, γ_m equal to 1.75 is used in all the following cases. The results for X_W are shown in Figures 6 and 7. It is seen that when the uncertainty related to the fatigue loads increases, then the reliability index based on the log-normal distribution model decrease more than the reliability index based on the Weibull distribution model. It is also seen that the reliability index is quite sensitive to the coefficient of variation of X_W.

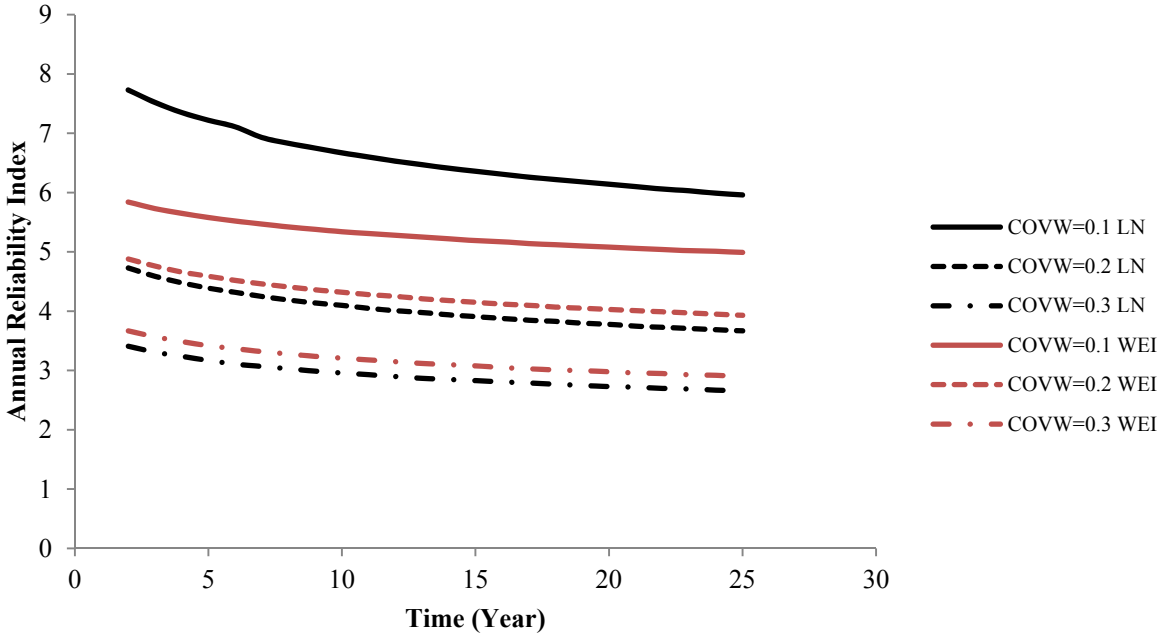

Figure 6. Annual reliability index for different uncertainty models for X_W. Test D21 T95 R = −1.

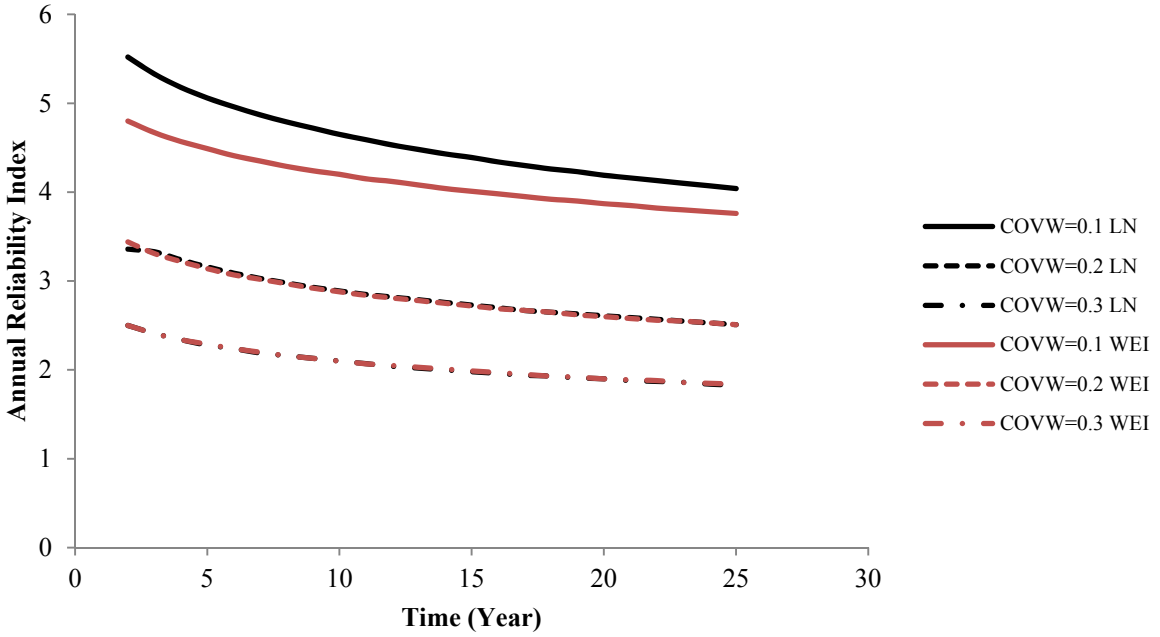

Figure 7. Annual reliability index for different uncertainty models for X_W. Test D21 T150 R = −1.

Next, the influence of the uncertainty of X_{SCF} is investigated. Figures 8 and 9 show the results for the coefficient of variation of X_{SCF} equal to 0.05, 0.15 and 0.25. The results are similar to those obtained for X_W. Furthermore, the geometrical size effect affects the resistance of the material against fatigue failure. As mentioned above, the results of "D21 T95 R = −1" and "D21 T150 R = −1" are used as basis for investigating the geometrical size effects.

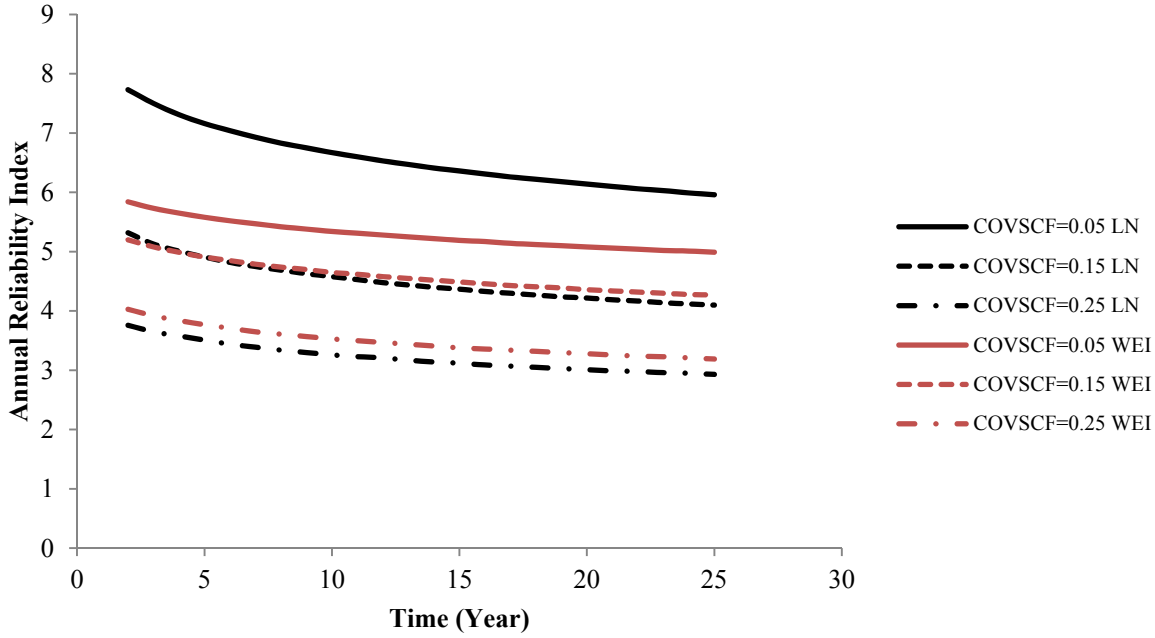

Figure 8. Annual reliability index for different uncertainty models for X_{SCF}. Test D21 T95 R = −1.

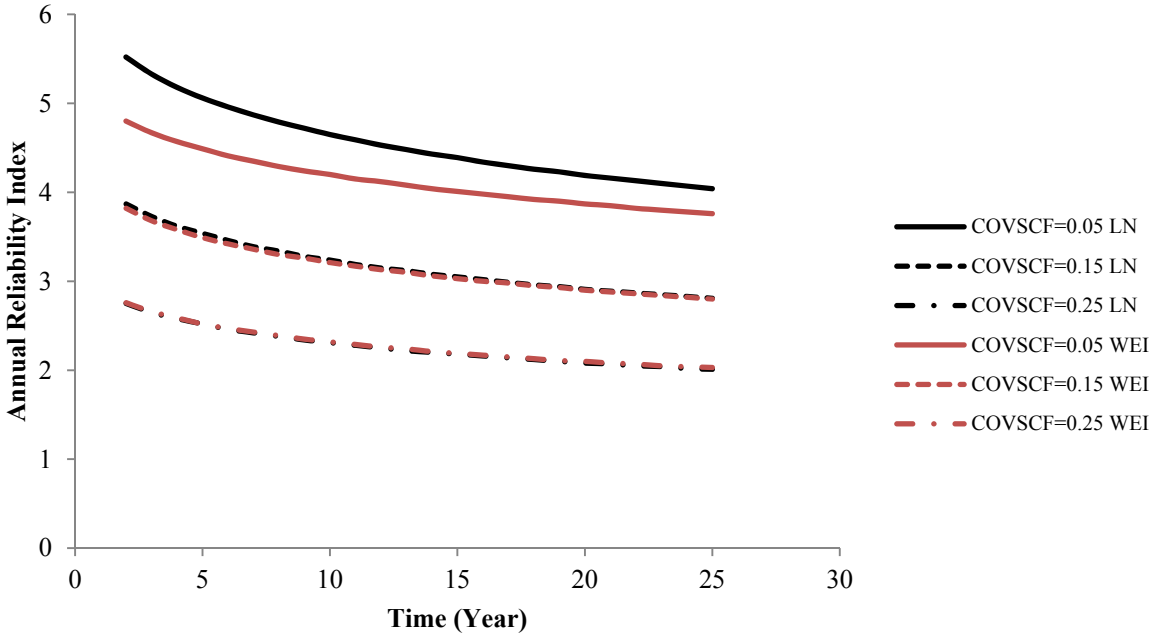

Figure 9. Annual reliability index for different uncertainty models for X_{SCF}. Test D21 T150 R = −1.

By comparing Figures 2 and 3, the fatigue life of specimen "D21 T95 R = −1" is higher than the fatigue life of "D21 T150 R= −1" and it is seen that when the volume of a component increase, the fatigue life of the component decrease. This effect is important to include in reliability assessments. Moreover, by comparing the Figures 6,7 and Figures 8,9 for various assumptions of the uncertainties of X_W and X_{SCF}, it is seen that the annual reliability index of T150 is (as expected) lower than T95 in all cases. Consequently, higher safety factor must be applied in the design process for larger components and the geometrical size effect may affect the design significantly.

8. Conclusions

In this paper, different stochastic models for fatigue failure of casted steel components in wind turbine drivetrain components are considered. Firstly, the fatigue life is modeled and various uncertainties that affect the stochastic models of failure are described including size effects. These uncertainties include model and statistical uncertainties. The basic uncertainty of the fatigue life is modeled by two distribution models, namely log-normal and Weibull distribution. It is described how the statistical parameters can be derived including the statistical uncertainties. Next, characteristic *SN*-curves are derived using structural reliability techniques.

A set of test data is used to illustrate the procedure to rationally model the uncertainties and next to estimate the reliability for generic cases. The results indicate that the characteristic *SN*-curves are almost the same using the Weibull and log-normal models, but the reliability obtained by the log-normal distribution model is generally higher than reliability index obtained using the Weibull distribution model. Further, the uncertainty of the load model is seen to influence the reliability level significantly. The same is the case for the size effect. This implies that safety factors used in deterministic design should reflect these uncertainties. This effect is not studied in this paper but will be done in future work.

Acknowledgments

The work is supported by the Strategic Research Center "REWIND–Knowledge based engineering for improved reliability of critical wind turbine components", Danish Research Council for Strategic Research, grant no. 10-093966.

Author Contributions

All the authors contributed to the data collection, analysis, and paper write up.

Conflicts of Interest

The authors declare no conflict of interest.

References

1. Hau, E. *Wind Turbines: Fundamentals, Technologies, Application, Economics*, 2nd ed.; Springer: New York, NY, USA, 2006.
2. Sheng, S.; Veers, P. Wind turbine drivetrain condition monitoring—an overview. In Proceedings of the Mechanical Failures Prevention Group: Applied Systems Health Management Conference 2011, Virginia Beach, VA, USA, 10−12 May 2011.
3. Mirzaei Rafsanjani, H.; Sørensen, J.D. Stochastic modeling of wind turbine drivetrain components. In *Safety, Reliability and Risk Analysis: Beyond the Horizon*; Proceedings of the European Safety and Reliability Conference, Amsterdam, The Netherlands, 29 September–2 October 2013; Steenbergen, R.D.J.M., van Gelder, P.H.A.J.M., Miraglia, S., Vrouwenvelder, A.C.W.M., Eds.; CRC Press LLC: Leiden, The Netherland, 2013; pp. 1221–1228.
4. Link, H.; LaCava, W.; Van Dam, J.; McNiff, B.; Sheng, S.; Wallen, R.; McDade, M.; Lambert, S.; Butterfield, S.; Oyague, F. *Gearbox Reliability Collaborative Project Report: Findings from Phase 1 and Phase 2 Testing*; Technical Report NREL/TP-5000-51885; National Renewable Energy Laboratory: Golden, CO, USA, 2011.
5. Soua, S.; Lieshout, P.V.; Perera, A.; Gan, T.; Bridge, B. Determination of the combined vibrational and acoustic emission signature of a wind turbine gearbox and generator shaft in service as a pre-requisite for effective condition monitoring. *Renew. Energy* **2013**, *51*, 175–181.
6. Liu, W.Y.; Zhang, W.H.; Han, J.G.; Wang, G.F. A new wind turbine fault diagnosis method based on the local mean decomposition. *Renew. Energy* **2012**, *48*, 411–415.
7. Dong, W.; Xing, Y.; Moan, T.; Gao, Z. Time domain-based gear contact fatigue analysis of a wind turbine drivetrain under dynamic conditions. *Int. J. Fatigue* **2013**, *48*, 133–146.
8. Shirani, M.; Härkegård, G. Fatigue life distribution and size effect in ductile cast iron for wind turbine components. *Eng. Fail. Anal.* **2011**, *18*, 12–24.
9. Madsen, H.O.; Krenk, S.; Lind, N.C. *Methods of Structural Safety*; Prentice-Hall: Englewood Cliff's, NJ, USA, 1986.
10. Oyague, F. *Gearbox Modeling and Load Simulation of a Baseline 750-kW Wind Turbine Using State-of-the-Art Simulation Codes*; Technical Report NREL/TP-500-41160; National Renewable Energy Laboratory: Golden, CO, USA, 2011.

11. Tavner, P.J.; Greenwood, D.M.; Whittle, M.W.G.; Gindele, R.; Faulstich, S.; Hahn, B. Study of weather and location effects on wind turbine failure rates. *Wind Energy* **2012**, *16*, 175–187.
12. Campbell, F.C. *Elements of Metallurgy and Engineering Alloys*; ASM International: Materials Park, OH, USA, 2008.
13. Mirzaei Rafsanjani, H.; Sørensen, J.D. Stochastic models of defects in wind turbine drivetrain components. In *Multiscale Modeling and Uncertainty Quantification of Materials and Structures*; Proceedings of the IUTAM Symposium, Santorini, Greece, 9–11 September 2013.
14. Shirani, M.; Härkegård, G. Casting defects and fatigue behavior of ductile cast iron for wind turbine components: A comprehensive study. *Mater. Werkst.* **2011**, *42*, 1059–1074.
15. Schittkowski, K. NLPQL: A fortran subroutine solving constrained nonlinear programming problems. *Ann. Oper. Res.* **1986**, *5*, 485–500.
16. Lindley, D.V. *Introduction to Probability and Statistics from a Bayesian Viewpoint*; Cambridge University Press: Cambridge, UK, 1976.
17. Byon, E.; Ding, Y. Season-dependent condition-based maintenance for a wind turbine using a partially observed Markov decision process. *IEEE Trans. Power Syst.* **2010**, *25*, 1823–1834.
18. Byon, E.; Ntaimo, L.; Ding, Y. Optimal maintenance strategies for wind turbine systems under stochastic weather conditions. *IEEE Trans. Reliab.* **2010**, *59*, 393–404.
19. Definition of a 5-MW Reference Wind Turbine for Offshore System Development. Available online: http://www.nrel.gov/docs/fy09osti/38060.pdf (accessed on 13 April 2015).
20. *Wind Turbines–Part 1: Design Requirements*; IEC: Geneva, Switzerland, 2015; CD IEC 61400-1 ed. 4.
21. Petersen, E.L.; Mortensen, N.G.; Landberg, L.; Højstrup, J.; Frank, H.P. *Wind Power Meteorology*; Risø National Laboratory: Roskilde, Denmark, 1997; Risø-I-1206(EN).
22. Wirsching, P.H. Fatigue reliability for offshore structures. *J. Struct. Eng. (ASCE)* **1984**, *10*, 2340–2356.
23. *Fatigue Design of Offshore Steel Structures*; DNV: Høvik, Norway, 2010; DNV-RP-C203.

B PAPER 2

Title: Stochastic models of defects in wind turbine drivetrain components.

Authors: Hesam Mirzaei Rafsanjani, John Dalsgaard Sørensen

Journal: In Multiscale Modeling and Uncertainty Quantification of Materials and Structures, 287-298

Year:2014

Stochastic Models of Defects in Wind Turbine Drivetrain Components

Hesam Mirzaei Rafsanjani and John Dalsgaard Sørensen

Abstract The drivetrain in a wind turbine nacelle typically consists of a variety of heavily loaded components, like the main shaft, bearings, gearbox and generator. The variations in environmental load challenge the performance of all the components of the drivetrain. Failure of each of these components of the drivetrain will lead to substantial economic losses such as cost of lost energy production, cost of repairs, cost of crew and cost of transportation. For offshore wind turbines, the marine environment affects the repair & maintenance process and in some case because of the rush environment, the maintenance team cannot operate properly and the wind turbine does not work for several days and consequently the cost of lost energy increases drastically. In this paper is presented stochastic models for fatigue failure based on test data and the accuracy of the models are compared.

Keywords Wind turbine • Reliability • Drivetrain • Defects • Stochastic model

1 Introduction

Reliability of wind turbine drivetrain components is very important for wind turbine manufacturers and owners. Offshore wind turbines are large structures exposed to wave excitations, highly dynamic wind loads influenced by the wind turbine control system and wakes from other wind turbines. Therefore, most components in a wind turbine experience highly dynamic and time-varying loads. These components may fail due to wear or fatigue and this can lead to unplanned shut down and repairs.

H. Mirzaei Rafsanjani (✉) • J.D. Sørensen
Department of Civil Engineering, Aalborg University, Sohngårdsholmsvej 57,
9000 Aalborg, Denmark
e-mail: hmr@civil.aau.dk; jds@civil.aau.dk

M. Papadrakakis and G. Stefanou (eds.), *Multiscale Modeling and Uncertainty Quantification of Materials and Structures*, DOI 10.1007/978-3-319-06331-7_19,

The drivetrain consists of a variety of heavily loaded components, such as the main shaft, bearings, gearbox and generator. The variability of the loads challenges the performance of all the components of drivetrain. The failure of each component of the drivetrain will lead to economic losses such as cost of lost energy production, cost of repairs, cost of crew and cost of transportation. The environmental exposure affects the repair & maintenance of offshore wind turbine. Sometimes, because of the harsh environment, the maintenance team cannot operate properly and therefore the wind turbine cannot be accessed for several days. Consequently, the cost of lost energy increases drastically.

Due to fluctuating loads, fatigue is one of the main failure modes in wind turbine components. The current design of large wind turbines against fatigue is usually based on the life design approach (Campbell 2008). In the safe life design, fatigue testing is carried out on baseline materials to produce S-N curves. For many years it has been assumed in designs that all loads and strengths are deterministic. The strength of an element was determined in such a way that it exceeded the load with a certain margin and accounted for by a safety factor defined as the ratio between the strength and the load (Dong et al. 2013). Recently, safety factors are changed to partial safety factors in new codes. Hence, characteristic values of the uncertain loads and resistances are specified and partial safety factors are applied to the loads and strengths in order to ensure that the structure is safe enough. Hence, the uncertainties in the loads, strengths and the modeling can be accounted partially for in such a semi-probabilistic safety format.

This paper focuses on probabilistic methods for assessment of the reliability and stochastic modeling of the fatigue strength using structural reliability methods; see Entezami et al. (2012) allowing a rational modeling of all uncertainties. An important aspect in modeling fatigue failure of large cast steel components is to take into account scale effects. Two approaches are considered in this paper for stochastic modeling of the fatigue life including scale effects. One method is based on the classical Weibull approach and the other on application of a LogNormal distribution as done e.g. for the fatigue life of welded steel details.

2 Wind Turbine Drivetrain

Currently, most operating wind turbines use a modular configuration (Hau 2006). Typically, all individual components of the drivetrain are mounted onto a bedplate. The basic drivetrain components are the main bearing, shaft, gearbox, brakes, high-speed shaft and the generator, see Hau (2006) and Lindley (1976). A typical configuration of these components in the nacelle of a wind turbine is shown in Fig. 1.

Reliability of wind turbine gearboxes is studied in a number of research projects, e.g. the GRC project at National Renewable Energy Laboratory (NREL), (Oyague 2009). This include as important areas research on fault diagnosis and condition monitoring. Several methods have been considered, such as vibration and acoustic emission (Soua et al. 2013) and Local mean decomposition (Liu et al. 2012).

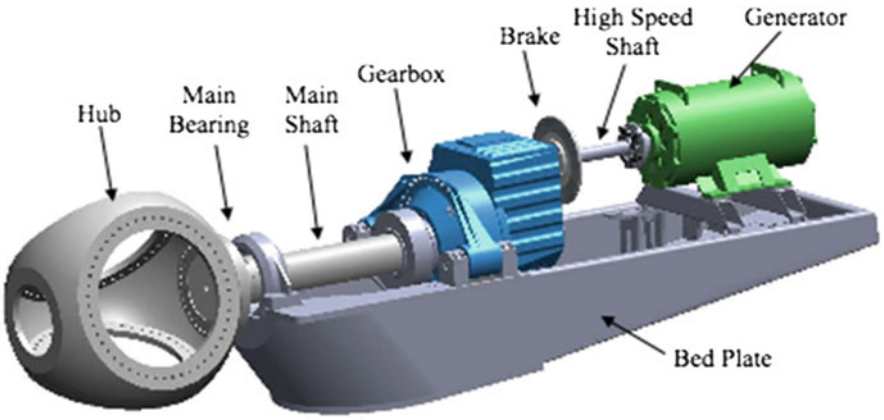

Fig. 1 Wind turbine drivetrain components (Oyague 2009)

Some studies on probabilistic modeling of failures in wind turbine drivetrain components have been carried out (Dong et al. 2013) but without a detailed stochastic modeling of the uncertainties related to the parameters in the limit state equations modeling each failure mode.

As mentioned above, most of the studies concentrated on gearbox failures. Moreover, in some studies failure of other parts like brake system (Entezami et al. 2012) is considered. By reviewing failure statistics of wind turbines, it is seen that focus is on reliability of blades, foundation and electrical parts whereas reliability of mechanical part such as bearing is only considered in few public studies.

Therefore, in this paper, the main bearing or main shaft are considered. Bearing and shaft of wind turbines are those having the highest downtimes in case of failure, see e.g. (Sheng and Veers 2011) and (Tavner et al. 2012). The current fatigue design is based on the life design approach (Shirani and Härkegård 2011a). In the safe life design S-N curves are based on tests as discussed above. However, the fatigue strength is typically highly uncertain and statistical uncertainties due to a limited number of tests can be important in modeling the fatigue strength. Moreover, model uncertainties related to e.g. application of the Miner rule for fatigue damage accumulation should be considered.

3 Fatigue Life Modeled by a LogNormal Distribution

The fatigue life can be modeled as the number of cycles to failure at a specified stress level. As the applied stress level decreases, the number of cycles to failure increases. The fatigue strength of metals is often assumed to follow the Basquin equation (Campbell 2008):

$$\sigma_a = \sigma_f (2N)^{-\frac{1}{m}} \tag{1}$$

where σ_a is the alternating stress amplitude, σ_f is the fatigue strength, $2\ N$ is the number of load reversals to failure, and $-1/m$ is the fatigue strength exponent. Equation (1) can also be written

$$N = \frac{1}{2}\left(\frac{\sigma_a}{\sigma_f}\right)^{-m} \tag{2}$$

In Eq. (2), σ_a is affected by geometrical size effects and can be estimated by the following equation (Shirani and Härkegård 2011a)

$$\frac{\sigma_a}{\sigma_{a0}} = \left(\frac{V}{V_0}\right)^{-\frac{1}{b_\sigma}} \Rightarrow \sigma_a = \sigma_{a0}\left(\frac{V}{V_0}\right)^{-\frac{1}{b_\sigma}} \tag{3}$$

where V_0 is the reference volume and σ_{a0} is the fatigue strength corresponding to the volume V_0. The stress exponent b_σ determines the effect of the specimen size on the fatigue life. By substitution of Eq. (3) in Eq. (2), the following equation is obtained:

$$N = \frac{1}{2}\left(\frac{\sigma_{a0}}{\sigma_f}\right)^{-m}\left(\frac{V}{V_0}\right)^{\frac{1}{b_n}} = \frac{1}{2}\left(\frac{\sigma_{a0}}{\sigma_f}\right)^{-m}\frac{1}{S_V^{b_n}} \tag{4}$$

The relative component volume influences the size effect and therefore the volume ratio is introduced by a scaling parameter s_V:

$$S_V = \frac{V}{V_0} \tag{5}$$

Moreover, the b_n in Eq. (4) is:

$$b_n = \frac{b_\sigma}{m} \tag{6}$$

The Eq. (4) can be rewritten in logarithmic format as follows

$$\log N = \log\left[\frac{1}{2}\left(\frac{\sigma_{a0}}{\sigma_f}\right)^{-m} S_V^{1/b_n}\right] \Rightarrow \log N = m\log\sigma_f - m\log\sigma_{a0} + \frac{1}{b_n}\log S_V - \log(2)$$

This equation is rewritten introducing an uncertainty term ε:

$$\log N = m\log\sigma_f - m\log\sigma_{a0} + \frac{1}{b_n}\log S_V - \log(2) + \varepsilon \tag{7}$$

where ε is assumed to be normally distributed with mean value $= 0$ and standard deviation $= \sigma_\varepsilon$. ε models the scatter in fatigue life and can be considered here

to cover both physical and model uncertainties related to imperfect knowledge or idealizations of the mathematical models used or uncertainty related to the choice of probability distribution types for the stochastic variables. It is noted that the test data considered below do not allow a bilinear *S-N* curve to be fitted.

The parameters in Eq. (7) can be estimated using available test data. In this paper test data extracted from Shirani and Härkegård (2011b) are used to exemplify the procedure for the stochastic modeling. Assuming that the Shirani data are representative the results of the statistical analysis can also be used to assess the reliability level for drivetrain components and to calibrate safety factors, see below.

In the following, the Maximum Likelihood Method is used for the statistical analysis. The likelihood function as function of the statistical parameters σ_f, m, and σ_ε to be estimated is written as follows accounting both for tests results where failure occurs and for test results where failure does not occur (run-outs):

$$L\left(\sigma_f, m, \sigma_\varepsilon\right) = \prod_{i=1}^{n_F} P\left[\log n_i = m\log\sigma_f - m\log\sigma_{a0,i} + \frac{1}{b_n}\log S_V + \varepsilon - \log 2\right] \times \prod_{i=1}^{n_R} P\left[\log n_i > m\log\sigma_f - m\log\sigma_{a0,i} + \frac{1}{b_n}\log S_V + \varepsilon - \log 2\right] \tag{8}$$

where n_i is the number of stress cycles to failure or run-out (no failure) with stress range equal to $\sigma_{a0,i}$ in test number *i*. n_F is the number of tests where failure occurs, and n_R is the number of tests where failure does not occur after n_i stress cycles (run-outs). $n = n_F + n_R$ is the total number of tests. σ_f, m, and σ_ε are estimated solving the optimization problem max $L(\sigma_f, m, \sigma_\varepsilon)$. This can be done using a standard nonlinear optimizer, e.g. the NLPQL algorithm, see Schittkowski (1986).

Since the parameters σ_f, m and σ_ε are estimated by the maximum-likelihood technique, they become asymptotically (number of data should be larger than 25–30) normally distributed stochastic variables with expected values equal to maximum-likelihood estimates and covariance matrix equal to, see Lindley (1976):

$$C_{\sigma_f,m,\sigma_\varepsilon} = \left[-H_{\sigma_f,m,\sigma_\varepsilon}\right]^{-1} = \begin{bmatrix} \sigma^2{}_{\sigma_f} & \rho_{\sigma_f,m}\sigma_{\sigma_f}\sigma_m & \rho_{\sigma_f,\sigma_\varepsilon}\sigma_{\sigma_f}\sigma_{\sigma_\varepsilon} \\ \rho_{\sigma_f,m}\sigma_{\sigma_f}\sigma_m & \sigma_m{}^2 & \rho_{m,\sigma_\varepsilon}\sigma_m\sigma_{\sigma_\varepsilon} \\ \rho_{\sigma_f,\sigma_\varepsilon}\sigma_{\sigma_f}\sigma_{\sigma_\varepsilon} & \rho_{m,\sigma_\varepsilon}\sigma_m\sigma_{\sigma_\varepsilon} & \sigma^2{}_{\sigma_\varepsilon} \end{bmatrix} \tag{9}$$

where $H_{\sigma_f,m,\sigma_\varepsilon}$ is the Hessian matrix with second-order derivatives of the log-likelihood function. σ_{σ_f}, σ_m, and $\sigma_{\sigma_\varepsilon}$ denote the standard deviation of σ_f, m and σ_ε respectively and ρ indicates correlation coefficients.

Alternatively to the LogNormal model for the S-N curve a Weibull model can be used, as described in the next section.

4 Fatigue Life Modeled by a Weibull Distribution

The influence of scale effects on damage modeling and fatigue life can from a theoretical basis be modeled by a Weibull model, see e.g. Madsen et al. (1986). Such a model is considered in this section assuming that the fatigue life can be modeled by a Weibull distribution. The distribution function for number of cycles to failure, N given stress range σ_{a0} is written:

$$F_N(n) = 1 - \exp\left[-\left(\frac{n}{N}\right)^{b_n}\right] \tag{10}$$

where b_n is a shape parameter. The corresponding density function becomes

$$f_N(n) = \frac{b_n}{N}\left(\frac{n}{N}\right)^{b_n-1} \exp\left[-\left(\frac{n}{N}\right)^{b_n}\right] \tag{11}$$

By substitution Eq. (4) and (6) in Eq. (11), the density function is written

$$f_N(n) = \frac{2b_n}{S_V^{1/b_n}}\left(\frac{\sigma_{a0}}{\sigma_f}\right)^m \left(\frac{2n}{S_V^{1/b_n}}\left(\frac{\sigma_{a0}}{\sigma_f}\right)^m\right)^{b_n-1} \exp\left[-\left(\frac{2n}{S_V^{1/b_n}}\left(\frac{\sigma_{a0}}{\sigma_f}\right)^m\right)^{b_n}\right] \tag{12}$$

The statistical parameters σ_f and m in Eq. (12) can be estimated by the Maximum Likelihood Method with the log-likelihood function:

$$\ln L\left(\sigma_f, m\right) = \ln\left(\prod_{i=1}^{n} f_N\left(n_i\right)\right) = \sum_{i=1}^{n_F} \ln\left(\frac{2b_n}{S_V^{1/b_n}}\left(\frac{\sigma_{a0,i}}{\sigma_f}\right)^m \left(\frac{2n_i}{S_V^{1/b_n}}\left(\frac{\sigma_{a0,i}}{\sigma_f}\right)^m\right)^{b_n-1} \exp\left[-\left(\frac{2n_i}{S_V^{1/b_n}}\left(\frac{\sigma_{a0,i}}{\sigma_f}\right)^m\right)^{b_n}\right]\right) + \sum_{i=1}^{n_R} \ln\left(\exp\left[-\left(\frac{2n_i}{S_V^{1/b_n}}\left(\frac{\sigma_{a0,i}}{\sigma_f}\right)^m\right)^{b_n}\right]\right) \tag{13}$$

where n_i is the number of stress cycles to fail or run-out (no failure) with stress range $\sigma_{a0,i}$ in test number i. n_F is the number of tests where failure occurs, and n_R is the number of tests where failure did not occur after n_i stress cycles (run-outs). $n = n_F + n_R$ is the total number of tests. σ_f and m are estimated solving the optimization problem max $L(\sigma_f, m)$, as described above.

5 Characteristic Values

In deterministic, code based design safety is introduced though application of deterministic values in terms of characteristic values and partial safety factors to obtain design values of both loads and strengths.

If statistical uncertainty is not taken into account then corresponding to a stress range, $\sigma_{a0,c}$ a characteristic value of the fatigue life, n_c defined as a 5 % quantile can be estimated directly from the distribution function of the fatigue life.

If statistical uncertainty is to be taken into account and the physical/model uncertainties for the fatigue life is modeled by a Lognormal distribution then a characteristic value for the fatigue life, n_c corresponding to the stress range, $\sigma_{a0,c}$ defined as a 5 % quantile can be obtained from

$$P\left(\log n_c > m\log\sigma_f - m\log\sigma_{a0,c} + \frac{1}{b_n}\log S_V + \varepsilon - \log 2\right) = 0.05 \qquad (14)$$

with a corresponding limit state equation written as

$$g\left(\sigma_f, m, \varepsilon, \sigma_\varepsilon\right) = m\log\sigma_f - m\log\sigma_{a0,c} + \frac{1}{b_n}\log S_V + \varepsilon - \log 2 - \log n_c \qquad (15)$$

Here the stochastic variables are ε, m, σ_ε and σ_f and they are introduced to model the physical/model and statistical uncertainties. For given $\sigma_{a0,c}$ (Eq. (15)) can be solved with respect to the characteristic fatigue life, n_c using e.g. FORM (First Order Reliability Methods), see Madsen et al. (1986).

Similarly if the fatigue life is modeled by a Weibull distribution and statistical uncertainty is accounted for then a limit state equation can be applied:

$$\begin{aligned} g\left(\sigma_f, m, \varepsilon, \sigma_\varepsilon\right) = {} & \log n_c + \log 2 - \frac{1}{b_n}\log\left(S_V\right) \\ & + m\log\left(\sigma_{a0,c}\right) - m\log\left(\sigma_f\right) - \log\left(-1\mathrm{n}(0.95)\right)^{1/b_n - \varepsilon} \end{aligned} \qquad (16)$$

In Eq. (16), $\varepsilon, \sigma_\varepsilon, m$ and σ_f model the physical/model and statistical uncertainties, respectively. As mentioned before, these parameters can be obtained from the test results.

6 Results

As mentioned above the data by Shirani and Härkegård (2011b) will be used to illustrate the above statistical analysis and reliability assessment for wind turbine components. The test data follows the specification listed in Table 1.

Table 1 The test plan (Shirani and Härkegård 2011b)

Material	Load ratio	Specimen	Number of specimen	Testing frequency
T95	0	Ø21	12	10
T95	−1	Ø21	12	10
T95	−1	Ø50	12	1
T150	−1	Ø21	18	10
T150	−1	120*140	9	40

Table 2 5 % quantile using LN distribution

Test	σ_f [MPA]	m	ε	σ_ε
D21 T95 R = 0	443.51	12.107	−1.1896	0.3220
D21 T95 R = −1	1,022.58	8.8793	−1.3270	0.3171
D50 T95 R = −1	1,003.92	8.3760	−1.2605	0.1652
D21 T150 R = −1	792.87	9.5477	−1.1181	0.2261
120*140 T150 R = −1	405.60	14.47	−1.5295	0.3524

Table 3 5 % quantile using Weibull distribution

Test	σ_f [MPA]	m	ε	σ_ε
D21 T95 R = 0	444.10	12.366	−1.579	0.3389
D21 T95 R = −1	974.68	9.1787	−1.4400	0.3528
D50 T95 R = −1	781.91	10.257	−1.6236	0.1657
D21 T150 R = −1	700.05	10.799	−1.5422	0.2571
120*140 T150 R = −1	412.59	14.39	−1.1564	0.3522

The material is EN-GJS-400-18-LT ductile cast iron with graphite nodules contained within a ferritic matrix (Sheng and Veers 2011). The specimens are extracted from two types of castings with 95 mm thickness, (95 mm × 200 mm × 750 mm) cast blocks, and 150 mm thickness, (150 mm × 300 mm × 1,550 mm) cast blocks. These blocks are illustrated in Table 1 by T95 and T150.

Two series of specimens were machined from T95 block, specimens with 21 mm and specimens with 50 mm diameter, see Sheng and Veers (2011). Specimens with 21 mm diameter were tested at load ratios $R = -1$ and $R = 0$, but specimens with 50 mm diameter were just tested at load ratio $R = -1$. Furthermore, two series of specimens were machined from T150 block, specimens with 21 mm and heavy section specimens with 120 × 140 mm cross section. All specimens were tested at load ratios R = −1 (Shirani and Härkegård 2011b).

The statistical analysis is performed following the methodology described in Sects. 3 and 4 for estimation of the parameters in the LogNormal and Weibull models. The results are shown in Tables 2 and 3 and 5 % quantiles are estimated as described above. The results of each test category are shown in Figs. 2, 3, 4, 5 and 6 showing test results for broken/failed and run-out specimens. Furthermore, the results of fit to LogNormal distribution and Weibull distribution are shown. Further, the figures show two types of 5 % quantiles for the LogNormal distribution, namely quantiles estimated when only failure data considered in calculating the 5 % quantile

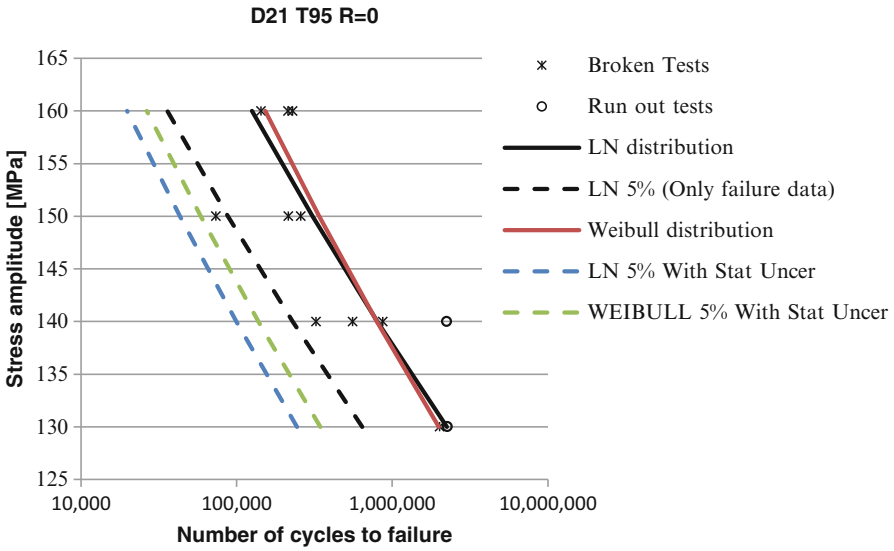

Fig. 2 Results for D21 T95 R0

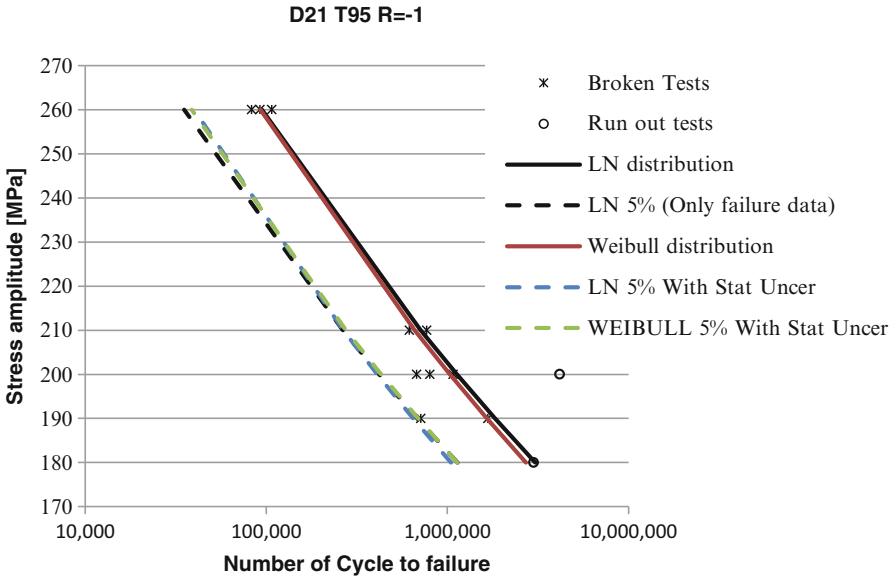

Fig. 3 Results for D21 T95 R-1

and the other quantile is estimated when the statistical uncertainties is taken into account. Moreover, the 5 % quantile of Weibull distribution is estimated when the statistical uncertainties are considered.

The results show that generally only a small difference is obtained between the mean (best fit) curves using Weibull and LogNormal distributions. Larger differences

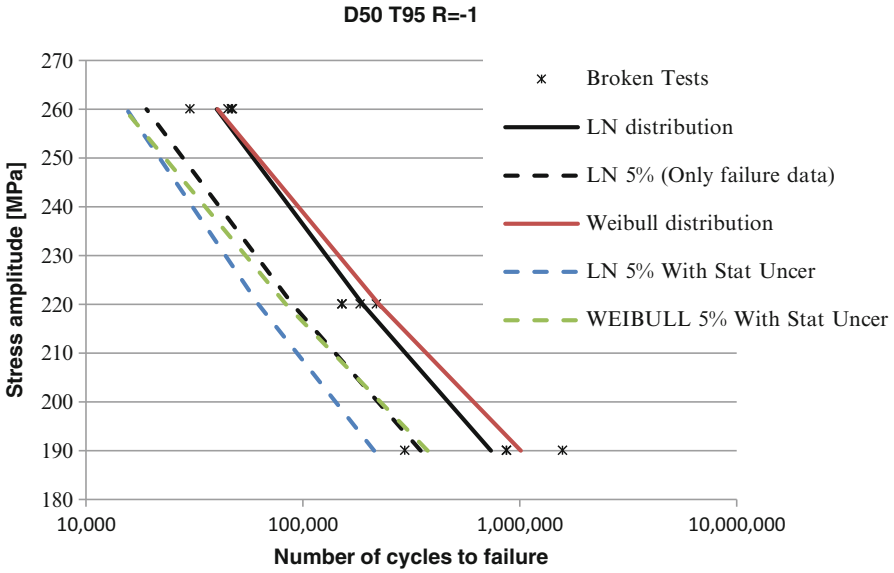

Fig. 4 Results for D50 T95 R-1

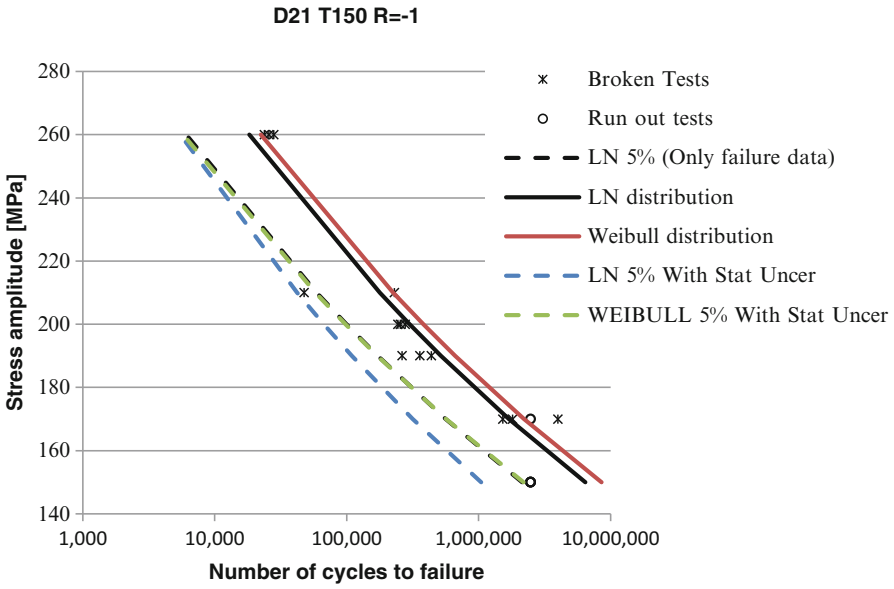

Fig. 5 Results for D21 T150 R-1

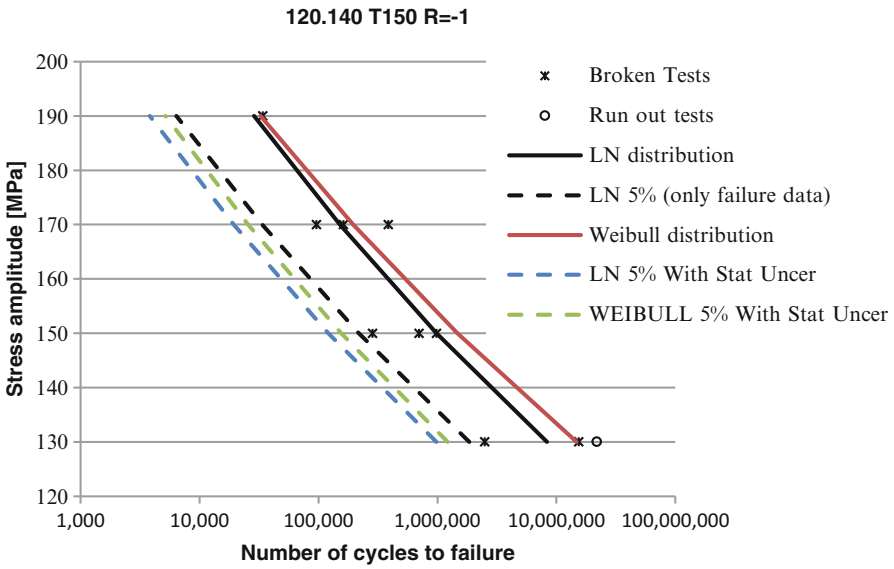

Fig. 6 Results for 120*140 T150 R-1

are seen in some cases when the 5 % quantiles are considered. Generally, the LogNormal distribution results in smaller number of cycles to failure than the Weibull distribution. Further, it is also seen that as expected smaller fatigue lives are obtained when statistical uncertainty is taken into account. Also it is seen in most cases to be important to take into account in the statistical analysis that some tests result in no-failure/run-out. As demonstrated in the examples this is easily accounted for using the Maximum Likelihood Method.

7 Conclusion

In this paper stochastic models for modeling fatigue failure in wind turbine drivetrain components are considered. Firstly, two stochastic models for uncertainties influencing fatigue failure are described based on a Weibull and a LogNormal distribution function. These uncertainties include model uncertainties, statistical uncertainties and size effects. It is described how the statistical parameters can be estimated using the Maximum Likelihood Method and how 5 % quantiles can be obtained taking into account statistical uncertainties though formulating limit state equations and applying FORM (First Order Reliability Methods).

In an illustrative example, statistical procedure is applied to a set of data to demonstrate the importance of taking into account both tests resulting in failure and in no-failure/run-out using the Maximum Likelihood Method. The results indicate

that generally only a small difference is obtained between the mean (best fit) curves using Weibull and LogNormal distributions. When 5 % quantiles (characteristic values) are compared larger differences are seen with the LogNormal model resulting in smaller number of cycles to failure than the Weibull model. Further, it is also seen that as expected smaller fatigue lives are obtained when statistical uncertainty is taken into account.

Acknowledgments The work is supported by the Strategic Research Center "REWIND – Knowledge based engineering for improved reliability of critical wind turbine components", Danish Research Council for Strategic Research, grant no. 10–093966.

References

Campbell FC (2008) Elements of metallurgy and engineering alloys. ASM International, Materials Park, pp 243–264

Dong W, Xing Y, Moan T, Gao Z (2013) Time domain-based gear contact fatigue analysis of a wind turbine drivetrain under dynamic conditions. Int J Fatigue 48:133–146

Entezami M, Hillmansen S, Weston P, Papaelias M (2012) Fault detection and diagnosis within a wind turbine mechanical braking system using condition monitoring. Renew Energy 47:175–182

Hau E (2006) Wind turbines: fundamentals, technologies, application, economics, 2nd edn. Springer, New York

Lindley DV (1976) Introduction to probability and statistics from a Bayesian viewpoint, vol 1 + 2. Cambridge University Press, Cambridge

Liu WY, Zhang WH, Han JG, Wang GF (2012) A new wind turbine fault diagnosis method based on the local mean decomposition. Renew Energy 48:411–415

Madsen HO, Krenk S, Lind NC (1986) Methods of structural safety. Prentice-Hall, Inc., Englewood cliffs

Oyague F (2009) Gearbox modeling and load simulation of a baseline 750-kW wind turbine using state-of-the-art simulation codes. National Renewable Energy Laboratory. Available via NREL. http://www.nrel.gov/docs/fy09osti/41160.pdf

Schittkowski K (1986) NLPQL: a fortran subroutine solving constrained nonlinear programming problems. Ann Oper Res 5:485–500

Sheng S, Veers P (2011) Wind turbine drivetrain condition monitoring – an overview. In: Machinery Failure Prevention Technology (MFPT) Society conference proceedings, Virginia Beach, VA, USA, 10–12 May 2011

Shirani M, Härkegård G (2011a) Fatigue life distribution and size effect in ductile cast iron for wind turbine components. Eng Fail Anal 18:12–24

Shirani M, Härkegård G (2011b) Casting defects and fatigue behavior of ductile cast iron for wind turbine components: a comprehensive study. Materialwiss Werkst 42:1059–1074

Soua S, Lieshout PV, Perera A, Gan T, Bridge B (2013) Determination of the combined vibrational and acoustic emission signature of a wind turbine gearbox and generator shaft in service as a pre-requisite for effective condition monitoring. Renew Energy 51:175–181

Tavner PJ, Greenwood DM, Whittle MWG, Gindele R, Faulstich S, Hahn B (2012) Study of weather and location effects on wind turbine failure rates. Wind Energy 16:175–187

C PAPER 3

Title: Statistical analysis of manufacturing defects on fatigue life of a wind turbine casted components.

Authors: Hesam Mirzaei Rafsanjani, John Dalsgaard Sørensen, Krishnendu Mukherjee, Søren Fæster, Asger Sturlason

Journal: International Conference on Safety & Reliability of Ship, Offshore & Subsea Structure, Glasgow, UK, 18th-20th August.

Year:2014

STATISTICAL ANALYSIS OF MANUFACTURING DEFECTS ON FATIGUE LIFE OF A WIND TURBINE CASTED COMPONENT

H. Mirzaei Rafsanjani & J. Dalsgaard Sørensen, *Aalborg University, Denmark*
K. Mukherjee & **S. Fæster**, *Technical University of Denmark, Denmark*
A. Sturlason, *Vestas Wind Systems A/S, Denmark*

ABSTRACT

Wind turbine components experience heavily variable loads during its lifetime and fatigue failure is a main failure mode of casted components during their design working life. The fatigue life is highly dependent on the microstructure (grain size and graphite form and size), number, type, location and size of defects in the casted components and is therefore rather uncertain and needs to be described by stochastic models. Uncertainties related to such defects influence prediction of the fatigue strengths and are therefore important in modelling and assessment of the reliability of wind turbine components. The defect distribution is usually affected by the manufacturing process. In this paper, two methods of casting, sand casting and chill casting are considered. These are compared in statistical analyses of a large number of representative test samples using two basic stochastic models for the fatigue life, namely LogNormal and Weibull distributions. The statistical analyses are performed using the Maximum Likelihood Method and the statistical uncertainty is estimated. Further, stochastic models for the fatigue life obtained from the statistical analyses are used for illustration to assess the reliability of a representative component in an offshore wind turbine.

1. INTRODUCTION

Offshore wind turbines are large structures exposed to wave excitations, highly dynamic wind loads and wakes from other wind turbines. Hence, the components of wind turbine experience stochastic loads varying during the design working life of offshore wind turbines. In this paper casted components are considered. If these may fail due to wear or fatigue very costly repairs and loss of production of energy are the results. The repair time of offshore wind turbine is affected by the environment conditions of the wind turbine. Hence, the repair time of offshore wind turbines can be several months, especially during wintertime.

Design of mechanical components in offshore wind turbine drivetrains by deterministic methods using safety factors are generally not able to account for the many uncertainties and thus a reliability assessment may be needed based on probabilistic methods [1]. The most common drivetrain configuration consists of a main shaft, main bearings, a gearbox and a generator [2], [3]. Further, casting is used for several components exposed to cyclic and variable loads and consequently fatigue failure is one of the main sources of failure for such components.

Current fatigue designs are typically based on the life design approach [4]. In the safe life design, fatigue testing is carried out on baseline material to produce *SN* curves. However, the fatigue strength is highly uncertain and statistical uncertainties due to a limited number of tests can be important to include in modelling of the fatigue strength. Moreover, the manufacturing process may affect the statistical uncertainties and different manufacturing processes may lead to different statistical models for the material strengths.

This paper focuses on statistical analysis of two different manufacturing processes for a casted wind turbine component. The manufacturing processes are “Sand Casting” and “Chill Casting”. For each manufacturing process, several fatigue tests in different loading stresses can be performed. The resulting fatigue strength can be used to estimate the physical and statistical uncertainties. Two approaches are considered in this paper for stochastic modelling of the fatigue life. One method is based on the classical Weibull approach and the other one is based on an application of a LogNormal distribution as done e.g. for the fatigue life of welded steel details. The statistical parameters in both models are estimated. Finally, the characteristic fatigue strengths are evaluated.

2. FATIGUE LIFE MODELELD BY A LOGNORMAL DISTRIBUTION

Fatigue failures occur typically due to the application of fluctuating stresses much lower than the stress required to cause failure during a single application of the stress. The fatigue life is the number of cycles to failure at a specified stress level, while the fatigue strength is the stress level below which failure does not occur for the given number of cycles. As the applied stress level decreases, the number of cycles to failure increases. The fatigue strength of metals is often assumed to follow the Basquin equation [5]:

$$\sigma_a = \sigma_f \left(2N\right)^{-\frac{1}{m}} \qquad (1)$$

where σ_a is the alternating stress amplitude, σ_f is the fatigue strength, N is the number of load cycle, and m is the fatigue strength exponent.

The probability of failure increases when the volume of the component increase due to scale effects since the likelihood of finding a critical micro-crack increases [4]. Thus the geometrical size effect affects the resistance of materials against fatigue failure. In most materials, fatigue initiates from mechanical discontinuities that may be considered as micro-cracks. The geometrical size effects can be modeled though σ_a by the following equation, see e.g. [4]

$$\frac{\sigma_a}{\sigma_{a0}} = \left(\frac{V}{V_0}\right)^{-\frac{1}{b_\sigma}} \Rightarrow \sigma_a = \sigma_{a0}\left(\frac{V}{V_0}\right)^{-\frac{1}{b_\sigma}} = \sigma_{a0}\left(s_V^{-\frac{1}{b_\sigma}}\right) \qquad (2)$$

where V_0 is the reference volume and σ_{a0} is the fatigue strength corresponding to the volume V_0. The stress exponent b_σ determines the effect of the specimen size on the fatigue life. By substitution Equation (2) in Equation (1), the following equation is obtained:

$$N = \frac{1}{2}\left(\frac{\sigma_{a0}}{\sigma_f}\right)^{-m}\left(\frac{V}{V_0}\right)^{\frac{1}{b_n}} = \frac{1}{2}\left(\frac{\sigma_{a0}}{\sigma_f}\right)^{-m} s_V^{\frac{1}{b_n}} \qquad (3)$$

Here b_n in equation (3) is:

$$b_n = \frac{b_\sigma}{m} \qquad (4)$$

In a log-log format the equation (3) is linear and can be rewritten as follows

$$\log N = m\log\sigma_f - m\log\sigma_{a0} + \frac{1}{b_n}\log s_V - \log(2) \qquad (5)$$

Further, this equation can be rewritten introducing an uncertainty term ε:

$$\log N = m\log\sigma_f - m\log\sigma_{a0} + \frac{1}{b_n}\log s_V - \log(2) + \varepsilon \qquad (6)$$

where ε is assumed to be normal distributed with mean value = 0 and standard deviation = σ_ε. ε models the scatter in fatigue life and can be considered here to cover both physical and model uncertainties related to imperfect knowledge or idealizations of the mathematical model used and uncertainty related to the choice of probability distribution types for the stochastic variables. It is noted that the test data applied in the example below do not allow a bilinear *SN* curve to be fitted; but the above model can easily be extended to model a bi-linear *SN* curve and a lower threshold can be introduced. The parameters in (6) can be estimated using available test data.

In the following, the Maximum Likelihood Method is used for the statistical analysis. The log-likelihood function is a function of the statistical parameters σ_f, m, and σ_ε, it will be estimated as follows accounting both for tests results where failure occurs and test results where failure does not occur (run-outs):

$$L\left(\sigma_f, m, \sigma_\varepsilon\right) = \prod_{i=1}^{n_F} P\left[\log n_i = m\log\sigma_f - m\log\sigma_{a0,i} + \frac{1}{b_n}\log s_V + \varepsilon - \log 2\right] \times \prod_{i=1}^{n_R} P\left[\log n_i > m\log\sigma_f - m\log\sigma_{a0,i} + \frac{1}{b_n}\log s_V + \varepsilon - \log 2\right] \qquad (7)$$

where n_i is the number of stress cycles to failure or run-out (no failure) with stress range equal to $\sigma_{a0,i}$ in test number i. n_F is the number of tests where failure occurs, and n_R is the number of tests where failure does not occur after n_i stress cycles (run-outs). $n = n_F + n_R$ is the total number of tests. σ_f, m, and σ_ε are estimated solving the optimization problem: max $L(\sigma_f, m, \sigma_\varepsilon)$. This can be done using a standard nonlinear optimizer, e.g. the NLPQL algorithm, see [6].

Since the parameters σ_f, m and σ_ε are estimated by the maximum-likelihood technique, they become asymptotically (number of data should be larger than 25-30) normally distributed stochastic variables with expected values equal to maximum-likelihood estimates and covariance matrix equal to, see [7]:

$$C_{\sigma_f,m,\sigma_\varepsilon} = \left[-H_{\sigma_f,m,\sigma_\varepsilon}\right]^{-1}$$
$$= \begin{bmatrix} \sigma^2_{\sigma_f} & \rho_{\sigma_f,m}\sigma_{\sigma_f}\sigma_m & \rho_{\sigma_f,\sigma_\varepsilon}\sigma_{\sigma_f}\sigma_{\sigma_\varepsilon} \\ \rho_{\sigma_f,m}\sigma_{\sigma_f}\sigma_m & \sigma^2_m & \rho_{m,\sigma_\varepsilon}\sigma_m\sigma_{\sigma_\varepsilon} \\ \rho_{\sigma_f,\sigma_\varepsilon}\sigma_{\sigma_f}\sigma_{\sigma_\varepsilon} & \rho_{m,\sigma_\varepsilon}\sigma_m\sigma_{\sigma_\varepsilon} & \sigma^2_{\sigma_\varepsilon} \end{bmatrix} \quad (8)$$

where $H_{\sigma_f,m,\sigma_\varepsilon}$ is the Hessian matrix with second-order derivatives of the log-likelihood function. σ_{σ_f}, σ_m and $\sigma_{\sigma_\varepsilon}$ denote the standard deviation of σ_f, m and σ_ε respectively and $\rho_{i,j}$ indicates correlation coefficients.

Alternatively to the LogNormal model for the *SN* curve a Weibull model can be used, as described in the next section.

3. FATIGUE LIFE MODELELD BY A WEIBULL DISTRIBUTION

As mentioned above, the fatigue strength is subject to uncertainties and therefore a stochastic modeling of life distribution is needed to study the fatigue life of components. The physical uncertainty related to the fatigue life can be modeled by a Weibull distribution. Then, the number of cycles to failure, N given stress range σ_{a0} is written:

$$F_N(n) = 1 - \exp\left[-\left(\frac{n}{N(\sigma_{a0})}\right)^{b_n}\right] \quad (9)$$

where b_n is a shape parameter. The corresponding density function becomes

$$f_N(n) = \frac{b_n}{N(\sigma_{a0})}\left(\frac{n}{N(\sigma_{a0})}\right)^{b_n-1}\exp\left[-\left(\frac{n}{N(\sigma_{a0})}\right)^{b_n}\right] \quad (10)$$

By substitution equations (3) and (4) in equation (10), the density function is written

$$f_N(n) = \frac{2b_n}{s_V^{1/b_n}}\left(\frac{\sigma_{a0}}{\sigma_f}\right)^m\left(\frac{2n}{s_V^{1/b_n}}\left(\frac{\sigma_{a0}}{\sigma_f}\right)^m\right)^{b_n-1} \times\exp\left[-\left(\frac{2n}{s_V^{1/b_n}}\left(\frac{\sigma_{a0}}{\sigma_f}\right)^m\right)^{b_n}\right] \quad (11)$$

The statistical parameters σ_f and m in equation (11) can be estimated by the maximum likelihood method with the likelihood function:

$$\ln L(\sigma_f,m) = \ln\left(\prod_{i=1}^{n} f_N(n_i)\right)$$
$$= \sum_{i=1}^{n_F}\ln\left(\frac{2b_n}{s_V^{1/b_n}}\left(\frac{\sigma_{a0,i}}{\sigma_f}\right)^m\left(\frac{2n_i}{s_V^{1/b_n}}\left(\frac{\sigma_{a0,i}}{\sigma_f}\right)^m\right)^{b_n-1}\exp\left[-\left(\frac{2n_i}{s_V^{1/b_n}}\left(\frac{\sigma_{a0,i}}{\sigma_f}\right)^m\right)^{b_n}\right]\right) \quad (12)$$
$$+\sum_{i=1}^{n_R}\ln\left(\exp\left[-\left(\frac{2n_i}{s_V^{1/b_n}}\left(\frac{\sigma_{a0,i}}{\sigma_f}\right)^m\right)^{b_n}\right]\right)$$

where n_i is the number of stress cycles to fail or run-out (no failure) with stress range $\sigma_{a0,i}$ in test number i. n_F is the number of tests where failure occurs, and n_R is the number of tests where failure did not occur after n_i stress cycles (run-outs). $n = n_F + n_R$ is the total number of tests. σ_f, m, and σ_ε are obtained solving the optimization problem max ln $L(\sigma_f, m, \sigma_\varepsilon)$, as described above.

4. CHARACTERISTIC VALUES

In deterministic, code based design safety is introduced though application of deterministic values in terms of characteristic values and safety factors to obtain design values of both loads and strengths. In the following a probabilistic basis is used to estimate the characteristic values by modelling of physical, measurement, statistical and model uncertainties. The characteristic values can be evaluated in two cases: "with statistical uncertainties" and "without statistical uncertainties".

If statistical uncertainty is not taken into account then corresponding to a given stress range, $\sigma_{a0,c}$ a characteristic value of the fatigue life, n_c defined as the 5% quantile can be estimated directly from the distribution function of the fatigue life.

If statistical uncertainty is to be taken into account and the physical/model uncertainties for the fatigue life is modelled by a LogNormal distribution then the characteristic value for the fatigue life, n_c corresponding to the stress range, $\sigma_{a0,c}$ defined as a 5% quantile can obtained from by

$$P\left(\log n_c > m\log\sigma_f - m\log\sigma_{a0,c} + \frac{1}{b_n}\log s_V + \varepsilon - \log 2\right) = 0.05 \quad (13)$$

with a corresponding limit state equation written as

$$g\left(\sigma_f, m, \varepsilon, \sigma_\varepsilon\right) = m\log\sigma_f - m\log\sigma_{a0,c} + \frac{1}{b_n}\log s_V + \varepsilon - \log 2 - \log n_c \quad (14)$$

Here, ε, m, and σ_f are modelled as stochastic variables as described above. For given $\sigma_{a0,c}$ equation (14) can be solved with respect to the characteristic fatigue life, n_c using e.g. FORM (First Order Reliability Methods), see [8].

Similarly, if the fatigue life is modeled by a Weibull distribution and statistical uncertainty is accounted for, then the characteristic value can be estimated using the following limit state equation:

$$g(\sigma_f, m, \varepsilon, \sigma_\varepsilon) = \log n_c + \log 2 - \frac{1}{b_n}\log s_V + m\log\sigma_{a0,c} - m\log\sigma_f - \log\left(-\ln(0.95)\right)^{1/b_n} - \varepsilon \quad (15)$$

In equation (15), ε, σ_ε, m and σ_f model the physical/model and statistical uncertainties, respectively. As mentioned before, these parameters can be obtained from test results.

5. RESULTS

This section presents results obtained using representative fatigue test data from test specimens manufactured by two different manufacturing processes of casted components. The manufacturing processes are "Sand Casting" and "Chill Casting". For each manufacturing process, several fatigue tests in different loading stresses were done. The numbers of test data are listed in Table (1).

Table 1- The test data

Manufacturing Method	Broken	Run-out
Sand Casting	713	114
Chill Casting	302	107

The statistical analysis is performed following the methodology described in section 2 and 3 for estimation of the parameters in the LogNormal and Weibull models. The results of the statistical analyses using the LogNormal and Weibull distributions are shown in table (2).

Further, the statistical analysis shows that σ_f and m are highly negative correlated. The results for the "Sand Casting" and "Chill Casting" are also shown in figure (1). The results show only a small difference between the curves for the LogNormal and Weibull distributions.

Table 2- Estimated statistical parameters from tests with LogNormal and Weibull distributions (normalized with respect to the mean value of 'Sand casting, LogNormal model')

Manufacturing method	Distribution type	σ_f[MPa]		m	
		mean	*Std dev*	*mean*	*Std dev*
Sand Casting	LogNormal	1	0.0064	1	0.005
	Weibull	0.95	0.0002	1.098	0.0000
Chill Casting	LogNormal	0.82	0.0050	1.608	0.010
	Weibull	0.71	0.0003	1.998	0.001

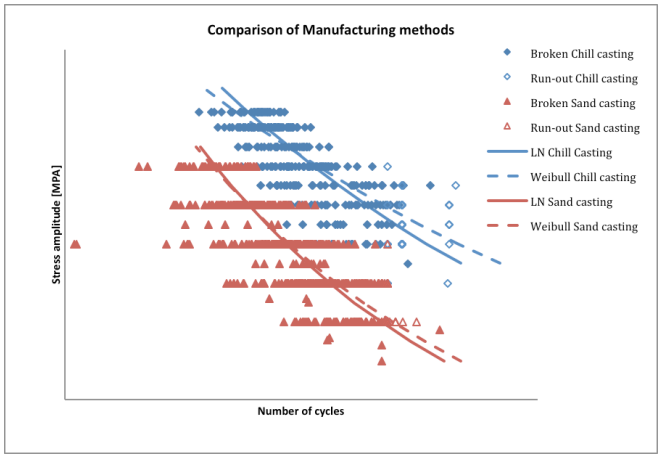

Figure 1. Comparison of "Sand Casting" and "Chill Casting"

It is seen that the specimens with "Chill Casting" manufacturing have higher fatigue strengths compare to "Sand Casting" manufacturing. It is also noted that the results are obtained considering both run-out (no-failure) and broken (failure) data (it must be noticed that run-out is not considered as broken data). The effect of including run-out data can be seen from the results in figures (2) and (3), where three different cases are considered:

- Estimation with run-out and broken data (denoted WR) (the run-out data is considered to evaluation the undefined parameter according to equations (7) and (12))
- Estimation without run-out data (denoted WOR)
- Estimation with run-out data considered as broken data (denoted ARB)

It seen that, the run-out data influences the fatigue life by increasing the fatigue life for smaller fatigue stress amplitudes showing that it is generally important to model the run-out data as 'run-out' data in the statistical analysis.

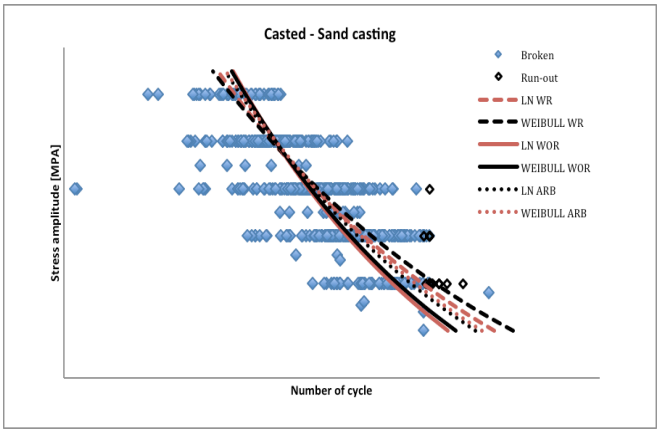

Figure 2. Effect of run-out data on estimation of fatigue life in Sand casting method

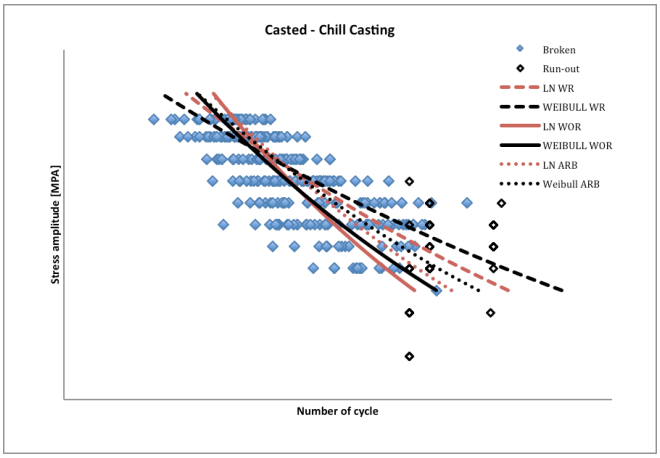

Figure 3. Effect of run-out data on estimation of fatigue life in chill casting method

Next, characteristic values are estimated as described above. First, the characteristic values are estimated without considering statistical uncertainties and next the statistical uncertainties are taken into account in estimation of the characteristic values. In figure (4) both mean values and characteristic values without statistical uncertainties are shown. It is seen that the characteristic values of Weibull distribution is lower than using the LogNormal distribution for both manufacturing methods.

Furthermore, the characteristic values are estimated when the statistical uncertainties are taken into account. The results are shown in figure (5). It is seen that also in this case the characteristic values obtained by the Weibull distribution are lower than those obtained by the LogNormal distribution for both manufacturing methods.

In figure (6), the characteristic values with statistical uncertainties and without statistical uncertainties are compared to each other. In this figure, 'WU' means "with statistical uncertainties" and 'WOU' means "without statistical uncertainties". It is seen that the statistical uncertainties in this example with a very large number of data only very slightly affect the characteristic values. Note that solid lines in figure (6) are mean values.

It must be noticed that in figures (4), (5) and (6), the run-out considered to estimation the parameters by equations (7) and (12).

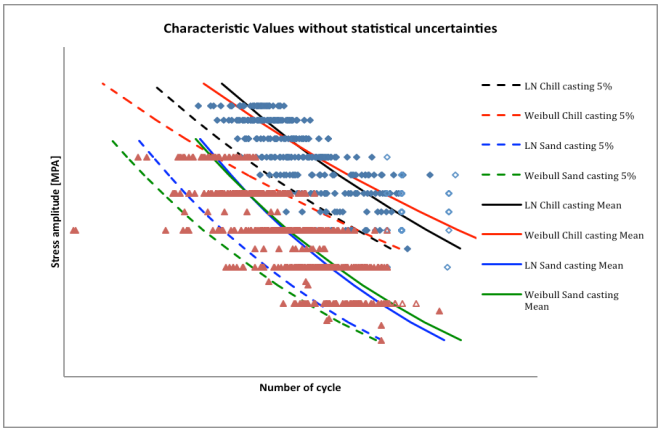

Figure 4. Characteristic values without statistical uncertainties

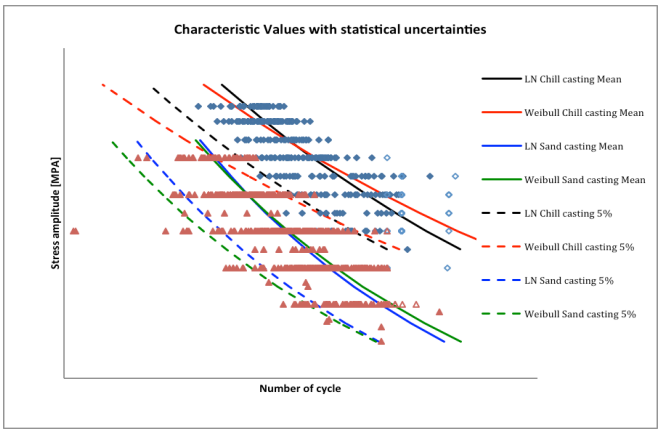

Figure 5. Characteristic values with statistical uncertainties

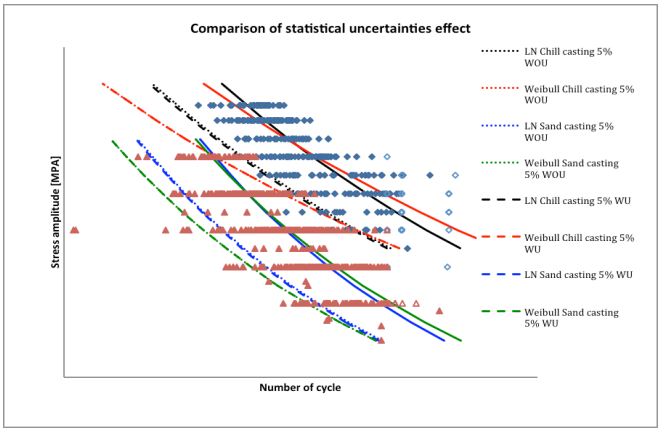

Figure 6. Comparison of statistical uncertainties effect

6. CONCLUSIONS

In this paper is considered two different casting methods often used for manufacturing casted components. A probabilistic approach is used to model the fatigue failure of both casting methods. Two basic stochastic models for the fatigue life are considered, namely the LogNormal and Weibull distributions. In these models, various uncertainties that affect the stochastic models of failure are modeled. These uncertainties include model and statistical uncertainties. Further, characteristic SN-curves are derived using structural reliability techniques. The characteristic curves are estimated using both without and with statistical uncertainties.

Using representative test data, the statistical model is applied to illustrate how the statistical analysis can be performed and characteristic values of the fatigue life estimated for wind turbine components. The results indicate that the "Chill Casting" manufacturing method as expected results in higher fatigue lives compare to "Sand Casting" method. It is also seen that the importance of run-out data in estimation of fatigue life and they must be considered to find the fatigue life of components.

The statistical models derived in this paper can be used for reliability assessments and for calibration of partial safety factors for fatigue assuming that the tests results are representative for typical applications.

ACKNOWLEDGEMENTS

The work is supported by the Strategic Research Center "REWIND – Knowledge based engineering for improved reliability of critical wind turbine components", Danish Research Council for Strategic Research, grant no. 10-093966. Fatigue test data is provided by Vestas Wind Systems A/S, Denmark.

REFERENCES

[1] H. Mirzaei Rafsanjani, J.D. Sørensen, 2013, 'Stochastic modeling of wind turbine drivetrain components', *Safety. Reliability and Risk Analysis: Beyond the Horizon*: Proceedings of the European safety and reliability conference, Esrel 2013, Amsterdam, The Netherlands, 29 September - 2 October 2013. ed. / R.D.J.M. Steenbergen; P.H.A.J.M. van Gelder; S. Miraglia; A.C.W.M. Vrouwenvelder. London: CRC Press LLC, 2013. pp. 1221-1228.

[2] E. Hau, 2006, 'Wind turbines: Fundamentals, Technologies, Application, Economics', Second ed., Springer, New York.

[3] P.J. Tavner, D.M. Greenwood, M.W.G. Whittle, R. Gindele, S. Faulstich, B. Hahn, 2012, 'Study of weather and location effects on wind turbine failure rates', *Wind Energy*, *Vol.* 16 pp. 175–187.

[4] M. Shirani, G. Härkegård, 2011, 'Fatigue life distribution and size effect in ductile cast iron for wind turbine components', *Engineering Failure Analysis, Vol.* 18 pp. 12-24.

[5] F.C. Campbell, 2008, 'Elements of metallurgy and engineering alloys', Ohio: Palo Alto.

[6] K. Schittkowski, 1986, 'NLPQL: A fortran subroutine solving constrained nonlinear programming problems', *Annals of Operations Research, Vol.* 5 pp. 485-500.

[7] D.V. Lindley, 1976, 'Introduction to Probability and Statistics from a Bayesian Viewpoint', Cambridge Univ. Press, Cambridge.

[8] H.O. Madsen, S. Krenk, N.C. Lind, 1986, 'Methods of structural safety', Prentice-Hall, Inc., Englewood cliffs, New Jersey.

D PAPER 4

Title: Fatigue Reliability analysis of wind turbine cast components.

Authors: Hesam Mirzaei Rafsanjani, John Dalsgaard Sørensen, Søren Fæster, Asger Sturlason

Journal: Submitted to Energies

Year:2016

energies

MDPI

Article

Fatigue Reliability analysis of wind Turbine Cast Components

Hesam Mirzaei Rafsanjani [1,*], John Dalsgaard Sørensen [1], Søren Fæster [2] and Asger Sturlason [3]

[1] Department of Civil Engineering, Aalborg University, Aalborg, Denmark 1; hmr@civil.aau.dk;
[2] Department of wind Energy, Technical University Denmark, Roskilde, Denmark; sfni@dtu.dk
[3] Vestas Technology & Service Solutions, Aarhus, Denmark; ast@vestas.com
* Correspondence: hmr@civil.aau.dk; Tel.: +45-41727434

Academic Editor: name
Received: date; Accepted: date; Published: date

Abstract: The fatigue life of wind turbine cast components is generally determined by defects from the casting process. These defects may reduce the fatigue life and they are generally distributed randomly in components. The foundries, cutting facilities and test facilities can affect the verification of properties by testing. Hence, it is important to have a tool to identify which foundry, cutting and/or test facility that produce components which based on the relevant uncertainties have the largest expected fatigue life or alternatively have the largest reliability to be used for decision making if additionally cost considerations are added. In this paper, a statistical approach is presented based on statistical hypothesis testing and Analysis of Covariance (ANCOVA) which can be applied to compare different groups (manufacturers, suppliers, test facilities, etc.) and to quantify the relevant uncertainties using available fatigue tests. Illustrative results are presented obtained by statistical analysis of a large set of fatigue data for casted test components typically used for wind turbines. Furthermore, the SN-curves for fatigue assessment are estimated based on the statistical analyses and by introduction of physical, model and statistical uncertainties used for illustration of reliability assessment.

Keywords: Reliability; Casting; Fatigue; ANCOVA; Wind turbines.

1. Introduction

Wind energy has become an attractive source of renewable energy, and its installed capacity worldwide has grown significantly in recent years [1]. Offshore wind turbines have been installed many places, especially in the North Sea and many new, larger wind farms are planned. Due to the harsh environmental conditions for offshore wind turbines, and the access difficulties for making maintenance and repairs, it is very important to minimize failures of wind turbine components including fatigue failures of casted components [2] in the wind turbine drivetrain.

Wind turbines are large structures exposed to wave excitations, highly dynamic wind loads and wakes from other wind turbines [3]. Thus, wind turbine components are exposed to stochastic loads that are varying randomly during the design working life. Due to highly variable loads, the components may fail due to fatigue, wear and other deterioration processes [3].

Casting defects are of high importance for the lifetime of structural casting. The fatigue life of cast iron components is often controlled by the growth of cracks initiated from defects such as shrinkage cavities and gas pores [4]. Further, different manufacturers apply different manufacturing processes of cast components resulting in different fatigue lives of the produced components.

This paper focuses on using Analysis of Covariance (ANCOVA) for comparing different groups / manufacturing steps of specimens from the casted components. An advantage of ANCOVA is that this method is able to handle different number of tests for various groups [5]. The result of

ANCOVA is useful in decision-making processes for companies and manufacturers to choose the better manufacturing process. This will lead to higher quality of manufactured components and increase the reliability of produced components. Further, the results of ANCOVA analysis is used for reliability assessment of wind turbine cast components. For this reason, the uncertainties related to model evaluation and the effect of each uncertainty on the reliability level on the components is evaluated. Moreover, a case study is presented to illustrate the application of ANCOVA to compare different manufacturing steps of casted components according to fatigue life results and also the reliability assessment of chosen cast components in wind turbine components based on the ANCOVA results.

2. Reliability analysis

Reliability of a component can be defined as the probability that the component under consideration has a proper performance throughout its lifetime. Structural reliability methods can be used to estimate the probability of failure/reliability which can be used for decision-making, e.g., with respect to design or planning of inspections, maintenance and repair [2].

Based on statistical analyses of statistically homogeneous datasets of fatigue lives, an appropriate stochastic model for the fatigue life can be established as described shortly below. Further, it is shown how a fatigue load model can be formulated based on simulations of the load effects for a specific wind turbine and represented by Markov matrices. Together with stochastic variables representing the uncertainties associated with the load assessment, and following the principles in e.g. [6] and [7], the reliability can be estimated by First Order Reliability Methods (FORM) or by simulation, see e.g. [8]. Finally, the stochastic model established on the basis of the above statistical analysis in combination with the reliability model for fatigue failure of wind turbine cast components can be applied for calibration of partial safety factors to a specified target reliability level, e.g. $5\ 10^{-4}$ per year as recommended in [7]. In section 4, the reliability assessment and methodology to evaluate the probability of failure is briefly explained, see [2] for more details.

3. Statistical analysis of fatigue data sets

A major challenge in statistical analysis of fatigue data is to establish statistically homogeneous dataset to be applied as basis for the statistical analyses. Analysis of variance (ANOVA) is a statistical method that can be used to analyze the differences between mean values of different groups of e.g. suppliers. In its simplest form, ANOVA provides a statistical test of whether or not the means of several groups are equal, and therefore generalizes the classical statistical *t*-test to more than two groups [9]. Based on hypothesis testing, the null hypothesis by the ANOVA method is that the mean values of several groups are equal, and on the other hand, the alternative hypothesis is that the mean values are not equal [10]. The level of significance represent the probability of making a type I error and is denoted by α. The level of significance should not be made too small, because the probability of making a type II error will then be increased. In this paper the value of $\alpha = 0.05$ is chosen.

ANOVAs are useful in comparing (testing) three or more groups. A decision of whether or not to accept the null hypothesis depends on a comparison of the computed values of the test statistics and the critical values. The ANOVA analysis can be performed computationally as follows; for further details see [10].

Step 1: Formulation of hypothesis – If a problem involves *k* groups, the following hypotheses are appropriate for comparing *k* group means [10]:

$$\begin{aligned} &\mathrm{H}_0 : \mu_1 = \mu_2 = \ldots = \mu_k \\ &\mathrm{H}_\mathrm{A} : \text{ at least one pair of group means are not equal} \end{aligned} \tag{1}$$

Step 2: Define the test statistic and its distribution – The hypotheses of step 1 can be tested using the following test statistic:

$$F = \frac{MS_b}{MS_w} \tag{2}$$

in which MS_b and MS_w are the mean squares quantifying between and within variations, respectively, and F is a random variable following an F distribution; for more details, see [10].

Step 3: The level of Significance: The level of significance is chosen to $\alpha = 5\%$ in this paper.

Step 4: Collect data and compute test statistic – The data should be collected and used to compute the value of the test statistics (F) in equation (2). Each data value is categorized according to the different groups to be compared statistically to each other.

Step 5: Determine the critical value of the test statistic – The critical value is a function of the level of significance and the degrees of freedom. If the computed value of step 4 is greater than the critical value, the null hypothesis of equation (1) should be rejected and the alternative hypothesis of equation (1) accepted.

In addition, the ANCOVA (Analysis of Covariance) always involves at least three variables to be introduced: an independent variable, a dependent variable, and a covariate. The covariate is the variable likely to be correlated with the dependent variable. For application for fatigue data, these variables are chosen as:

- The independent variable is the group types that we consider to compare to each other (for example test facilities or supplier).
- The dependent variable is the fatigue life, N and it is dependent on test stress amplitude and the type of group.
- The covariate is the test stress amplitude, σ [5].

The major distinction between the two analyses (ANOVA and ANCOVA) is that in ANOVA the error term is related to the variation of log$N$ around individual group means, whereas the ANCOVA error term is based on variations of log$N$ scores around regression lines. The effect of the smaller within-group variation associated with ANCOVA is an increase of the power of the analysis. Note that the ANOVA distributions have a larger overlap than the ANCOVA distributions [5]. The analysis of covariance is a combination of the linear models employed in analysis of variance and regression [11].

If it is assumed that data from k groups is available then the starting point for ANCOVA is exactly the same as for ANOVA; the total sum of squares is computed. It is noted that ANCOVA can be used for linear regression methods and therefore the analysis is carried out using the "logarithm of fatigue life (log$N$)" and the "logarithm of test stress amplitude (logσ)". Hence, the covariate variable (x) is logσ and dependent variable (y) is log$N$. Assuming that there is a linear relationship between the dependent variable and the covariate, we find that an appropriate statistical model is:

$$\log N_{ij} = \mu + \tau_i + \beta\left(\log \sigma_{ij} - \log \overline{\sigma_{\bullet\bullet}}\right) + \varepsilon_{ij} \quad \begin{cases} i = 1,2,...,m_j \\ j = 1,2,...,k \end{cases} \tag{3}$$

where logN_{ij} is the i-th observation on the response variable in the j-th group, logσ_{ij} is the measurement made on the covariate variable corresponding to logN_{ij}, $\log \overline{\sigma_{\bullet\bullet}}$ is the mean of all the values, μ is an overall mean, τ_j is the effect/influence of the j-th group, β is a linear regression coefficient indicating the dependency of logN_{ij} on logσ_{ij}, and ε_{ij} is a random error component. It is assumed that the errors ε_{ij} are normal distributed with mean value = 0 and standard deviation of σ_ε. The null hypothesis is "the group effects is zero ($\sum_{j=1}^{k} \tau_j = 0$)" and if the null hypothesis is accepted then logσ_{ij} is not affected by the groups.

3.1. Adjusted Mean

An adjusted mean is the mean dependent variable that would be expected or is predicted for each group, if the covariate variable mean is equal to the grand covariate mean. The grand covariate mean is a unique $\log\sigma_u$ and the adjusted fatigue life in each group is estimated according to this stress amplitude. In this way, for each group there is a unique point ($\log\sigma_u$, $\log N_{j,adj}$). This value would be different in different groups, and these values can be used to compare the state of regression lines to each other. According to adjusted means and slopes of regression lines, there are four types of regression line configurations:

- Completely different (Figure 1.a)
- Intercept (same intercepts) (Figure 1.b)
- Parallel (same slope but without intercept) (Figure 1.c)
- Coincidence (Exactly same lines) (Figure 1.d)

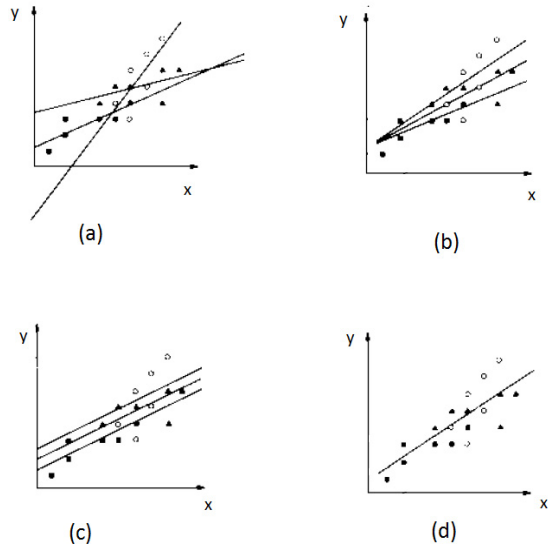

Figure 1. Relation between regression lines; [12]

By adjustment point and slope for each group, comparisons can be performed. As mentioned above the purpose of ANCOVA is to test the null hypothesis that two or more adjusted population means are equal. Alternatively, the purpose could be formulated as to test the equality of two or more regression intercepts. Under the assumption of parallel regression lines, the difference between intercepts must be equal to the difference between adjusted means. The formula for the computation of adjusted means is

$$\log N_{j,adj} = \log \overline{N_{\bullet j}} - b_w \left(\log \overline{\sigma_{\bullet j}} - \log \overline{\sigma_{\bullet\bullet}} \right) \quad (4)$$

where

$\log N_{j,adj}$ is the adjusted mean for j-th group

$\log \overline{N_{\bullet j}}$ is the unadjusted mean (mean of fatigue life) for j-th group

b_w is the pooled within-group regression coefficient (for details see [5] and [11])

$\log \overline{\sigma_{\bullet j}}$ is the mean of stress amplitude for j-th group

$\log \overline{\sigma_{\bullet\bullet}}$ is the grand covariate mean (i.e. the mean of the stress amplitudes for all test results)

3.2. Testing homogeneity of regression slopes

An assumption underlying the use of ANCOVA is that the population regression slopes are equal. If the slopes are not equal, the "Type of groups" effects differ at different levels of the stress amplitude; consequently, the adjusted stress amplitude can be misleading because they do not convey this important information. When the slopes are the same, the adjusted means are adequate descriptive measures because the differences of fatigue life are the same at different levels of the stress amplitude.

If the slopes for the populations in an experiment are equal, that is, $\beta_1^{(\text{group 1})} = \beta_1^{(\text{group 2})} = \ldots = \beta_1^{(\text{group k})}$, a reasonable way of estimating the value of this common slope from the samples is by computing an average of the sample b_1 values:

$$b_1^{(\text{Group j})} = \frac{\sum_{i=1}^{m_j}\left(\log N_{ij}\right)\left(\log \sigma_{ij}\right) - \frac{\left(\sum_{i=1}^{m_j}\log N_{ij}\right)\left(\sum_{i=1}^{m_j}\log \sigma_{ij}\right)}{m_j}}{\sum_{i=1}^{m_j}\left(\log \sigma_{ij}\right)^2 - \frac{\left(\sum_{i=1}^{m_j}\log \sigma_{ij}\right)^2}{m_j}} \quad (5)$$

where from equation (5) we have

$$b_w = \sum_{j=1}^{k} b_1^{(\text{Group j})} \quad (6)$$

The slope b_w is the best estimate of the population slope β_1, which is the slope assumed to be common on all groups. As long as $\beta_1^{(\text{group 1})} = \beta_1^{(\text{group 2})} = \ldots = \beta_1^{(\text{group k})}$, the estimate b_w is a useful statistical value to use. Now the problem is to decide whether all groups have the same slope. The homogeneity of the regression *F*-test is designed to answer the question of the equality of the population slopes. The null hypothesis associated with this test is:

$$H_0 : \beta_1^{(\text{group 1})} = \beta_1^{(\text{group 2})} = \ldots = \beta_1^{(\text{group k})} \quad (7)$$

The steps involved in the computation of the test are described next:

Steps 1 and 2: Computation of within-group sum of squares and within-group residual sum of squares (*SSres*$_w$)

This parameter can be evaluated by following equation (for further detail see [5] and [11]):

$$E_{yy} = \sum_{j=1}^{k}\left[\sum_{i=1}^{m_j}\left(\log N_{ij}\right)^2 - \frac{\left(\sum_{i=1}^{m_j}\log N_{ij}\right)^2}{m_j}\right] \quad (8)$$

$$E_{xy} = \sum_{j=1}^{k}\left[\sum_{i=1}^{m_j}\left(\log N_{ij}\right)\left(\log \sigma_{ij}\right) - \frac{\left(\sum_{i=1}^{m_j}\log N_{ij}\right)\left(\sum_{i=1}^{m_j}\log \sigma_{ij}\right)}{m_j}\right] \quad (9)$$

$$E_{xx} = \sum_{j=1}^{k} \left[\sum_{i=1}^{m_j} \left(\log \sigma_{ij} \right)^2 - \frac{\left(\sum_{i=1}^{m_j} \log \sigma_{ij} \right)^2}{m_j} \right] \tag{10}$$

$$SSreg_W = \frac{\left(E_{xy} \right)^2}{E_{xx}} \tag{11}$$

$$SSres_w = E_{yy} - SSreg_W \tag{12}$$

Step 3: Computation of individual sum of squares residual (*SSres*$_i$)

The third step involves computation of the sum of squares residual for each group separately and then add these residuals to obtain the sum of individual residual sum of squares (*SSres*$_j$). The difference in the computations of *SSres*$_w$ and *SSres*$_j$ is that *SSres*$_w$ involves computing the residual sum of squares around the single b_w value whereas *SSres*$_j$ involves the computation of the residual sum of squares around the b_j values fitted to each group separately (equation 13).

$$SSres_j = \left[\sum_{i=1}^{m_j} \left(\log N_{ij} \right)^2 - \frac{\left(\sum_{i=1}^{m_j} \log N_{ij} \right)^2}{m_j} \right] - \left[\frac{\sum_{i=1}^{m_j} \left(\log N_{ij} \right) \left(\log \sigma_{ij} \right) - \frac{\left(\sum_{i=1}^{m_j} \log N_{ij} \right) \left(\sum_{i=1}^{m_j} \log \sigma_{ij} \right)}{m_j}}{\sum_{i=1}^{m_j} \left(\log \sigma_{ij} \right)^2 - \frac{\left(\sum_{i=1}^{m_j} \log \sigma_{ij} \right)^2}{m_j}} \right] \tag{13}$$

Step 4: Computation of heterogeneity of slopes sum of squares

The discrepancy between *SSres*$_w$ and *SSres*$_i$ reflects the extent to which the individual regression slopes are different from the within-group slope b_w; hence, the heterogeneity of slopes *SS* is "*SS*$_{het}$ = *SSres*$_w$ - *SSres*$_i$", see [5].

Step 5. Computation of *F*-ratio. The summary table for the *F*-test is as follow. If the obtained *F* is equal to or greater than $F_{[\alpha, J-1, N-2J]}$, then the null hypothesis $H_0 : \beta_1^{(\text{group 1})} = \beta_1^{(\text{group 2})} = \ldots = \beta_1^{(\text{group k})}$ is rejected.

Table 1. Computation table for the Heterogeneity of slope.

Source	*SS*	*DF*	Mean square	*F*
Heterogeneity of slopes	SS_{het}	*k*-1	$MS_{het} = SS_{het} / (k-1)$	$MS_{AT} / MSres_w$
Individual residual (res$_i$)	$SSres_i$	*M*-2*k*	$MSres_i = SSres_i / (M-2k)$	
Within residual (res$_w$)	$SSres_w$	*M*-*k*-1	-	

In this method, diagnostic checking of the covariance model is based on residual analysis. Furthermore, the measure of uncertainty is not directly related to the uncertainty of SN-curve. The uncertainty of SN-curves used in the next section has been evaluated by Maximum Likelihood Method [MLM] [2].

4. Reliability assessment

The fatigue strength of metals is often assumed to follow the Basquin equation (the equation is based on fully reversed fatigue ($R = -1$), i.e. the mean value is zero) and is written [12].

$$N = K(\Delta\sigma)^{-m} \tag{14}$$

where N is the number of stress cycles to failure with constant stress ranges $\Delta\sigma$. K and m are material parameters dependent on the fatigue critical detail. The fatigue strength $\Delta\sigma_F$ may e.g. be defined as the value of S for e.g. $N_D = 2.10^6$ [7]. If one fatigue critical detail is considered, then the annual probability of failure is obtained from:

$$\Delta P_{F,t} = P_{\mathrm{COL|FAT}} P(\text{Fatigue failure in year } t) \tag{15}$$

where $P(\text{Fatigue failure in year } t)$ is the probability of failure in year t and $P_{\mathrm{COL|FAT}}$ is the probability of collapse of the structure given fatigue failure - modelling the importance of the detail / consequence of failure. The probability of failure in year t given survival up to year t is estimated by

$$\Delta P_{F,t} = P_{COL|FAT}\big(P(g(t) \le 0) - P(g(t-1) \le 0)\big)/P(g(t) > 0) \tag{16}$$

where the limit state equation is based on application of SN-curves, Miner's rule for linear accumulation of fatigue damage and by introducing stochastic variables accounting for uncertainties in fatigue loading and strength. The design equation can be written as follow, if used in a deterministic code-based verification:

$$D = \sum_i \frac{n_{i,S} T_L}{N(\Delta\sigma, \Delta\sigma_F, \gamma_F, \gamma_m, \Delta K, z)} = 1 \tag{17}$$

where $n_{i,S}$ represents the number of cycles per year at a specific stress level and T_L is the design lifetime. It is assumed that for a wind turbine component, the total number of stress ranges for a given fatigue critical detail can be grouped in n_σ groups/intervals such that, the number of stress ranges in group i is $n_{i,S}$ per year. In this paper, the Level II reliability method is used to estimate the reliability of the components [7]. The design parameter z is obtained from (17) assuming that the fatigue partial safety factors are given. Thereby the reliability analyses become normalized in the way that the reliability is linked to the partial safety factors and it is assumed that the structure is designed to the limit though the design parameter z in the design equation.

For deterministic design the following partial safety factors are introduced [13]:

γ_f a fatigue load partial safety factor multiplied to the fatigue stress ranges obtained by e.g. rainflow counting.

γ_m a fatigue strength partial safety factor. The design value of the fatigue strength is obtained by dividing the characteristic fatigue strength by γ_m.

The characteristic fatigue strength can be defined in various ways, namely based on:

- the mean minus two standard deviations of $\log K$.
- the 5% quantile of $\log K$, i.e. the mean minus 1.65 times the standard deviation of $\log K$.
- the mean of $\log K$.

The corresponding limit state equation to be used in the reliability analysis is written:

$$g(t) = \Delta - \sum_i \frac{n_{i,S} t}{N(X_W, X_{SCF}, \Delta\sigma, \Delta\sigma_F, \Delta K, z)} \tag{18}$$

where X_W is a stochastic variable modelling model uncertainty related to determination of fatigue loads and X_{SCF} is a stochastic variable modelling model uncertainty related to determination of

stresses given fatigue loads. In addition, Δ models model uncertainty related to Miner's rule for linear damage accumulation [2].

In Equation (18), Δ, X_W and X_{SCF} are assumed to be log-normal distributed with mean values equal to 1 and coefficients of variation COV_Δ, COV_W and COV_{SCF}, respectively. The coefficient of variations are estimated based partly subjectively, but following generally the recommendations used as basis for the material partial safety factors in IEC 61400-1, and also considering information from e.g. [14]. The importance of the choices of the coefficient of variations is investigated by sensitivity analyses. It is noted that the reliability level obtained is in accordance with the target reliability corresponding to an annual probability failure of the order 5×10^{-4} (annual reliability index 3.3) [15].

In Table 2, the stochastic model is shown. It is noted that m and $\Delta\sigma_f$ are correlated with statistical parameters extracted from [2]. The stochastic model is considered as representative for the fatigue strength represented by SN-curves. It is assumed that the design lifetime is T_L = 25 year [13].

Table 2. Stochastic model of fatigue strength based on SN-curves.

Variable	Definition	Distribution	Expected Value	Coefficient of Variation
Δ	Model uncertainty related to Miner's rule	LN*	1	COV_Δ = 0.3
X_{SCF}	Model uncertainty related to determination of stresses given fatigue load	LN	1	COV_{SCF}
X_W	Model uncertainty related to determination of fatigue loads	LN	1	COV_W
m	Slope SN-curve (Statistical uncertainty)	N**	Extracted from test results, [2]	
$\Delta\sigma_f$ [Mpa]	Fatigue Strength (Statistical uncertainty)	N	Extracted from test results, [2]	

* Log-Normal Distribution; ** Normal Distribution

If the SN-curves are obtained by a limited number of tests then statistical uncertainty has to be accounted. Table 3 shows indicative values of $\gamma_f\gamma_m$ for the target reliability index equal to 3.3 as function of the total coefficient of variation of the fatigue load: $COV_{load} = \sqrt{COV_W^2 + COV_{SCF}^2}$. It is noted that more fatigue test data should be investigated to validate the indicative values in Table 3.

Table 3. Indicative partial safety factors $\gamma_f\gamma_m$ as function of COV for fatigue load.

$\Delta\beta_{\min,FAT} \setminus COV_{load}$	0.00	0.05	0.10	0.15	0.20	0.25	0.30
3,3 ($5\ 10^{-4}$)	1.62	1.63	1.67	1.74	1.83	1.95	2.11

5. Result and Discussion

This section presents results obtained using representative fatigue test data from test specimens of cast components. The casted specimens are manufactured by two different manufacturing processes. The manufacturing processes are "Sand Casting" and "Chill Casting". In this section, the ANCOVA method is used to compare the different test laboratories and different extractions of samples for the tests and obtaining the fatigue test data.

5-1- Comparison of different test laboratories

The fatigue tests are carried out by four different Test laboratories. Table 4 shows the number of tests in each group. The comparison between groups (Tests labs) is performed using sand casting

results because there is only one group with chill casting. In this configuration, the run-out samples are considered as broken samples with very high cycles in order not to exclude them from the analysis. A summary of the ANCOVA calculations is shown in Table 5.

The value of b_w shows that the stress amplitude and fatigue life are negatively correlated. First it is tested if the choice of test laboratory does not affect the fatigue test results:

The null hypothesis is: H_0: The choice of test laboratory does not affect the fatigue test results.

Table 4. Number of test results by Test laboratories.

Testing Laboratories	Sand Casting		Chill Casting		Total
	Broken	Run-out	Broken	Run-out	
Group 1	28	2	-	-	30
Group 2	609	109	302	107	1127
Group 3	57	3	-	-	60
Group 4	19	-	-	-	19
Summation	713	114	302	107	1236

Table 5. Summary of calculation for Test laboratories comparison.

Parameter	Value	Parameter	Value
S_{yy}	574	$SSres_w$	196
$SSres_t$	206	SS_{AT}	9.6
$SSreg_w$	377	b_w	-8.9

* *SS*: Sum of squares

The *F*-ratio is calculated according to section 3. The study involves one covariate, four groups and 827 test results. The *F*-ratio calculation is summarized in Table 6.

Table 6. Computation Table for the Test laboratories comparison.

Source of Variation	Sum of squares	Degrees of freedom	Mean square	*F*	*p-value*
Adjusted (AT)	9.56	3	3.2	13.3	0.00
Error (res_w)	196	822	0.2		
Total residual (res_t)	205	825	-		

The obtained *F* is then compared with the critical value of *F* with 3 and 822 degrees of freedom and level of significance equal to 5%; $F_{(0.05,\ 3,822)}$ is 2.62, and the null hypothesis of "The choice of test laboratory does not affect the fatigue test results" is rejected. Next, the homogeneity of slopes of regression lines is considered, i.e. it is tested if the slopes of the different regressions lines are equal. The null hypothesis is written: $H_0 : \beta_1^{(Group1)} = \beta_1^{(Group2)} = \beta_1^{(Group3)} = \beta_1^{(Group4)}$

The summary of the calculation is shown in Table 7.

Table 7. Computation Heterogeneity of slopes for Test laboratories comparison.

Source	*SS*	*DF*	Mean square	*F*	*p-value*
Heterogeneity of slopes	1.2	3	0.41	1.71	0.16
Individual residual (res_i)	194	821	0.24		
Within residual (res_w)	196	824	-		

The critical value is $F_{(0.05,\ 3,\ 821)} = 2.62$; hence the null hypothesis is accepted. It is concluded that the slope of the regression lines are similar. Figure 2 shows the results for the regression lines (note the results are normalized). It is seen that the "Group 2" have the highest fatigue life and "Group 1" have the lowest fatigue life compare to the other Testing places and the groups have the same slope.

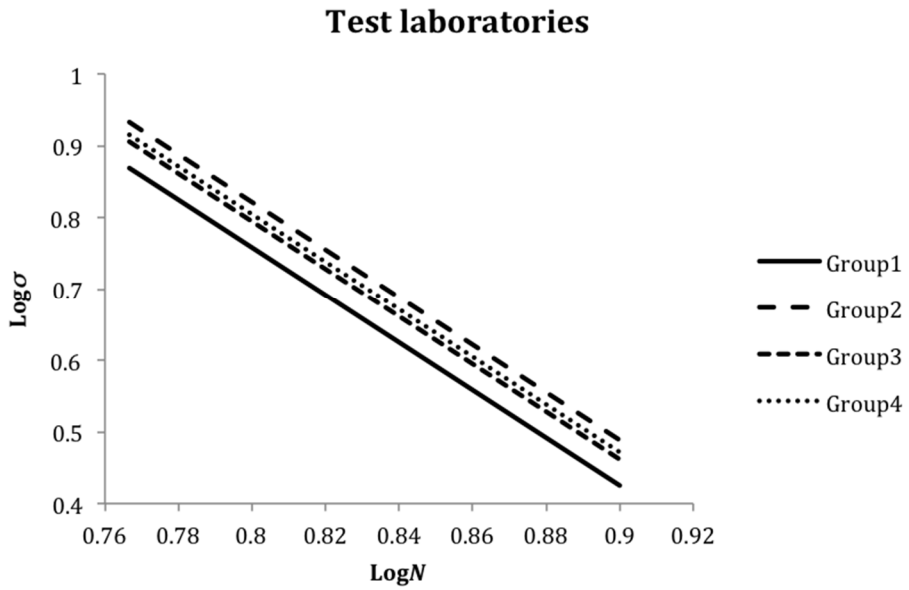

Figure 2. Comparison of "Testing Laboratories" on logarithmic scale

5-2- Comparison of different cutting facilities

The components from where samples are taken are cut up at different facilities. Table 8 shows the number of tests in each group. It is noted that the groups of cutting facilities are not the same as groups for testing laboratories.

Table 8. Number of test results by cutting facilities.

Cutting Facilities	Sand Casting		Chill Casting		Total
	Broken	Run-out	Broken	Run-out	
Group 1	107	8	96	3	214
Group 2	18	3	-	-	21
Group 3	95	14	-	-	109
Group 4	148	26	107	53	334
Group 5	345	63	99	51	558
Summation	713	114	302	107	1236

In this case, the comparison between groups is performed using sand casting and chill casting. The result of ANCOVA for sand casting and chill casting are shown in Table 9 and Table 10, respectively.

Table 9. Computation Table for the cutting facilities based on sand casting method.

Source of Variation	Sum of squares	Degrees of freedom	Mean square	*F*	*p-value*
Adjusted (AT)	16	4	3.8	16.3	0.00
Error (res_w)	191	821	0.2		
Total residual (res_t)	206	825	-		

Table 10. Computation Table for the cutting facilities based on chill casting method.

Source of Variation	Sum of squares	Degrees of freedom	Mean square	*F*	*p-value*
Adjusted (AT)	42	2	21.0	111	0.00
Error (res_w)	77	405	0.19		
Total residual (res_t)	119	407	-		

The obtained *F* statistics is then compared with the critical value. In both casting methods, the null hypothesis of "The choice of cutting facilities does not affect the fatigue test results" is rejected. Next, the homogeneity of regression test (slope of regression lines) is considered. The summaries of the calculation are shown in Table 11 and Table 12.

Table 11. Computation Heterogeneity of slopes for cutting facilities based on sand casting.

Source	*SS*	*DF*	Mean square	*F*	*p-value*
Heterogeneity of slopes	3.0	4	0.75	3.28	0.011
Individual residual (res_i)	181	817	0.23		
Within residual (res_w)	190	821	-		

Table 12. Computation Heterogeneity of slopes for cutting facilities based on chill casting.

Source	*SS*	*DF*	Mean square	*F*	*p-value*
Heterogeneity of slopes	3.4	2	1.68	9.24	0.000
Individual residual (res_i)	73.2	403	0.18		
Within residual (res_w)	76.6	405	-		

Based on Table 11 and Table 12, the null hypothesis is rejected and slopes of regression lines are not the same. Figure 3 and Figure 4 show the results for the regression lines of sand casting and chill casting, respectively (note the results are normalized).

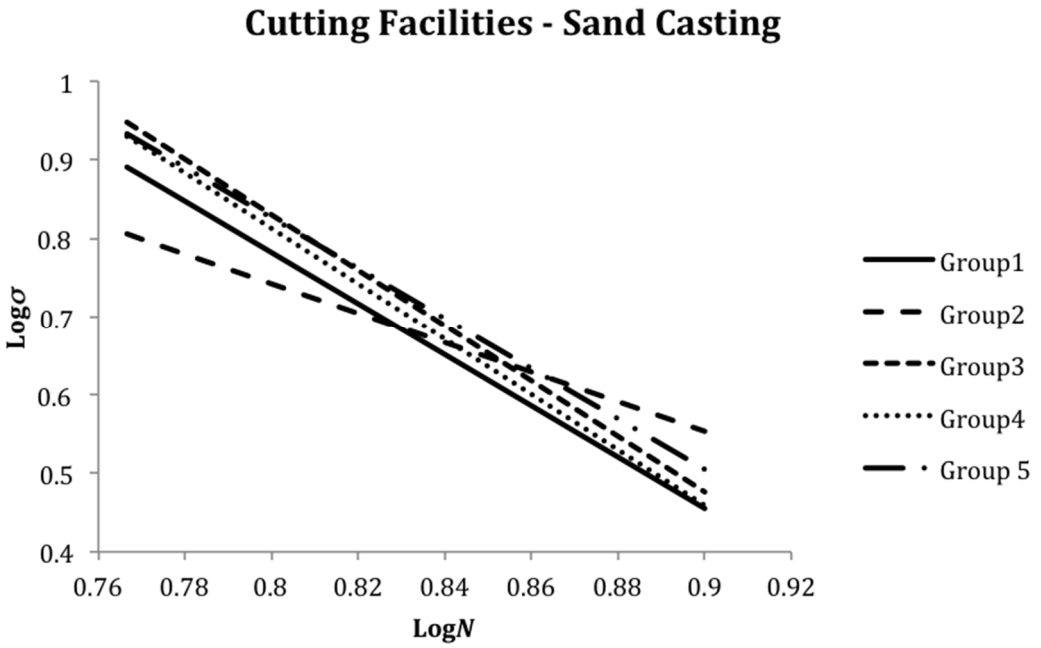

Figure 3. Comparison of "Cutting Facilities" on logarithmic scale for Sand Casting

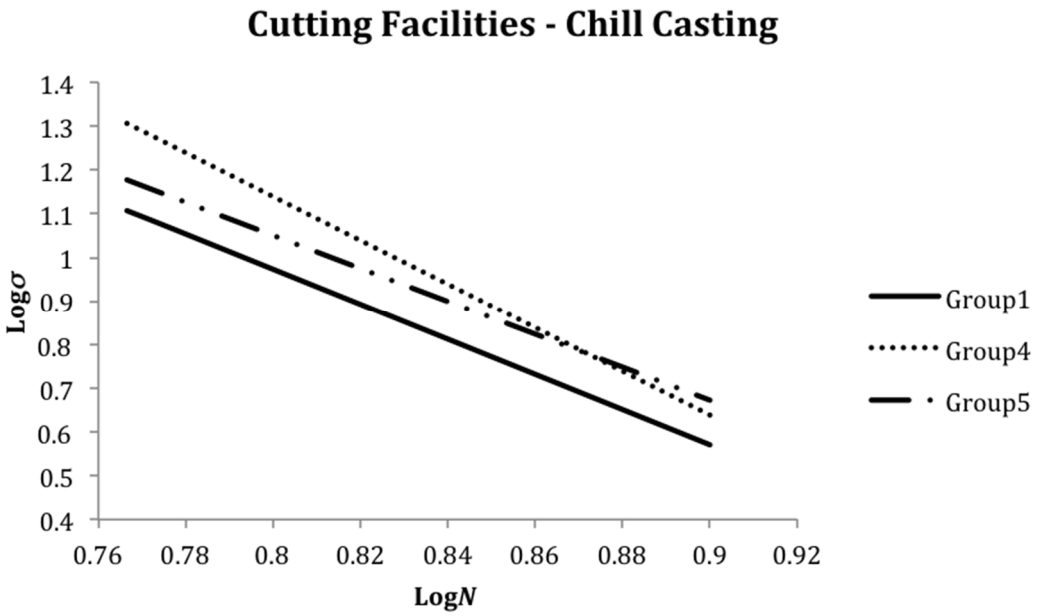

Figure 4. Comparison of "Cutting Facilities" on logarithmic scale for Chill Casting

According to Figure 3 and Figure 4, group 2 has a different slope compare to the other groups but the other groups are similar to each other. For sand casting quite small differences between fatigue lives are obtained for cutting facilities 1, 3, 4 and 5. For chill casting relatively larger differences in fatigue lives are obtained for cutting facilities 1, 4 and 5.

5-3– Reliability analysis – examples

In following, the SN-curves that were derived in the above sections are used for reliability analysis in a case study. The parameters used for analysis are listed in Table 13. By using the design equation (17), the design values (z) are determined for each group, see Table 15 and 16.

Table 13. Statistical parameters for reliability assessment of samples.

COV_{Δ}	COV_{SCF}	COV_{W}	COV_{load}	γ_f	γ_m
0.3	0.1	0.05	0.11	0.95	1.75

Table 14. Design-values (z) for Testing lab groups (obtained from equation (17)).

Groups	Group 1	Group 2	Group 3	Group 4
z-value	0.228	0.203	0.214	0.210

Table 15. Design-values (z) for cutting facilities groups (obtained from equation (17)).

Groups	Group 1	Group 2	Group 3	Group 4	Group 5
z-value	0.226	0.510	0.178	0.184	0.214

The reliability indices as function of time for the groups of testing laboratories (section 5.1) are estimated and are shown in Figure 5. Note that in this figure the annual reliability index is shown. The data from Group 2 result in the largest reliability level compared to the other groups. Moreover, the annual reliability index for cutting samples groups (section 5.2) is shown in Figure 6. It is seen that the annual reliability indices at the end of the lifetime is of the order of 3.3, corresponding to the target annual reliability index = 3.3.

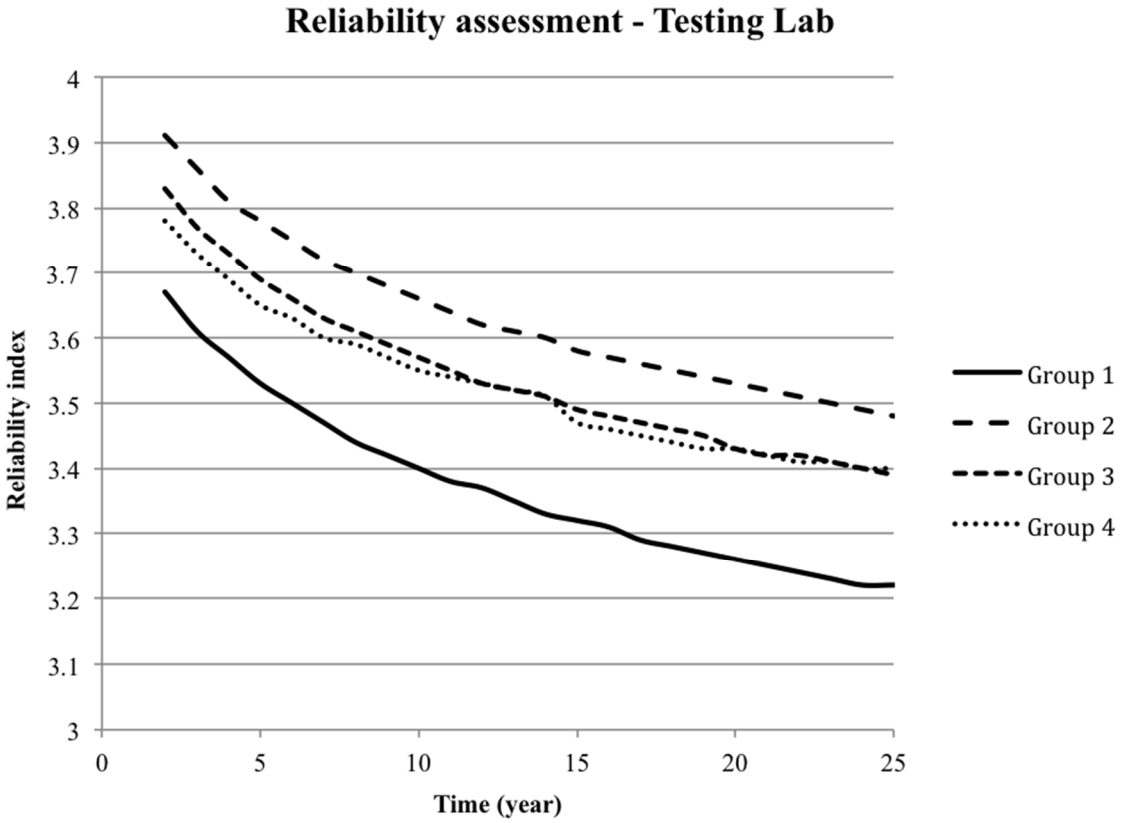

330

331 **Figure 5.** Annual reliability index for different groups based on test laboratories categories
332 (Sand casting)

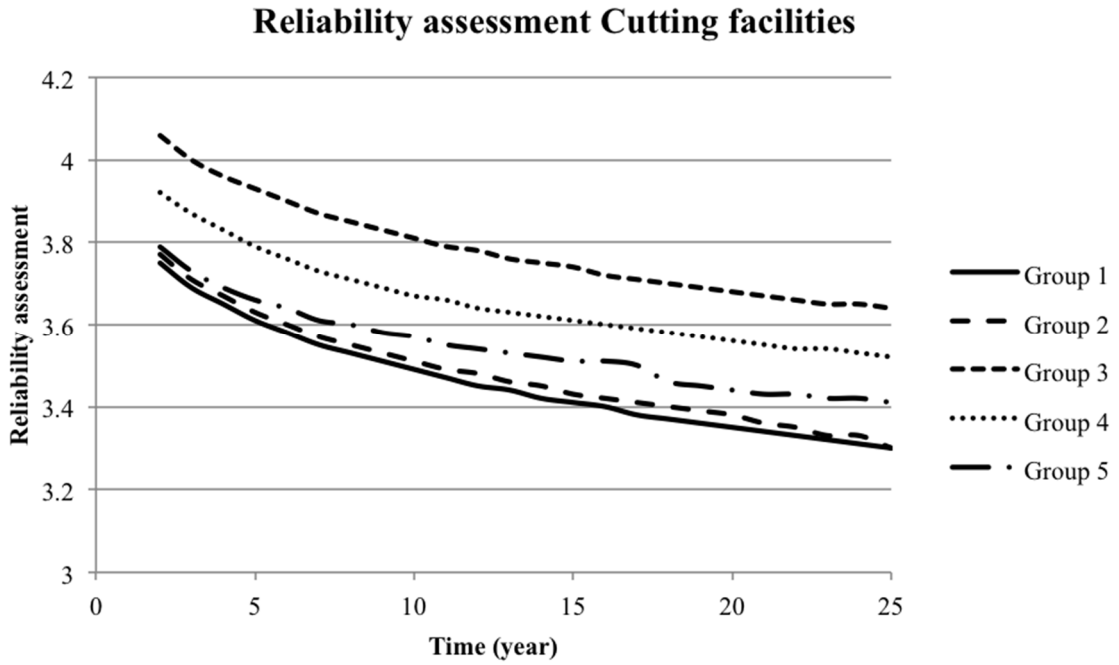

333

334 **Figure 6.** Annual reliability index for different groups based on cutting facilities categories
335 (Sand casting)

6 – Conclusions

In this paper, the ANCOVA method is used to compare different groups related to the manufacturing process and associated quality control of cast components. The ANCOVA method is applied for fatigue failure data. Test data is used to illustrate the implementation of the ANCOVA method. The different test laboratories and cutting facilities are compared to each other. The results obtained from the ANCOVA analysis can be used for decision-making on which tests laboratories and cutting facilities to be included in a statistical analysis in order to make sure that the statistical analyses are performed on data from a statistically homogeneous population. More parameters can be included, if relevant.

Further, it is presented how to apply the statistical results from the ANCOVA analysis to estimate the reliability for generic cases, and to assess the required safety factors for deterministic design such that a given target reliability level is obtained. It is noted, that more data and more example structures are needed to perform a more general reliability-based calibration of safety factors by the proposed approach.

Acknowledgments: The work is supported by the Strategic Research Center "REWIND – Knowledge based engineering for improved reliability of critical wind turbine components", Danish Research Council for Strategic Research, grant no. 10-093966. Fatigue test data is provided by Vestas Wind Systems A/S, Denmark.

Author Contributions: The Hesam Mirzaei Rafsanjani contributed to defining the overall problem and proposed the core scientific idea to solve it. The Hesam Mirzaei Rafsanjani established the ANCOVA analysis of SN curve models for fatigue samples that has been tested in RISØ center (DTU Roskilde campus) and they had been provided by industrial partner of project. The test samples provided by "Asger Sturlason" and tests was carried out in RISØ center by "Søren Fæster". The Hesam Mirzaei Rafsanjani conducted all the numerical simulations included in the paper and interpreted all the results with the help of the supervisor (co-author John Dalsgaard Sørenesen). Further, the Hesam Mirzaei Rafsanjani wrote the manuscript and revised it according to co-author comments.

Conflicts of Interest: The authors declare no conflict of interest.

References

1. Tavner, P.J.; Greenwood, D.M.; Whittle, M.W.G.; Gindele, R.; Faulstich, S.; & Hahn, B. Study of weather and location effects on wind turbine failure rates. *Wind Energy* **2012**, *16*, 175–187. http://dx.doi.org/10.1002/we.538
2. Rafsanjani, H.M.; Sørensen, J.D. Reliability analysis of fatigue failure of cast components for wind turbines. *Energies* **2015**, *8*, 2908-2923. http://dx.doi.org/10.3390/en8042908
3. Rafsanjani, H.M.; Sørensen, J.D. Stochastic models of defects in wind turbine drivetrain components. In *Multiscale Modeling and Uncertainty Quantification of Materials and Structures*. Papadrakakis, M., Stefanou, G., Eds.; Springer International Publishing, Switzerland, 2014, pp. 287-298.
4. Shirani, M.; Härkegård, G. Damage tolerant design of cast components based on defects detected by 3D X-ray computed tomography. *International Journal of Fatigue* **2012**, *41*, 188-198. http://dx.doi.org/10.1016/j.ijfatigue.2011.09.011
5. Huitema, B.E. *The Analysis of Covariance and Alternatives Statistical Methods for Experiments, Quasi-Experiments, and Single-Case Studies*. Wiley: New Jersey, USA, 2011.
6. Sørensen, J.D.; Toft, H.S. Probabilistic design of wind turbines, *Energies* **2010**, *3*, 24-257. http://dx.doi.org/10.3390/en3020241
7. Sørensen, J.D.; Toft, H.S. Safety Factors – IEC 61400-1 ed. 4 – background document. DTU Wind Energy-E-report-0066 (EN), **2014**.
8. Madesn, H.O.; Krenk, S.; Lind, N.C. *Methods of Structural Safety.* Dover Publications, 1986.
9. Zimmerman, D.W. A Note on Interpretation of the Paired-Samples t Test. *Journal of Educational and Behavioral Statistics* **1997**, *22*(3), 349–360. http://dx.doi.org/10.2307/1165289
10. Ayyub, B.M.; McCuen, R.H. *Probability, Statistics, and Reliability for Engineers and Scientists*, Second Ed., CRC: Chapman & Hall, USA, 2002.
11. Montgomery, D.C. *Design and Analysis of Experiments*, Eighth Ed., Wiley, 2013.

12. Silk, J. Analysis of covariance and comparison of regression lines. *Geo Abstracts,* University of East Anglia, 1979.
13. Sørensen, J.D. Reliability assessment of wind turbines. 12th International Conference on Applications of Statistics and Probability in Civil Engineering, *ICASP12.* Vancouver, Canada, 12-15 July 2015.
14. DNV-RP-C203. Fatigue design of offshore steel structures. Høvik, Norway, 2010.
15. IEC 61400. Wind Turbine- Part 1: Design Requirements. Geneva, 2015.

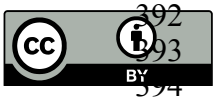

E PAPER 5

Title: Fatigue reliability of casted wind turbine drivetrain components due to defects.

Authors: Hesam Mirzaei Rafsanjani, John Dalsgaard Sørensen

Journal: 12th International Conference on Application of Statistics and Probability in Civil Engineering, ICASP12, Vancouver, Canada, 12th-15th July

Year:2015

Fatigue Reliability of Casted Wind Turbine Components Due to Defects

Hesam Mirzaei Rafsanjani
PhD Fellow, Dept. of Civil Engineering, Aalborg University, Aalborg, Denmark

John Dalsgaard Sørensen
Professor, Dept. of Civil Engineering, Aalborg University, Aalborg, Denmark

ABSTRACT: Manufacturing of casted components often leads to some (small) defects that are distributed in the volume of the components. These defects are different according to their size, type, orientation and etc. In this paper a probabilistic model is proposed for modeling manufacturing defects and their influence on the fatigue strength of the components. The fatigue life is dependent on the number, type, location and size of the defects in the component and is therefore quite uncertain and needs to be described by stochastic models. In this paper, the Poisson distribution for modeling of defects of component are considered and the surface and sub-surface defects categorized. Furthermore, a model to estimate the probability of failure by fatigue due to the defects is proposed. This model is used to estimate the failure location of component and it is compared to models of defect distributions and locations. Further, an upper bound of reliability is estimated using a modified Miner rule approach for fatigue damage accumulation.

1. INTRODUCTION

Wind energy is a rapid growing industry in the renewable energy sector with large potentials for contributing significantly to the future energy production. A main focus for wind turbine manufactures and operators is to increase the reliability of wind turbines and to decrease the cost of energy. Offshore wind turbines are exposed to wave excitations, highly dynamic wind loads and wakes from other wind turbines. Therefore, most components in a wind turbine experience highly dynamic and time-varying loads (Mirzaei & Sørensen, 2014). These components may fail due to wear or fatigue and this can lead to unplanned shut down repairs that may be very costly.

Design of mechanical components in the wind turbine drivetrain by deterministic methods using safety factors are generally not able to account rationally for the many uncertainties. Therefore, alternatively reliability assessments may be performed using probabilistic methods where stochastic modeling of failures and uncertainties is performed. Modeling of the fatigue failure of casted wind turbine components can be used for predicting the expected time-to-failure which is an important indicator to be used in planning of operation and maintenance. In order to estimate the probability of failure of casted components careful modeling of the aleatory (physical) and epistemic (model, statistical and measurement) uncertainties has to be performed (Sheng & Veers, 2011).

Current fatigue designs are typically based on the safe life design approach (Shirani & Härkegård, 2010). In the safe life design, fatigue testing is carried out on baseline material to produce *SN* curves. However, the manufacturing process may affect *SN*-curves and the statistical uncertainties and different manufacturing processes may lead to the need to use different statistical models for the material strengths.

The fatigue life of cast iron is often controlled by the growth of cracks initiated from defects such as shrinkage cavities and gas pores

(Shirani & Härkegård, 2012). To predict the fatigue life, defects are considered as pre-existent cracks and fatigue life and fatigue limit are controlled by the crack propagation law and by the threshold of the stress intensity range, respectively.

Early-life failures are often the result of poor manufacturing and inadequate design. A substantial proportion of early-life failure is also due to the presence of defects in the material. An important factor affecting the strength of components is the presence of defects due to processing, manufacturing or mechanical damage occurring during service (Todinov, 2006). Further, the fatigue life is highly dependent on the number, type, location, size of defects and the applied stress on the component during its design working life. Defects can thus be categorized in different groups.

This paper focuses on statistical models of defect distribution in wind turbine components and development of probabilistic models of fatigue strength. To model the defect distribution, the location of defects (interior or surface) defects has to be modelled and the number of defects in each volume must also be modeled. It is noted that size, type, number, orientation and stress surface of defects affect the probability of failure. First, the distribution of defects in the specimen volume has to be modeled incl. clustering of defects in the interior and the surface of the specimens. The fatigue strength is estimated based on the defect distribution. Finally, the stochastic models for the defects and for the fatigue life given defects are used to estimate the probability of failure of components.

2. DEFECT DISTRIBUTION MODEL

Manufacturing of components often leads to some (small) defects that are distributed in the volume of the components. These defects are different according their size, type, orientation and etc. and influence the load-bearing capacity of the components (Toft et al., 2011). Hence, an important factor affecting the strength of components is the presence of defects from processing and/or manufacturing.

An important problem related to materials containing defects is to model the uncertainty by a defect density function for the component volume. In some cases, clustering of defects is important and strongly influencing the probability of failure. Clustering of two or more defects within a small volume often decrease dangerously the load-bearing capacity and increases the stress concentration. Hence, the number of defects in each volume and the size / dimension of the defects should be modeled according to their size, type, orientation and etc.

In order to determine the probability of fracture (failure), all initiating defects are divided into categories depending on their type (Todinov, 2000). In the categories, each defect, according to its size, shape, and orientation etc., is characterized by a specific level of local maximum tensile stress, at which fatigue is triggered. Each type of defect i is characterized by a cumulative distribution function for the number of fatigue load cycles to failure, $F_{N,I}(n, R, \sigma)$, giving the probability that fatigue failure does not occur at a local maximum tensile stress equal to σ and a given R-ratio, that is the ratio of the minimum stress experienced during a cycle to the maximum stress experienced during a cycle.

Hence, suppose that in a specimen with volume V_T, M types of defects exist (Todinov, 2000). It is important to emphasize that the nucleation of fatigue cracks in the groups of defects are assumed as statistically independent events. In other words, a fatigue crack in a particular group is not affected by fatigue crack in other groups. This assumption is related to the condition of nucleation on a particular defect depending only on the local maximum tensile stress and on the strength and orientation of the defect. According to this, the defects can be categorized in M groups of defects such that the size, type and orientation etc. of defects in each group are very close to each other. It is noted that each type of defects is characterized by a

cumulative distribution function $F_{N,I}(n, R, \sigma)$ for the number of load cycles to failure, see below.

Furthermore, it is assume that the number of defects of group j can be modeled by a multi-dimensional Poisson process. Thus, if D is any region in the multi-dimensional space for which the area or volume of the region and $N(D)$ is the number of defects in D, then

$$P\left(N\left(D\right)=k\right)=\frac{\left(\lambda\left|D\right|\right)^{k}e^{-\lambda\left|D\right|}}{k!} \quad (1)$$

is the probability that the number of defects in D is k. Equivalently, the density function of the number of defects in group j in volume V of component is (Ravi Chandran and Jha, 2005):

$$P\left(k\right)=\frac{\left(\lambda_j V\right)^{k}e^{-\lambda_j V}}{k!} \quad (2)$$

where λ_j is the average number of defects of group j (there is M different groups of defects). The probability of occurrence of the number of defects in different parts of the specimen can now be assessed using the Poisson model. Eq. (1) and (2) are the general equations for modeling the defect distribution of the j-th group of defects. In the next step, the whole component is modeled. Suppose, that in a specimen with volume V_T, a smaller volume dV_i is stressed to a tensile stress $\sigma_{i,j}$ which is assumed to be uniform inside the volume dV_i, result in

$$V_T=\sum_{i=1}^{N_V}dV_i \quad (3)$$

where N_V is the number of volumes dV_i in volume V_T. Fatigue cracks are assumed to initiate from surface cracks / defects or sub-surface cracks / defects. Volume dV_i in Eq. (3) is rewritten as (Ravi Chandan and Jha, 2005):

$$dV_i=\left(A_i+dA_i\right)dl \quad (4)$$

where, A_i is interior area of each smaller volume and dA_i is the area of the surface rim of a certain width wrapping around A_i such that the total cross-sectional area of the sample is A_i+dA_i (Figure 1). It is noted that the above equation can model other specimen's volumes too.

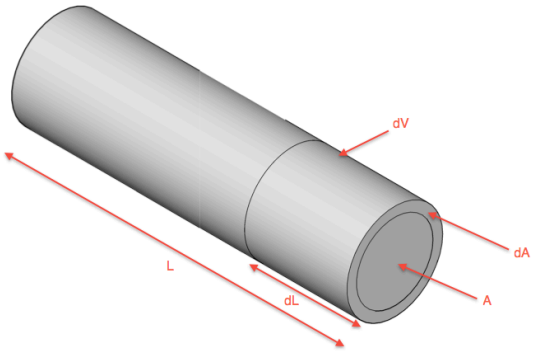

Figure 1: The model segment of Specimen Volume.

The probabilities of defect occurrence in different parts of the specimen can now be assessed using the Poisson distribution. Whether a specimen fail by internal or surface crack initiation is determined depending on whether there is a cluster of defect at that location (Ravi Chandran and Jha, 2005). In this context, three cases are considered:

- If there is a finite probability that there are cluster defects in the interior and no cluster defects in the surface rim volume, implying the specimens to fail only by internal initiation.
- If there is a finite probability that there are cluster defects in the surface rim region and no cluster defect in the interior, implying the specimens to fail only by surface-initiation.
- If cluster defects exist both in the interior as well as in the surface rim volumes, then, the specimen is likely to fail by surface-initiation only, because it is known that fatigue crack initiation at surface typically is accelerated by the air environment.

The probability of occurrence of interior defects, $P_{int,j}$, is the probability that one or more defects from group j in A_i with no such defects present in dA_i. This can be written on the basis of Eq. (2) and (4) as

$$P_{\text{int},i,j}\left(k\right)=\frac{\left(\lambda_j\left(A_i dl\right)\right)^{k}e^{-\lambda_j\left(A_i dl\right)}}{k!}e^{-\lambda_j\left(dA_i dl\right)} \quad (5)$$

Similarly, the probability of occurrence of surface defects, $P_{surf,j}$, is equal to the probability that at least one or more defect from group *j* will occur in dA_i regardless of a defect from group *j* being absent or present in the interior area A_i. In other words, the occurrence of a defect in the interior does not matter as long as one surface defect is present, since it will preferentially initiate a critical fatigue crack which is more critical than a defect in A_i due to environmental effects. The probability of surface-crack initiation is then given by the probability of presence of one or more defects in dA_i

$$P_{surf,i,j}\left(k\right)=\frac{\left(\lambda_j\left(dA_i dl\right)\right)^k e^{-\lambda_j\left(dA_i dl\right)}}{k!} \tag{6}$$

In following, the probability of fatigue failure of component due to existence of defects will be modeled.

3. PROBABILTY OF FATIGUE FAILURE

In the previous section, the defect location in the volume V_T is modeled by a Poisson distribution. The volume V_T is modeled as a "series system" of volumes $\mathrm{d}V_i$ since failure in any of the volumes $\mathrm{d}V_i$ is assumed to result in 'collapse'. The probability of failure of each volume $\mathrm{d}V_i$, is denoted $P_{f,i}$. The probability $P_{f,i}$ is dependent on

- Probability of existence of defect in volume $\mathrm{d}V_i$.
- Probability of fatigue failure if a defect exists in volume $\mathrm{d}V_i$.

As mentioned above, the defects are categorized in *M* groups. For each one of these groups, the probability of failure is to be evaluated. Hence, the probability of failure of each volume $\mathrm{d}V_i$ is written

$$P_{f,i}=\sum_{j=1}^{M}\Big[P\left(\text{defect of j-th group exist in } dV_i\right) \times P\left(\text{fatigue failure}\middle|\text{defect from j-th type/size exist}\right)\Big] \tag{7}$$

Eq. (7) is applied for both interior and surface defects and in each volume $\mathrm{d}V_i$.

As described above it is assumed that the defects follow a homogeneous Poisson process in the volume $\mathrm{d}V_i$. The distribution function $F_{N,j}(n,R,\sigma_{i,j})$ is assumed to follow a Weibull distribution (Fjeldstad, Wormsen and Härkegård, 2008)

$$F_{N,j}\left(n,R,\sigma_{i,j}\right)=1-\exp\left[-\left(\frac{n}{N_j(R,\sigma_{i,j})}\right)^{b_{n,j}}\right] \tag{8}$$

where $N_j(R,\sigma_{i,j})$ and $b_{n,j}$ are the shape and scale parameters of Weibull distribution and they are subject to statistical uncertainties if modelled on basis of test data and should be evaluated by statistical analysis methods such as Maximum Likelihood Method or Bootstrapping using available data sets. *n* is the actual number of cycles in the lifetime $[0, T_L]$ with stress range σ, where T_L is life time of component. Hence *n* can be written as:

$$n=\nu * T_L \tag{9}$$

where ν is the number of load cycles with the stress range $\sigma_{i,j}$ per year. Eq. (8) should be determined for all *M* groups of defects. Let $F_{N,j}(n,R,\sigma_{i,j})$ denote the conditional individual probability that the fatigue life characterizing a single defect from *j*-th group on the component's volume will be smaller than *n* cycles, given that the defect resides in the component volume.

The probability of failure in volume $\mathrm{d}V_i$ can next be determined by subtracting from unity the probability of the complementary event that none of the defects fatigue lives will be smaller than *n* cycles (Todinov, 2006). This probability, $p^0_{(r,i,j)}$ of the compound event: exactly *r* defects from group *j*-th exist in the volume $\mathrm{d}V_i$ of the component and their fatigue lives will not smaller than *n* can be modeled by:

$$p^0_{(r,i,j)}=P\left(r \text{ defects in } dV_i\right) \times P\left(\text{none fatigue failure less than n cycle}\middle| r \text{ defects}\right) \tag{10}$$

This probability correspond to the probability of two events:

- Exactly r defects from group j-th exist in volume dV_i
- None of fatigue lives associated with the r defects will be smaller than n cycles.

The probability $p^0_{i,j}$ that "component's fatigue life will be greater than n cycle" is determined on basis of a union of disjoint probabilities $p^0_{(r,i,j)}$. Consequently, the probability of the event $p^0_{i,j}$ is a sum of the probabilities defined by:

$$p^0_{i,j} = \sum_r p^0_{(r,i,j)} \tag{11}$$

Eq. (11) can be generalized modeling interior and surface defects. If m defects are interior defects in volume dV_i, then r-m defects will be surface defects. Hence, Eq. (11) can be written as (as mentioned before):

$$p^0_{i,j}(n,R,\sigma_{i,j}) = \begin{cases} \sum_{k=0}^{m} P_{\text{int},i,j}(k) \times \left[1 - F_{N,j}(n,R,\sigma_{i,j})\right]^k & m = r \\ \sum_{l=0}^{r-m} P_{surf,i,j}(l) \times \left[1 - F_{N,j}(n,R,\sigma_{i,j})\right]^l & r > m \end{cases} \tag{12}$$

Then, the probability of failure due to defect from group j for the sub-components with volume dV_i becomes

$$P_{f,i,j} = 1 - p^0_{i,j} \tag{13}$$

Eq. (13) can be generalized for multiple groups. Thus, the probability that component's fatigue life will be greater than n cycle according to Eq. (13) is

$$p^0_i(n,R,\sigma_{i,j}) = \prod_{j=1}^{M} p^0_{i,j}(n,R,\sigma_{i,j}) \tag{14}$$

Hence, the probability of failure of fatigue for volume dV_i can be written as

$$P_{f,i}\left(n,R,\sigma_{i,j}\right) = 1 - p^0_i\left(n,R,\sigma_{i,j}\right) = 1 - \prod_{j=1}^{M} p^0_{i,j}\left(n,R,\sigma_{i,j}\right) \tag{15}$$

The volume V_T is assumed to be modeled as a "series system" of independent volumes dV_i. Hence, the probability of failure of volume V_T, can be written as

$$P_f\left(n,R,\sigma_{i,j}\right) = 1 - \prod_{i=0}^{N_V}\left(1 - P_{f,i}\left(n,R,\sigma_{i,j}\right)\right) \tag{16}$$

This failure probability is a function of:

- The stress level $\sigma_{i,j}$
- Time t because $n=\nu^*t$

$P_f\left(n,R,\sigma_{i,j}\right)$ is the probability of failure in the life time $[0,t]$ when $n=\nu^*t$. Eq. (16) is the probability of failure for volume V_T. In these equations, the size, type, orientation, stress of defects are considered but when there are clusters of defects in components, the distance between each defects play very important role on fatigue life and should be introduced in the models, e.g. following the models in (Toft et al., 2011).

4. RESULTS

In this section, the probabilistic model described in previous sections is illustrated using the data and defects observed in (Shirani 2012). The data considered are from specimen numbers 45, 49, 50 and 51. In Figure 2 is shown the geometry of the specimens and the coordinate system used.

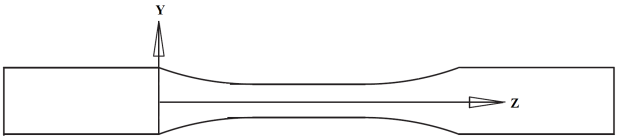

Figure 2: The fatigue test Specimen.

Table 1 shows for each specimen, the location of the observed fracture surfaces with respect to the z-axis; for more details see (Shirani 2012). Moreover, dl in Eq. (4) is chosen to 2 mm, and the probability of failure is estimated by Eq. (15) with n chosen to 2,000,000 cycles for all specimens. Further, $N_j(R,\sigma_{i,j})$ and $b_{n,j}$ in Eq. (8) are estimated for each group of defects such that the $N_j(R,\sigma_{i,j})$ values are taken as the predicted values by (Shirani 2012), see the following tables. $b_{n,j}$ is taken as 1.5.

Table 1: Location of fracture surface on z-axis for test specimens (Shirani 2012).

Specimen Number	*Fracture surface observed (Shirani 2012) [mm]*
45	*98*
49	*138*
50	*53*
51	*96*

Specimen number 45: The observed defects and the probability of failure estimated by Eq. (15) are shown in Figure 3. It is noted, that the probability of failure in Figure 3, and in the following figures, is the probability of failure for each sub-volume dV_i estimated by Eq. (15) with dl = 2 mm, i.e. it is thus not the probability of failure of whole specimen.

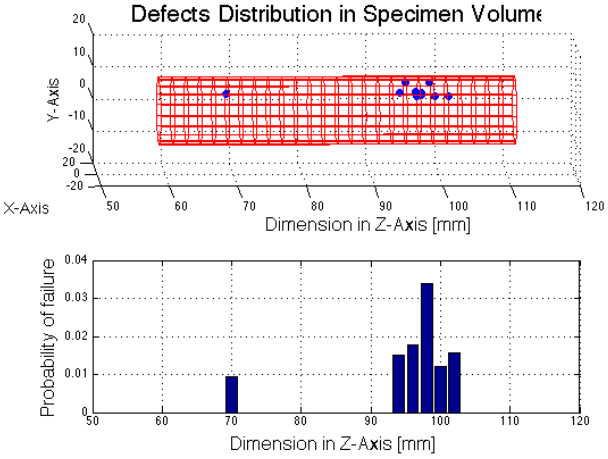

Figure 3: Observed defects and probability of failure in dV_i along the length of specimen 45

According to (Shirani 2012) the two largest defects (based on defects volumes) for specimen number 45 are located at z = 98.87 mm and 97.55 mm (see Table 2). The defect volumes are 26.44 mm^3 and 24.72 mm^3, respectively. According to Figure 3, the sub-volume at 97 - 99 mm has the highest probability of failure (upper bound estimated by Eq. (15)). Further, the smaller defect number 8 is also located in this sub-volume and contributes to the probability of failure. This sub-volume with the highest estimated probability of failure, and thereby the most critical sub-volume corresponds to the observed fracture surface, see Table 1.

Table 2: Specimen number 45 (Shirani, 2012).

Num.	*Volume (mm^3)*	*X (mm)*	*Y (mm)*	*Z (mm)*	*$N_j(R,\sigma_{i,j})$ Predicted life (cycles)*
1	*26.44*	*7.37*	*6.11*	*98.87*	*690,134*
2	*24.72*	*4.29*	*3.03*	*97.55*	*774,977*
3	*5.39*	*3.74*	*3.14*	*101.5*	*1,946,904*
4	*4.65*	*8.03*	*2.59*	*95.13*	*1,963,542*
5	*7.48*	*5.22*	*1.27*	*94.36*	*2,046,626*
6	*3.92*	*3.96*	*1.93*	*99.42*	*2,774,349*
7	*1.93*	*4.73*	*2.70*	*69.04*	*3,758,844*
8	*2.21*	*5.06*	*1.27*	*97.55*	*4,065,269*
9	*2.28*	*5.33*	*2.48*	*96.67*	*4,501,964*
10	*1.24*	*4.4*	*0.39*	*96.78*	*4,898,411*

Specimen number 49: The observed defects and the probability of failure (estimated by Eq. (15)) are shown in Figure 4. The largest probability of failure is in the sub-volume dV_i between 139 and 141 mm (Table 3).

According to Table 3, defect number 3, 4 and 10 are in the mentioned sub-volume. The observed fracture surface (at 138 mm) is very close to the sub-volume with the highest estimated probability of failure.

Table 3: Specimen number 49 (Shirani, 2012).

Num.	*Volume (mm^3)*	*X (mm)*	*Y (mm)*	*Z (mm)*	*$N_j(R,\sigma_{i,j})$ Predicted life (cycles)*
1	*4.2*	*-1.87*	*8.67*	*92.25*	*2,811,521*
2	*2.52*	*3.41*	*-4.31*	*72.55*	*3,886,311*
3	*2.41*	*-3.41*	*2.29*	*140.68*	*4,429,748*
4	*2.39*	*-8.92*	*2.07*	*139.25*	*5,088,111*
5	*2.02*	*6.82*	*3.61*	*102.93*	*4,106,853*
6	*2.23*	*9.35*	*0.31*	*102.05*	*4,409,628*
7	*1.43*	*0.33*	*-4.75*	*75.19*	*5,328,563*
8	*1.16*	*7.7*	*0.09*	*102.49*	*6,903,317*
9	*1.13*	*8.58*	*4.27*	*101.28*	*7,124165*
10	*1.04*	*-5.17*	*0.31*	*139.8*	*5,296,975*

Specimen number 50: The two sub-volumes with the largest probabilities of failure are at the 53-55 mm and 57-59 mm sub-volumes, see Figure 5.

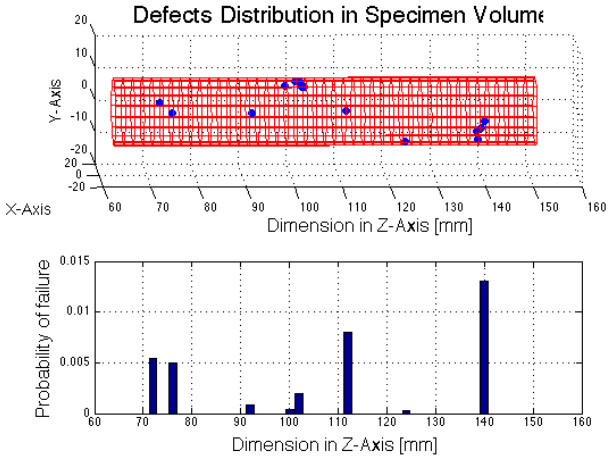

Figure 4: Observed defects and probability of failure of dV_i along the length of specimen 49.

According to Table 4, the defects number 3, 6, 7, 9 and 10 are inside the 53-55 mm sub-volume, i.e. 5 out of the 10 largest defects are located very close to where failure is observed (at 53 mm). Hence, failure is likely due to the cluster of defects that are very close to each other. It is noted that the largest defect (based on volume of defects) is located at 55.15 mm. Because this defect is located in the interior of the specimen, the probability of failure of this defect is lower than cluster of defects between surfaces 53-55 mm. These results are very similar to results in (Shirani 2012).

Table 4: Specimen number 50 (Shirani, 2012)

Num.	*Volume (mm^3)*	*X (mm)*	*Y (mm)*	*Z (mm)*	*$N_j(R,\sigma_{i,j})$ Predicted life (cycles)*
1	*12.82*	*-1.24*	*-7.32*	*55.15*	*1,174,747*
2	*7.89*	*-0.39*	*-1.98*	*57.82*	*1,734,182*
3	*6.37*	*0.68*	*-2.84*	*54.72*	*1,843,818*
4	*4.35*	*-3.7*	*-6.68*	*57.07*	*2,169,724*
5	*3.54*	*4.52*	*-7.75*	*52.91*	*2,355,450*
6	*3.41*	*-0.39*	*-5.61*	*54.08*	*2,529,115*
7	*1.47*	*4.42*	*-4.33*	*53.44*	*4,166,833*
8	*0.74*	*-2.2*	*-6.04*	*58.57*	*6,381,366*
9	*0.97*	*2.82*	*-3.9*	*53.76*	*6,588,717*
10	*0.96*	*6.98*	*-5.83*	*53.76*	*6,964,649*

Specimen number 51: According to Table 5, the two largest defects are located at 97.85 mm and 98.29 mm on *z*-axis. Further, the defects number 4, 8, 9 and 10 are also located between or near the sub-volume 97-99 mm.

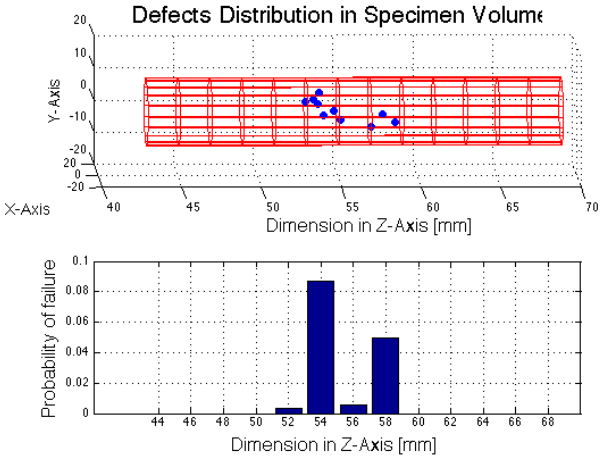

Figure 5: Observed defects and probability of failure of dV_i along the length of specimen 50.

Table 5: Specimen number 51 (Shirani, 2012)

Num.	*Volume (mm^3)*	*X (mm)*	*Y (mm)*	*Z (mm)*	*$N_j(R,\sigma_{i,j})$ Predicted life (cycles)*
1	*1.86*	*7.7*	*-4.06*	*97.85*	*3,901,121*
2	*1.53*	*6.49*	*-4.73*	*98.29*	*4,312,266*
3	*1.99*	*-2.75*	*-8.51*	*102.04*	*4,761,026*
4	*2.1*	*-1.09*	*-9.17*	*98.29*	*5,617,233*
5	*0.74*	*-5.4*	*-6.75*	*122.86*	*6,307,730*
6	*0.69*	*4.3*	*-8.06*	*67*	*7,585,928*
7	*0.54*	*-5.98*	*0.52*	*123.74*	*8,320,367*
8	*0.53*	*7.05*	*-5.83*	*97.3*	*8,789,104*
9	*0.47*	*0.87*	*-4.31*	*98.18*	*8,789,104*
10	*0.4*	*0.76*	*-3.65*	*98.84*	*9,019,978*

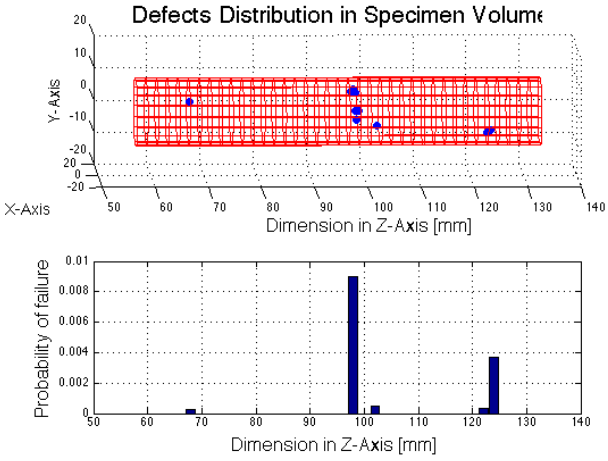

Figure 6: Observed defects and probability of failure of dV_i along the length of specimen 51.

The largest estimated probability of failure is in the sub-volume 97-99 mm, corresponding to the observed location of the fracture (at 96 mm).

5. CONCLUSION

In this paper is presented generic models for estimation of the probability of fatigue failure due to manufacturing defects in casted components, e.g. for wind turbine components. The defects are categorized in different groups according to their size, type, orientation and etc. For each group, a Poisson distribution is used to model the distribution of defects. Further, the defects are divided in two sub-groups of interior and surface defects.

Next, the component volume is divided in smaller volume to obtain approximately homogeneous stresses in small sub-volumes. In each sub-volume sections, the probability of failure is modeled. The probability of failure is a function of i) existence of defect(s) in sub-volumes, ii) the conditional probability of failure due to existence of defect(s) in sub-volumes. In this model, the interior and surface defects are separated from each other. The model accounts for cluster of defects.

For each sub-volume, the probability of failure is modeled. As the component volume is assumed to be considered as a series system of sub-volumes, the probability of failure of the whole components can be estimated according to a series systems probability of failure models.

Finally, the model is illustrated by application to test results. The results indicate that the probabilistic model is able to estimate a location of highest probability of failure quite close to the actual location of failure of the tests.

6. ACKNOWLEDGMENT

The work is supported by the Strategic Research Center "REWIND – Knowledge based engineering for improved reliability of critical wind turbine components", Danish Research Council for Strategic Research, grant no. 10-093966.

7. REFERENCES

Fjeldstad, A., Wormsen, A., and Härkegård, G. (2010). "Simulation of fatigue crack growth in components with random defects" *Engineering Fracture Mechanics*, 75, 1184-1203.

Mirzaei Rafsanjani, H., and Sørensen, J. D. (2014). "Stochastic models of defects in wind turbine drivetrain components?" In: Papadrakakis M, Stefanou G, editors. *Multiscale Modeling and Uncertainty and Uncertainty Quantification of Materials and Structures.* Switzerland: Springer; 287-298.

Ravi Chandran, K. S., and Jha, S. K. (2005). "Duality of the S-N fatigue curve caused by competing failure modes in a titanium alloy and the role of Poisson defect statistics" *Acta Materialia*, 53, 1867-1881.

Sheng, S., and Veers, P. (2011, May). "Wind turbine drivetrain condition monitoring – An overview" Paper presented at Mechanical Failure Prevention Group: Applied Systems Health Management Conference, Virginia Beach, Virginia.

Shirani, M., and Härkegård, G. (2010). "Fatigue life distribution and size effect in ductile cast iron for wind turbine components" *Engineering Failure Analysis*, 18, 12-24.

Shirani, M., and Härkegård, G. (2012). "Damage tolerant design of cast components based on defects detected by 3D X-ray computed tomography" *International Journal of Fatigue*, 41, 188-198.

Todinov, M. T. (2000). "Probability of fracture initiated by defects" *Materials Science and Engineering*, A276, 39-47.

Todinov, M. T. (2006). "Equations and a fast algorithm for determining the probability of failure initiated by flaws" *International Journal of Solids and Structures*, 43, 5182-5195.

Toft, H. S., Branner, K., Berring, P. and Sørensen, J. D. (2011). "Defect distribution and reliability assessment of wind turbine blades" *Engineering Structures*, 33, 171-180.

F PAPER 6

Title: Effect of defects distribution on fatigue life of wind turbine components.

Authors: Hesam Mirzaei Rafsanjani, John Dalsgaard Sørensen

Journal: Procedia IUTAM, 13, 144-150.

Year:2015

Available online at www.sciencedirect.com

ScienceDirect

Procedia IUTAM 13 (2015) 144 – 150

Procedia IUTAM

www.elsevier.com/locate/procedia

IUTAM Symposium on "Dynamical Analysis of Multibody Systems with Design Uncertainties"

Effect of defects distribution on fatigue life of wind turbine components

Hesam Mirzaei Rafsanjani*, John Dalsgaard Sørensen

Aalborg University, Sohngaardsholmvej 57, Aalborg 9000, Denmark

Abstract

The reliability of the component of a wind turbine is often highly dependent on defects introduced during the manufacturing process. In this paper a stochastic model is proposed for modeling these defects and the influence on the fatigue life is considered. Basically the defects assumed distributed by a Poisson process / field where the defects form clusters that consist of a parent defect and related defects around the parent defect. The fatigue life is dependent on the number, type, location and size of the defects in the component and is therefore quite uncertain and needs to be described by stochastic models. In this paper, the Poisson distribution for modeling of defects of component are considered and the surface and sub-surface defects categorized. Furthermore, a model to estimate the probability of failure by fatigue due to the defects is proposed. Moreover, the relation between defect distribution and fatigue life of component explained.

Peer-review under responsibility of organizing committee of Institute of Engineering and Computational Mechanics University of Stuttgart.

Keywords: Fatigue life; Wind turbine; defect distribution.

1. Introduction

Wind energy has become an attractive source of renewable energy, and its installed capacity worldwide has grown significantly in recent years. Understanding the availability of wind turbines is vital to maximize wind turbine energy production and minimize the payback period. The wind turbine components are exposed to stochastic

* Corresponding author. Tel.: +45-99408557.
E-mail address: hmr@civil.aau.dk

Peer-review under responsibility of organizing committee of Institute of Engineering and Computational Mechanics University of Stuttgart.
doi:10.1016/j.piutam.2015.01.014

loads varying during the design working life of wind turbines. In this paper casted component are considered. Due to highly variable loads, these components may fail due to wear and / or fatigue.

Current fatigue designs are typically based on the life design approach[1]. In the safe life design, fatigue testing is carried out on baseline material to produce *SN* curves. However, the fatigue strength is highly uncertain and statistical uncertainties due to a limited number of tests can be important to be included in modeling the fatigue strength. Moreover, the manufacturing process may affect the statistical uncertainties and different manufacturing processes may lead to the need to use different statistical models for the material strengths[2].

The fatigue life of cast iron is often controlled by the growth of cracks initiated from defects such as shrinkage cavities and gas pores[3]. Since fatigue cracks are frequently observed early in life, it is usually assumed that the crack initiation stage is negligible. To predict the fatigue life, defects are considered as pre-existent cracks and fatigue life and fatigue limit are controlled by the crack propagation law and by the threshold of the stress intensity range, respectively. Thus, to predict the fatigue life of cast components by a damage tolerant approach, the position and size of the defects contained in the component are required.

Early-life failures are often the result of poor manufacturing and inadequate design. A substantial proportion of early-life failure is also due to the presence of defects in the material. An important factor affecting the strength of components is the presence of defects due to processing, manufacturing or mechanical damage occurring during service[4]. Furthermore, most of the existing models relate the probability of failure initiated by defects to the probability of finding defects of particular sizes in the stressed volume.

This paper focuses on statistical models of defect distribution in wind turbine components. To model the defect distribution, the location of defects (interior or surface) defects must be determined and the number of defects in each volume must also be modeled. It is noted that size, type, number, orientation and stress surface of defects affect the probability of failure. First, the distribution of defects in the specimen volume has to be modeled incl. cluster of defects in the interior and surface of the specimens. Finally, the relation between fatigue failure and defects has to be modeled. Further, the probability of failure is considered based on the models of distribution of defects.

2. Defect distribution model

Manufacturing of components often leads to some (small) defects that are distributed in the volume of the components. These defects are different according their size, type, orientation and etc. and influence the load-bearing capacity of the components[5]. E.g. fatigue failures are often the result of manufacturing defects. Further, a substantial proportion of the fatigue failures are related to random variations of strengths in a complex function of material properties, design configuration and dimensions. An important factor affecting the strength of components is the presence of defects from processing or manufacturing.

An important problem related to materials containing defects is determining the defect density in the component volume. In some cases, clustering of defects is strongly correlated with the probability of failure. Clustering of two or more defects within a small volume often decrease dangerously the load-bearing capacity and increases the stress concentration. Hence, the number of defects in each volume and the size / dimension of the defects should be modeled according to their size, type, orientation and etc.

In order to determine the probability of fracture and distribution of fracture stress, all initiating defects are divided into categories depending on their type[6]. In the categories, each defect, according to its size, shape, and orientation etc., is characterized by a specific level of local maximum tensile stress, at which it triggers fatigue crack initiation. Each type of defect i is characterized by a cumulative distribution function $F_{N,i}(n;\sigma)$, giving the probability that fatigue crack will be initiated at a local maximum tensile stress smaller than or equal to σ.

Hence, suppose that in a specimen with volume V_T, M types of defects exist[6]. It is important to emphasize that the acts of nucleation of fatigue cracks in the groups of defects are independent events. In other words, a fatigue crack nucleation in a particular group is not affected by fatigue crack nucleation in other groups. This assumption is related to the condition of nucleation on a particular defect depending only on the local maximum tensile stress and on the strength and orientation of the defect[6]. According to this, the defects can be categorized in M groups of defects such that the size, type and orientation etc. of defects in each group are very close to each other. It is noted that each type of defects is characterized by a cumulative distribution function $F_{N,i}(n;\sigma)$ for the number of load cycles to failure, see below.

Furthermore, it is assume that the number of defects of group j can be modeled by a multi-dimensional Poisson process. Thus, if D is any region in the multi-dimensional space for which the area or volume of the region, $|D|$ is finite. If $N(D)$ is the number of defects in D, then

$$P\left(N\left(D\right)=k\right)=\frac{\left(\lambda\left|D\right|\right)^{k}e^{-\lambda\left|D\right|}}{k!} \tag{1}$$

is the probability that the number of defects in D is k. Equivalently, the density function of the number of defects in group j in volume V of component is[7]:

$$P\left(k\right)=\frac{\left(\lambda_j V\right)^{k}e^{-\lambda_j V}}{k!} \tag{2}$$

where λ_j is the average number of defects of group j (there is M different groups of defects). The probabilities of occurrence of number of defects in different parts of the specimen can now be assessed using the Poisson distribution. The probabilities of occurrence of no defect and one defect or more in volume V are given by:

$$P\left(k=0\right)=e^{-\lambda_j V} \tag{3}$$

$$P\left(k\geq 1\right)=1-P\left(k=0\right)=1-e^{-\lambda_j V} \tag{4}$$

Equations (1 – 4) are general equations for modeling the defect distributions of j-th group of defects. As mentioned above, there are M groups of defects that are categorized according to their defect size, type, orientation and etc.

In the next step, the whole component is modeled. Suppose that in a specimen with volume V_T, a smaller volume $\mathrm{d}V_i$ is stressed to a tensile stress σ_i which is assumed to be uniform inside the volume $\mathrm{d}V_i$. The fracture stress associated with the stressed volume $\mathrm{d}V_i$ is the minimum stress σ_i at which a defect in the volume will initiate fatigue failure.

$$V_T=\sum_{i=1}^{N_V}dV_i \tag{5}$$

where N_V is the number of volumes $\mathrm{d}V_i$ in volume V_T. Fatigue cracks are assumed to initiate from surface cracks / defects or sub-surface cracks / defects. Volume $\mathrm{d}V_i$ in equation (5) is rewritten as:

$$dV_i=\left(A_i+dA_i\right)dl \tag{6}$$

where, A_i is interior area of each smaller volume and dA_i is the area of the surface rim of a certain width wrapping around A_i such that the total cross-sectional area of the sample is A_i+dA_i. Note that, it is assumed that all volumes are cylindrical (Figure 1). It must be noticed that the above equation can model other volumes too.

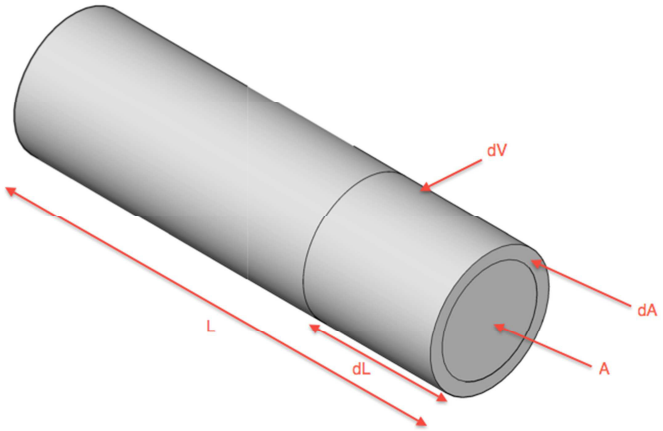

Fig. 1. The geometry of specimen volume.

The probabilities of defect occurrence in different parts of the specimen can now be assessed using the Poisson distribution. Whether a specimen would fail by internal or surface crack initiation is determined by whether there is a cluster of defect at that location[7]. In this context, three cases are considered:

- If there is a finite probability that there are cluster defects in the interior and no cluster defects in the surface rim volume, implying the specimens to fail only by internal initiation.
- If there is a finite probability that there are cluster defects in the surface rim region and no cluster defect in the interior, implying the specimens to fail only by surface-initiation.
- If cluster defects exist both in the interior as well as in the surface rim volumes, then, the specimen is likely to fail by surface-initiation only, because it is known that fatigue crack initiation at surface is accelerated by the air environment

The probability of occurrence of interior defects, $P_{int,j}$, is the probability that one or more defects from group j in A_i with no such defects present in dA_i. This can be written on the basis of Equations (5) and (6) as[7]

$$P_{\text{int},j} = \left(1 - e^{-\lambda_j\left(A_i dl\right)}\right) e^{-\lambda_j\left(dA_i dl\right)} \tag{7}$$

Similarly, the probability of occurrence of surface defects, $P_{surf,j}$, is equal to the probability that at least one or more defect from group j will occur in dA_i regardless of a defect from group j being absent or present in the interior area A_i. In other words, the occurrence of a defect in the interior does not matter as long as one surface defect is present, since it will preferentially initiate a critical fatigue crack due to environmental effects[7]. The probability of surface-crack initiation is then given by the probability of presence of one or more defects in dA_i

$$P_{surf,j} = 1 - e^{-\lambda_j\left(dA_i dl\right)} \tag{8}$$

In the next section, the probability of failure of component due to existence of defects will be modeled.

3. Probability of failure according to defect distribution

In the previous section, the defect location in the volume V_T is modeled by a Poisson distribution. The volume V_T is modeled as a "series system" of volumes dV_i. The probability of failure of each volume dV_i, is $P_{f,i}$. The probability $P_{f,i}$ is dependent on

- Probability of existence of defect in volume dV_i.
- Probability of failure when the defect exists in volume dV_i.

As mentioned above, the defects are categorized in M groups. For each one of these groups, the probability of failure should be evaluated. Hence, the probability of failure of each volume dV_i is written

$$P_{f,i} = \sum_{j=1}^{M} \left[P\left(\text{defect of j-th group exist in } dV_i\right) \times P\left(\text{fatigue failure} \middle| \text{defect from j-th group exist}\right) \right] \tag{9}$$

Equation (9) is established for both interior and surface defects and in each volume dV_i.

It is assumed that the defects follow a homogeneous Poisson process in the volume dV_i. Defects are characterized by the distribution function $F_{N,j}$ for the number of load cycles to fatigue failure due to existence of defect(s) from the j-th group. The distribution function $F_{N,j}$ is assumed to follow a Weibull distribution[2]

$$F_{N,j}\left(n;\sigma\right) = 1 - \exp\left[-\left(\frac{2n}{S_V^{1/b_n}} \left(\frac{\sigma_{a0}}{\sigma_{f,j}} \right)^{m_j} \right)^{b_n} \right] \tag{10}$$

where σ_{a0} is the alternating stress amplitude, $\sigma_{f,j}$ is the fatigue strength according to a specific defect group, n is the number of load cycles to failure, m_j is the fatigue strength exponent when defect is from group j and S_V is ratio of volumes (the ratio of dV_i/V_0 , the V_0 is the volume of test specimens that used for estimation the Weibull model). The values of m_j and $\sigma_{f,j}$ are subject to statistical uncertainties and should be evaluated by statistical analysis methods such as Maximum Likelihood Method or Bootstrapping based on the available data sets. The Weibull distribution should be determined for all M groups of defects.

The probability of failure in the volume dV_i can next be determined by subtracting from unity the probability of the complementary event that none of the defects will initiate failure[4]. This probability, $p^0_{(r,i,j)}$ of the compound event: exactly r defects from group j-th exist in the volume dV_i of the component and none of them initiates failure can be modeled by[4]:

$$p^0_{(r,i,j)} = P\left(r \text{ defects in } dV_i\right) \times P\left(\text{none of defects will initiate failure} \middle| r \text{ defects}\right) \tag{11}$$

This probability is the probability of two statistically independent events:

- exactly r defects from group j-th exist in volume dV_i
- none of defects will initiate failure.

The event $p^0_{i,j}$ that "no failure will be initiated at a stress level σ_i in the volume dV_i" is a union of disjoint events $p^0_{(r,i,j)}$, that no fracture will be initiated if the sample volume dV_i contains r = 0, 1, 2, …, n defects. Consequently, the probability of the event $p^0_{i,j}$ is a sum of the probabilities defined by:

$$p_{i,j}^{0} = \sum_{r} p_{(r,i,j)}^{0} \tag{12}$$

Equation (12) can be generalized modeling interior and surface defects. If m defects are interior defects in volume $\mathrm{d}V_i$, then r-m defects will be surface defects. Hence, equation (12) can be written as:

$$p_{i,j}^{0} = \sum_{k=0}^{m} P_{\mathrm{int},i,j} \times \left[1 - F_{N,j}\right]^{k} + \sum_{l=0}^{r-m} P_{surf,i,j} \times \left[1 - F_{N,j}\right]^{l} \tag{13}$$

By substitution equations (7) and (8) in equation (13), equation (13) is rewritten as

$$p_{i,j}^{0} = \sum_{k=0}^{m} \left(1 - e^{-\lambda_j \left(A_i dl\right)}\right) e^{-\lambda_j \left(dA_i dl\right)} \times \left[1 - F_{N,j}\right]^{k} + \sum_{l=0}^{r-m} \left(1 - e^{-\lambda_j \left(dA_i dl\right)}\right) \times \left[1 - F_{N,j}\right]^{l} \tag{14}$$

Equation (14) can be rewritten to

$$p_{i,j}^{0} = \left(1 - e^{-\lambda_j \left(A_i dl\right)}\right) \left\{ \sum_{k=0}^{m} e^{-\lambda_j \left(dA_i dl\right)} \times \left[1 - F_{N,j}\right]^{k} + \sum_{l=0}^{r-m} \left[1 - F_{N,j}\right]^{l} \right\} \tag{15}$$

Then, the probability of failure due to defect from group j for the sub-components with volume $\mathrm{d}V_i$ becomes

$$P_{f,i,j} = 1 - p_{i,j}^{0} = 1 - \left(1 - e^{-\lambda_j \left(A_i dl\right)}\right) \left\{ \sum_{k=0}^{m} e^{-\lambda_j \left(dA_i dl\right)} \times \left[1 - F_{N,j}\right]^{k} + \sum_{l=0}^{r-m} \left[1 - F_{N,j}\right]^{l} \right\} \tag{16}$$

Equation (16) can be generalized for multiple groups. As mentioned above, the defects can be categorized in M groups of defects that for each group the probability of failure can be evaluated. Thus, the probability that no failure will be initiated according to equation (15) is

$$p_{i}^{0} = \prod_{j=1}^{M} p_{j}^{0} = \prod_{j=1}^{M} \left\{ \sum_{k=0}^{m} \left(1 - e^{-\lambda_j \left(A_i dl\right)}\right) e^{-\lambda_j \left(dA_i dl\right)} \times \left[1 - F_{N,j}\right]^{k} + \sum_{l=0}^{r-m} \left(1 - e^{-\lambda_j \left(dA_i dl\right)}\right) \times \left[1 - F_{N,j}\right]^{l} \right\} \tag{17}$$

where λ_j and $F_{N,j}$ are the defect number density and the probability of initiating failure characterizing a defect from the j-th group of defects. Hence, the probability of failure of fatigue for volume $\mathrm{d}V_i$ can be written as

$$P_{f,i} = 1 - p_{i}^{0} = 1 - \prod_{j=1}^{M} \left\{ \sum_{k=0}^{m} \left(1 - e^{-\lambda_j \left(A_i dl\right)}\right) e^{-\lambda_j \left(dA_i dl\right)} \times \left[1 - F_{N,j}\right]^{k} + \sum_{l=0}^{r-m} \left(1 - e^{-\lambda_j \left(dA_i dl\right)}\right) \times \left[1 - F_{N,j}\right]^{l} \right\} \tag{18}$$

The volume V_T is assumed to be modeled as a "series system" of independent volumes $\mathrm{d}V_i$. Hence, the probability of failure of volume V_T, can be written as

$$P_{f} = 1 - \prod_{i=0}^{N_V} \left(1 - P_{f,i}\right) \tag{19}$$

Equation (20) is the probability of failure for volume V_T. This model estimate the probability of failure of components estimated according to a defects distribution in the component volume. It is noted, that the cumulative distribution function $F_{N,i}(n;\sigma)$, is a critical point of this model and can be estimated based on fatigue test data.

In these equations, the size, type, orientation, stress of defects considered but when there is a cluster of defects in component, the distance between each defects play very important role on fatigue life.

4. Conclusion

In this paper is considered basic models for assessment of the probability of fatigue failure due to manufacturing defects on casted components. The defects are categorized in different groups according to their size, type, orientation and etc. For each group, a Poisson distribution is used to model the distribution of defects in component volumes. Further, the defects are divided in two sub-groups of interior and surface defects.

Next, the component volume is divided in smaller volume to make homogeneous stress in small volumes. In each sub-volume sections, the probability of failure is modeled. The probability of failure is a function of i) existence of defect(s) in sub-volumes, ii) the conditional probability of failure due to existence of defect(s) in sub-volumes. In this model, the interior and surface defects are separated from each other. For each sub-volume, the probability of failure is modeled. As the component volume can be considered as a series system of sub-volumes, the probability of failure of components formulated according to a series systems probability of failure model.

Modeling the distance between defects in 3D dimension is very difficult due to completely random shape of defects in components. This point is considered in further work to increase the precision of introduced model.

Acknowledgements

The work is supported by the Strategic Research Center “REWIND – Knowledge based engineering for improved reliability of critical wind turbine components”, Danish Research Council for Strategic Research, grant no. 10-093966.

References

1. Shirani M, Härkegård G. Fatigue life distribution and size effect in ductile cast iron for wind turbine components. *Eng Fail Anal* 2010;**18**; 12-24.
2. Mirzaei Rafsanjani H, Sørensen JD. Stochastic models of defects in wind turbine drivetrain components. In: Papadrakakis M, Stefanou G, editors. *Multiscale Modeling and Uncertainty Quantification of Materials and Structures.* Switzerland: Springer; 2014. p. 287-298.
3. Shirani M, Härkegård G. Damage tolerant design of cast components based on defects detected by 3D X-ray computed tomography. *Int J Fatigue* 2012;**41**; 188-198.
4. Todinov MT. Equations and a fast algorithm for determining the probability of failure initiated by flaws. *Int J Solids Struct* 2006;**43**; 5182-5195.
5. Toft HS, Branner K, Berring P, Sørensen JD. Defect distribution and reliability assessment of wind turbine blades. *Eng Struct* 2011;**33**; 171-180.
6. Todinov MT. Probability of fracture initiated by defects. *Mater Sci Eng* 2000;**A276**; 39-47.
7. Ravi Chandran KS, Jha SK. Duality of the S-N fatigue curve caused by competing failure modes in a titanium alloy and the role of Poisson defect statistics, *Acta Mater* 2005;**53**; 1867-1881.

APPENDIX A

The list of nodules associated with the biggest nodule volumes for specimen 269-1 (Sand Casting).

Num.	*Volume (mm^3)*	*Surface (mm^2)*	*PZ (mm^2)*	*X (mm)*	*Y (mm)*	*Z (mm)*
1	0.018	0.282	0.038	1.157	0.049	-19.066
2	0.018	1.050	0.026	-1.235	-0.257	-33.722
3	0.016	0.405	0.042	-1.449	-0.686	-23.647
4	0.012	0.860	0.023	-1.233	-1.758	-35.600
5	0.011	0.812	0.017	-1.393	2.204	-36.680
6	0.006	0.161	0.021	-1.614	-0.989	-23.299
7	0.005	0.144	0.013	0.692	3.394	-39.302
8	0.005	0.177	0.008	0.639	1.621	-39.257
9	0.005	0.081	0.017	-1.558	3.043	-39.384
10	0.004	0.089	0.014	0.382	1.716	-29.787
11	0.004	0.080	0.019	-0.321	1.880	-28.919
12	0.004	0.073	0.016	-2.025	-1.047	-26.865
13	0.004	0.094	0.016	-0.948	-0.708	-24.595
14	0.004	0.097	0.012	-0.779	-1.855	-36.196
15	0.004	0.151	0.009	0.708	2.007	-39.396

The list of nodules associated with the biggest nodule volumes for specimen 269-19 (Sand Casting).

Num.	*Volume (mm^3)*	*Surface (mm^2)*	*PZ (mm^2)*	*X (mm)*	*Y (mm)*	*Z (mm)*
1	0.017	0.323	0.046	-0.999	2.211	-22.873
2	0.014	0.236	0.027	-0.884	2.307	-22.562
3	0.007	0.195	0.017	-1.357	0.063	-24.984
4	0.005	0.098	0.014	1.388	0.867	-27.221
5	0.005	0.117	0.015	2.528	0.603	-29.841
6	0.005	0.111	0.021	-1.382	1.477	-18.464
7	0.005	0.093	0.018	0.966	0.008	-29.204
8	0.005	0.101	0.014	1.774	0.087	-28.570
9	0.004	0.105	0.015	-0.859	0.631	-26.245
10	0.003	0.079	0.017	-0.259	1.723	-27.435
11	0.003	0.079	0.016	0.421	0.735	-27.663
12	0.003	0.119	0.013	1.901	-1.250	-29.311
13	0.003	0.072	0.009	-1.315	0.979	-27.327
14	0.003	0.087	0.009	2.140	0.626	-29.693
15	0.003	0.056	0.011	2.175	-1.174	-28.612

The list of nodules associated with the biggest nodule volumes for specimen 308-8 (Sand Casting).

Num.	*Volume (mm^3)*	*Surface (mm^2)*	*PZ (mm^2)*	*X (mm)*	*Y (mm)*	*Z (mm)*
1	0.012	0.360	0.026	-0.167	-2.382	-15.453
2	0.009	0.160	0.026	0.048	-0.005	-36.989
3	0.006	0.194	0.015	-0.374	1.284	-15.354
4	0.006	0.171	0.009	-1.587	-0.522	-20.487
5	0.005	0.321	0.012	-0.248	-1.347	-17.047
6	0.005	0.209	0.016	0.086	-1.006	-24.508
7	0.004	0.214	0.014	-0.309	-1.199	-28.542
8	0.004	0.289	0.011	-1.122	2.680	-29.006
9	0.004	0.082	0.015	-2.190	-1.399	-18.949
10	0.004	0.066	0.014	1.514	0.185	-17.644
11	0.004	0.094	0.014	1.689	3.249	-15.392
12	0.004	0.096	0.013	1.546	2.697	-36.644
13	0.004	0.104	0.013	-1.473	1.107	-15.179
14	0.003	0.106	0.013	1.877	0.444	-17.269
15	0.003	0.088	0.012	-0.906	0.775	-30.175

The list of nodules associated with the biggest nodule volumes for specimen 338-13 (Sand Casting).

Num.	*Volume (mm^3)*	*Surface (mm^2)*	*PZ (mm^2)*	*X (mm)*	*Y (mm)*	*Z (mm)*
1	0.023	0.535	0.047	0.423	1.738	-20.176
2	0.015	0.267	0.029	-0.733	2.109	-12.288
3	0.011	0.297	0.040	0.588	1.569	-20.704
4	0.008	0.196	0.018	0.479	1.541	-21.120
5	0.005	0.180	0.008	0.226	-0.576	-27.145
6	0.003	0.104	0.008	-0.105	2.205	-20.125
7	0.003	0.150	0.009	1.692	-1.662	-34.378
8	0.003	0.152	0.008	3.420	-0.374	-34.927
9	0.003	0.111	0.008	-2.182	-0.468	-22.912
10	0.003	0.074	0.009	-0.655	-0.928	-27.831
11	0.003	0.073	0.015	-0.676	2.366	-13.163
12	0.003	0.058	0.009	0.435	0.519	-27.945
13	0.003	0.067	0.009	-1.117	2.485	-12.805
14	0.003	0.104	0.011	0.188	2.546	-24.321
15	0.003	0.088	0.006	-1.182	2.135	-20.438

The list of nodules associated with the biggest nodule volumes for specimen 626-2 (Chill Casting).

Num.	*Volume (mm^3)*	*Surface (mm^2)*	*PZ (mm^2)*	*X (mm)*	*Y (mm)*	*Z (mm)*
1	0.0008	0.0767	0.0022	-0.5725	-0.0158	-21.1777
2	0.0007	0.0609	0.0022	1.3509	-1.2683	-26.3802
3	0.0006	0.0575	0.0017	1.2932	1.3176	-22.1812
4	0.0006	0.0557	0.0022	1.1679	0.1625	-22.2149
5	0.0006	0.0542	0.0016	-0.7762	1.3659	-24.2442
6	0.0006	0.0505	0.0028	1.1010	-0.1392	-26.0876
7	0.0006	0.0508	0.0028	0.2971	-1.0249	-29.1290
8	0.0006	0.0523	0.0015	0.9841	0.8132	-27.6746
9	0.0006	0.0481	0.0030	1.6888	-0.4419	-26.4111
10	0.0006	0.0468	0.0029	-1.6059	0.4627	-23.1146
11	0.0005	0.0490	0.0025	0.9819	1.7020	-22.4130
12	0.0005	0.0487	0.0027	1.4577	0.0408	-23.5855
13	0.0005	0.0499	0.0027	-0.5497	-1.2563	-23.5691
14	0.0005	0.0419	0.0015	-0.4920	-1.2653	-28.5208
15	0.0005	0.0425	0.0017	-0.8439	-0.8798	-21.6996

The list of nodules associated with the biggest nodule volumes for specimen 656-1 (Chill Casting).

Num.	*Volume (mm^3)*	*Surface (mm^2)*	*PZ (mm^2)*	*X (mm)*	*Y (mm)*	*Z (mm)*
1	0.0013	0.1040	0.0038	0.3747	-1.1015	-25.0064
2	0.0012	0.0942	0.0036	0.6580	0.3216	-23.0084
3	0.0012	0.0945	0.0041	-1.1535	-0.0429	-25.7517
4	0.0011	0.0932	0.0042	-0.7000	-0.4957	-26.2596
5	0.0011	0.0908	0.0031	1.5084	-0.4240	-26.9413
6	0.0010	0.0834	0.0028	-1.4593	0.6724	-27.6891
7	0.0009	0.0773	0.0026	0.5943	-0.7527	-23.2151
8	0.0009	0.0670	0.0046	0.0084	1.3588	-24.6927
9	0.0009	0.0657	0.0034	-1.1292	-0.5519	-24.4590
10	0.0008	0.0679	0.0044	-1.0658	-1.5174	-25.0515
11	0.0008	0.0602	0.0045	-0.0973	1.6272	-23.7696
12	0.0008	0.0589	0.0028	-1.1238	1.0075	-24.1286
13	0.0007	0.0534	0.0030	0.9738	1.4103	-24.8836
14	0.0007	0.0557	0.0026	-0.2157	0.0985	-29.1799
15	0.0007	0.0552	0.0022	0.8398	0.8226	-23.2050

The list of nodules associated with the biggest nodule volumes for specimen 656-4 (Chill Casting).

Num.	*Volume (mm^3)*	*Surface (mm^2)*	*PZ (mm^2)*	*X (mm)*	*Y (mm)*	*Z (mm)*
1	0.0015	0.1290	0.0027	-0.0208	1.4368	-25.2957
2	0.0015	0.1120	0.0053	-0.3678	0.9465	-24.5339
3	0.0010	0.0821	0.0037	-0.9901	1.6504	-24.0766
4	0.0009	0.0701	0.0018	-0.3759	1.4523	-24.2731
5	0.0009	0.0605	0.0028	-0.9020	0.8666	-22.5023
6	0.0008	0.0671	0.0033	-0.9311	1.0414	-23.1757
7	0.0008	0.0592	0.0042	0.9168	1.3961	-25.2765
8	0.0008	0.0621	0.0025	-1.5087	-0.1365	-23.7054
9	0.0008	0.0682	0.0031	-0.8916	0.5980	-24.6419
10	0.0007	0.0607	0.0019	-0.3494	-0.9817	-22.3708
11	0.0007	0.0573	0.0027	1.0029	-0.9956	-23.2776
12	0.0007	0.0566	0.0023	-0.7952	-0.3634	-29.1371
13	0.0007	0.0581	0.0027	0.1657	1.8129	-25.0824
14	0.0007	0.0544	0.0020	-0.5855	-0.3306	-23.1449
15	0.0007	0.0488	0.0030	-0.3877	0.3610	-22.9404

The list of nodules associated with the biggest nodule volumes for specimen 656-13 (Chill Casting).

Num.	*Volume (mm^3)*	*Surface (mm^2)*	*PZ (mm^2)*	*X (mm)*	*Y (mm)*	*Z (mm)*
1	0.0014	0.1160	0.0048	-0.4599	0.9743	-23.0071
2	0.0010	0.0850	0.0025	-0.0769	1.3835	-22.9173
3	0.0008	0.0634	0.0021	-1.4314	-0.4521	-24.0407
4	0.0008	0.0662	0.0022	-0.0172	-1.3604	-28.4429
5	0.0008	0.0624	0.0035	1.3026	0.1491	-29.7494
6	0.0008	0.0637	0.0031	0.6123	0.4737	-24.3174
7	0.0008	0.0610	0.0039	0.0209	0.0232	-28.8022
8	0.0007	0.0526	0.0044	-1.4100	-1.0207	-28.5613
9	0.0007	0.0593	0.0023	0.9056	-1.2932	-24.3947
10	0.0007	0.0512	0.0031	0.4479	0.5373	-28.4924
11	0.0007	0.0520	0.0020	0.7675	1.4556	-23.9745
12	0.0007	0.0513	0.0025	0.9579	0.3196	-25.0211
13	0.0007	0.0560	0.0029	1.1576	-0.1634	-29.0819
14	0.0007	0.0538	0.0035	0.5295	-1.2553	-24.4284
15	0.0007	0.0493	0.0026	-0.1175	-1.1864	-26.5579

APPENDIX B

The main statistical descriptors of all nodules in specimen 269-1.

	Volume [mm^3]	**Equivalent Size [mm]**	**Area [mm^2]**	**Sphericity**	**Aspect Ratio**	**Proj.Surf. [mm^2]**
Mean	4.6e-4	0.18	0.01	0.91	0.83	3.0e-3
STD	4.8e-4	0.07	0.02	0.11	0.12	2.0e-3
Min	5.0e-7	0.02	1.4e-4	0.14	0.17	1.0e-5
Max	0.02	0.70	1.05	1.0	1.0	0.04
Median	3.4e-4	0.19	0.01	0.95	0.86	3.0e-3

The main statistical descriptors of all nodules in specimen 269-19.

	Volume [mm^3]	**Equivalent Size [mm]**	**Area [mm^2]**	**Sphericity**	**Aspect Ratio**	**Proj.Surf. [mm^2]**
Mean	3.2e-4	0.17	0.01	0.89	0.82	2.0e-3
STD	3.6e-4	0.06	0.01	0.13	0.14	2.0e-3
Min	6.1e-7	0.02	1.6e-4	0.24	0.16	2.0e-5
Max	0.02	0.69	0.32	1.0	1.0	0.05
Median	2.2e-4	0.16	0.01	0.96	0.86	2.0e-3

The main statistical descriptors of all nodules in specimen 308-8.

	Volume [mm^3]	**Equivalent Size [mm]**	**Area [mm^2]**	**Sphericity**	**Aspect Ratio**	**Proj.Surf. [mm^2]**
Mean	3.7e-4	0.17	0.01	0.90	0.82	2.0e-3
STD	4.2e-4	0.07	0.01	0.11	0.13	2.0e-3
Min	6.1e-7	0.02	1.6e-4	0.19	0.14	2e-5
Max	0.01	0.61	0.36	1.0	1.0	0.03
Median	2.4e-4	0.17	0.01	0.95	0.85	2.0e-3

The main statistical descriptors of all nodules in specimen 338-13.

	Volume [mm^3]	**Equivalent Size [mm]**	**Area [mm^2]**	**Sphericity**	**Aspect Ratio**	**Proj.Surf. [mm^2]**
Mean	2.3e-4	0.15	0.01	0.89	0.81	2.0e-3
STD	2.9e-4	0.05	0.01	0.13	0.14	1.0e-3
Min	6.1e-7	0.02	1.6e-4	0.27	0.13	2.0e-5
Max	0.02	0.76	0.54	1.0	1.0	0.05
Median	1.4e-4	0.14	0.01	0.95	0.84	1.0e-3

The main statistical descriptors of all nodules in specimen 626-2.

	Volume [mm^3]	**Equivalent Size [mm]**	**Area [mm^2]**	**Sphericity**	**Aspect Ratio**	**Proj.Surf. [mm^2]**
Mean	1.7e-5	0.06	2.0e-3	0.84	0.67	2.8e-4
STD	2.18e-5	0.02	2.0e-3	0.12	0.15	1.9e-4
Min	6.1e-7	0.02	1.6e-4	0.26	0.10	2.0e-5
Max	8.2e-4	0.25	0.08	1.0	1.0	4.0e-3
Median	1.1e-5	0.06	0.01	0.85	0.67	2.4e-4

The main statistical descriptors of all nodules in specimen 656-1.

	Volume [mm^3]	**Equivalent Size [mm]**	**Area [mm^2]**	**Sphericity**	**Aspect Ratio**	**Proj.Surf. [mm^2]**
Mean	2.8e-5	0.07	3.0e-3	0.85	0.71	4.0e-4
STD	3.4e-5	0.02	3.0e-3	0.13	0.15	2.6e-4
Min	6.1e-7	0.02	1.6e-4	0.25	0.11	2.0e-5
Max	1.0e-3	0.29	0.10	1.0	1.0	5.0e-3
Median	1.8e-5	0.07	2.0e-3	0.86	0.71	3.4e-4

The main statistical descriptors of all nodules in specimen 656-4.

	Volume [mm^3]	**Equivalent Size [mm]**	**Area [mm^2]**	**Sphericity**	**Aspect Ratio**	**Proj.Surf. [mm^2]**
Mean	2.2e-5	0.07	2.0e-3	0.85	0.71	3.5e-4
STD	2.8e-5	0.02	2.0e-3	0.13	0.16	2.3e-4
Min	6.1e-7	0.02	1.6e-4	0.23	0.11	2.0e-5
Max	1.0e-3	0.31	0.13	1.0	1.0	5.0e-3
Median	1.5e-5	0.07	2.0e-3	0.86	0.71	2.9e-4

The main statistical descriptors of all nodules in specimen 656-13.

	Volume [mm^3]	**Equivalent Size [mm]**	**Area [mm^2]**	**Sphericity**	**Aspect Ratio**	**Proj.Surf. [mm^2]**
Mean	2.3e-5	0.07	2.0e-3	0.85	0.71	3.5e-4
STD	2.8e-5	0.02	2.0e-3	0.13	0.16	2.3e-4
Min	6.0e-7	0.02	1.6e-4	0.25	0.13	2.0e-5
Max	1.0e-3	0.30	0.12	1.0	1.0	5.0e-3
Median	1.5e-5	0.07	1.0e-3	0.86	0.71	3.0e-4

APPENDIX C

GEV distribution parameters for different threshold probabilities of specimen 269-1.

	Shape parameter, ζ	**Scale parameter, σ [mm]**	**Location parameter, μ [mm]**	**Number of nodules**
Total	-0.112	0.010	0.024	20730
PS80	0.294	0.003	0.041	3719
PS85	0.374	0.002	0.044	2444
PS90	0.493	0.002	0.047	1247
PS95	0.509	0.002	0.052	342
PS96	0.673	0.002	0.054	242
PS97	0.725	0.002	0.056	135
PS98	1.022	0.002	0.059	65
PS99	-	-	-	25

GEV distribution parameter for different threshold probabilities of specimen 269-19.

	Shape parameter, ζ	**Scale parameter, σ [mm]**	**Location parameter, μ [mm]**	**Number of nodules**
Total	-0.080	0.008	0.021	26663
PS80	0.313	0.003	0.036	5252
PS85	0.361	0.003	0.038	3729
PS90	0.472	0.002	0.040	2194
PS95	0.535	0.002	0.045	755
PS96	0.582	0.002	0.046	565
PS97	0.601	0.002	0.048	377
PS98	0.701	0.002	0.051	220
PS99	0.752	0.002	0.055	101

GEV distribution parameter for different threshold probabilities of specimen 308-8.

	Shape parameter, ξ	**Scale parameter, σ [mm]**	**Location parameter, μ [mm]**	**Number of nodules**
Total	-0.142	0.010	0.021	22195
PS80	0.185	0.003	0.039	4396
PS85	0.226	0.003	0.041	3270
PS90	0.310	0.002	0.044	2061
PS95	0.453	0.002	0.048	783
PS96	0.581	0.002	0.049	569
PS97	0.497	0.002	0.051	338
PS98	0.535	0.002	0.054	188
PS99	0.572	0.002	0.058	72

GEV distribution parameter for different threshold probabilities of specimen 338-13.

	Shape parameter, ξ	**Scale parameter, σ [mm]**	**Location parameter, μ [mm]**	**Number of nodules**
Total	-0.061	0.007	0.018	38069
PS80	0.325	0.003	0.032	8079
PS85	0.348	0.003	0.033	6001
PS90	0.351	0.002	0.036	3764
PS95	0.415	0.002	0.039	1670
PS96	0.471	0.002	0.041	1290
PS97	0.557	0.002	0.042	877
PS98	0.553	0.002	0.045	484
PS99	0.644	0.002	0.049	195

GEV distribution parameter for different threshold probabilities of specimen 626-2.

	Shape parameter, ζ	**Scale parameter, σ [mm]**	**Location parameter, μ [mm]**	**Number of nodules**
Total	-0.039	0.002	0.008	222528
PS95	0.487	0.001	0.015	10854
PS96	0.493	0.001	0.016	8853
PS97	0.511	0.001	0.016	6573
PS98	0.499	0.001	0.017	4681
PS99	0.502	0.001	0.018	2512
PS995	0.468	0.001	0.020	1363
PS996	0.485	0.001	0.020	1136
PS997	0.437	0.001	0.021	901
PS998	0.421	0.001	0.021	660
PS999	0.436	0.001	0.022	400

GEV distribution parameter for different threshold probabilities of specimen 656-1.

	Shape parameter, ζ	**Scale parameter, σ [mm]**	**Location parameter, μ [mm]**	**Number of nodules**
Total	-0.053	0.003	0.009	184674
PS95	0.484	0.001	0.018	9003
PS96	0.489	0.001	0.019	7168
PS97	0.495	0.001	0.019	5524
PS98	0.514	0.001	0.020	3754
PS99	0.529	0.001	0.022	1958
PS995	0.493	0.001	0.023	1072
PS996	0.520	0.001	0.024	886
PS997	0.534	0.001	0.024	708

PS998	0.484	0.001	0.018	9003
PS999	0.489	0.001	0.019	7168

GEV distribution parameter for different threshold probabilities of specimen 656-4.

	Shape parameter, ζ	**Scale parameter, σ [mm]**	**Location parameter, μ [mm]**	**Number of nodules**
Total	-0.051	0.002	0.009	225415
PS95	0.485	0.001	0.017	11076
PS96	0.492	0.001	0.017	8935
PS97	0.499	0.001	0.018	6677
PS98	0.498	0.001	0.019	4629
PS99	0.511	0.001	0.020	2554
PS995	0.526	0.001	0.022	1421
PS996	0.501	0.001	0.022	1194
PS997	0.500	0.001	0.023	928
PS998	0.521	0.001	0.023	696
PS999	0.456	0.001	0.025	403

GEV distribution parameter for different threshold probabilities of specimen 656-13.

	Shape parameter, ζ	**Scale parameter, σ [mm]**	**Location parameter, μ [mm]**	**Number of nodules**
Total	-0.047	0.002	0.009	220608
PS95	0.526	0.001	0.017	10292
PS96	0.536	0.001	0.017	8344
PS97	0.519	0.001	0.018	6489
PS98	0.512	0.001	0.019	4441
PS99	0.474	0.001	0.020	2521
PS995	0.459	0.001	0.022	1438
PS996	0.457	0.001	0.022	1253

PS997	0.465	0.001	0.023	1004
PS998	0.442	0.001	0.024	757
PS999	0.433	0.001	0.025	465

APPENDIX D

In This Appendix, the qq-plot for nodule sizes for different specimens are shown based on the GEV and Weibull distribtuinos.

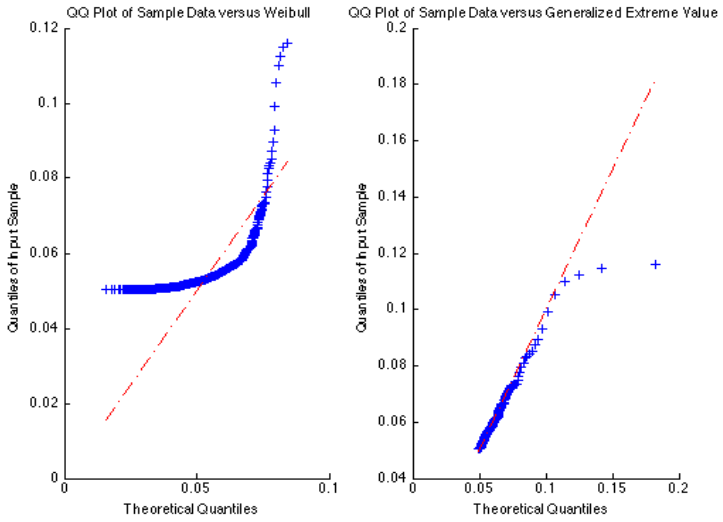

qq-plot of GEV and Weibull distributions for specimen 269-1 (PS95)

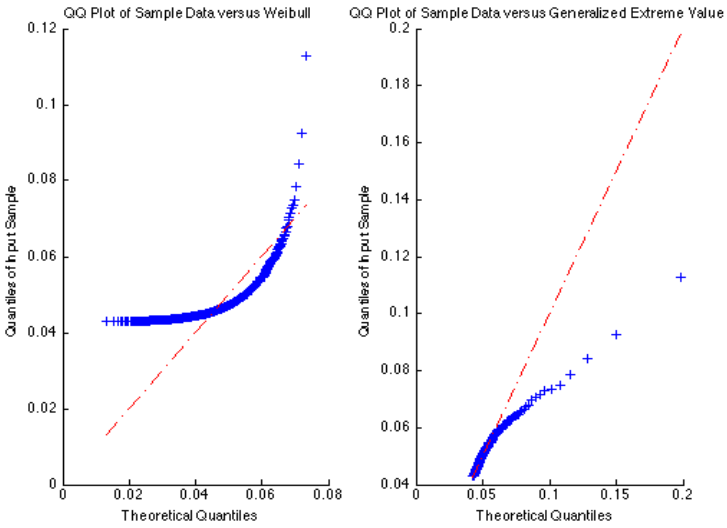

qq-plot of GEV and Weibull distributions for specimen 269-19 (PS95)

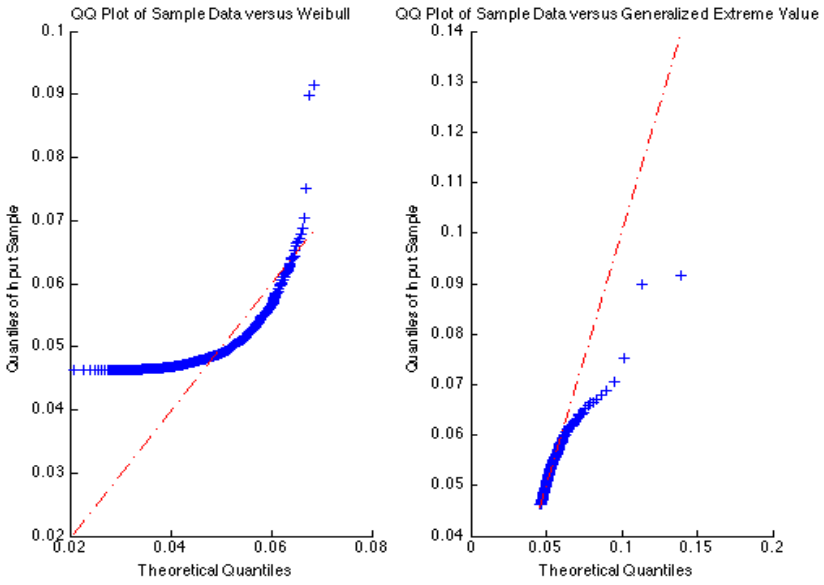

qq-plot of GEV and Weibull distributions for specimen 308-8 (PS95)

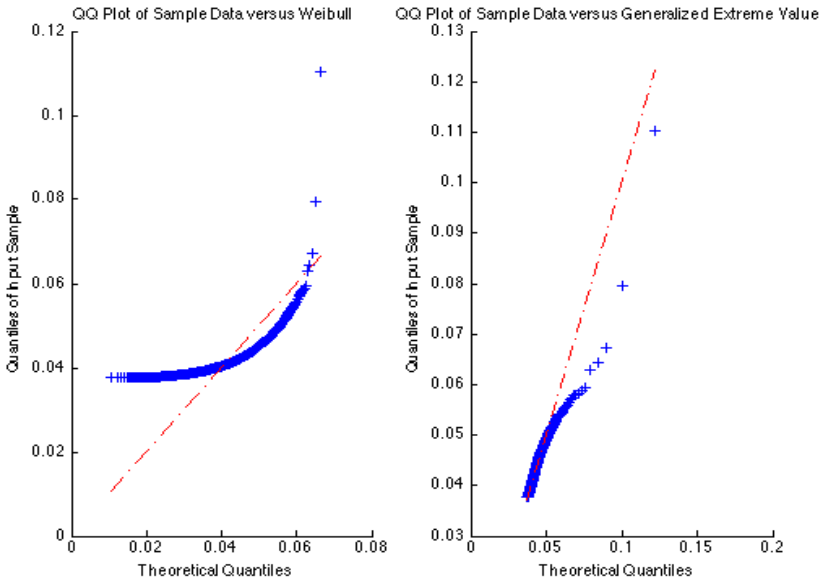

qq-plot of GEV and Weibull distributions for specimen 338-13 (PS95)

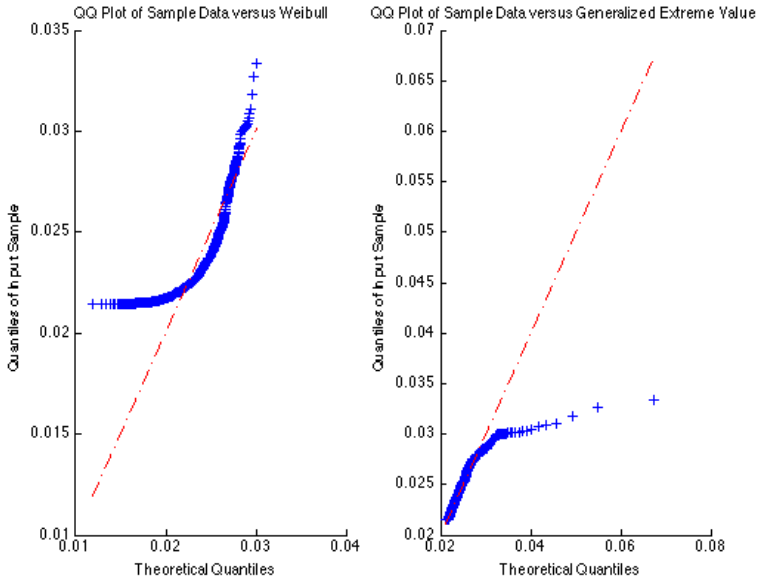

qq-plot of GEV and Weibull distributions for specimen 626-2 (PS999)

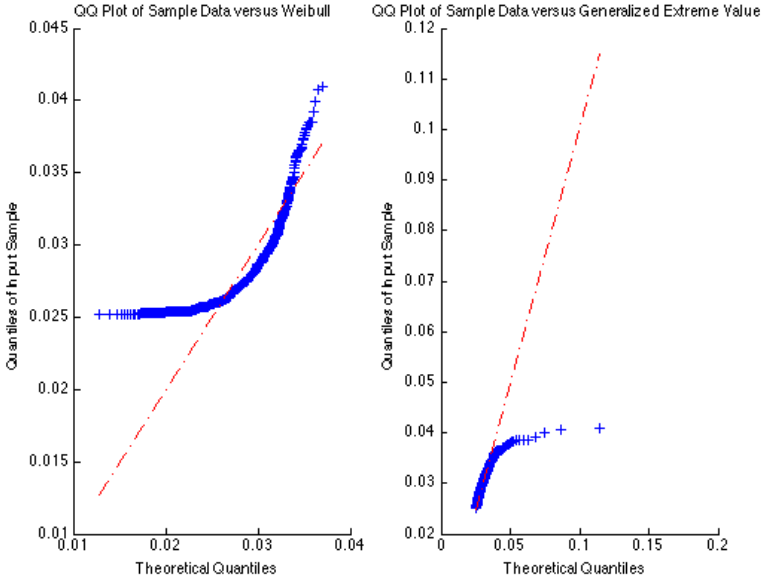

qq-plot of GEV and Weibull distributions for specimen 656-1 (PS999)

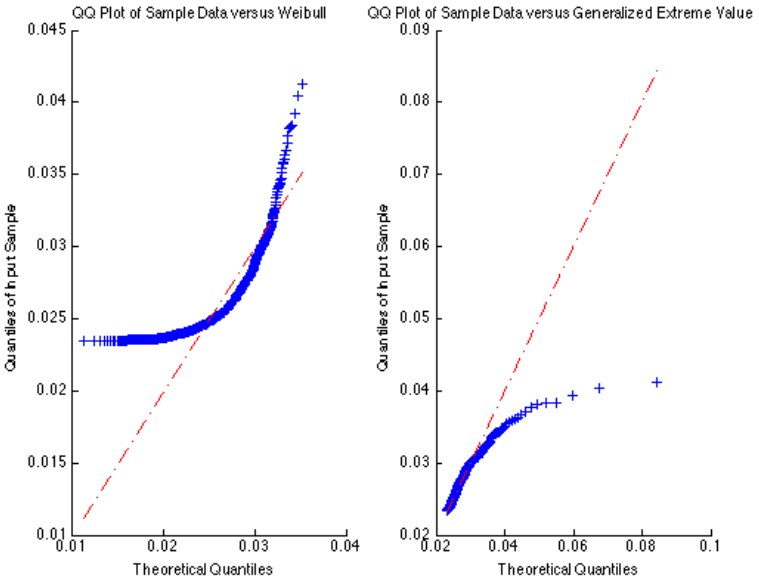

qq-plot of GEV and Weibull distributions for specimen 656-4 (PS999)

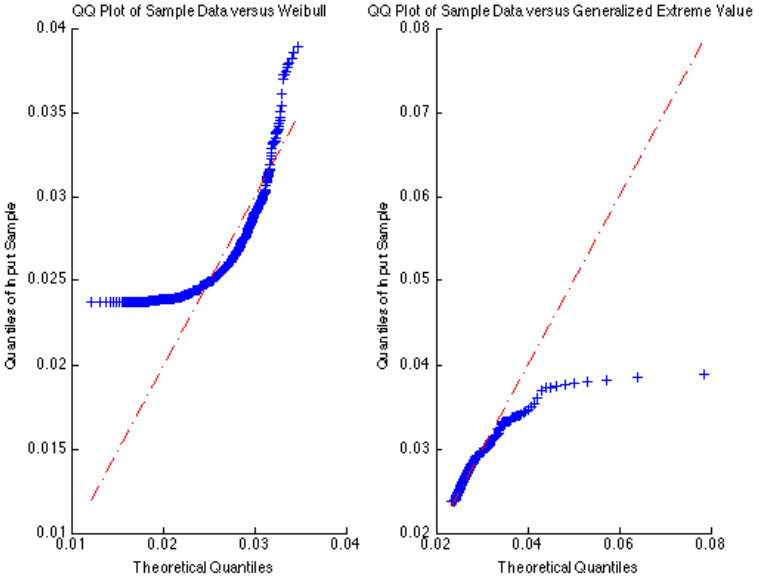

qq-plot of GEV and Weibull distributions for specimen 656-13 (PS999)

APPENDIX E

In This Appendix, the evaluation of the "Sphericity" versus "Equivalent Size" for each specimen is shown as below.

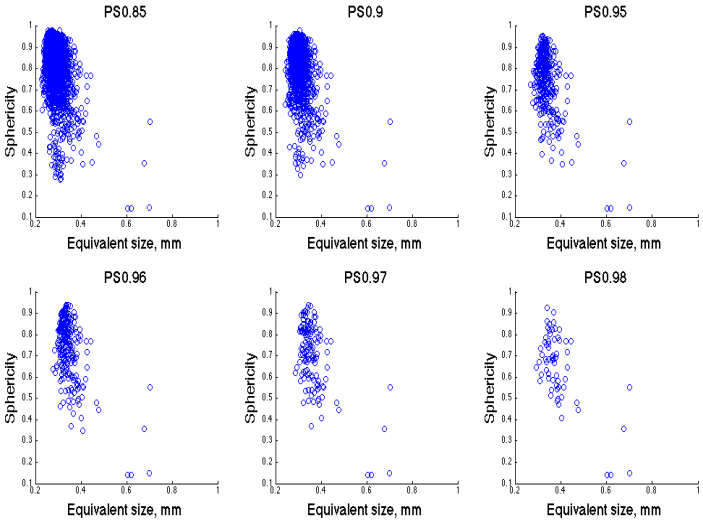

Sphericity vs.Equivalent Size for 269-1

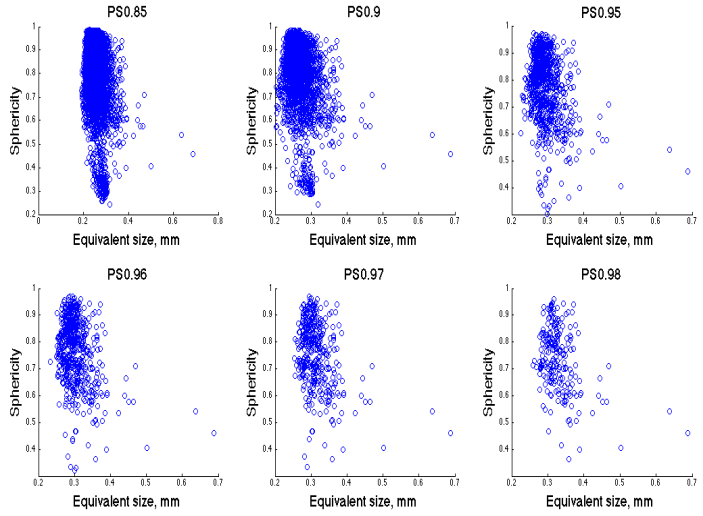

Sphericity vs.Equivalent Size for 269-19

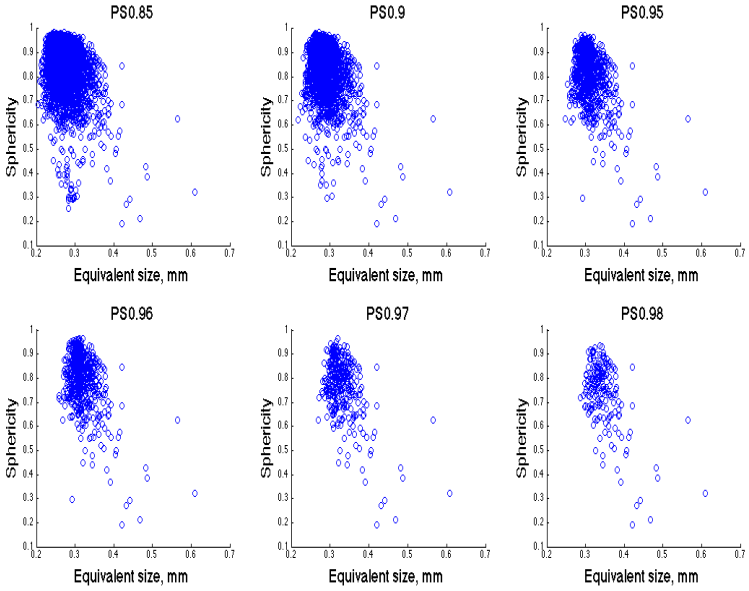

Sphericity vs.Equivalent Size for 308-8

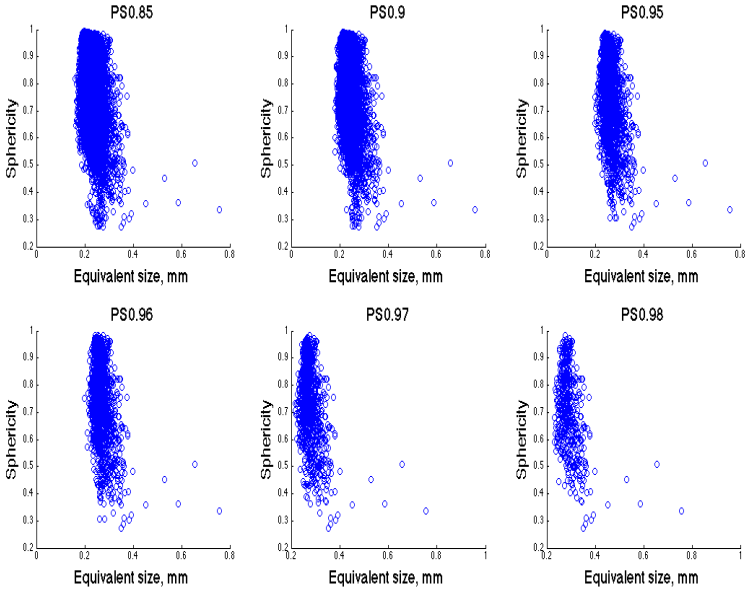

Sphericity vs.Equivalent Size for 338-13

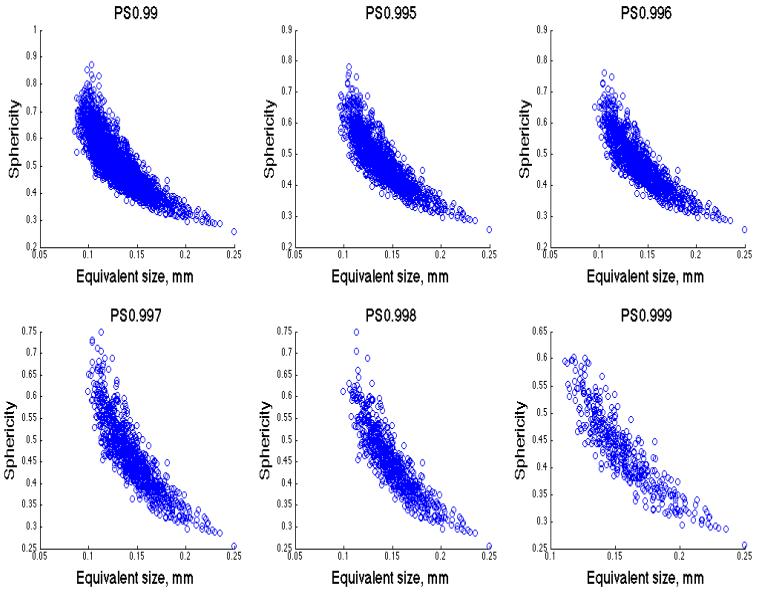

Sphericity vs.Equivalent Size for 626-2

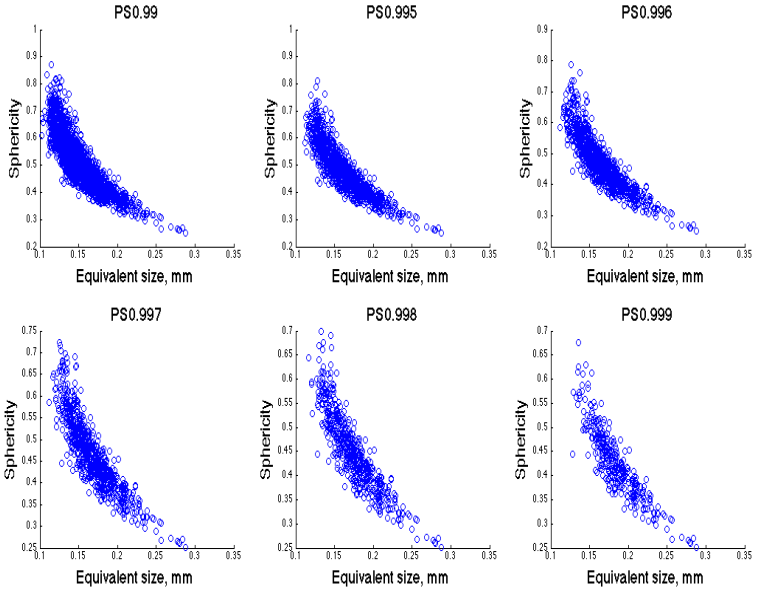

Sphericity vs.Equivalent Size for 656-1

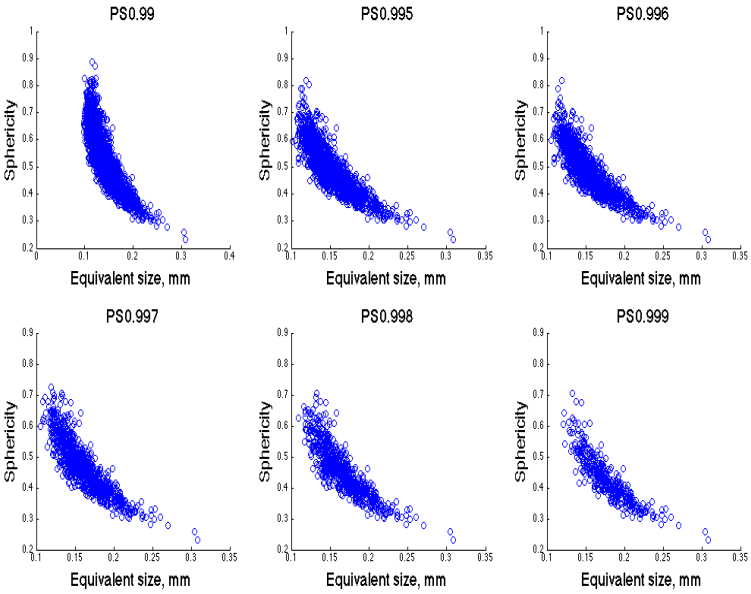

Sphericity vs.Equivalent Size for 656-4

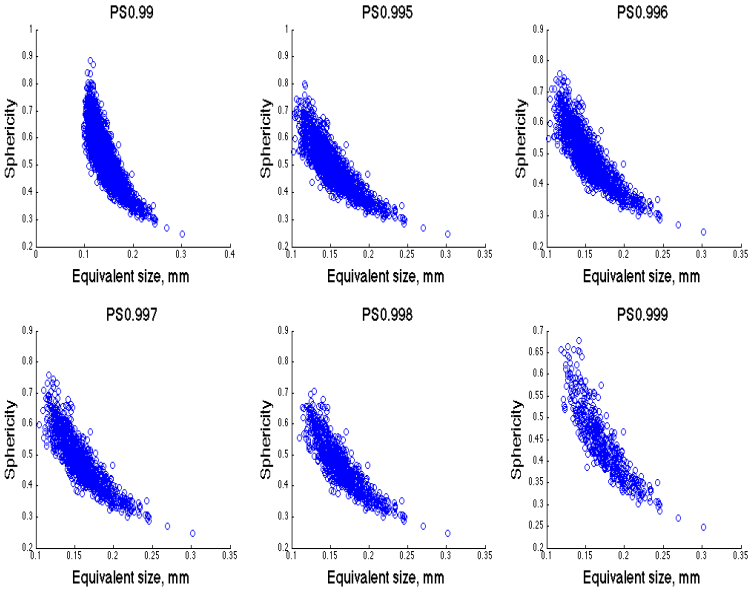

Sphericity vs.Equivalent Size for 656-13

APPENDIX F

In This Appendix, the evaluation of the “Aspect Ratio” versus “Equivalent Size” for each specimen is shown as below.

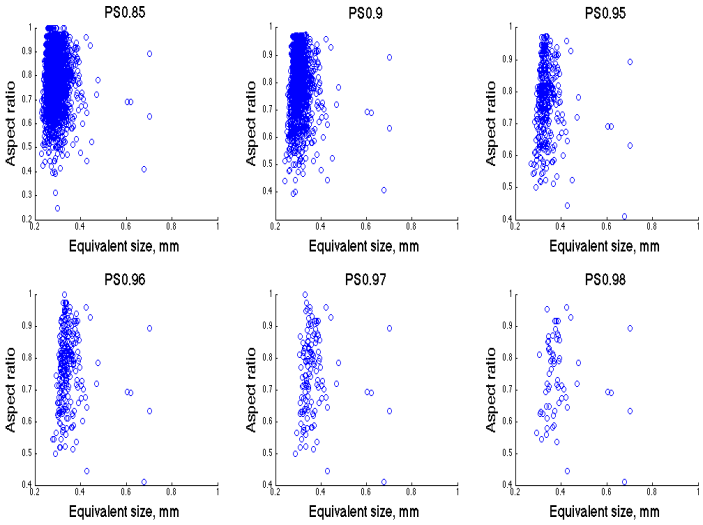

Aspect Ratio vs.Equivalent Size for 269-1

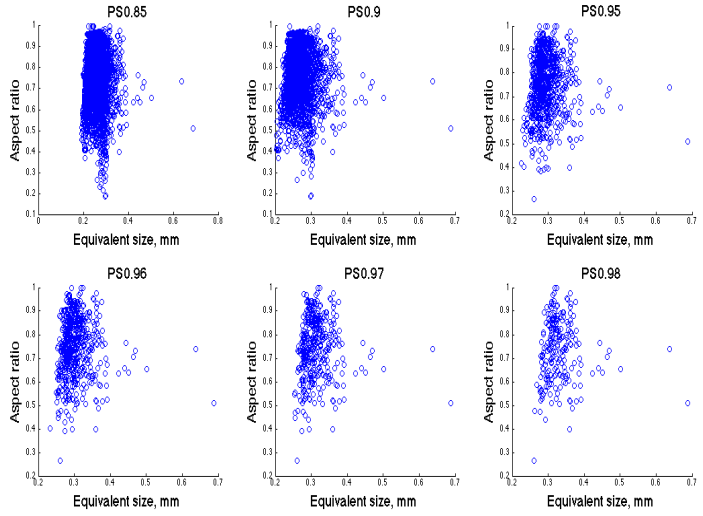

Aspect Ratio vs.Equivalent Size for 269-19

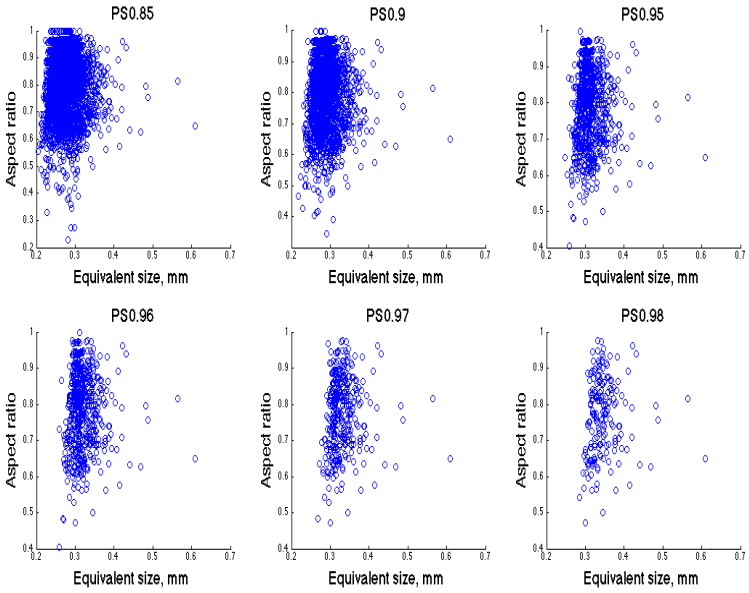

Aspect Ratio vs.Equivalent Size for 308-8

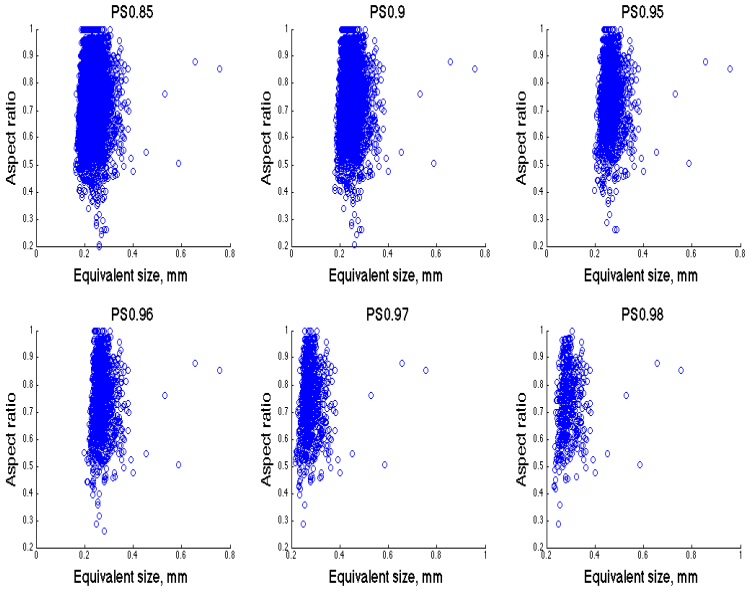

Aspect Ratio vs.Equivalent Size for 338-13

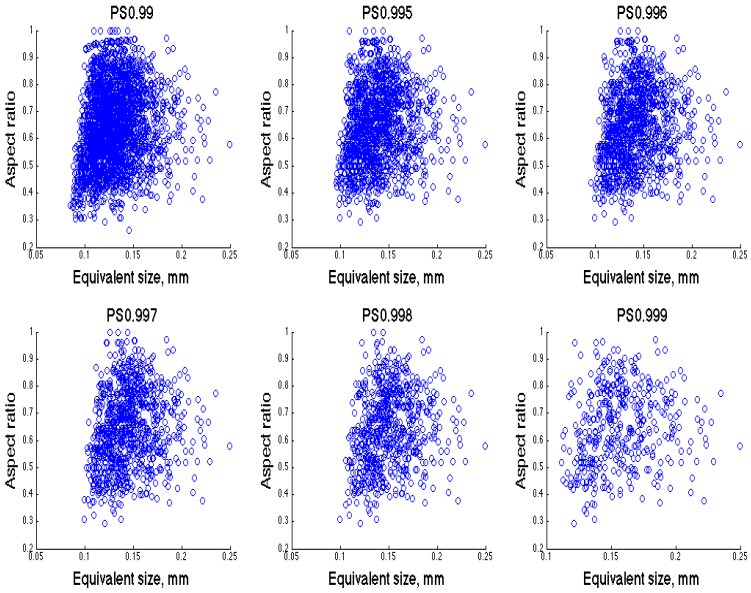

Aspect Ratio vs.Equivalent Size for 626-2

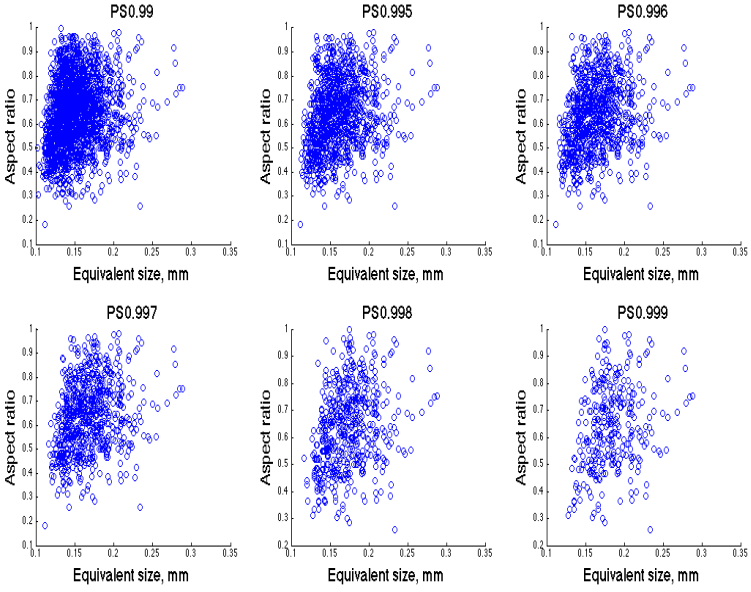

Aspect Ratio vs.Equivalent Size for 656-1

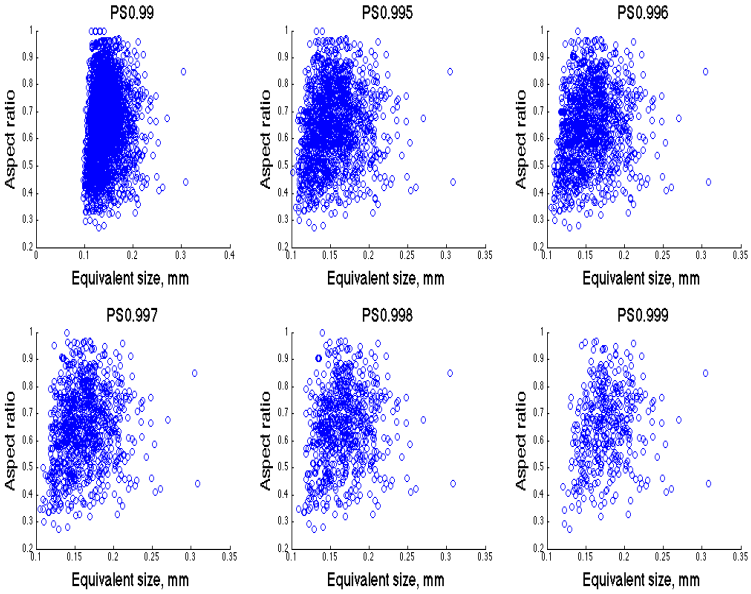

Aspect Ratio vs.Equivalent Size for 656-4

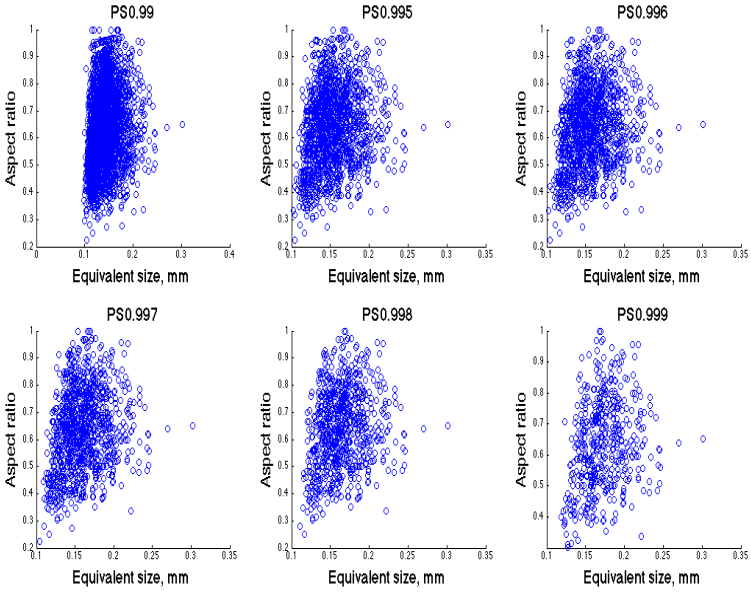

Aspect Ratio vs.Equivalent Size for 656-13

APPENDIX G

Examples of COV_W (Sørensen & Toft, 2014)

COV_{Wind}	Uncertainty is assessment of fatigue wind load
0.10-0.15	*Site assessment:* • More than 2 years of climatic data, corrected with MCP techniques. • Wind measurements above and below wind turbine hub height. • Flat terrain with low roughness *Dynamic response:* • Structural dynamic effects through modal analysis, with at least 4 modes considered for blade and tower. • Mass and stiffness properties defined with FEM and validated with real scale specimens. • Eigenvalues and damping validated with real scale tests. *Aerodynamic coefficients:* • Airfoil data experimentally validated in wind tunnel at different Re numbers • Airfoil data including 3D effects • Attached flow in all operating regimes • BEM, including Dynamic stall and Tip and hub loss included • Dynamic wake inflow model • Quality control of shape of manufactured blades
0.15-0.20	*Site assessment:* • Minimum 1 year of climatic data. • Wind measurements at hub height and below. • Non-complex site with medium roughness. *Dynamic response:* • Structural dynamic effects through modal analysis, with 2 modes considered for blade and tower. • Mass and stiffness properties defined with FEM but not validated with real scale specimens. • Eigenvalues and damping not validated with real scale tests. *Aerodynamic coefficients:* • Airfoil data based on CFD, but not measured in wind tunnel. • 3D effects not included in airfoil data • Attached flow in all operating regimes • BEM, but not including dynamic stall effects nor tip and hub losses • Static wake inflow model
0.20-0.25	*Site assessment:* • Less than 1 year of data, not corrected with MCP techniques Wind measurements below hub height. • Complex terrain. *Dynamic response:* • Structural dynamic effects not considered *Aerodynamic coefficients:* • Airfoil data based on similar airfoils or for a single Re number. • 3D effects not included in airfoil data • Stall flow in relevant operating regimes • BEM, but not including dynamic stall effects nor tip and hub losses • No model for wake effects • Dirt and erosion on blades

Examples of COV_{SCF} (Sørensen & Toft, 2014)

COV_{SCF}	Fatigue critical detail
0.00	Statically determinate systems with simple fatigue critical details (e.g. girth welds) where FEM analyses are performed
0.05	Statically determinate systems with complex fatigue critical details (e.g. multi-planar joints) where FEM analyses are performed
0.10	Statically in-determinate systems with complex fatigue critical details (e.g. doubler plates) where FEM analyses are performed
0.15	2 dimensional tubular joints using SCF parametric equations
0.20	Tubular joints in structures where tubular stiffness is modeled by Local Joint Flexibility (LJF) models and SCF parametric equations are used

SUMMARY

Wind energy is one of several energy sources in the world and a rapidly growing industry in the energy sector. When placed in offshore or onshore locations, wind turbines are exposed to wave excitations, highly dynamic wind loads and/or the wakes from other wind turbines. Therefore, most components in a wind turbine experience highly dynamic and time-varying loads. These components may fail due to wear or fatigue, and this can lead to unplanned shutdown repairs that are very costly. The design by deterministic methods using safety factors is generally unable to account for the many uncertainties. Thus, a reliability assessment should be based on probabilistic methods where stochastic modeling of failures is performed. This thesis focuses on probabilistic models and the stochastic modeling of the fatigue life of the wind turbine drivetrain.

Hence, two approaches are considered for stochastic modeling of the fatigue life. One method is based on the classical Weibull approach and the other on application of a log-normal distribution. The statistical parameters in both models are estimated and applied in reliability assessments. Furthermore, the thesis includes a study of the effect of defects/nodules on fatigue life of cast iron samples. The cast iron samples scanned by 3D tomography equipment at the DTU Wind Energy (Risø campus), and the distribution of nodules are used to estimate the fatigue life.

ISSN (online): 2246-1248
ISBN (online): 978-87-7112-859-8

AALBORG **UNIVERSITETSFORLAG**